AFFDL-TR-70-143

AIRPLANE FLYING CHARACTERISTICS IN TURBULENCE

E. D. ONSTOTT
E. P. SALMON

FOREWORD

This report was prepared by the Northrop Corporation, Aircraft Division, Hawthorne, California under USAF Contract No. F33615-70-C-1156. The contract work was performed under Project No. 8219, "Stability and Control for Air Force Missiles, Aerospace Vehicles and Aircraft," Task No. 821904, "Control System Theory Applied to Combat Aircraft Flight Control Design," Work Unit No. 024, "Airplane Flying Characteristics in Atmospheric Turbulence." The program was administered by the Air Force Flight Dynamics Laboratory, Air Force Systems Command, Wright-Patterson Air Force Base, Ohio. The program monitor and project engineer was Mr. Frank L. George (FGC).

The reporting period extends from 17 November 1969 through 11 September 1970. This report was sumitted on 30 November 1970 and the internal Northrop Report is NOR 70-139.

This technical report has been reviewed and is approved.

C. B. Westbrook
Chief, Control Criteria Branch
Flight Control Division
AF Flight Dynamics Laboratory

ABSTRACT

A method for predicting the performance of the total pilot-vehicle system has been developed for the lateral dynamics of Class IV airplanes. This method, which is based on pilot model theory and multiloop analysis, predicts tracking errors for command tracking tasks and also for attitude hold tracking tasks in turbulence. The predictions are in terms of root mean square time domain statistics and are obtained by means of a fully automated multiloop analysis performance prediction program available from the United States Air Force. Thus, system performance can be evaluated analytically in terms of familiar time domain root mean square statistics. The validity and accuracy of this method has been ascertained by means of moving base simulation on the Northrop Large Amplitude Flight Simulator operating in five degree of freedom motion.

TABLE OF CONTENTS

SECTION		PAGE
I	INTRODUCTION	1
	A. Scope and Purpose of This Report	1
	B. Specification of Flying Qualities	1
	C. Quasi-Linear Analysis	2
	D. The Anderson Rating Prediction Method	3
	E. Conventional Aircraft in Turbulence	4
II	TOTAL SYSTEM PERFORMANCE PREDICTIONS	5
	A. Four Approaches to Pilot-Vehicle Analysis	5
	B. Performance Measures	6
	C. Lateral System Models for Compensatory Tracking	7
	D. Pilot Model Theory	11
	E. Turbulence Models	20
III	DEMONSTRATION OF THE METHOD	22
	A. Bank Angle Task Prediction	22
	B. The Simulation	23
	C. Bank Angle Simulation Data	24
	D. Heading Task Prediction	67
IV	FURTHER CONSIDERATIONS OF SYSTEMS ANALYSIS	89
	A. Superposition in the Pilot	89
	B. Anderson Formulas for Command Tracking in Turbulence	90
	C. Reduced Time Delay as a Model for Acceleration Cues	90
V	APPLICATION TO AIRPLANE SPECIFICATION AND DESIGN	95
	A. Specification Criteria	95
	B. Applications to Airplane Design	96
	C. Design Study Example	96

TABLE OF CONTENTS (Continued)

SECTION		PAGE
VI	CONCLUSIONS	98
	A. Bank Angle Study	98
	B. Heading Study	98
	C. Specification Criteria	99
	D. Application to Airplane Design	99
	E. Final Remarks	99
REFERENCES		101
APPENDIX I	MULTILOOP ANALYSIS	103
APPENDIX II	GUIDE TO THE MULTILOOP ANALYSIS PROGRAM	119
APPENDIX III	SIMULATION	145

LIST OF ILLUSTRATIONS

FIGURE		PAGE
1	Pilot-Vehicle System	8
2	Bank Angle Closure in Turbulence	10
3	Bank Angle Closure in Command Tracking	10
4	Heading Closure with Yaw Damper	12
5	VTOL Predicted vs Actual Pilot Ratings	14
6	VTOL Position Closure	15
7	Padé Time Delay Approximations	18
8	Configuration T-33 AB-2.6 Gain Variation	25
9	Configuration T-33 AB-2.6 Lead Variation	26
10	T-33 AB 2.6 Roll Task Simulation	27
11	Configuration T-33 AB-2.7 Gain Variation	29
12	Configuration T-33 AB-2.7 Lead Variation	30
13	T-33 AB 2.7 Roll Task Simulation	31
14	Configuration T-33 AB-3.1 Gain Variation	32
15	Configuration T-33 AB-3.1 Lead Variation	33
16	T-33 AB 3.1 Roll Task Simulation	34
17	Configuration T-33 AB-3.3 Gain Variation	35
18	Configuration T-33 AB-3.3 Lead Variation	36
19	T-33 AB 3.3 Roll Task Simulation	37
20	Configuration T-33 BB-2.3 Gain Variation	38
21	Configuration T-33 BB-2.3 Lead Variation	39
22	T-33 BB 2.3 Roll Task Simulation	40
23	Configuration T-33 BC-2.2 Gain Variation	42
24	Configuration T-33 BC-2.2 Lead Variation	43
25	T-33 BC 2.2 Roll Task Simulation	44
26	Configuration T-33 BC-2.3 Gain Variation	45
27	Configuration T-33 BC-2.3 Lead Variation	46
28	T-33 BC 2.3 Roll Task Simulation	47
29	Configuration T-33 BC-2.4 Gain Variation	48
30	Configuration T-33 BC-2.4 Lead Variation	49

LIST OF ILLUSTRATIONS (Continued)

FIGURE		PAGE
31	T-33 BC 2.4 Roll Task Simulation	50
32	Configuration F-5 Gain Variation	51
33	Configuration F-5 Lead Variation	52
34	F-5 Roll Task Simulation.	53
35	F-5 Delay Variation	54
36	T-33 AB-2.6 Delay Variation	55
37	Configuration F-5	56
38	Configuration F-5	57
39	Configuration F-5	58
40	Configuration F-5	59
41	Configuration F-5	60
42	Configuration F-5	61
43	Pilot Rating vs Bank Angle Error for Gust Response	62
44	Bank Angle Gust Tracking	63
45	Bank Angle Command Tracking	63
46	Bank Angle Gust Tracking	64
47	Command Tracking vs Gust Tracking	65
48	T-33 AB 2.6 Heading Task Simulation	69
49	T-33 AB 2.6 Heading Task Simulation	70
50	T-33 AB 2.7 Heading Task Simulation	71
51	T-33 AB 2.7 Heading Task Simulation	72
52	T-33 AB 3.1 Heading Task Simulation	73
53	T-33 AB 3.1 Heading Task Simulation	74
54	T-33 AB 3.3 Heading Task Simulation	75
55	T-33 AB 3.3 Heading Task Simulation	76
56	T-33 BB 2.3 Heading Task Simulation	77
57	T-33 BB 2.3 Heading Task Simulation	78
58	T-33 BC 2.2 Heading Task Simulation	79
59	T-33 BC 2.2 Heading Task Simulation	80
60	T-33 BC 2.3 Heading Task Simulation	81
61	T-33 BC 2.3 Heading Task Simulation	82
62	T-33 BC 2.4 Heading Task Simulation	83
63	T-33 BC 2.4 Heading Task Simulation	84

LIST OF ILLUSTRATIONS (Continued)

FIGURE		PAGE
64	F-5 SAS Heading Task Simulation	85
65	F-5 SAS Heading Task Simulation	86
66	Heading Command Tracking	87
67	Heading Gust Tracking	87
68	Heading Gust Tracking	88
69	Heading Gust Tracking	88
70	Command Tracking with Turbulence, RMS Average	91
71	Command Tracking with Turbulence, Arithmetic Average	92
72	Comparison of Acceleration and Reduced Time Delay Pilot Models	94
73	Multiloop Block Diagram	108
74	Form I Multiloop Diagram	112
75	Form II Multiloop Diagram	113
76	Form III Multiloop Diagram	114
77	Multiloop Analysis Program Flow Chart	122
78	Bank Angle Command Block Diagram	134
79	Bank Angle Turbulence Block Diagram	134
80	Multiloop Analysis Program Output	139
81	Multiloop Program Input	142
82	Large-Amplitude 3-Axis Flight Simulator	154
83	Response of Vertical Translated Motion System at Pilot's Station to Steady Sinusoidal Motion	154
84	Simulator Drive Philosophy	156
85	Simulator Frequency Response	157

LIST OF TABLES

TABLE		PAGE
I	Transformation to Dimensional Derivatives and Transformation to Prime Convention	123
II	Equations of Motion	124
III	Required Transfer Functions	125
IV	N-Symbol Polynomials	127
V	Pilot Model Notation	132
VI	Transfer Functions	135
VII	Performance Summary Large-Amplitude 3-Axis Flight Simulator	154
VIII	Lateral-Directional Airframe Equations	161
IX	Longitudinal Airframe Equations	162
X	Euler Angle Equations	163
XI	Simulator Beam Equations	163
XII	Simulator Cockpit Equations	164
XIII	Gust Simulation	165
XIV	Tracking Signal	165
XV	Root Mean Square Computations	165
XVI	Simulator Cockpit Instruments	166
XVII	T-33 Data	167
XVIII	T-33 Simulated Configurations	168
IX	F-5 Data	169
XX	Simulator Data	170
XXI	Bank Angle Pilot Rating Data	171

SYMBOLS

a_{ij} - Coefficients in equations of motion

b - Airplane wing span, ft

C_D = $D/\frac{1}{2} \rho V_o^2 S$, Airplane drag coefficient

C_{D_o} - Drag coefficient at zero angle of attack

C_{D_α} = $\partial C_D / \partial \alpha$, Nondimensional drag coefficient derivative with respect to angle of attack, 1/rad

$C_{D_\alpha 2}$ = $\partial C_D / \partial \alpha^2$, Nondimensional drag coefficient derivative with respect to angle of attack squared, $1/rad^2$

C_ℓ = $L/\frac{1}{2} \rho V_o^2 S b$, Airplane rolling moment coefficient

C_{ℓ_r} = $\partial C_\ell / \partial (rb/2V_o)$, Nondimensional rolling moment coefficient derivative with respect to yawing rate, 1/rad

C_{ℓ_β} = $\partial C_\ell / \partial \beta$, Nondimensional rolling moment coefficient derivative with respect to sideslip, 1/rad

C_L = $L/\frac{1}{2} \rho_o V_o^2 S$, Airplane lift coefficient

C_{L_o} - Lift coefficient at zero angle of attack

C_{L_α} = $\partial C_L / \partial \alpha$, Nondimensional lift coefficient derivative with respect to angle of attack, 1/rad

$C_{L_{\delta e}}$ = $\partial C_L / \partial \delta e$ Nondimensional lift coefficient derivative with respect to elevator control, 1/rad

C_n = $N/\frac{1}{2} \rho_o V_o^2 S b$, Airplane yawing moment coefficient

C_{n_p} = $\partial C_n / \partial (pb/2 V_o)$, Nondimensional yawing moment coefficient derivative with respect to rolling rate, 1/rad

$C_{n_{\delta_a}}$ = $\partial C_n / \partial \delta_a$, Nondimensional yawing moment coefficient derivative with respect to aileron control 1/rad

D - Drag, lb

$D_{q\,1}$ - pilot model delay numerator in q loop

$D_{q\,2}$ - pilot model delay denominator in q loop

$e_i^{-\tau s}$ - ith Padé approximation of $e^{-\tau s}$

F - greatest common denominator

F_{ij} - forcing function coefficients

g - acceleration due to gravity, ft/sec^2

G(s) - transfer function

G_{ij} - feedback transfer function

H(s) - transfer function, tracking command filter

i = 1, 2, 3, 4, 5, a, r,

I_n - rms contour integral

I_x - moment of inertia about x-axis, $ft\text{-}lb\text{-}sec^2$

I_y - moment of inertia about y-axis, $ft\text{-}lb\text{-}sec^2$

I_z - moment of inertia about z-axis, $ft\text{-}lb\text{-}sec^2$

I_{xz} - product of inertia, $ft\text{-}lb\text{-}sec^2$

j - imaginary base

K, K_i - constant, pilot model gain in i loop

K_q - pilot model gain in q loop

L - turbulence scale length

L_p = $(1/I_x)\ (\partial L/\partial p)$, rad/sec

L_r = $(1/I_x)\ (\partial L/\partial r)$, rad/sec

L_β = $(1/I_x)\ (\partial L/\partial \beta)$, rad/sec^2

L_{δ_a} = $(1/I_x)\ (\partial L/\partial \delta_a)$, $1/sec^2$ -in

L_{δ_r} = $(1/I_x)\ (\partial L/\partial \delta_r)$, $1/sec^2$ -in

L_i' = $\left|L_i + (I_{xz}/I_x)\ N_i\right| \ / \ \left|1 - (I_{xz}^2 / I_x I_z)\right|$; $i = \beta, \beta_{\delta_a}, \delta_r, p, r$

m	- W/g, lb-sec^2/ft
M	- Pitching moment, ft-lb
ms	- mean square
M_q	= $(1/I_z)\ (\partial M/\partial q)$, rad/sec
N_p	= $(1/I_z)\ (\partial N/\partial p)$, rad/sec
N_r	= $(1/I_z)\ (\partial N/\partial r)$, rad/sec
N_β	= $(1/I_z)\ (\partial N/\partial \beta)$, rad/sec^2
N_{δ_a}	= $(1/I_z)\ (\partial N/\partial \delta_a)$, 1/sec^2-rad
N_{δ_r}	= $(1/I_z)\ (\partial N/\partial \delta_r)$, 1/sec^2-rad
N'_i	= $\left[N_i + (I_{xz}/I_x)L_i\right] / \left[1-(I_{xz}^2/I_xI_z)\right]$; i = β, δ_a, δ_r, p, r
$N_{q_i \delta_j}$	- dynamic numerator
$N^{qi\ qj}_{\delta k\ \delta i}$	- coupling numerator
p	- roll rate, rad/sec
P_{q2}	- pilot model lead in q loop
P_{q2}	- pilot model lag in q loop
PR	- predicted or reported pilot rating
q, q_i	= ϕ, ψ, β, σ, x
$q \rightarrow \delta$	- system loop closure q to δ
q_o	= $1/2\,\rho V_o^2$, dynamic pressure, lbs/ft^2
r	- yaw rate, rudder
rms	- root mean square
s	- Laplace operator
T_I	- pilot model lag in seconds
T_L	- pilot model lead in seconds
U_o	- V_o
V_o	- Initial true velocity, ft/sec
ΔV	- Perturbation true velocity, ft/sec

W	- Airplane weight, lb
W.N.	- white noise
x, y, z	- Stability axes (i.e., a right hand orthogonal body-axis system with origin at the center of gravity, the z-axis in the plane of symmetry and the x-axis aligned with the relative wind of zero sideslip trimmed flight)
Y	- side force, lb
Y_q or Y_{p_q}	- pilot transfer function controlling q
$Y^*_{\delta_r}$	= $(1/m\ V_o)\ (\partial Y/\partial \delta_r)$, 1/sec-rad
α	- Angle of attack, rad
β	- sideslip angle
δa	- aileron command, rad
δg_β	- lateral gust
δ_i	- ith control surface
δ_r	- rudder command, rad
Δ	- airframe characteristic polynomial
Δ_{sys}	- system characteristic polynomial
n_i	- ith disturbance
ϕ	- bank angle
ϕ_c	- bank angle command
ϕ_e	- bank angle tracking error, closed loop
ϕ_ϵ	- bank angle system error, open loop
Φ_{cc}	- command power spectrum
Φ_{g_β}	- turbulence power spectrum
Φ_{nn}	- remnant power spectrum
ψ	- heading angle
ψ_c	- heading angle command
ψ_e	- heading tracking error
ψ_ϵ	- heading angle system error

ρ	- Atmospheric density, lbs-sec^2/ft^4
ρ^2	- correlation coefficient determines remnant
σ , σ_q	- rms system tracking error
σ_m	- minimum tracking error
τ	- pilot model time delay in seconds
ω	- frequency
ω_c	- crossover frequency
$\left[\ \right]^-$	- realizable part of

I. INTRODUCTION

A. Scope and Purpose of this Report

The research reported here contributes to a continuing Air Force program aimed at developing better flying qualities prediction techniques suitable for performance specification. Although the primary responsibility of this effort was flying qualities prediction in turbulence, general methods have been developed that are applicable to a large number of pilot vehicle system problems. The underlying concept, incorporating the human pilot into the mathematical description of the total system, has been widely used in the past to evaluate certain aspects of the dynamics of piloted flight. This kind of analysis yields important information about the frequency domain characteristics of the system but has had two typical drawbacks. The first is the difficulty of carrying out lengthy algebraic computations which must be repeated many times, and the second is the uncertain interpretation of frequency domain results in terms of time domain performance. These limitations have now been largely removed through the development of a digitally automated method which computes root mean square (rms) performance of a broad class of single or multiple loop pilot-vehicle systems. Thus, this report not only will present these methods along with partial confirmation by moving base simulation, but also will serve as the manual to an easily used digital program that computes the total pilot-vehicle system performance for command tracking or attitude hold tasks in the presence of specified atmospheric turbulence.

B. Specification of Flying Qualities

There are several recognized limitations to the current Military Specification "Flying Qualities of Piloted Airplanes" which have prompted the current research into closed loop pilot-vehicle analysis. The correlation between open loop dynamic characteristics of airplanes and the flying qualities during piloted flight is the basis for most items of the Specification. Since closing a feedback loop around a dynamic system effects gross changes in the system dynamics, such a correlation will be valid for only those airplanes which do not depart too far from conventional design. In addition, the increasing use of flight control augmentation devices means that current flying qualities criteria may not be sufficient for the evaluation of modern high performance airplanes. Thus a standardized procedure is needed which can directly evaluate an airplane in terms of its closed loop piloted characteristics. In order for this approach to be compatible with the established Air Force evaluation ratings of Levels 1, 2, or 3,

numerical performance predictions are needed which include subjective handling qualities affecting pilot workload.

Another area of concern is the lack of any precise method of establishing flying qualities requirements for performance in atmospheric turbulence. Acceptable representations of gust spectra have been established, and their use has been cited in some paragraphs of the Specification. However, no criteria have been developed for acceptable flying qualities in turbulence and no precise technique for evaluating airplane performance in turbulence has been available. This, again, needs to be handled by closed loop pilot-vehicle methods since both the susceptibility of airplanes to gust disturbances and the pilot's ability to reduce them must be assessed. Furthermore, the difficulties attendant with flight testing in turbulence can be avoided by the use of analytical evaluation procedures. This approach not only avoids the problems of searching out suitable turbulence for flight testing, but also circumvents the use of pilot ratings as a turbulence performance parameter. Pilot ratings have proved to be insufficient for flying qualities in turbulence evaluations and a better approach is to develop criteria based on physically measurable quantities that can be analytically predicted. The performance measure considered in this report is root mean square tracking error of the total pilot-vehicle system, a parameter which is possibly responsible for differences in pilot ratings between flight in still and in turbulent air (Reference 1).

An especially important use of the methods presented in this report is in aircraft design. Since these evaluation techniques depend only on a knowledge of the aerodynamic and control derivatives, the flying qualities of the piloted vehicle can be assessed at the earliest design stage. Even though turbulence criteria are not yet established, it is possible to perform comparative studies between proposed configurations and operational aircraft of known characteristics. In this way not only the turbulence tracking qualities, but also the closed loop command tracking capabilities of any design can be predicted for such tasks as target tracking and weapons delivery in a still or gusty environment.

C. Quasi-linear Analysis

One of the most fruitful areas of closed loop pilot-vehicle system research has been quasi-linear multiloop analysis (References 2, 3). The basic assumption is that the actual nonlinear, time varying and perhaps stochastic pilot-vehicle system can be closely approximated by a suitable linear model. Since the pilot may be operating on several control axes simultaneously, several loops must be studied as a single system.

In general, these loop closures will be coupled through the linear equations of motion representing the vehicle. This results in complex transfer functions containing terms formed from the representations of the pilot along with factors associated with the isolated vehicle. Once the pilot-vehicle transfer functions have been derived, they can be studied to determine the frequency domain nature of piloted control tasks. In this way, information can be obtained regarding the total system bandwidth, damping, and the extent of compensation the pilot must adopt for acceptable performance. Many years of research into this approach to flying qualities has led to the development of pilot models that have proven to be of great use in understanding pilot activity and the relationship between airplane parameters and acceptable flying qualities.

This type of system modeling can also be used to obtain quantitative performance measures of the pilot-vehicle system. Root mean square error can be computed from the quasi-linear models and has been used in such studies by Durand on carrier landing analysis (Reference 4). The pilot models usually are determined through the verbal adjustment rules (Reference 2) but the approach taken for the turbulence research is to optimize the pilot models with respect to the total system root mean square error performance. Thus the emphasis here is on modeling the total pilot-vehicle system performance, an approach also taken by Kensinger (Reference 5) who obtained excellent agreement between analytical and simulator results.

D. The Anderson Rating Prediction Method

An important extension of these closed loop analysis methods has been recently made by R.O. Anderson (Reference 6). Working with VTOL hover data, he constructed a linear function as a predictor of pilot rating that shows remarkable agreement with a large amount of data from diverse sources. Although the formula requires the measured quantities of pilot lead and system tracking error, it has been extended to a purely analytical prediction method. By assuming that the pilot optimizes his performance with respect to the Anderson formula, the pilot rating can be computed from a knowledge of only the stability and control derivatives of the airplane. This extended predictive technique dubbed "The Paper Pilot" was developed by R.O. Anderson and J.D. Dillow (Reference 7) and has amply demonstrated the usefulness of this approach which has led to a proposed flying qualities specification.

E. Conventional Aircraft in Turbulence

The success of the Anderson-Dillow method immediately suggests using a similar approach for conventional aircraft to study tracking tasks in turbulence. This program has been partially completed and the results are the main topic of this report. There were three main objectives of the research, (a) to determine how well performance can be predicted by analytical techniques, (b) determine by simulation how well system performance correlates with pilot rating as a function of turbulence level, and (c) suggest an approach to developing turbulence specification criteria based on closed loop pilot-vehicle analysis. The work has been limited to conventional lateral dynamics and methods have been developed and digitally implemented for computing not only the closed loop pilot-vehicle system transfer functions, but also the tracking error predictions, a major contribution to the Anderson rating formula. These predictions have been confirmed for four pilot tasks by moving base simulation on the Northrop Large Amplitude Flight Simulator. The success of this verification indicates that closed loop criteria for flying qualities in turbulence will be possible and that the technology developed during this effort can be used to evaluate many handling qualities features of airplanes in the earliest design stages.

II. TOTAL SYSTEM PERFORMANCE PREDICTIONS

A. Four Approaches to Pilot-Vehicle Analysis

There are four basic approaches that have been used in pilot-vehicle closed loop analysis. Although they share the basic idea of developing a mathematical representation for the pilot, the specific modeling of the system is accomplished by several different methods.

The first successful method was developed largely by Systems Technology, Inc. and represents the system in the frequency domain where the problem can be handled by multiloop analysis. The pilot models are adjusted by a set of verbal adjustment rules and the performance is evaluated in terms of the closed loop system eigenvalues, bandwidth, damping, phase and gain margins and other frequency domain performance parameters. The object of the adjustment rules is to achieve optimum performance, postulated, but not directly evaluated, as root mean square (rms) error (Reference 2).

A second way of approaching the problem is through optimal control theory. The importance of optimal performance as a basic objective of pilot model adjustment indicates that optimal control theory can be applied. This has been done with success (Reference 8) although the resulting methods are difficult.

A third approach is represented by the Anderson pilot rating prediction method (Reference 6). This will be described in Part C. Here root mean square error performance is combined with pilot workload to give an index that is the predicted pilot rating. The pilot model has a fixed form and the workload is obtained from the amount of lead the pilot model requires. The parameters of the pilot model are optimized with respect to this rating index so that the minimum obtained is the predicted pilot rating. Anderson has had considerable success with the relatively simple dynamics of VTOL hover and this approach appears to be promising for conventional airplanes.

The fourth way of approaching closed loop pilot-vehicle analysis is the underlying concept of this study of flying qualities in turbulence. Fixed form pilot models are used in multiloop system descriptions and root mean square error calculations are made using the multiloop total system transfer functions. The pilot models are then optimized with respect to root mean square error to give predictions of the total system performance. This technique has also been successfully used by Kensinger (Reference 5). The validity and accuracy of this approach has been ascertained by moving base simulation and the results of the study are presented in Section III.

Since this report is to serve as an introduction to both pilot-vehicle analysis and the turbulence performance prediction methods developed during this research effort, it is necessary to present some of the basic features of these techniques. The brief discussions of this chapter contain the most important aspects of several contributing theories and constitute an essentially complete guide to the use of the prediction procedure. A more detailed knowledge of these areas is undoubtedly useful and the reader is invited especially to consider the report by McRuer and Graham on pilot model theory (Reference 2) and the Anderson VTOL specification (Reference 6) as essential to a proper working knowledge of the subject. The underlying mathematics and other peripheral data have been relegated to appendices in order to keep this presentation brief and germane. A computer program has been prepared to carry out the algebra of the multiloop analysis and rms error calculations. This has proved to be indispensable since these computations are lengthy unless fully automated. Appendix II constitutes a user's guide and the program itself is available upon request from the United States Air Force. Individual users will possibly want to modify and extend the basic digital program to fit particular problems, although the variety of lateral situations already covered is large. These changes can be easily carried out by the user with the aid of Appendix II. In order to understand what this program computes and what it means in terms of time domain performance statistics, performance measures are discussed first.

B. Performance Measures

The use of root mean square (rms) as a performance measure not only is convenient and physically appealing, but has proved to be appropriate for the study of pilot-vehicle performance. This is the case because most stochastic processes encountered in flying qualities research can be suitably approximated by Gaussian processes which belong to the class of processes for which the mean and variance are a complete statistical description. Therefore, rms quantities are naturally associated with the statistical analysis. By using the total system pilot vehicle transfer function to compute rms performance for a Gaussian tracking task, the analysis can proceed by considering the familiar statistics of the time domain. In the case of VTOL performance in precision hover, Anderson assumed a Gaussian gust environment and computed the rms system performance by means of a contour integral, and the same method was adopted for this study of conventional lateral dynamics. Suppose that for some control axis q and forcing function i that the q/i transfer function for the total systems is given by the rational function

$$q/i = G(s) \tag{1}$$

If i represents a Gaussian process with zero mean and power spectrum Φ_{ii} then the rms value of q per unit rms i is given (Reference 9) by

$$\text{rms } q = \frac{\frac{1}{2\pi j}\int_{-j\infty}^{j\infty} \Phi_{ii}(s)\,|G(s)|^2\,ds}{\frac{1}{2\pi j}\int_{-j\infty}^{j\infty} \Phi_{ii}(s)\,ds} \tag{2}$$

These integrals can be easily evaluated by a rapid digital program that is discussed in Appendix II. Since Φ_{ii} can be spectrally factored, the forcing function which models say, a random tracking command signal or gust term in the equations of motion can be represented as a transfer function H (s) where

$$H(s) = \left[\Phi_{ii}(s)\right]^- \tag{3}$$

is the realizable part of the spectral factoring

$$\Phi_{ii}(s) = \left[\Phi_{ii}(s)\right]^+ \left[\Phi_{ii}(s)\right]^-$$

Thus the desired command tracking signal is obtained by passing white noise through the filter H(s).

Since the integration is over all frequencies ω, the rms value is exact for an infinite sampling time. The assumption that G (s) is a rational function is no more than the quasilinear approximation which represents both the pilot and the vehicle by purely linear dynamics. Now that the method for computing rms q is clear, it is necessary to discuss the way in which the system transfer function G (s) is obtained.

C. Lateral System Models for Compensatory Tracking

If Y_q represents the describing transfer function of the pilot acting on the command tracking error q, then the total system selected for study can be represented by the block diagram of Figure 1. By selecting appropriate functions Y_ϕ, Y_ψ and Y_β, and applying either the injected gust or a command tracking signal at one of the input ports, a specific compensatory tracking task can be selected. Furthermore, Y_r can be used to model an augmentation system such as a yaw damper, and control or actuator dynamics can be included by including their dynamics with the pilot models.

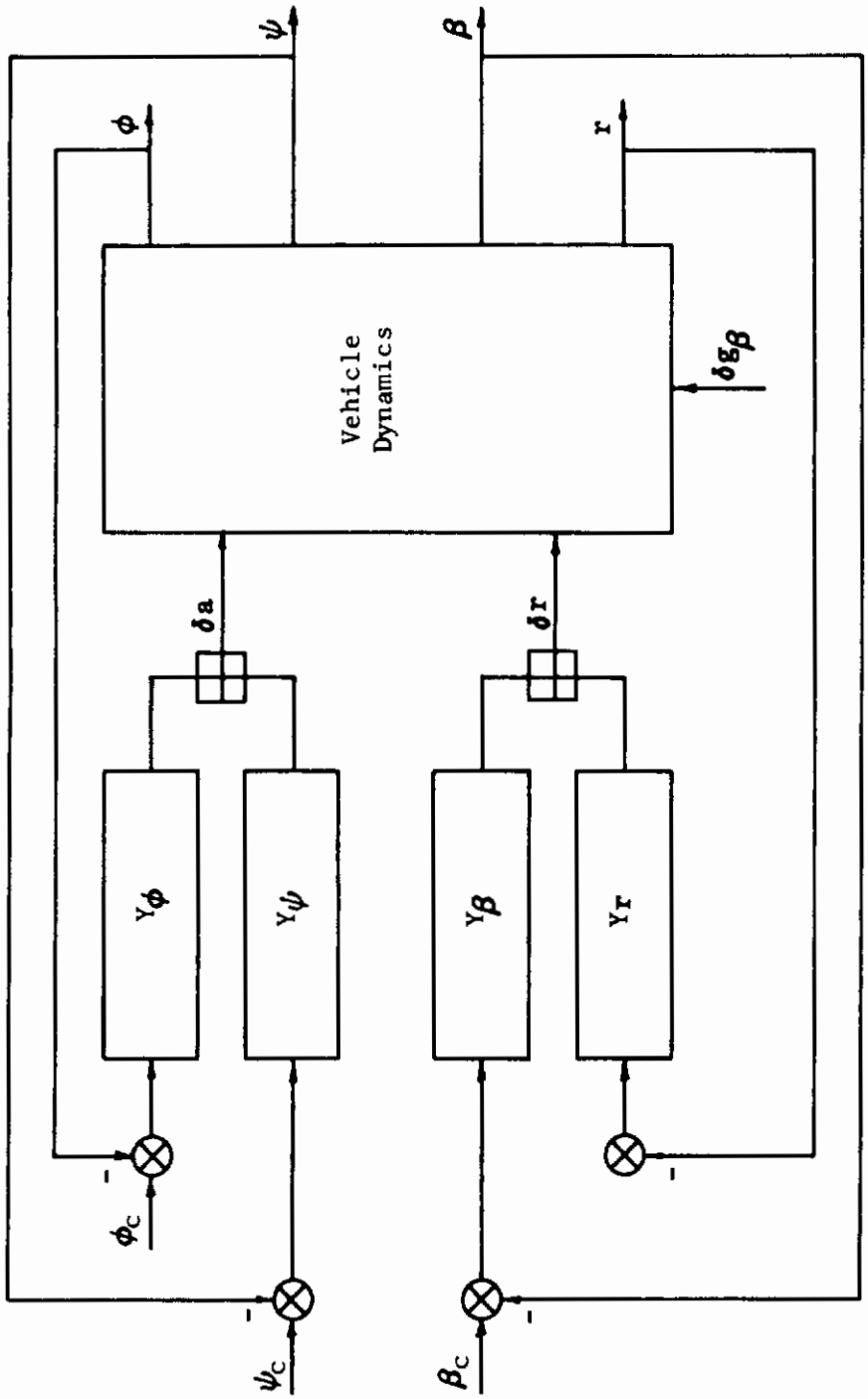

FIGURE 1 PILOT-VEHICLE SYSTEM

For example, consider the main task to be discussed later, bank angle attitude hold in turbulence in which the pilot is asked to keep the aircraft wings level. Since he does not act on heading or sideslip the pilot models Y_ψ and Y_β are set equal to zero which effectively removes the heading and sideslip loops as shown in Figure 2. If δ_{g_β} represents the gust injected into the equations of motion and $\phi \rightarrow \delta a$ denotes the bank angle through aileron loop closure, then the total system open loop transfer function of bank angle to δ_{g_β} is written

$$\phi/\delta_{g_\beta}\Big|_{\phi \rightarrow \delta a} = G(s) \tag{4}$$

since the bank angle ϕ is the system error of interest ϕ_e. Thus if H (s) is scaled for, say, 10 ft/sec rms lateral gust, then

$$\text{rms } \phi_e = \frac{1}{2\pi j} \int_{-j\infty}^{j\infty} \left| H(s)\, \phi/\delta_{g_\beta}\Big|_{\phi \rightarrow \delta a} \right|^2 ds \tag{5}$$

gives the rms bank angle error for the task in 10 ft/sec turbulence. The actual computations of $\phi/\delta_{g_\beta}\big|_{\phi \rightarrow \delta a}$ requires the expansion of several determinants and is completely automated along with the computations for many other system task models in the digital program discussed in Appendix II.

In a similar way the system performance for a Gaussian command tracking task ϕ_c represented by white noise passed through the linear filter H (s) can be computed. The system here is shown in Figure 3 which also shows the way in which ϕ_e is obtained. In this case ϕ_c represents a random signal obtained by filtering white noise which has a constant power spectrum by the filter H (s). The open loop transfer function $\phi/\phi_\epsilon\big|_{\phi \rightarrow \delta a}$ can thus be used to obtain

$$\phi_e = \phi_c - \phi_c \left(\frac{\phi/\phi_\epsilon\big|_{\phi \rightarrow \delta a}}{1 + \phi/\phi_\epsilon\big|_{\phi \rightarrow \delta a}} \right) \tag{6}$$

so that the system rms error is given by

$$\text{rms } \phi_e = \frac{1}{2\pi j} \int_{-j\infty}^{j\infty} \left| H(s) - H(s) \left(\frac{\phi/\phi_\epsilon\big|_{\phi \rightarrow \delta a}}{1 + \phi/\phi_\epsilon\big|_{\phi \rightarrow \delta a}} \right) \right|^2 ds \tag{7}$$

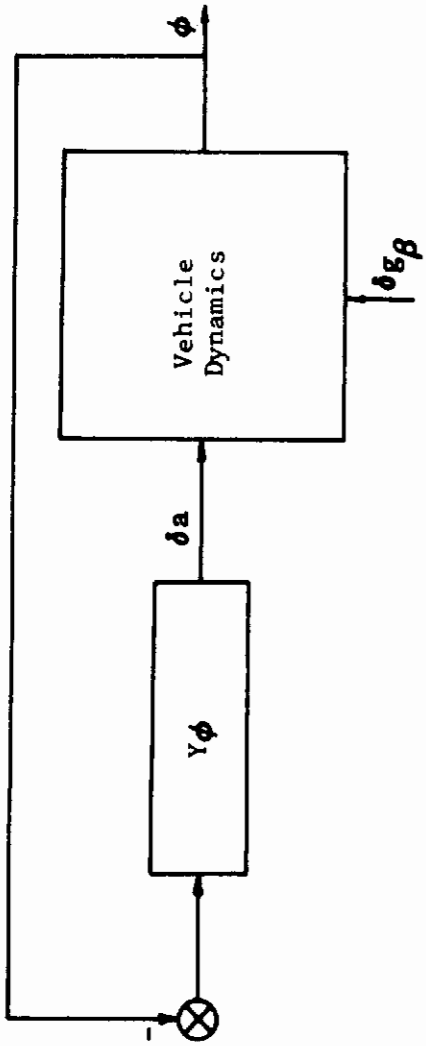

FIGURE 2 BANK ANGLE CLOSURE IN TURBULENCE

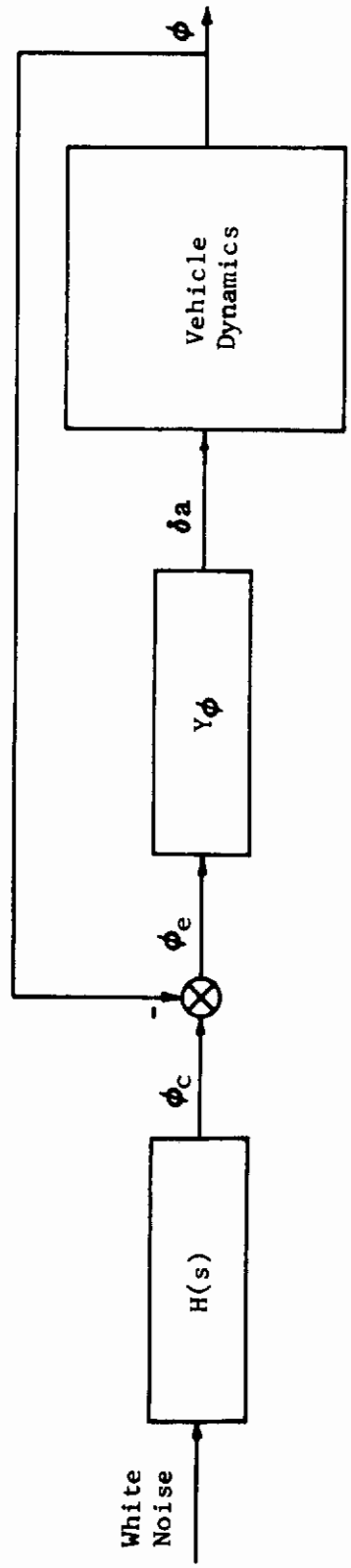

FIGURE 3 BANK ANGLE CLOSURE IN COMMAND TRACKING

Another example is the pilot task of maintaining heading in turbulence. If a yaw damper Y_r is used, the system is as shown in Figure 4. Letting the augmenter and heading closures be designated by $r \rightarrow \delta r$ and $\psi \rightarrow \delta a$, the open loop transfer function is then written

$$\left.\frac{\psi/\psi_\epsilon}{\begin{array}{l} r \rightarrow \delta r \\ \phi \rightarrow \delta a \\ \psi \rightarrow \delta a \end{array}}\right| = G(s) \qquad (8)$$

D. Pilot Model Theory

The many studies of pilot dynamics that have been undertaken during the last two decades show striking agreement on the form of the pilot describing transfer function. Of the many reports available, one of the most useful is Reference 2 which contains most of the basic theory of pilot models along with methods for pilot model parameter selection.

Essentially, the pilot describing function consists of a gain coefficient, first order lead, first order lag, and a pure time delay of τ seconds. Thus the general pilot model has the form

$$Y_q = K_q \frac{(T_L s + 1)}{(T_I s + 1)} e^{-\tau s} \qquad (9)$$

Of the four parameters K_q, T_L, T_I, and τ, only the first three can be chosen by the pilot. The parameter τ depends on the pilot task and, though variable, is not generally selectable by the pilot. This τ is an effective time delay and includes neuromuscular lag. The selection of K_q, T_L, and T_I is arrived at through adaptation and is made so that the best performance is obtained with respect to some criterion. The exact nature of this performance index for tracking has been subject to a large amount of study, but the exact form is still unknown. Nevertheless, it has been found that the pilot penalizes the aircraft for both tracking errors and workload, (Reference 10). This tradeoff between tracking error and the effort necessary to reduce it has been successfully modeled by R.O. Anderson for VTOL precision hover tasks. Using system rms tracking error as a measure of performance σ and pilot lead T_L as an indicator of

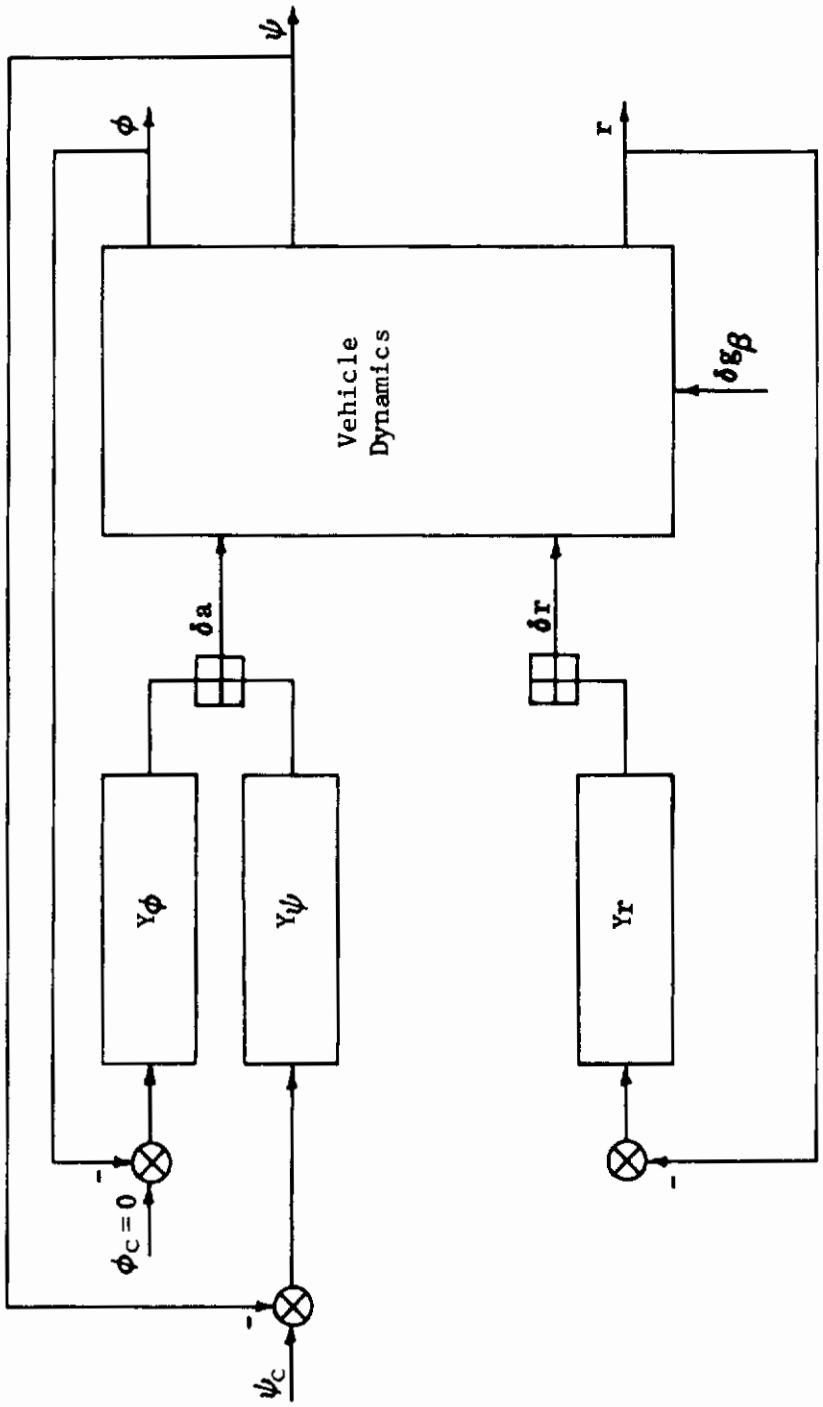

FIGURE 4 HEADING CLOSURE WITH YAW DAMPER

workload, he postulated a linear combination of these quantities as a predictor of pilot rating PR in the form

$$PR = K_1 \sigma + K_2 T_L + K_3 + \cdots \tag{10}$$

By choosing the coefficients K_j according to recent data, Reference 10, he was able to predict the pilot ratings for a large number of cases, some of which are shown in Figure 1 of Reference 6 and reproduced here as Figure 5. Since the usefulness of such a method is its ability to predict the pilot rating, Dillow and Anderson developed a conjugate gradient optimization scheme (Reference 7) that minimizes PR by assuming a mathematical model for the pilot vehicle system and then varying the pilot model parameters. It is useful to examine the actual system for longitudinal precision hover above a fixed point which is shown in Figure 6. Here there are two pilot models required, one in pitch attitude θ and one in ground displacement x. Let T_{L_θ} and T_{L_x} denote the pilot lead time constants in seconds for pitch and position displacement, and let σ_q and σ_x denote the rms values of pitch rate in radians per second and displacement in feet. Then a measure of system hover performance σ is postulated as

$$\sigma = \sigma_x + 10\,\sigma_q \tag{11}$$

If a minimum σ is adopted, $\sigma_m = .8$ for the VTOL data, the rating formula to predict Cooper Ratings, PR (Reference 6) takes the following form

$$PR = \frac{\sigma - \sigma_m}{\sigma_m} + 2.5\,T_{L_\theta} + T_{L_x} + 1.0 \tag{12}$$

subject to the following restrictions based on measured pilot parameters

$$\begin{cases} 0 \le \dfrac{\sigma - \sigma_m}{\sigma_m} \le 2.50 \\ 0 \le 2.5\,T_{L_\theta} \le 3.25 \\ 0 \le T_{L_x} \le 1.2 \end{cases} \tag{13}$$

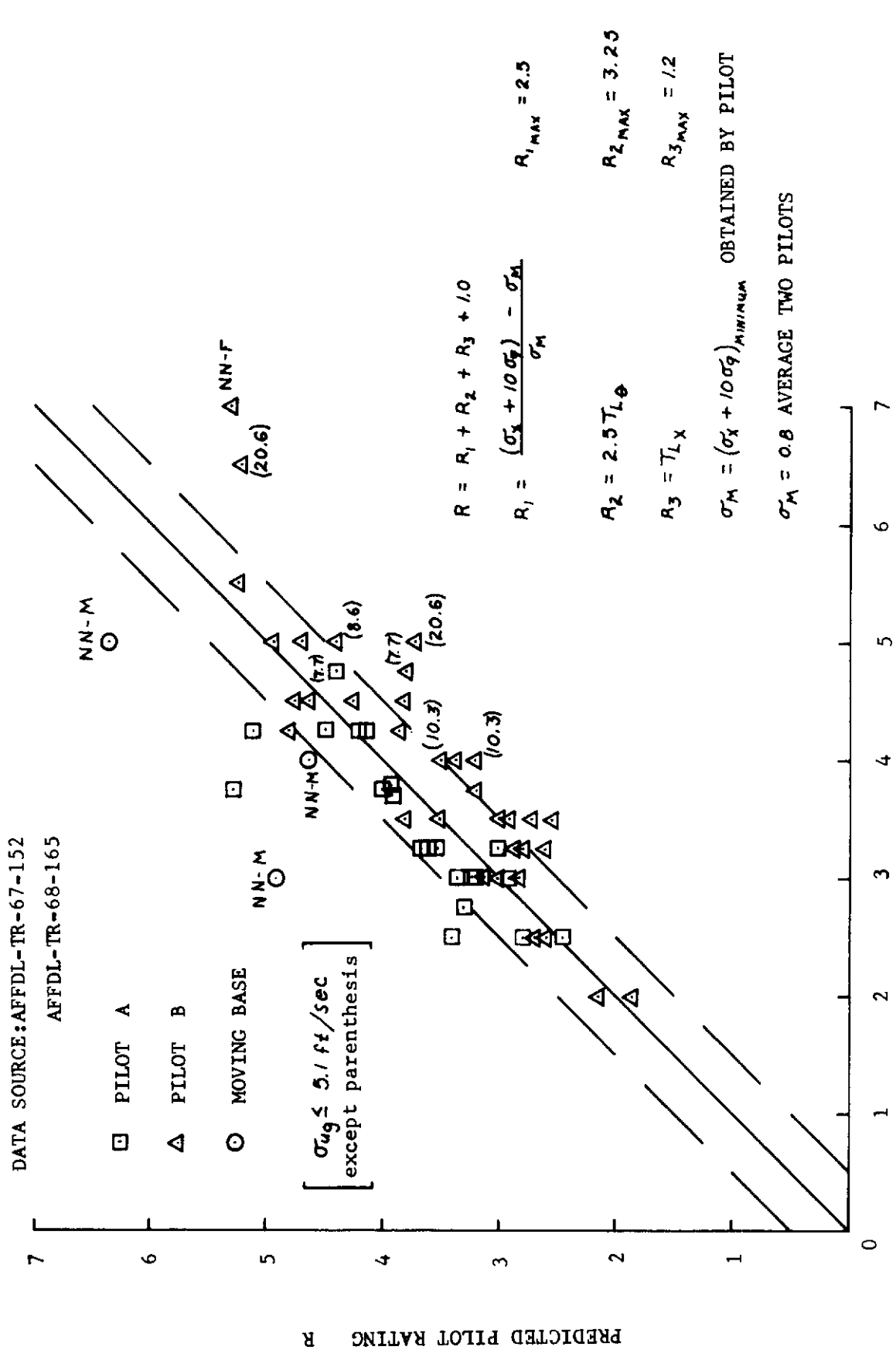

FIGURE 5 VTOL PREDICTED vs ACTUAL PILOT RATINGS

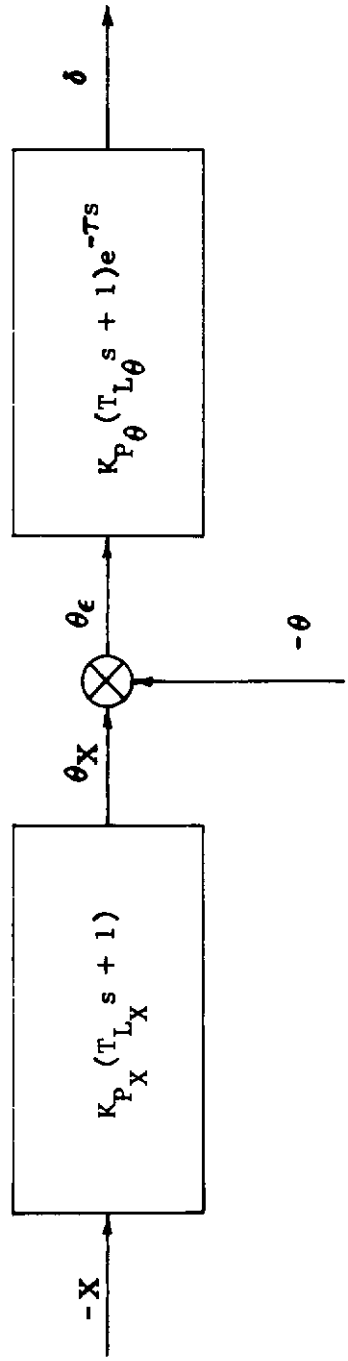

FIGURE 6 VTOL POSITION CLOSURE

Since the hover task is performed in a gusty environment, turbulence modeled by a Dryden Gaussian form was used at an rms level of 5 ft/sec. The proposed VTOL specification allows the designer to use any pilot model of the above form to meet the required pilot ratings subject to conditions including system stability and a time delay of $\tau = .44$ sec.

Although a program for the lateral dynamics of conventional airplanes as broad as this has not been carried out, it is clear that in addition to the usefulness to design, the ability to predict the system performance tracking errors in turbulence is an essential part of establishing specification criteria. Once methods have been established that are good predictors of system tracking errors, it will be possible to attempt the construction of an Anderson type formula for lateral dynamics of conventional airplanes. These prediction methods have been developed in this report for several pilot task situations and both the analytic and experimental results will be presented in Section III.

In order to arrive at the optimum pilot model, many variations of the parameters must be made. The labor involved in this is very greatly reduced by using the digital computer program described in Appendix II, but a knowledge of the describing function adjustment rules of Reference 2 is most useful.

For a single pilot model system, the parameters should be selected such that

1. The system is stable.
2. A first order lag T_I is adopted if this improves low frequency characteristics and this does not introduce high frequency destabilizing effects that cannot be overcome by a single first order lead.
3. A first order lead T_L is adopted if a noticeable improvement in performance is achieved, but should be as low as possible and should satisfy $T_L \leq 1.2$.
4. The gain K_q is adjusted to give the optimum performance in some sense analogous to minimum root mean square tracking error σ_e.

The time delay τ has to be determined from experiment, and the success of modeling the system depends critically on this value. Since the quasilinear assumption requires that the system model be purely a rational function of s, the time delay $e^{-\tau s}$ must be approximated by a rational function of s. The most often used expression is the first order Padé formula $e_1^{-\tau s}$ given by

$$e^{-\tau s} \doteq e_1^{-\tau s} = -\frac{s - 2/\tau}{s + 2/\tau} \tag{14}$$

Since the digital program can accept high order pilot models, a comparison of results between first order and higher order Padé approximations was made. The results show that the computed system tracking errors in each case are nearly the same, but that the first order form fails to indicate the correct stability boundaries. It turns out that this causes little difficulty and suitable precautions are easily taken. For reference, a table of the first five orders $e_1^{-\tau s}$ through $e_5^{-\tau s}$ is found in Figure 7.

An often useful way to obtain a good initial estimate for the pilot parameters is by means of the crossover pilot model. If $Y_c(s)$ represents the vehicle transfer function, then according to the model, the pilot describing function Y_q is adjusted so that

$$Y_c(i\omega)\, Y_q(i\omega) \doteq \frac{\omega_c\, e^{-j\omega\tau}}{j\omega} \tag{15}$$

in the vicinity of the crossover frequency ω_c. This approximation displays better amplitude than phase accuracy, but usually describes the fundamental features of the pilot-vehicle system.

The above models for the pilot are based on the quasilinear assumption, although the human is known to engage in such nonlinearities as sampling, bang-bang control, uncorrelated noise injection and thresholds. By means of the power spectra of the forcing function and the pilot's output, the amount of linearly uncorrelated power called the remnant can be measured. If Φ_{ii} and Φ_{cc} represent these spectra, then the linearly uncorrelated part of the pilot's output can be regarded as uncorrelated noise with power spectrum Φ_{nn} injected at the output. The linear pilot model output to input describing function for closed loop operation is given by

$$H(s) = \frac{Y_q}{1 + Y_q\, Y_c} \tag{16}$$

and the power spectra of the output including remnant is

$$\Phi_{cc}(\omega) \quad H(i\omega)\, H(-i\omega)\, \Phi_{ii}(\omega) + \Phi_{nn}(\omega) \tag{17}$$

The square of the correlation coefficient for linearly correlated input and output is then given by

$$\rho^2 \quad \frac{H(i\omega)\, H(-i\omega)\, \Phi_{ii}}{\Phi_{cc}} \tag{18}$$

$$\rho^2 \quad 1 - \frac{\Phi_{nn}}{\Phi_{cc}} \tag{19}$$

$$e_1^{-x} \doteq \frac{2 - x}{2 + x}$$

$$e_2^{-x} \doteq \frac{12 - 6x + x^2}{12 + 6x + x^2}$$

$$e_3^{-x} \doteq \frac{120 - 60x + 12x^2 - x^3}{120 + 60x + 12x^2 + x^3}$$

$$e_4^{-x} \doteq \frac{1680 - 840x + 180x^2 - 20x^3 + x^4}{1680 + 840x + 180x^2 + 20x^3 + x^4}$$

$$e_5^{-x} \doteq \frac{30240 - 15120x + 3360x^2 - 420x^3 + 30x^4 - x^5}{30240 + 15120x + 3360x^2 + 420x^3 + 30x^4 + x^5}$$

where $x = \tau s$

FIGURE 7 Padé Time Delay Approximations

Data on the value of ρ are difficult to obtain; but often show values of ρ near one, though lower values are frequently reported. The interpretation of ρ in terms of performance depends on many factors such as the measurement methods and ϕ_{ii}. The analysis and simulation performed during this effort has established that the effect of remnant on bank angle tracking prediction is very small and of little consequence. In more complex tasks, the remnant undoubtedly is more significant although many of the nonlinearities listed above can be modeled by an increased effective time delay.

A useful test for optimality of the pilot is as follows. Let q_c be the command signal, q_r the system response, c the pilot output, and finally $e = q_c - q_r$. Then the pilot is optimum with respect to the performance index

$$\overline{e^2} + K\,\overline{c^2} \tag{20}$$

if the following relation holds

$$\overline{e^2} = \overline{q_c^2} - \overline{q_r^2} - 2K\,\overline{c^2} \tag{21}$$

This result, which follows from Weiner filter optimization by spectral factoring, is useful in determining the influence of controller on the human pilot. By matching experimental data to the above formula, the value of K can be determined. A derivation of the formula, along with further details, is found in Reference 16.

The development of multiloop pilot models depends on the above techniques since each closure of the pilot is represented by the quasilinear form developed above. In this case, optimization with respect to some index, such as rms tracking error or an Anderson formula, is much more difficult and requires a choice of weighting factors for the different control axes. This occurs in the VTOL study where a factor K is used to form the index

$$\sigma_x + K\sigma_q \tag{22}$$

A supplementary analysis that should be employed in the study of many examples is the root locus method. By examining the loop closures, particularly in multiloop problems, the nature of the system dynamics can be easily assessed. This analysis should be employed wherever there is the least difficulty in obtaining pilot closures or when undertaking a new type of problem. In this way, the closed loop system eigenvalues can be found so that a complete knowledge of the pilot-vehicle natural frequencies and damping ratios is available. The actual determination of these numbers is automatic since the system characteristic polynomial is factored every time the multiloop

program is used. In addition, the open loop transfer functions are optionally printed out and can be used to generate the loci from any of the widely available root locus programs.

E. Turbulence Models

In order to keep the analysis and simulation of nine selected configurations as simple as possible, only the turbulence component of greatest effect on lateral flying qualities was employed, namely the lateral β gust. The incorporation of this lateral turbulence into the system equations is mathematically similar to the representation of the rudder and aileron where the input to the system consists of the δa or δr forcing function multiplied by the approximate force and moment in each equation of motion. The lateral β gust δg_β is such a forcing function and since it represents fluctuations of β, the correct coefficients are the aerodynamic coefficients of β. The multiloop system transfer functions for lateral β gust inputs are given in Appendix II.

The β gust can be modeled by either the spectrally factorable Dryden model or a rational approximation to the von Karman model. Since the Dryden form is easily utilized for both the analysis and the simulation it is adopted here. An extensive study of turbulence representations is contained in References 11 and 12.

The spectral form of the lateral β or v gust is

$$\Phi_{g_\beta}(\omega) = \sigma_v^2 \frac{L}{V_o} \cdot \frac{1 + 3\left(\frac{L\omega}{V_o}\right)^2}{\left[1 + \left(\frac{L\omega}{V_o}\right)^2\right]^2} \tag{23}$$

where L is the lateral scale length, and V_o is the airspeed, and σ_v is the rms gust level in rad/sec. This is easily factored to give the transfer function by which white noise can be filtered to give the required gust. This filter is

$$H(i\omega) = K \frac{1 + \frac{\sqrt{3}\,L}{V_o}(i\omega)}{\left[1 + \frac{L}{V_o}(i\omega)\right]^2} \tag{24}$$

where K is used to scale the filter to the desired rms gust level in ft/sec.

Some further discussion on the question of turbulence modeling for in-flight simulation is given in Reference 13.

Now that a presentation of the prediction technique is complete, the analytical and experimental results of the next chapter can be presented.

III DEMONSTRATION OF THE METHOD

In order to demonstrate the accuracy of the multiloop prediction method, a brief moving-base simulation of Class IV airplanes was completed for several command tracking and gust tracking tasks. Eight configurations flown by Cornell in the Air Force variable stability T-33 (Reference 14) were simulated along with the F-5. The stability and control derivatives and a complete description of the simulation mechanics are contained in Appendix III. Both bank angle and heading control tasks were included. Since bank angle tracking was the main object of study it is discussed first.

A. Bank Angle Task Prediction

A preliminary analysis of the F-5 and a large number of T-33 configurations was undertaken to obtain familiarity with the broadest possible tracking characteristics. In all cases command tracking, Figure 3, and attitude hold tracking in turbulence, Figure 2, were studied. After examining many cases, it was found that an estimate for the pilot lead of $T_L = .5$ sec and the values of τ discussed below usually led to approximately minimum rms bank angle error, ϕ_e, for both tracking tasks. The roll time constant T_R for these airplanes was between .5 sec and 1.3 sec so that the optimum pilot models control the roll subsidence mode, a result which has been often reported (Reference 2). Using this pilot compensation, a graph of rms bank angle error ϕ_e versus pilot gain K_ϕ was computed. The gains were selected so that the optimum K_ϕ was included, and then a plot rms ϕ_e versus T_L was obtained using the optimum value of K_ϕ. In this way the sensitivity of the system response to pilot model variations can be assessed as well as the closeness to the actual optimum model. Since the $T_L = .5$ sec is near optimum in terms at performance in every case, the predicted tracking performance is then the minimum rms ϕ_e attained by the K_ϕ versus rms ϕ_e graph.

The value of the effective time delay τ requires careful selection. For the command tracking task in still air where inertial acceleration cues are less important than in turbulence tasks, the value $\tau = .44$ sec was used for the prediction analysis. This time delay has also been used by Anderson (Reference 6 to model tracking tasks where acceleration cues are small. The method chosen to model the acceleration motion cues for turbulence tasks was to adopt a time delay of $\tau = .3$ seconds which provide good modeling of the system. Further analytical results concerning the equivalence of reduced time delays and acceleration cues are presented in Section IV.

By using the appropriate value of τ and the pilot lead $T_L = .5$ sec, the rms ϕ_e versus K_ϕ gain variation graph and the rms ϕ_e versus T_L lead variation graph were computed for the F-5 and over forty T-33 configurations. Of these, the F-5 was selected for further study and simulation along with eight T-33 airplanes exhibiting a wide variety of optimum performance and prediction graph characteristics. The predictions obtained from the graph have proved to be accurate not only in the rms performance levels, but also in other features of handling qualities related to the shape of the gain and lead variation graphs.

A Dryden form filter of the form discussed earlier was used to model the gust for both the analysis and the simulation and was scaled, using the initial true velocity V_o, to 10 ft/sec rms lateral gust. The command tracking signal used for the analysis and the simulation is represented by white noise filtered through

$$H(s) = \frac{K}{(s + .5)^2} \tag{25}$$

where K is used to scale the tracking signal to 10° rms.

The following representative gain and lead variation graphs, which will be discussed individually in Part C, are all computed for a time delay of $\tau = .3$ sec including the command tracking graphs which show representative dynamics although the command tracking predictions are computed for $\tau = .44$ sec. The actual predicted value for command tracking can be read from the prediction line on the command tracking simulator data graphs at the 10° rms tracking signal level.

A case-by-case discussion of the bank angle data follows a brief discussion of the simulation.

B. The Simulation

The Northrop Large Amplitude Flight Simulator was used in five degrees of freedom motion, omitting only the motion along the X-axis, for the six-degree-of-freedom lateral and longitudinal equations. The longitudinal dynamics were held constant for all configurations and presented an easy task; the longitudinal pilot instructions were to hold approximate altitude.

The lateral simulation was an IFR flight condition with full instrumentation in the cockpit. In order to present better bank angle information than is available from the attitude director indicator (ADI), a vertical bar with horizontal travel (the bank

steering bar of the ADI) was used to show ϕ_e. For both the gust and the command tracking, the pilot instruction was to keep the error as small as possible in an rms sense, but to work at a level that could be maintained during a two-minute period.

A complete description of the mechanization of the simulation, along with other pertinent information, is contained in Appendix III. In all cases the pilots were allowed to become familiar with the airplane before data were taken. Three pilots, whose backgrounds are also in Appendix III, were used and owing to the similarity of their performance, they have not been identified in the following simulator graphs.

Each simulator flight lasted about 2 minutes. The pilot was allowed to acquire the task and data were then taken for periods of 100 seconds using mean square analog circuits. The mean square tracking error was measured in this way along with the mean square values of the command tracking and the gust which fluctuated considerably from flight to flight.

Although there was some evidence of learning, no recorded flights were omitted from the data, and all moving-base data obtained are contained in the following pages. Fixed-base data are designated by asterisk, but fixed base data for some configurations could not be shown because of scaling. Averages of fixed base data are included in a later figure, Figure 46.

The Air Force variable stability T-33 configurations used in this study are reported in Reference 14, along with pilot comments. The airplanes are grouped into series such as AB 2, and the entry in each group is identified by its position, e.g., AB 2.6 designates the sixth configuration listed under AB 2.

C. Bank Angle Simulation Data

AB 2.6 - Figure 8 shows the command (tracking) and gust (tracking) response for the indicated pilot model. The gust response rms ϕ_e vs K_ϕ graph shows that the pilot should be able to reduce gust-induced bank angle and that his gain is not too critical. Figure 9 shows that, although the lead of $T_L = .5$ seconds is near optimum for the gain $K_\phi = 4.5$, lower values of T_L do not cause noticeable deterioration of the performance. The tracking performance is good (in comparison to the other airplanes studied), and the open-loop disturbance level in gust is also relatively low. Thus, a gust tracking performance of rms $\phi_e = 1.5°$ for 10 ft/sec rms turbulence is predicted, and is indicated by the line in the gust tracking graph of Figure 10. The command tracking prediction has been computed separately to give the predicted figure of rms $\phi_e = 2.0°$ for a 10° rms command signal. Reference 14 gives a Cooper rating of 3.0.

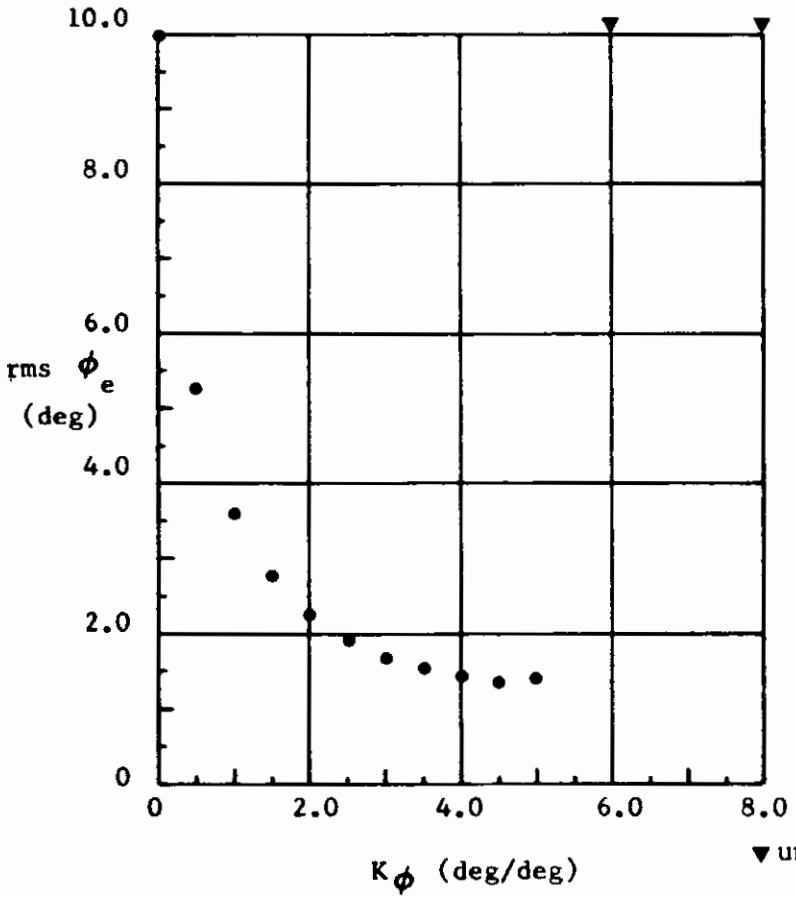

COMMAND TRACKING
RMS COMMAND INPUT = 10°

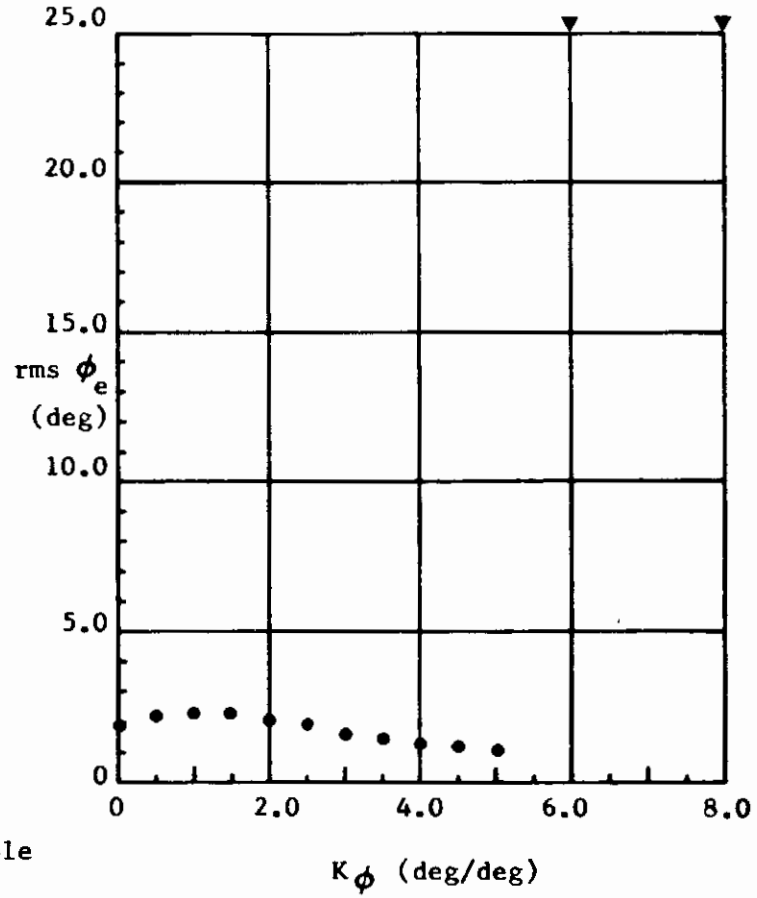

GUST TRACKING
RMS GUST INPUT LEVEL = 10 fps

Pilot Models

$$Y_{p_\beta} = 0$$

$$Y_{p_\phi} = K_\phi (.5s + 1) e^{-.3s}$$

$$Y_{p_\psi} = 0$$

FIGURE 8 **CONFIGURATION** *T-33 AB-2.6*
GAIN VARIATION

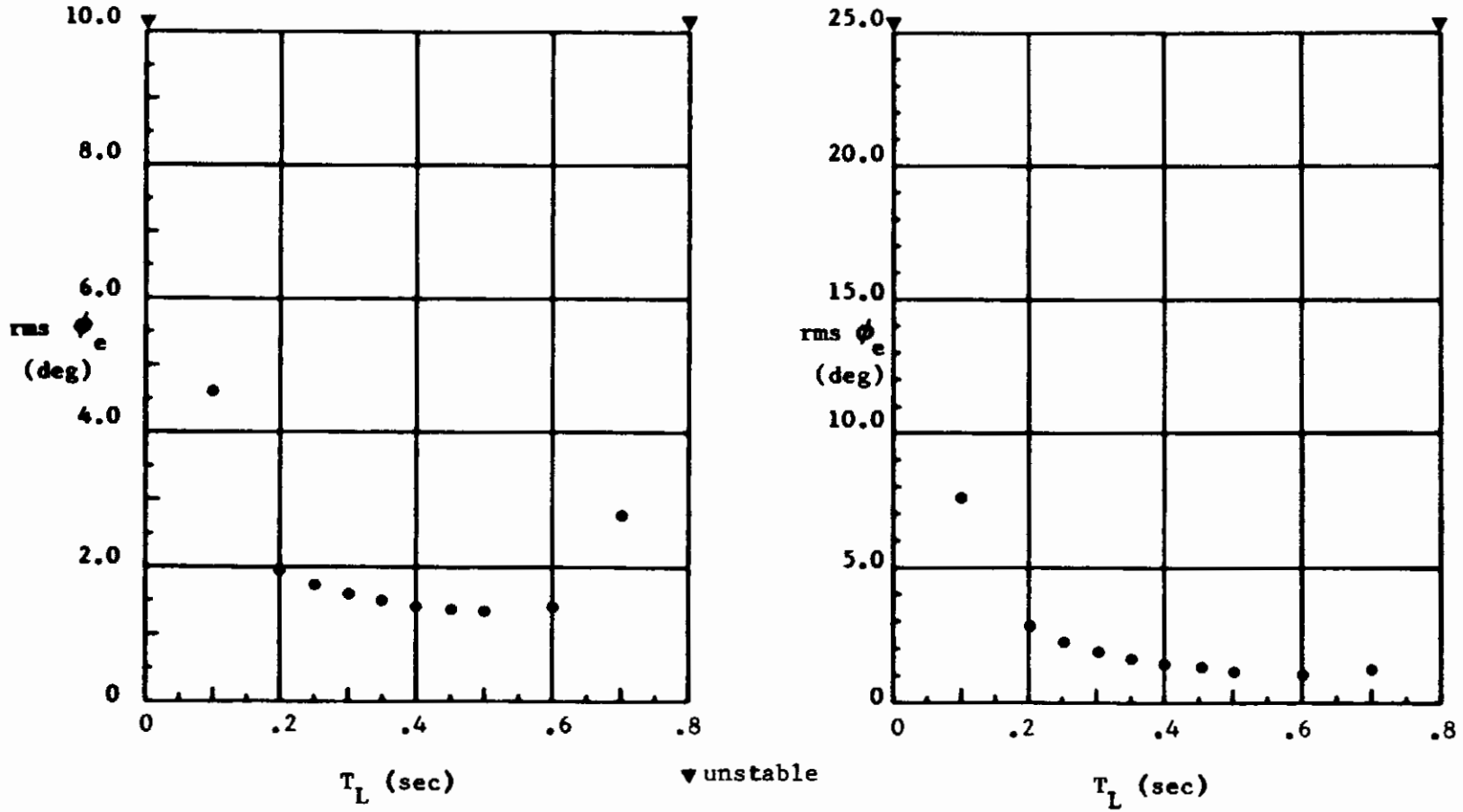

COMMAND TRACKING
RMS COMMAND INPUT = 10°

GUST TRACKING
RMS GUST INPUT LEVEL = 10 fps

Pilot Models

$$Y_{p_\beta} = 0$$

$$Y_{p_\phi} = 4.5(T_L s + 1)e^{-.3s}$$

$$Y_{p_\psi} = 0$$

FIGURE 9 **CONFIGURATION** T-33 AB-2.6
LEAD VARIATION

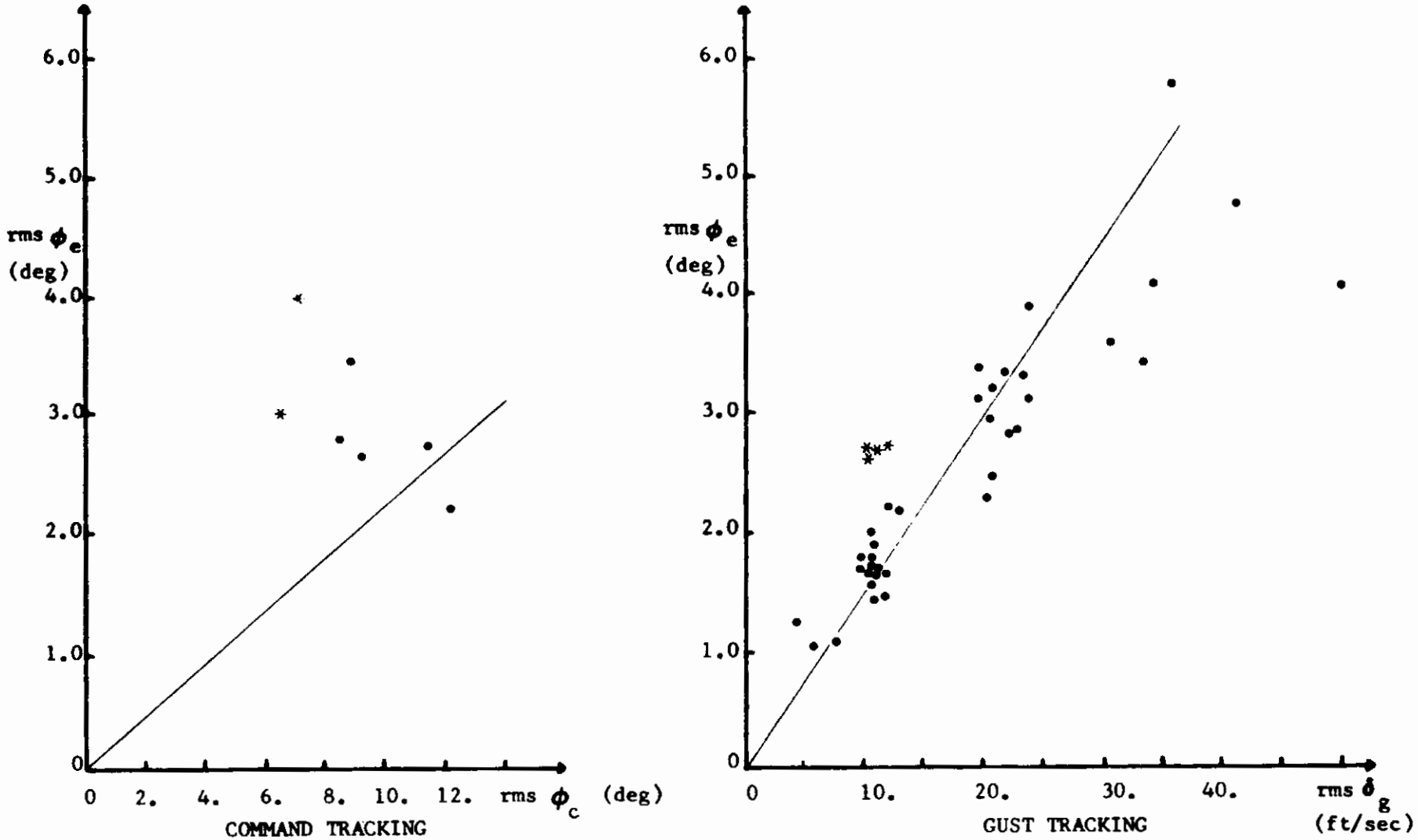

FIGURE 10 T-33 AB 2.6 ROLL TASK SIMULATION

• measured * fixed base

—— predicted

The bank angle tracking ability of AB 2.6 is also reported to be good, and the pilot, W.W.K., of this simulation, reported this airplane pleasant to fly. Since this appeared to be a realistic configuration, a large amount of data was taken. The agreement for both tasks is good, although the lower frequency nature of the tracking task causes more scatter in the data points.

AB 2.7 - Figures 11, 12, and 13 show the predictions and simulation data for this case. The configuration is very similar to AB 2.6, but pilot W.W.K. reported that AB 2.7 has more associated yaw and side acceleration. He also reported that at higher gust levels rms $\delta g_\beta > 20$ ft/sec the roughness of the ride increased his motivation to control the airplane. This shows up in the data points below the line at these levels. The tracking characteristics are similar to AB 2.6, and Reference 14 gives a Cooper rating of 3.0 to this configuration also.

AB 3.1 - Figures 14 and 15 show that the open loop gust response is very small and that pilot activity cannot reduce the error by any appreciable amount. Pilot W.W.K., after flying for a while, reported spontaneously that he could not reduce the bank angle errors, but that it did not seem to matter since they were very small. Again, the simulator results agree well at the 10 ft/sec value, but show lower values than predicted when more side acceleration is felt at 20 ft/sec turbulence (Figure 16). The tracking prediction shows that this airplane is not as good as AB 2.6 or AB 2.7, a result also apparent in the simulator data. Reference 14 indicates a Cooper rating of 7.0, which seems to reflect this. The two data points far above the prediction line are believed to be caused by a temporarily biased output of the noise generator, but were reported for completeness.

AB 3.3 - Figures 17, 18, and 19 show that this airplane is similar to the AB 3.1 except that the tracking performance is better. This is possibly reflected in the Reference 14 Cooper rating of 5.5, although the simulator data are too scattered to tell. Again, the gust performance is better than predicted at high gust levels and the fixed-base data for gust are well displaced above the line.

BB 2.3 - This airplane is an interesting example since it displays one of the best command tracking predictions (Figures 20 and 21) of the airplanes studied, yet the gust tracking characteristics are not very good. The large slope of Figure 22 shows that the airplane is more susceptible to gust disturbances than AB 3.1 and AB 3.3. An important feature of handling qualities of this airplane was reported by the pilot, W.W.K. He stated that he must use a constant high gain and that he could not relax without the errors increasing noticeably. This is indicated by the shape of the gust

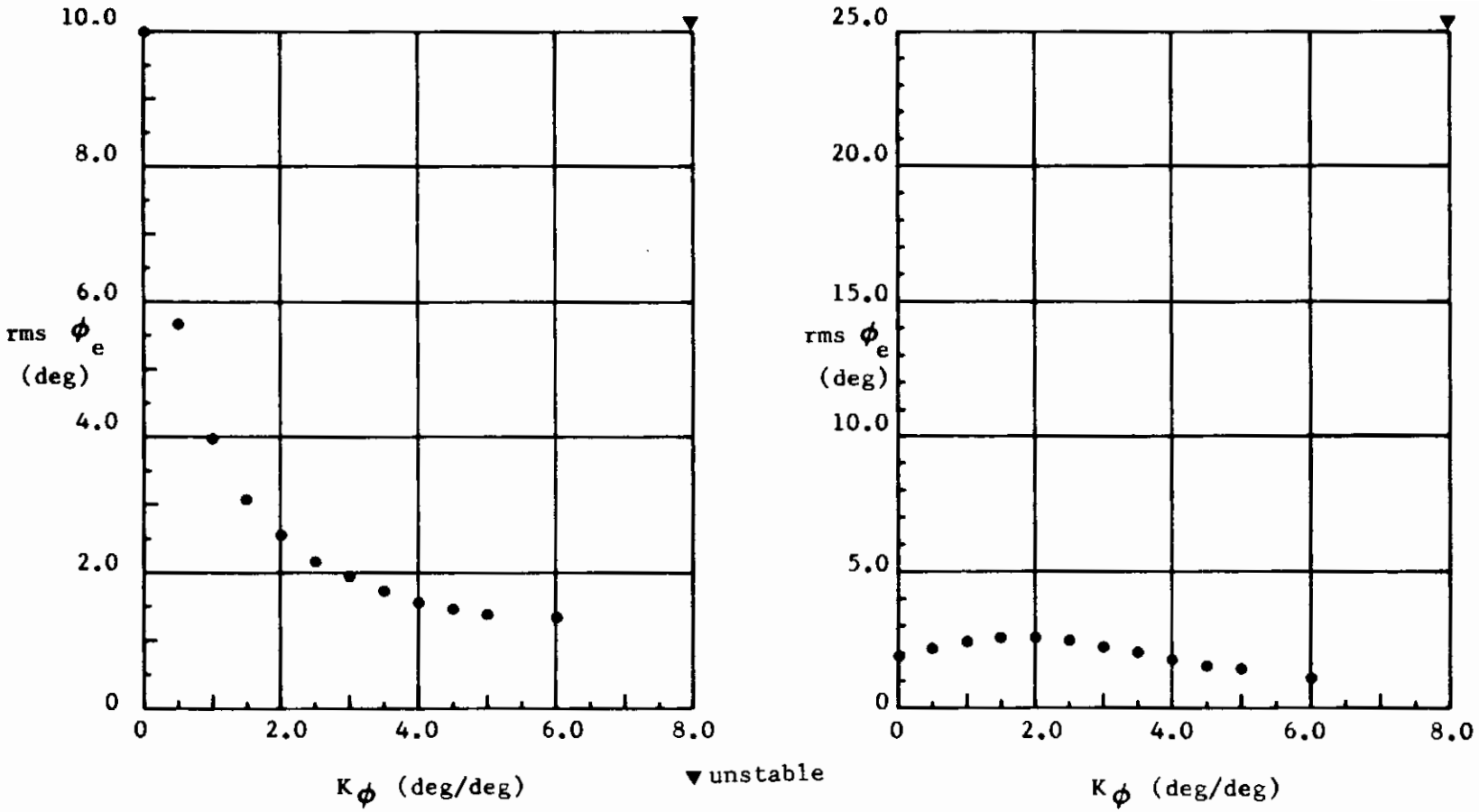

COMMAND TRACKING
RMS COMMAND INPUT = 10°

GUST TRACKING
RMS GUST INPUT LEVEL = 10 fps

Pilot Models

$$Y_{p_\beta} = 0$$

$$Y_{p_\phi} = K_\phi (.5s + 1) e^{-.3s}$$

$$Y_{p_\psi} = 0$$

FIGURE 11 CONFIGURATION T-33 AB-2.7
GAIN VARIATION

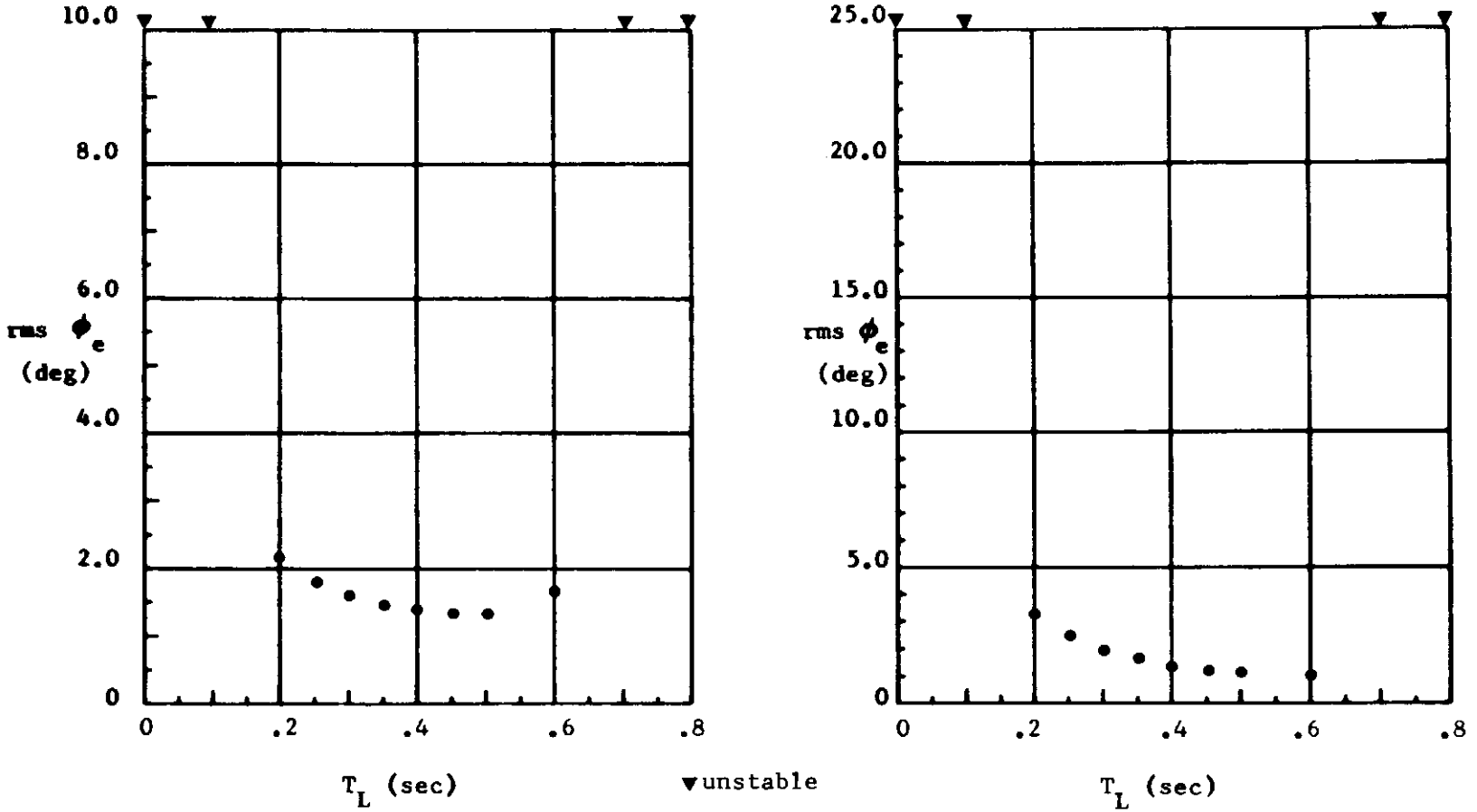

COMMAND TRACKING
RMS COMMAND INPUT = 10°

GUST TRACKING
RMS GUST INPUT LEVEL = 10 fps

Pilot Models

$$Y_{p_\beta} = 0$$

$$Y_{p_\phi} = 6.0(T_L S + 1)\, e^{-.3S}$$

$$Y_{p_\psi} = 0$$

FIGURE 12 **CONFIGURATION** *T-33 AB-2.7*
LEAD VARIATION

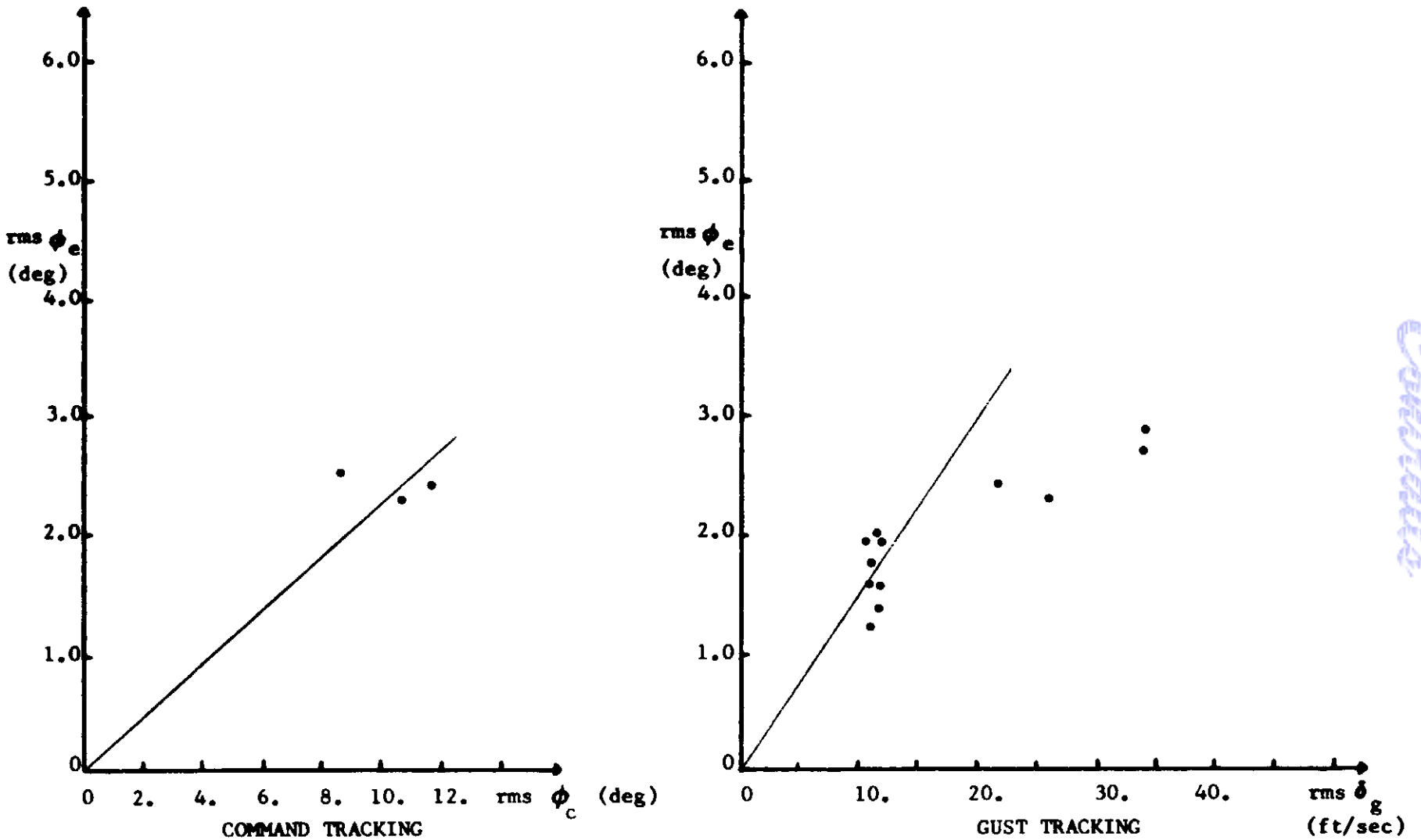

FIGURE 13 T-33 AB 2.7 ROLL TASK SIMULATION

• measured

—— predicted

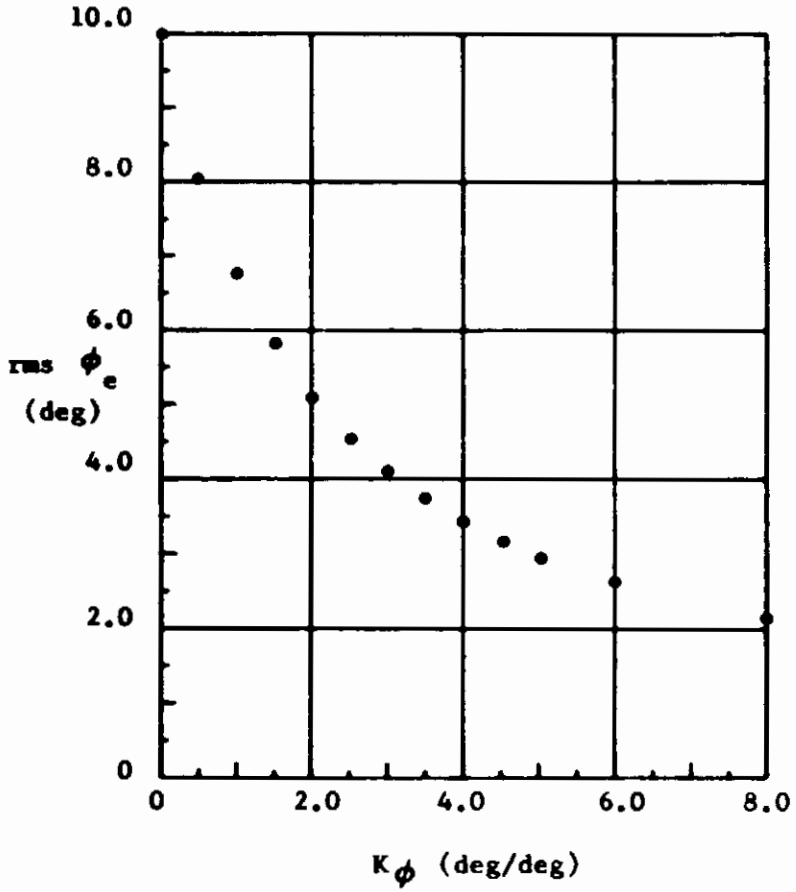

COMMAND TRACKING
RMS COMMAND INPUT = 10°

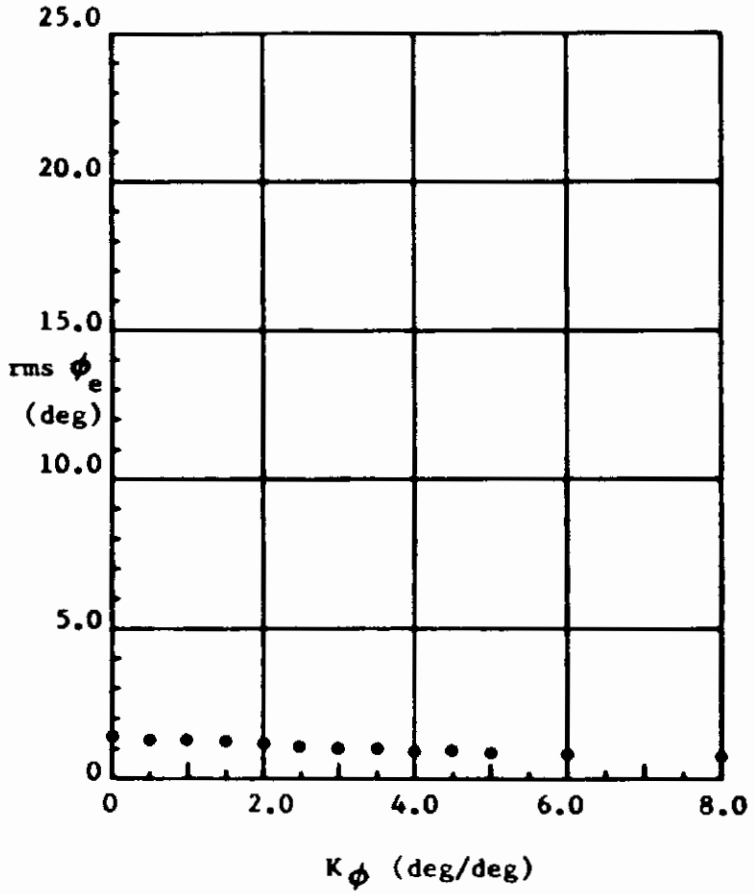

GUST TRACKING
RMS GUST INPUT LEVEL = 10 fps

Pilot Models

$$Y_{p_\beta} = 0$$

$$Y_{p_\phi} = K_\phi (.5S + 1) e^{-.3S}$$

$$Y_{p_\psi} = 0$$

FIGURE 14 **CONFIGURATION** *T-33 AB-3.1*
GAIN VARIATION

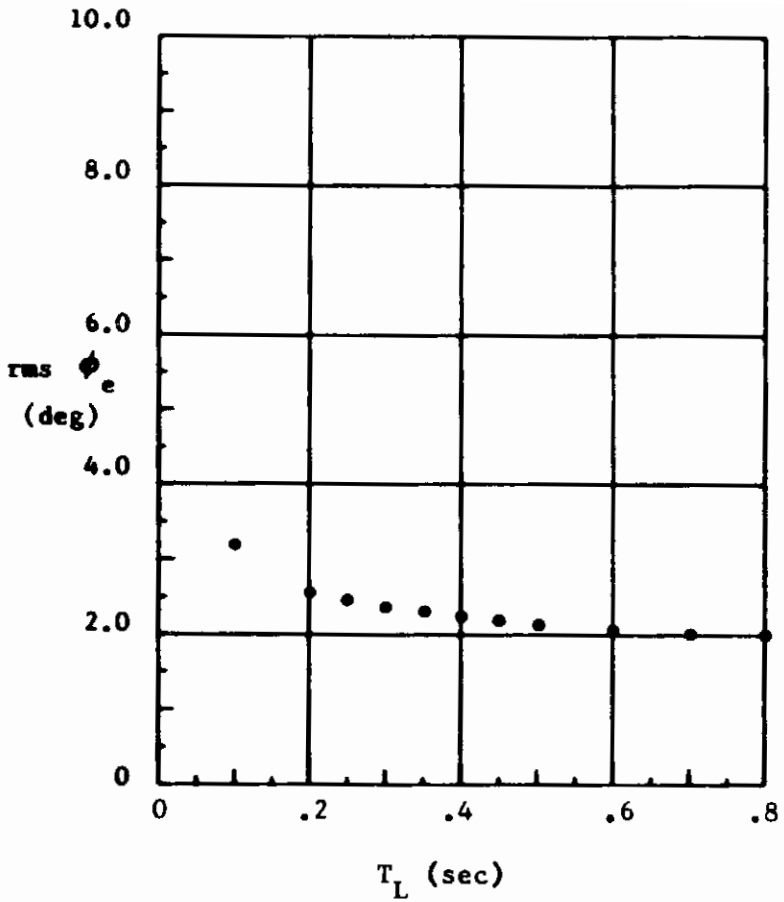

COMMAND TRACKING
RMS COMMAND INPUT = 10°

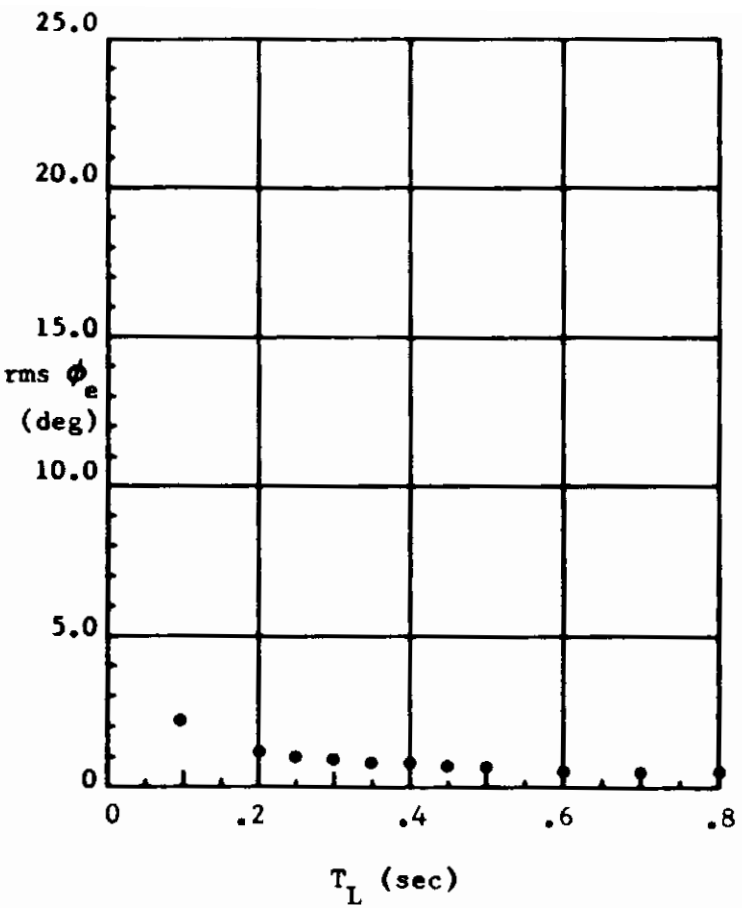

GUST TRACKING
RMS GUST INPUT LEVEL = 10 fps

Pilot Models

$$Y_{p_\beta} = 0$$

$$Y_{p_\phi} = 8.0(T_L s + 1)e^{-.3s}$$

$$Y_{p_\psi} = 0$$

FIGURE 15 **CONFIGURATION** *T-33 AB-3.1*
LEAD VARIATION

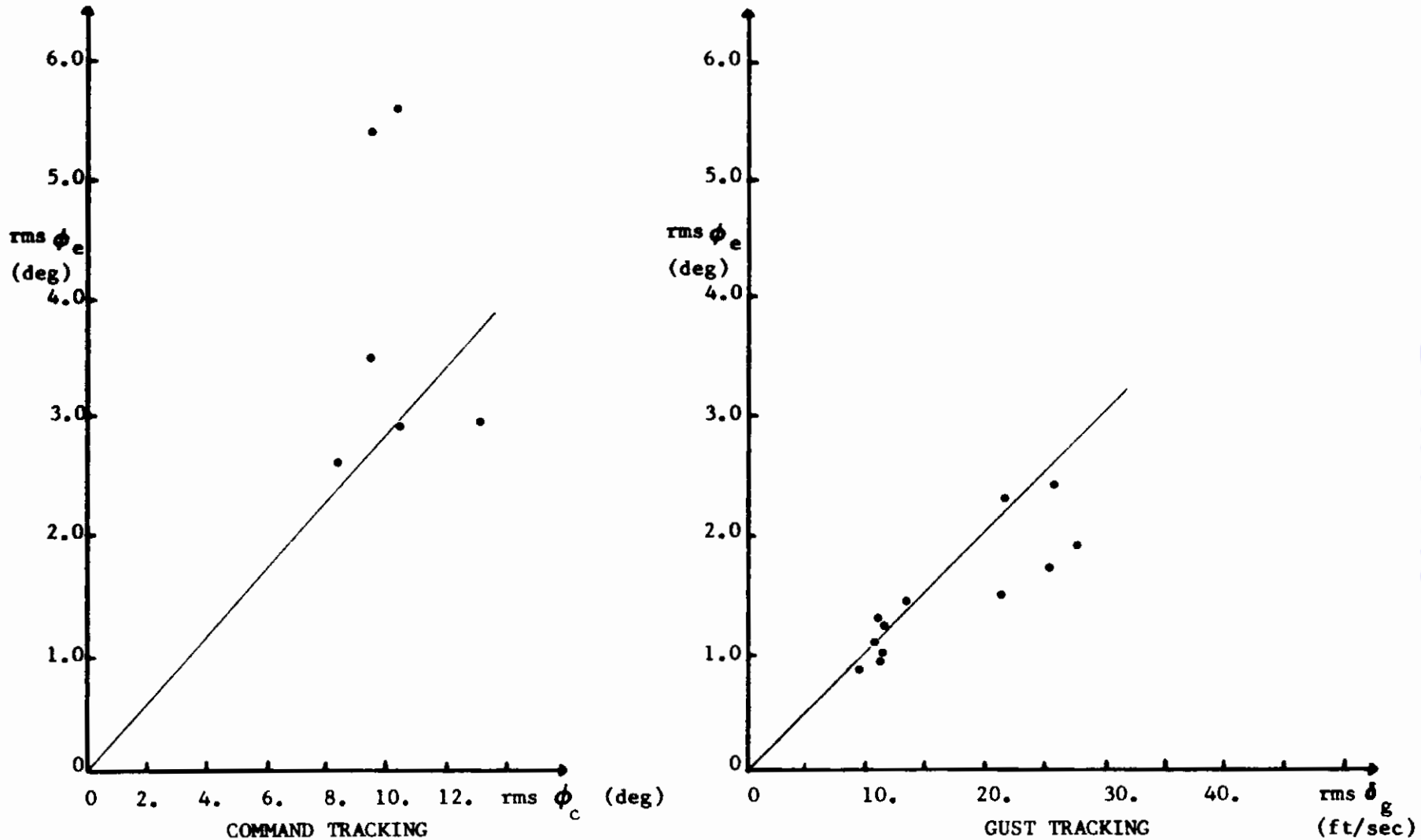

FIGURE 16 T-33 AB 3.1 ROLL TASK SIMULATION

• measured

—— predicted

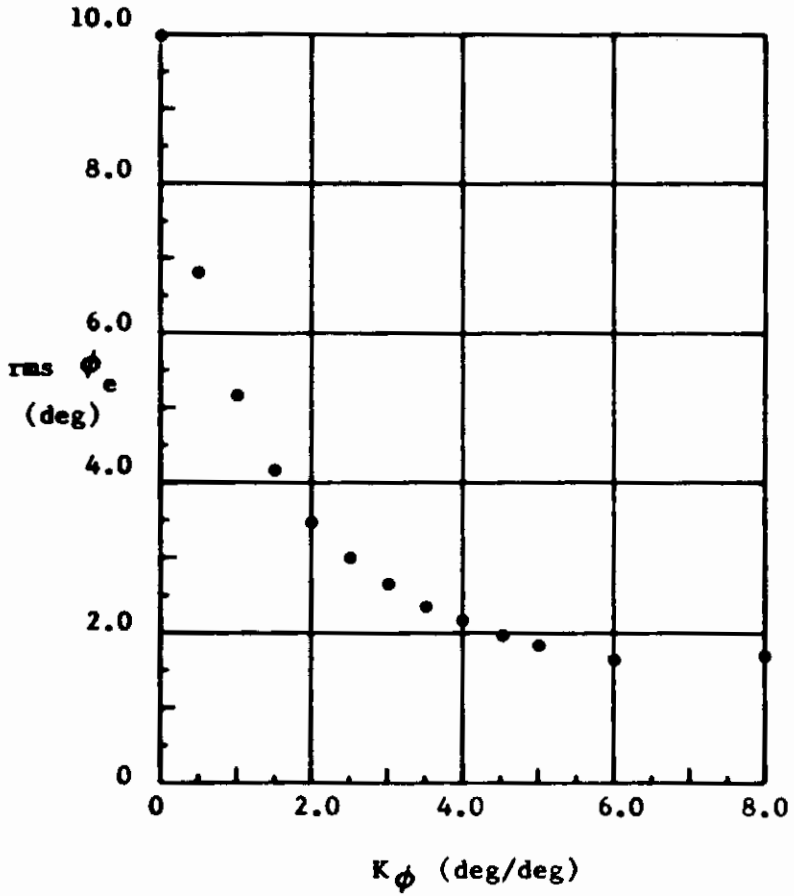

COMMAND TRACKING
RMS COMMAND INPUT = 10°

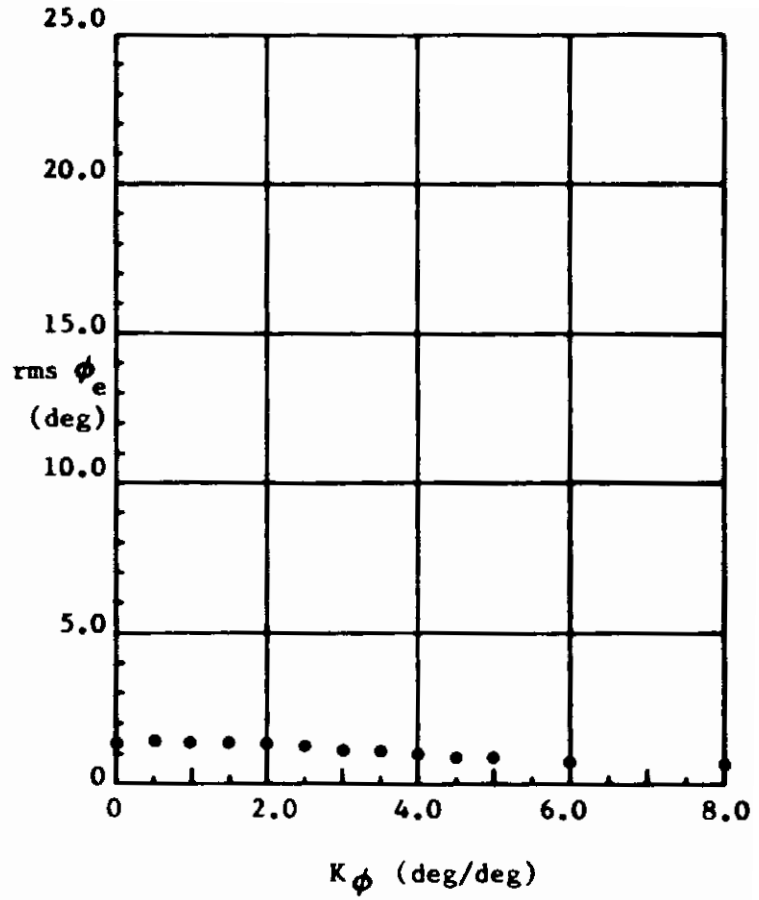

GUST TRACKING
RMS GUST INPUT LEVEL = 10 fps

Pilot Models

$$Y_{p_\beta} = 0$$

$$Y_{p_\phi} = K_\phi (.5s+1) e^{-.3s}$$

$$Y_{p_\psi} = 0$$

FIGURE 17 CONFIGURATION T-33 AB-3.3
GAIN VARIATION

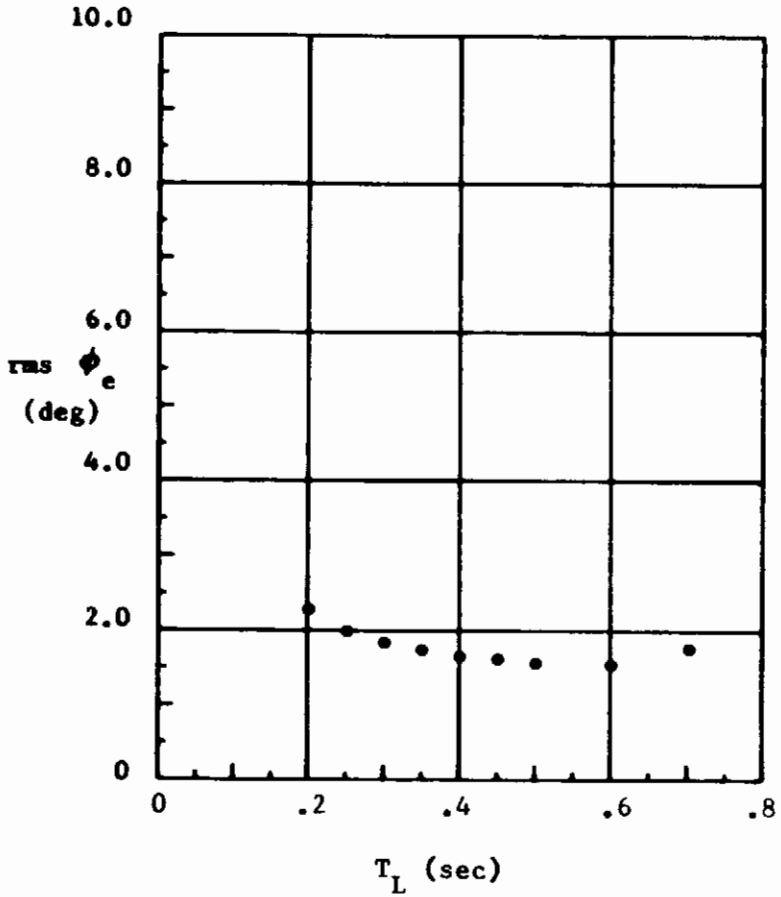

COMMAND TRACKING
RMS COMMAND INPUT = 10°

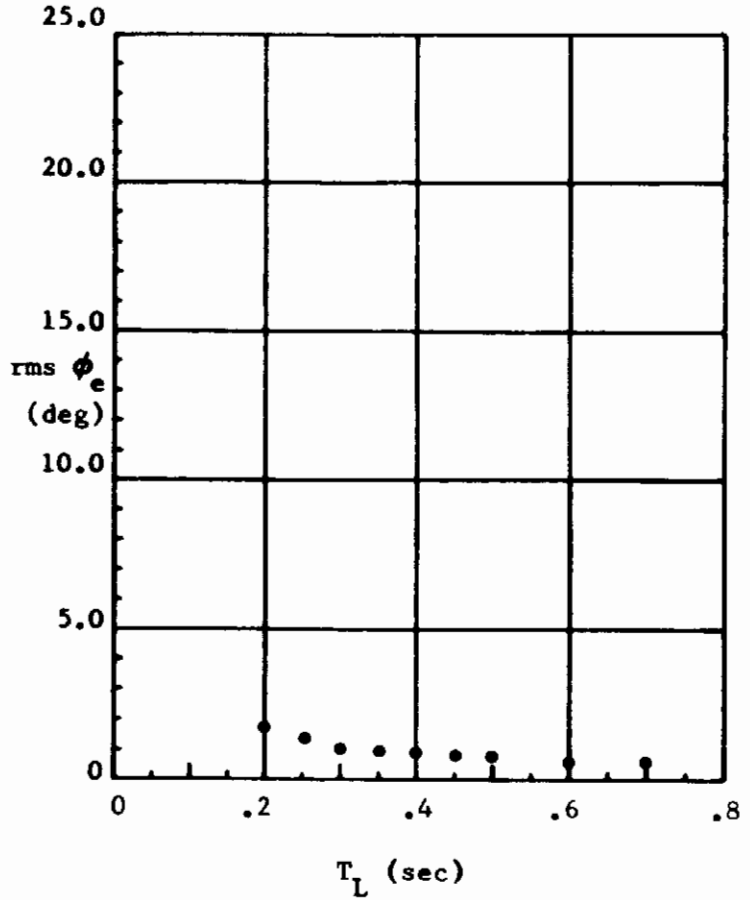

GUST TRACKING
RMS GUST INPUT LEVEL = 10 fps

Pilot Models

$$Y_{p_\beta} = 0$$

$$Y_{p_\phi} = 6.5(T_L S + 1)e^{-.35S}$$

$$Y_{p_\psi} = 0$$

FIGURE 18 **CONFIGURATION** *T-33 AB-3.3*
LEAD VARIATION

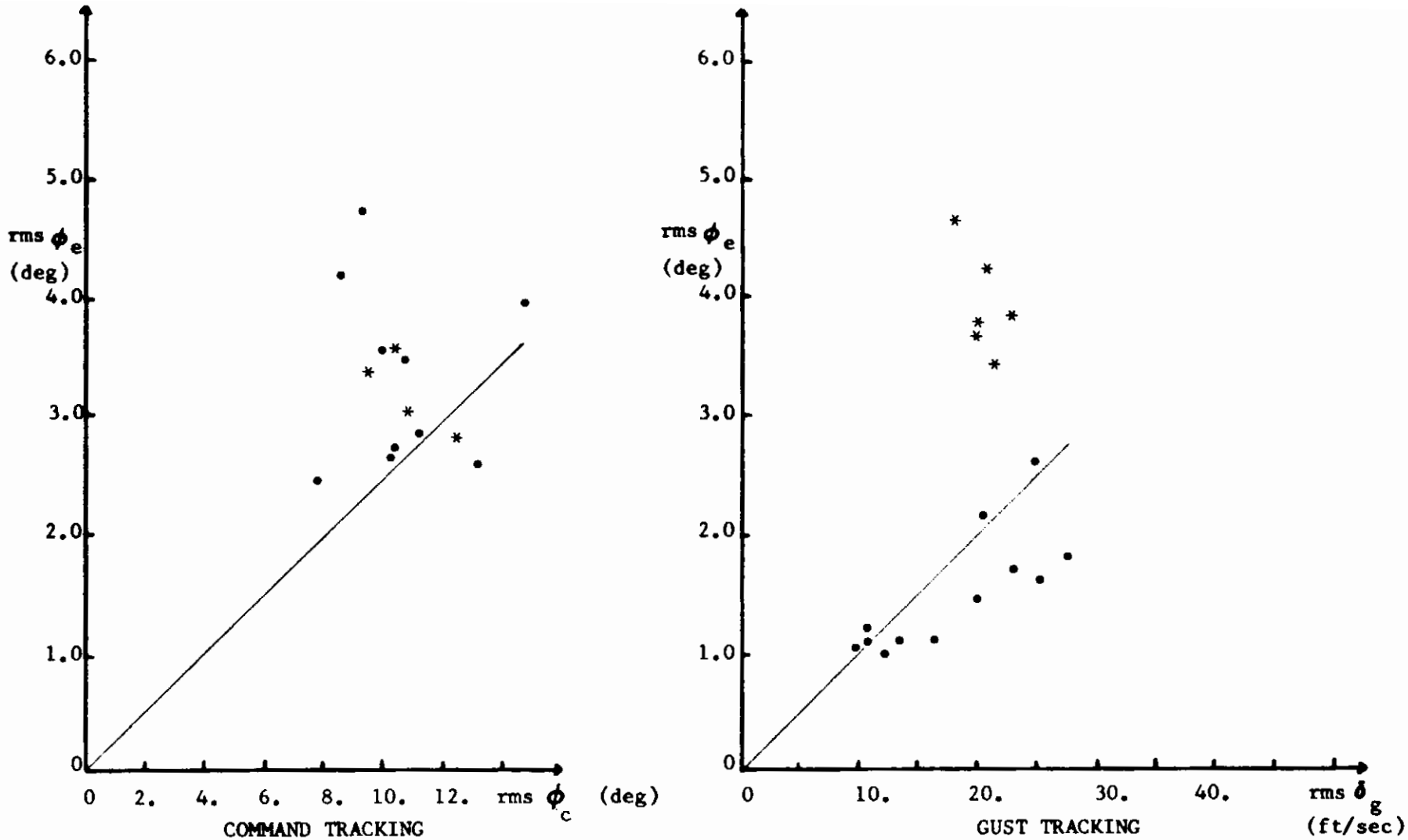

FIGURE 19 T-33 AB 3.3 ROLL TASK SIMULATION

• measured * fixed base

—— predicted

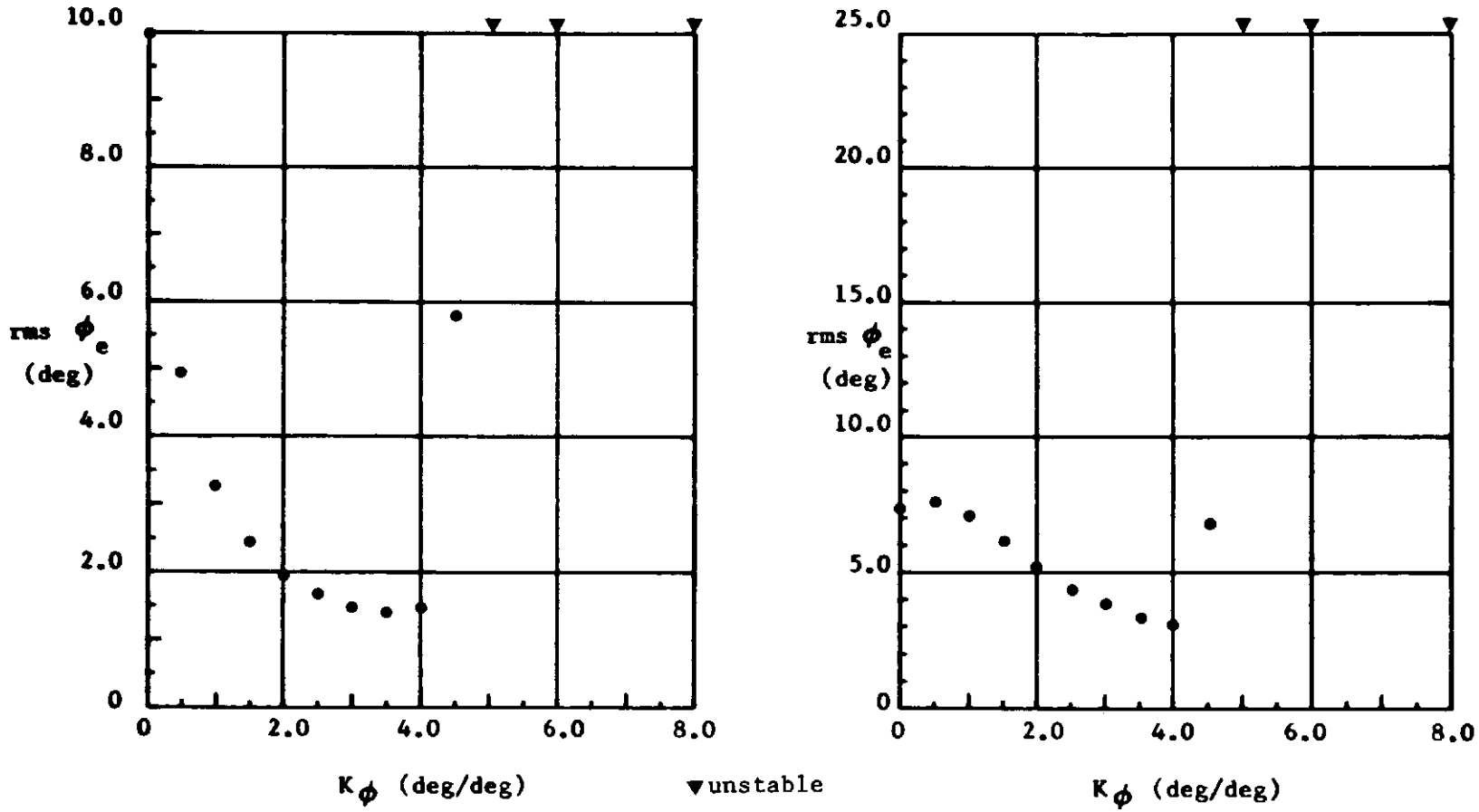

COMMAND TRACKING
RMS COMMAND INPUT = 10°

GUST TRACKING
RMS GUST INPUT LEVEL = 10 fps

Pilot Models

$Y_{p_\beta} = 0$

$Y_{p_\phi} = K_\phi (.55 + 1) e^{-.3s}$

$Y_{p_\psi} = 0$

FIGURE 20 CONFIGURATION T-33 BB-2.3
GAIN VARIATION

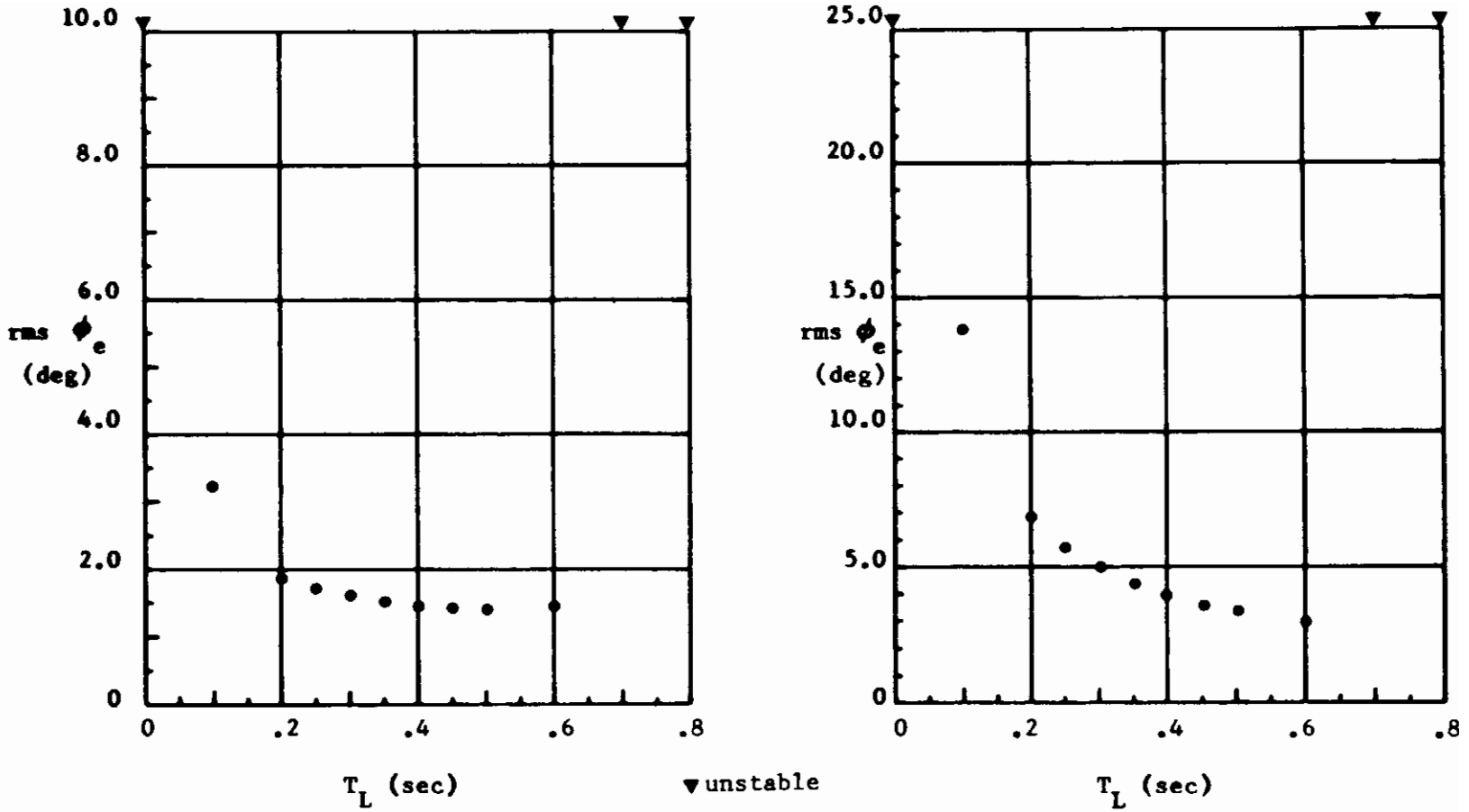

COMMAND TRACKING
RMS COMMAND INPUT = 10°

GUST TRACKING
RMS GUST INPUT LEVEL = 10 fps

Pilot Models

$Y_{p_\beta} = 0$

$Y_{p_\phi} = 3.5(T_L s + 1)e^{-.3s}$

$Y_{p_\psi} = 0$

FIGURE 21 **CONFIGURATION** *T-33 BB-2.3*
LEAD VARIATION

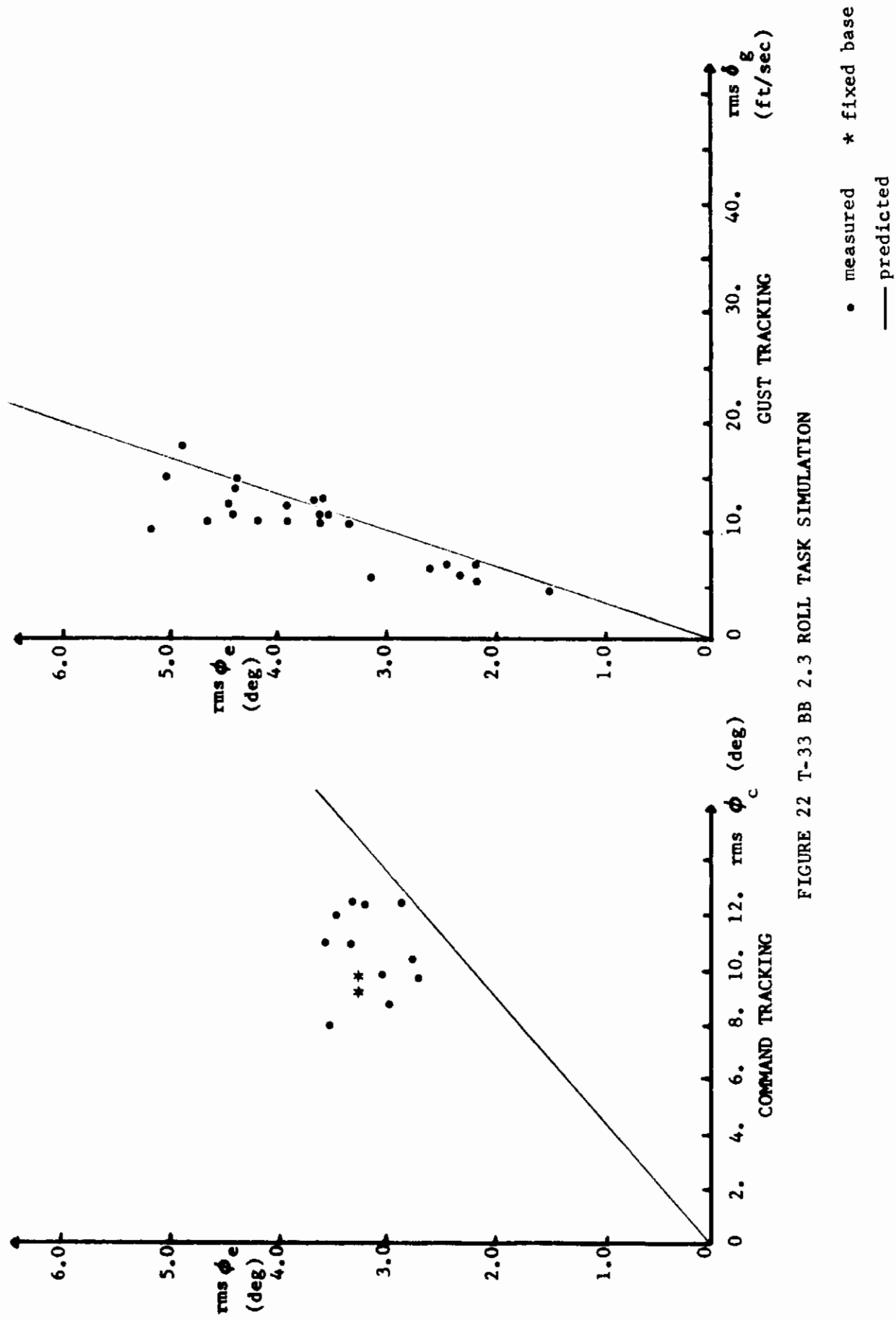

FIGURE 22 T-33 BB 2.3 ROLL TASK SIMULATION

response rms ϕ_e vs K_ϕ graph. The general difference between the flying qualities for tracking and gust tracking for BB 2.3 was further illustrated when the gust flights were completed and the familiarization with the tracking flights begun; the pilot, W.W.K., did not recognize the airplane and remarked that the new airplane was much better. The airplane is generally well behaved and is given a Cooper rating of 2.0 in Reference 14.

BC 2.2 - Figures 23 and 24 show that the predicted performance of BC 2.2 is inferior to BB 2.3. This is confirmed by the simulation as shown in Figure 25. Pilot W.W.K. reported that configuration was just controllable and that he did not dare relax, a reflection of the slope of the gust response graphs rms ϕ_e vs K_ϕ and rms ϕ_e vs T_L. Reference 14 reports that there is difficulty in precise bank angle control and gives BC 2.2 a Cooper rating of 5.0.

BC 2.3 - The comments of BC 2.2 also apply to BC 2.3, including the Cooper rating of 5.0. The gust tracking is worse, but the predictions remain accurate as shown in Figures 26, 27, and 28.

BC 2.4 - This airplane is given a Cooper rating of 7.5 by Reference 14, which also reports that the bank angle control is not sufficiently good for precision tracking. Figures 29 and 30 show the predictions of greater rms ϕ_e for the gust tracking. Pilot W.W.K. reported that the airplane was hard to fly and that he had to get immediate control and could not ease into the gust task, a possible manifestation of the hump in the gust rms ϕ_e vs K_ϕ graph. Again, the accuracy of the predictions is confirmed by simulation, as shown in Figure 31.

F-5 - Figures 32, 33, and 34 show the predictions for this airplane, a standard configuration of the F-5 which reportedly has exceptionally good tracking characteristics. This is illustrated by the command tracking performance prediction which is lower than all other airplanes studied. Since the F-5 is a representative Class IV airplane, it was selected for further analytical study.

The above studies assume a fixed time delay τ and consider perturbations of K_ϕ and T_L about the values of optimum K_ϕ and T_L = .5 seconds. In order to examine the effect of different values of T_L and τ, perturbations about these points were made. Figure 35 shows the effects of varying τ in the rms ϕ_e vs K_ϕ graphs for command tracking and a similar study for AB 2.6 yields the graph shown in Figure 36. A two parameter variation of T_L and K_ϕ is shown in Figures 37 through 42. These essentially map the rms ϕ_e surface with K_ϕ and T_L as coordinates. Viewed in this way, the figures are cross sections of constant T_L and it is clear that the surface rms ϕ_e becomes nearly

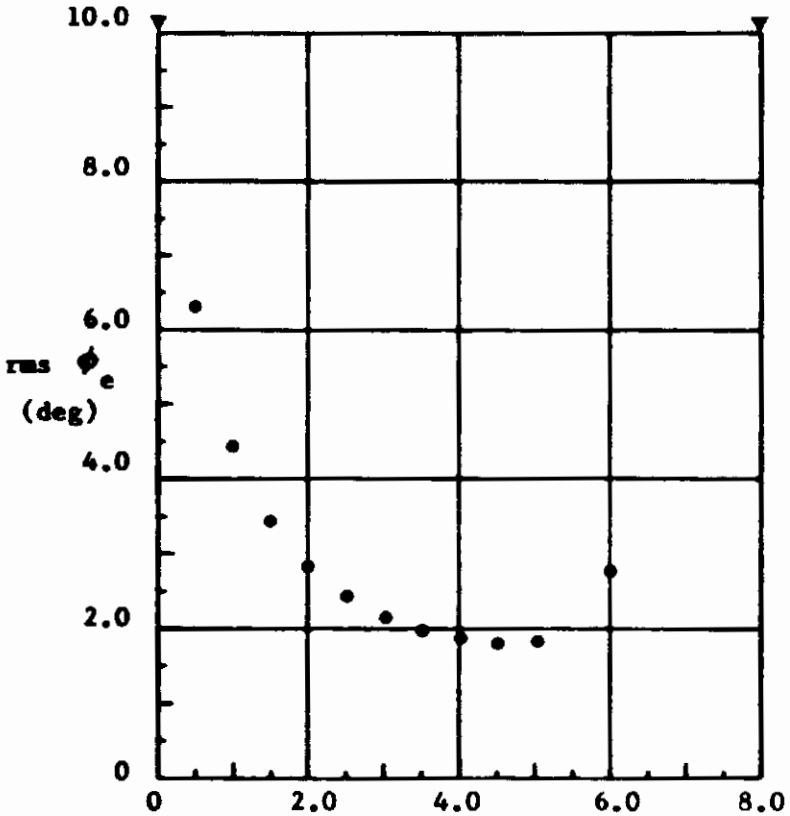

COMMAND TRACKING
RMS COMMAND INPUT = 10°

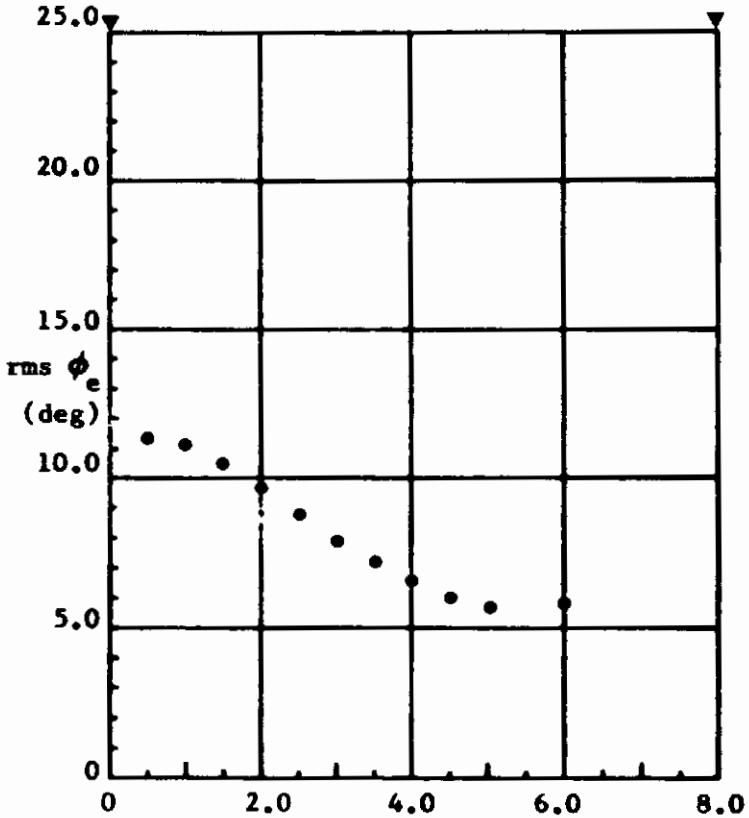

GUST TRACKING
RMS GUST INPUT LEVEL = 10 fps

Pilot Models

$$Y_{p_\beta} = 0$$

$$Y_{p_\phi} = K_\phi (.5s + 1) e^{-.3s}$$

$$Y_{p_\psi} = 0$$

FIGURE 23 **CONFIGURATION T-33 8C-2.2**
GAIN VARIATION

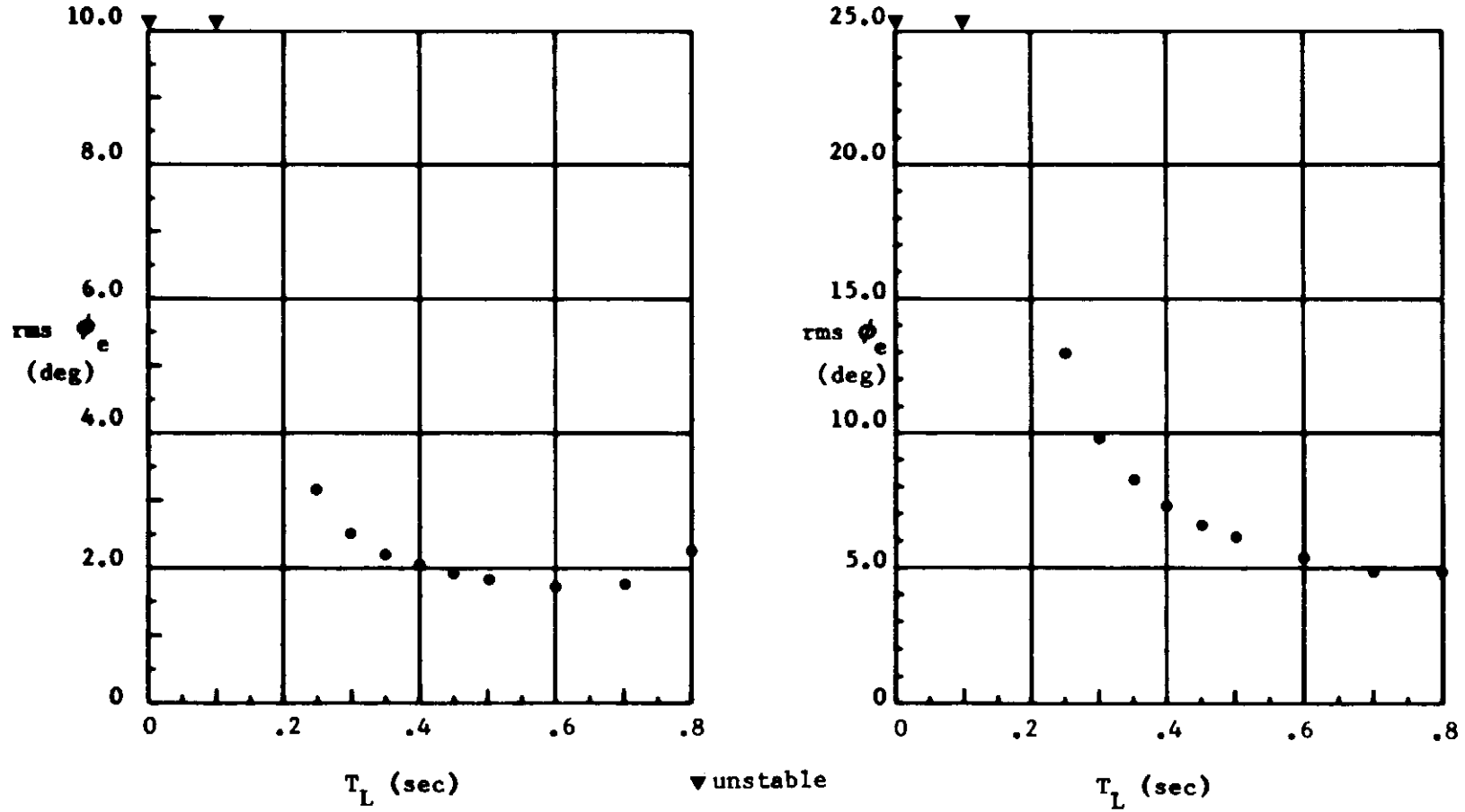

COMMAND TRACKING
RMS COMMAND INPUT = 10°

GUST TRACKING
RMS GUST INPUT LEVEL = 10 fps

Pilot Models

$$Y_{p_\beta} = 0$$

$$Y_{p_\phi} = 4.5(T_L s + 1) e^{-.3s}$$

$$Y_{p_\psi} = 0$$

FIGURE 24 CONFIGURATION T-33 BC-22
LEAD VARIATION

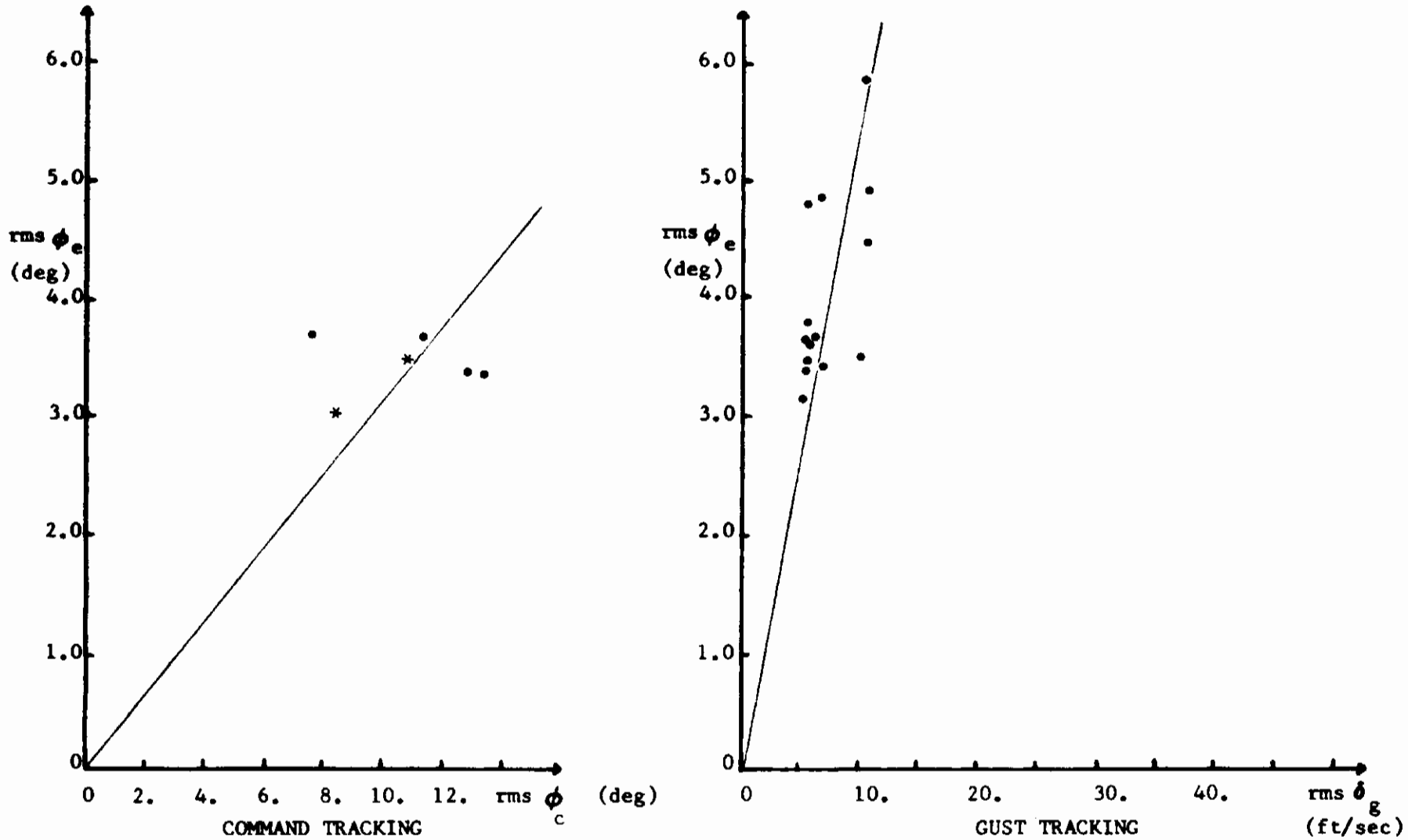

FIGURE 25 T-33 BC 2.2 ROLL TASK SIMULATION

• measured * fixed base

—— predicted

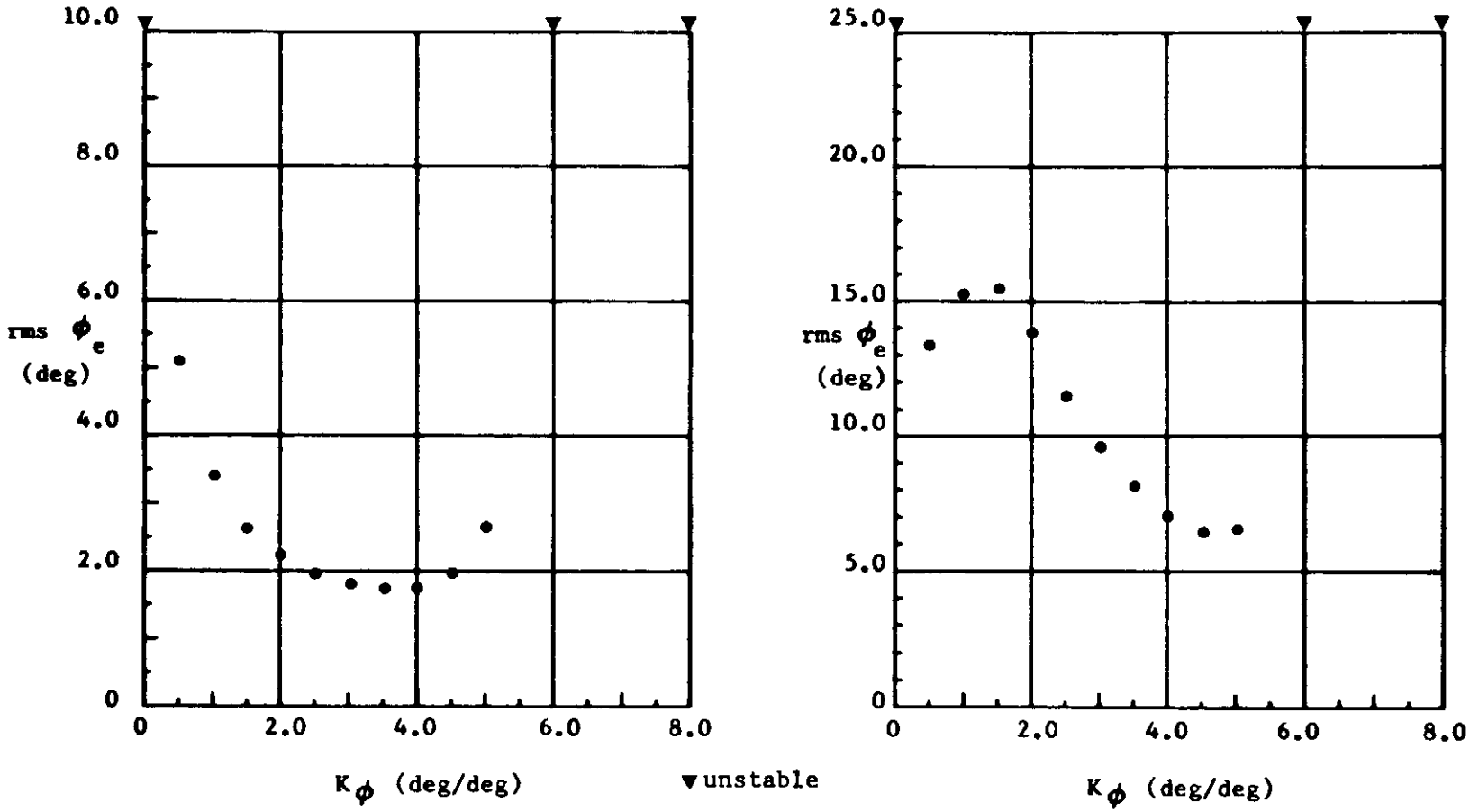

COMMAND TRACKING
RMS COMMAND INPUT = 10°

GUST TRACKING
RMS GUST INPUT LEVEL = 10 fps

Pilot Models

$$Y_{p_\beta} = 0$$

$$Y_{p_\phi} = K_\phi (.5S + 1) e^{-.3S}$$

$$Y_{p_\psi} = 0$$

FIGURE 26 **CONFIGURATION T-33 BC-2.3**
GAIN VARIATION

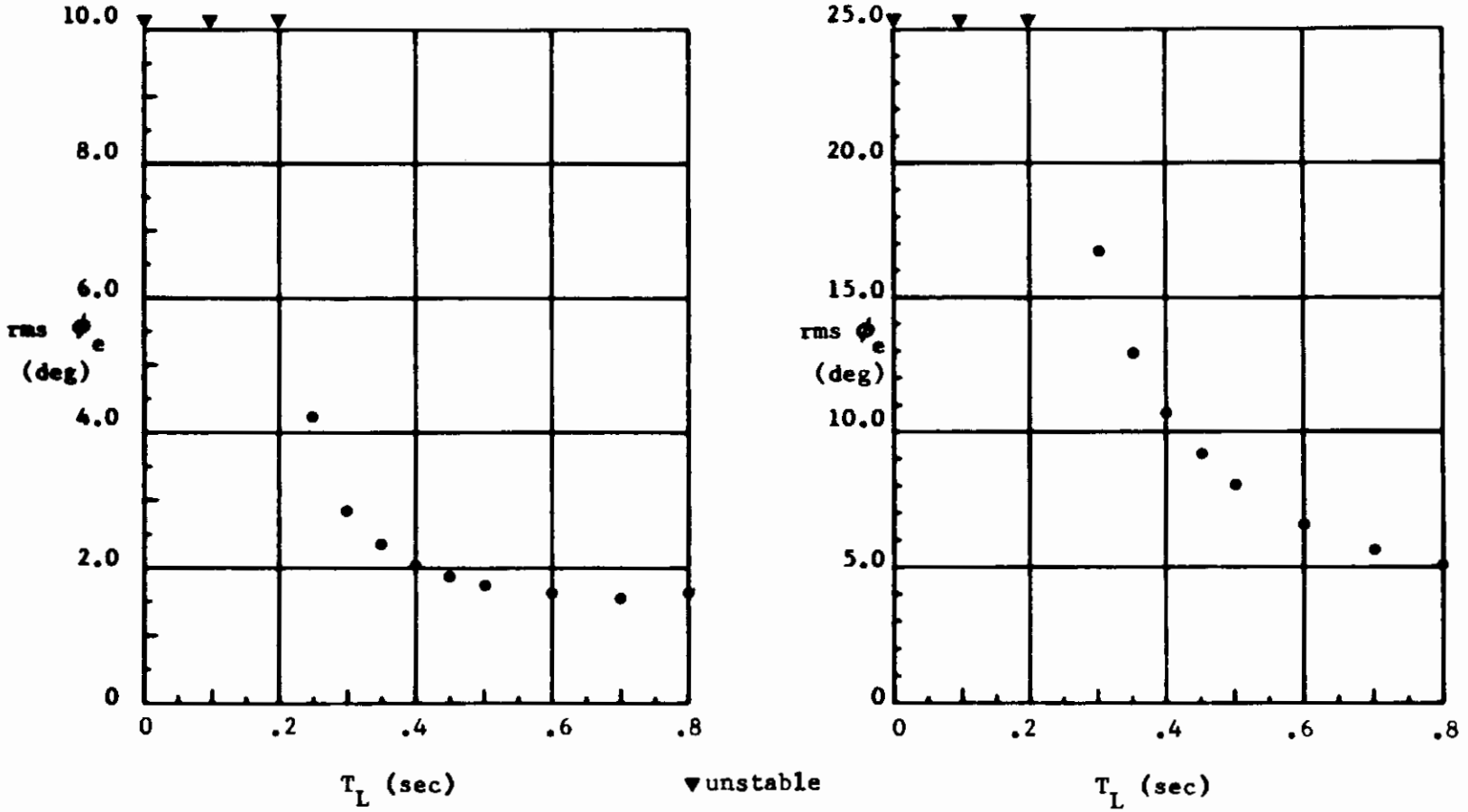

COMMAND TRACKING
RMS COMMAND INPUT = 10°

GUST TRACKING
RMS GUST INPUT LEVEL = 10 fps

Pilot Models

$$Y_{p_\beta} = 0$$

$$Y_{p_\phi} = 3.5\,(T_L s + 1)\,e^{-.35}$$

$$Y_{p_\psi} = 0$$

FIGURE 27 **CONFIGURATION** T-33 BC-2.3
LEAD VARIATION

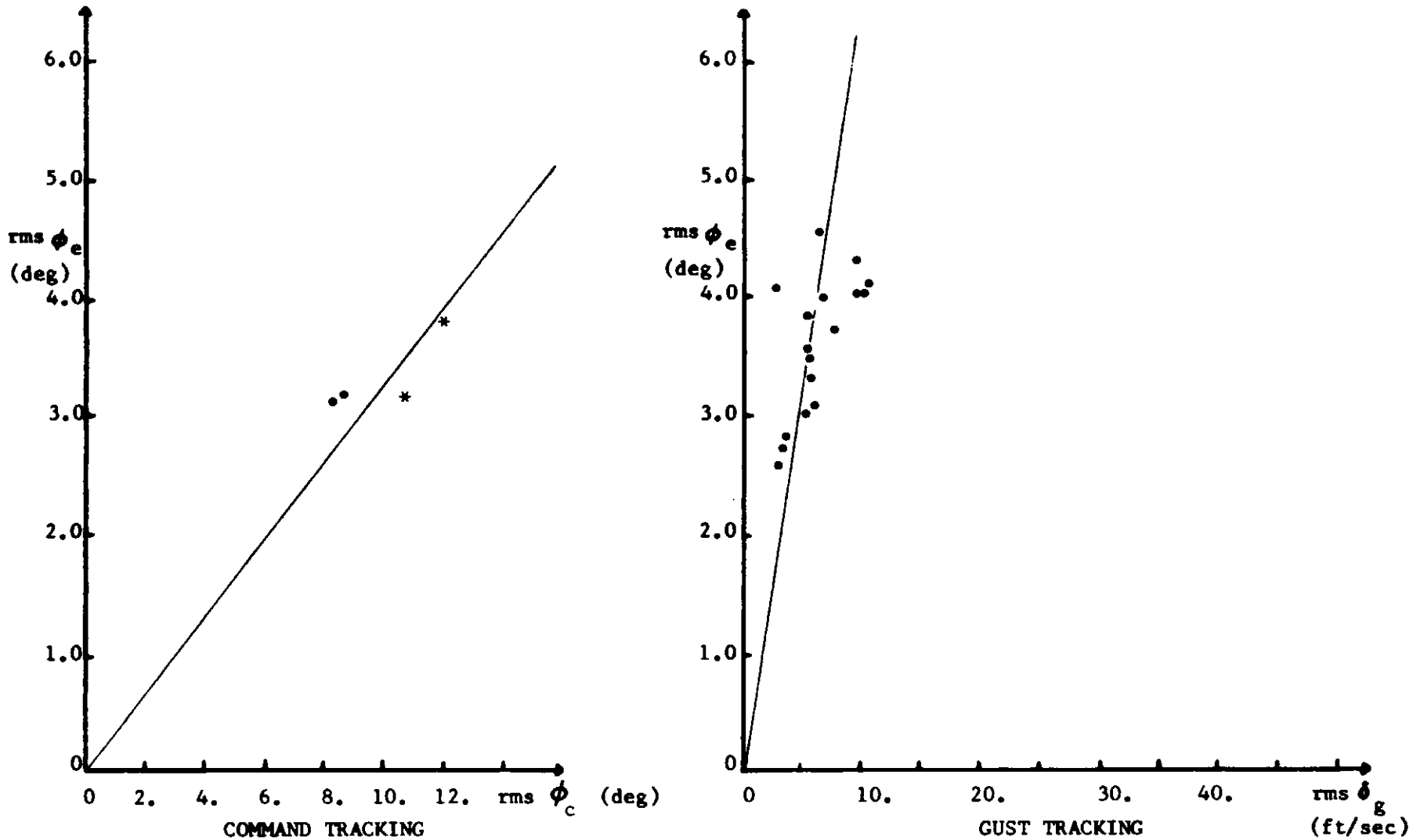

FIGURE 28 T-33 BC 2.3 ROLL TASK SIMULATION

• measured * fixed base

—— predicted

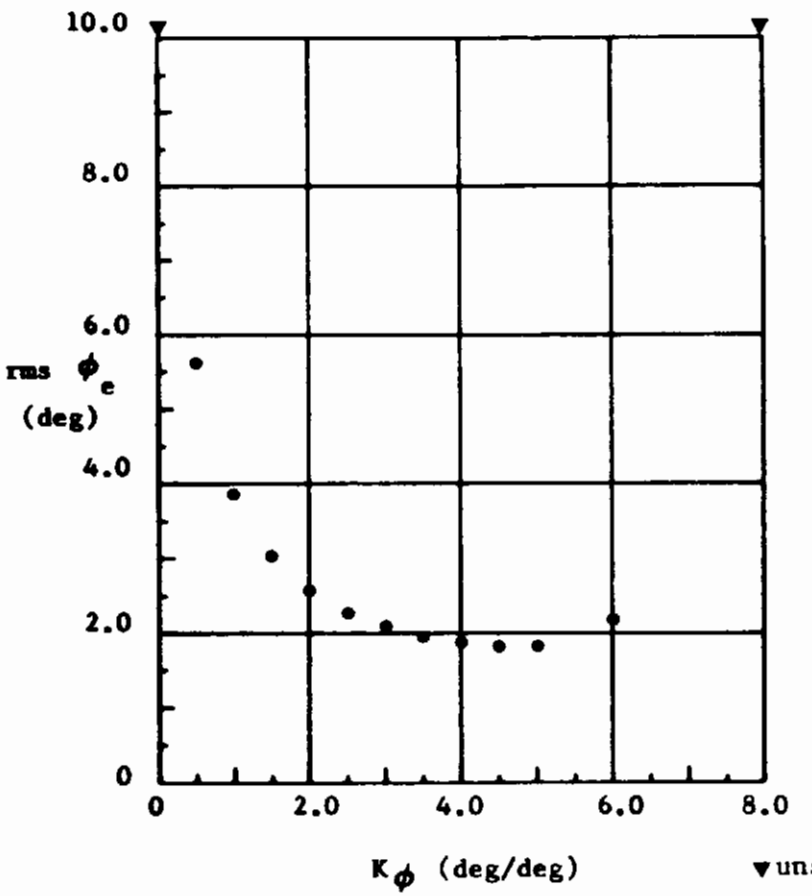

COMMAND TRACKING
RMS COMMAND INPUT = 10°

▼unstable

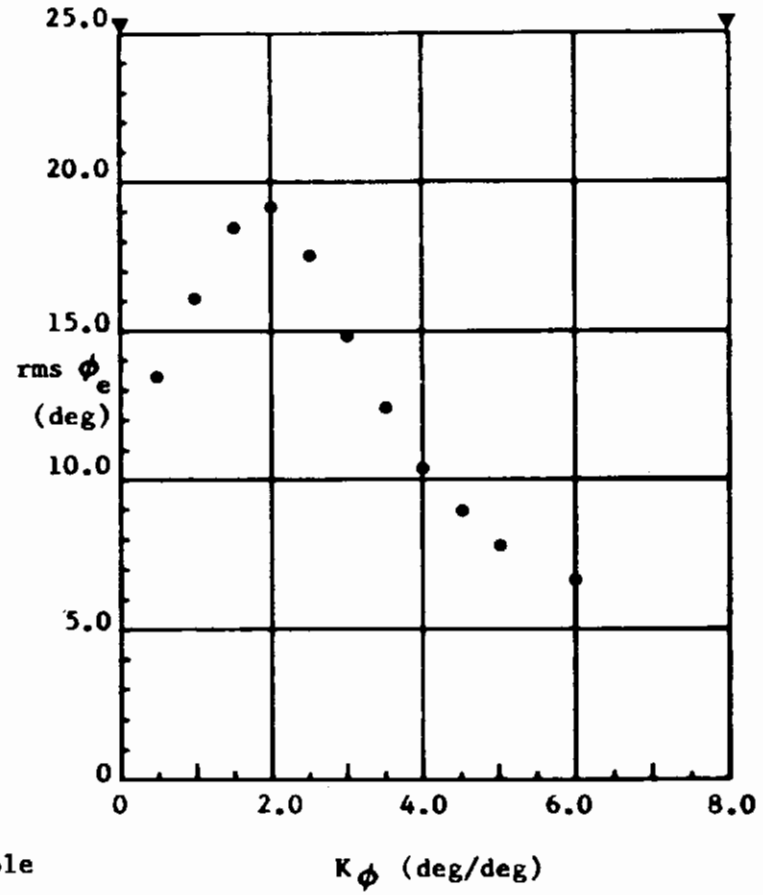

GUST TRACKING
RMS GUST INPUT LEVEL = 10 fps

Pilot Models

$$Y_{p_\beta} = 0$$

$$Y_{p_\phi} = K_\phi (.5S + 1) e^{-.3S}$$

$$Y_{p_\psi} = 0$$

FIGURE 29 CONFIGURATION T-33 BC-2.4
GAIN VARIATION

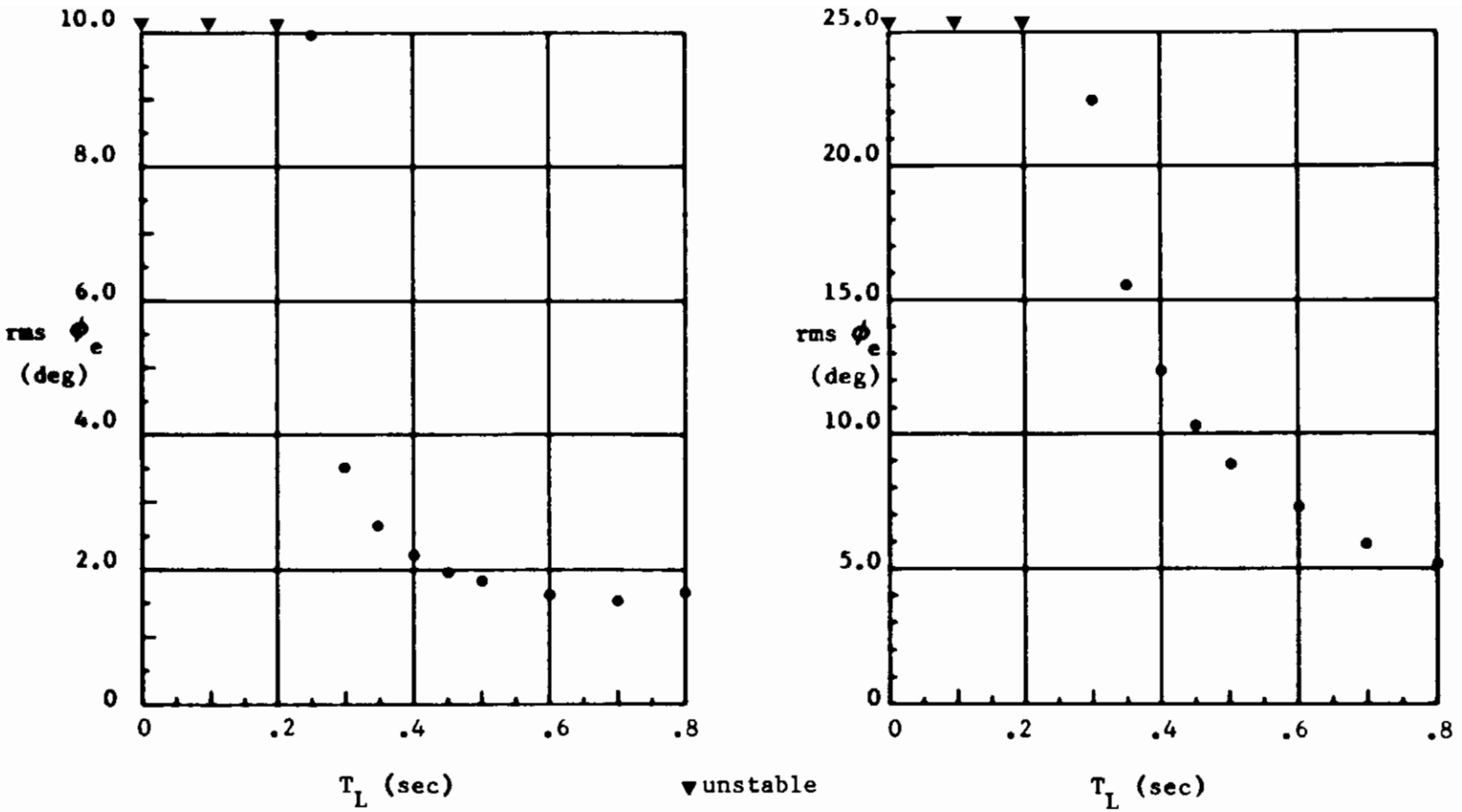

COMMAND TRACKING
RMS COMMAND INPUT = 10°

GUST TRACKING
RMS GUST INPUT LEVEL = 10 fps

Pilot Models

$$Y_{p_\beta} = 0$$

$$Y_{p_\phi} = 4.5(T_L S + 1)\, e^{-.35}$$

$$Y_{p_\psi} = 0$$

FIGURE 30 **CONFIGURATION** T-33 BC-2.4
LEAD VARIATION

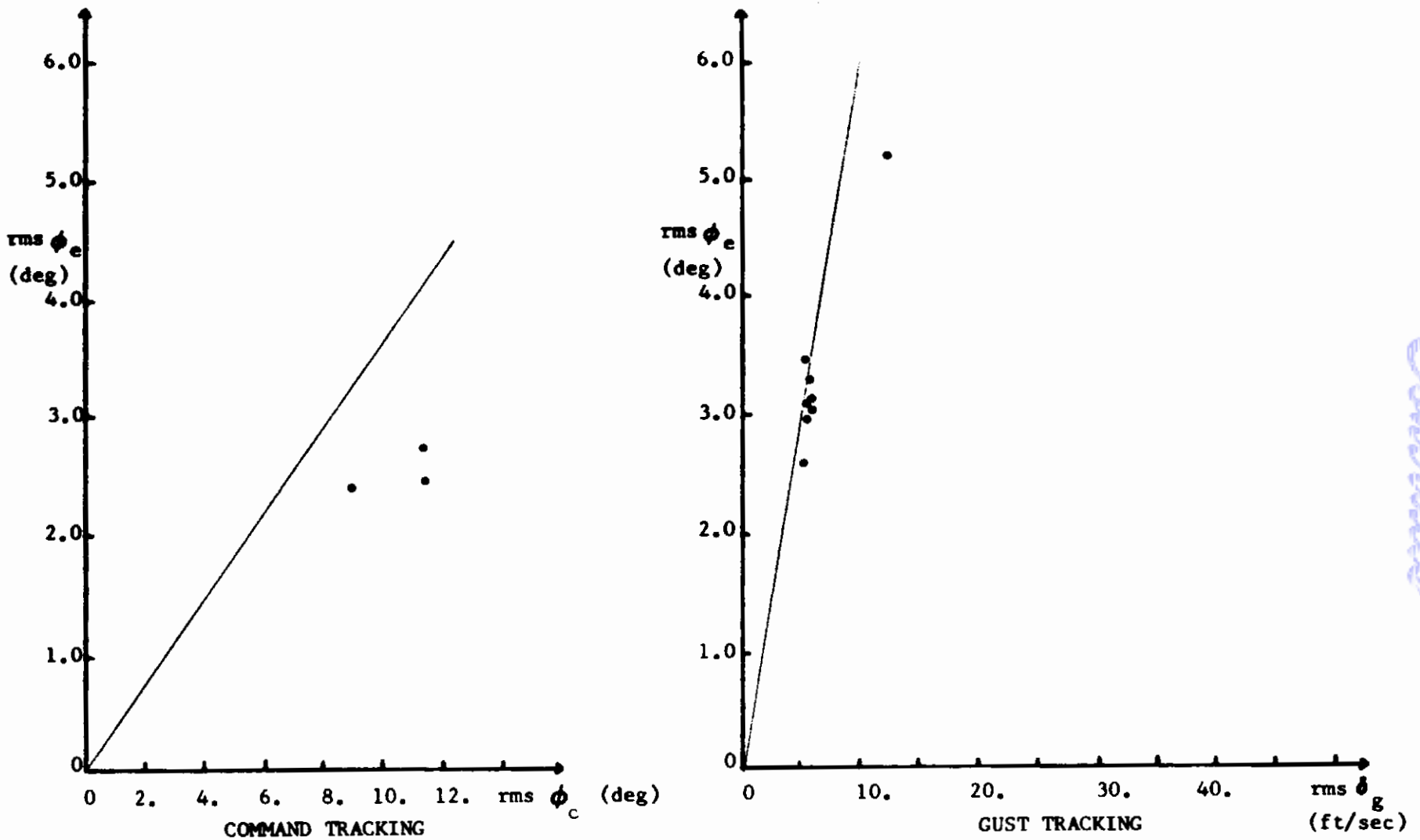

FIGURE 31 T-33 BC 2.4 ROLL TASK SIMULATION

• measured

—— predicted

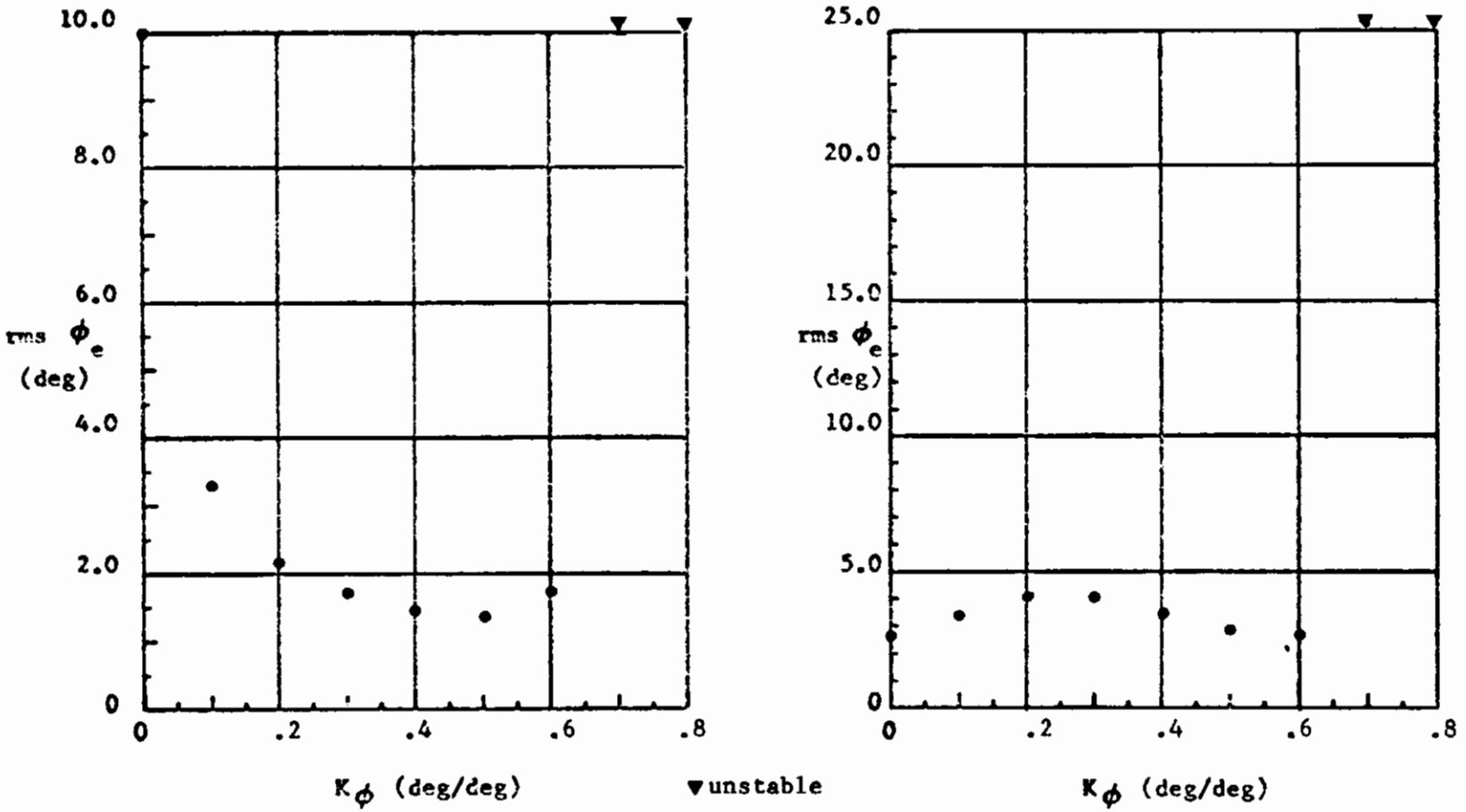

COMMAND TRACKING
RMS COMMAND INPUT = 10°

GUST TRACKING
RMS GUST INPUT LEVEL = 10 fps

Pilot Models

$$Y_{p_\beta} = 0$$

$$Y_{p_\phi} = K_\phi(.5s+1)e^{-.3s}$$

$$Y_{p_\psi} = 0$$

FIGURE 32 CONFIGURATION F-5
GAIN VARIATION

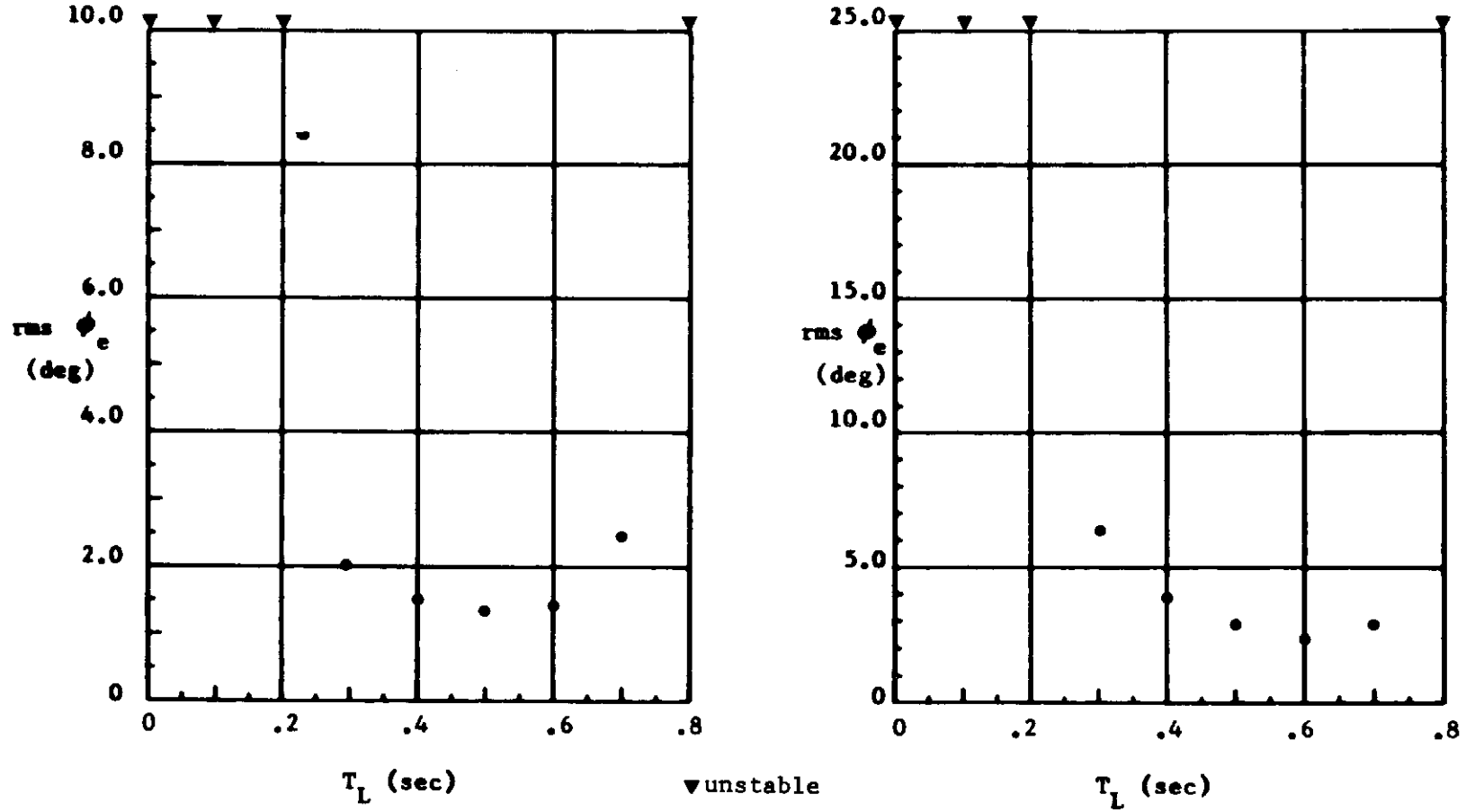

COMMAND TRACKING
RMS COMMAND INPUT = 10°

GUST TRACKING
RMS GUST INPUT LEVEL = 10 fps

Pilot Models

$Y_{p_\beta} = 0$

$Y_{p_\phi} = .5(T_L s + 1)e^{-.35}$

$Y_{p_\psi} = 0$

FIGURE 33 **CONFIGURATION** F-5
LEAD VARIATION

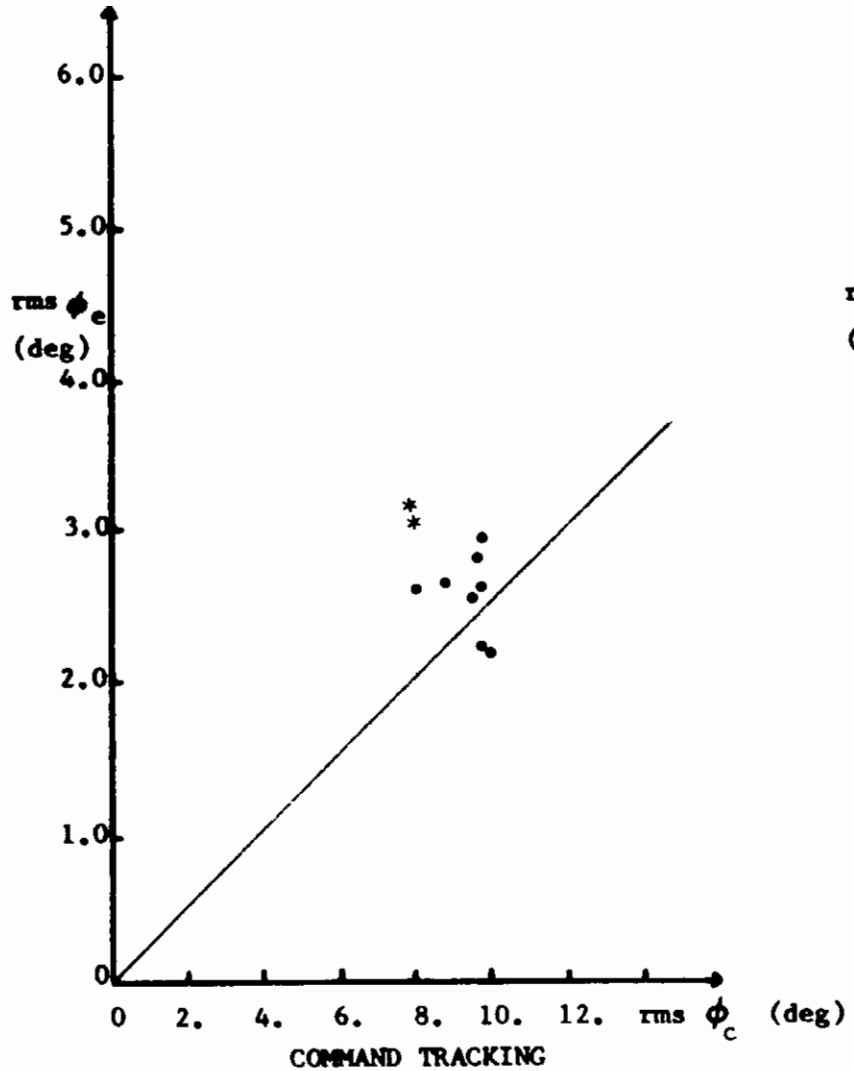

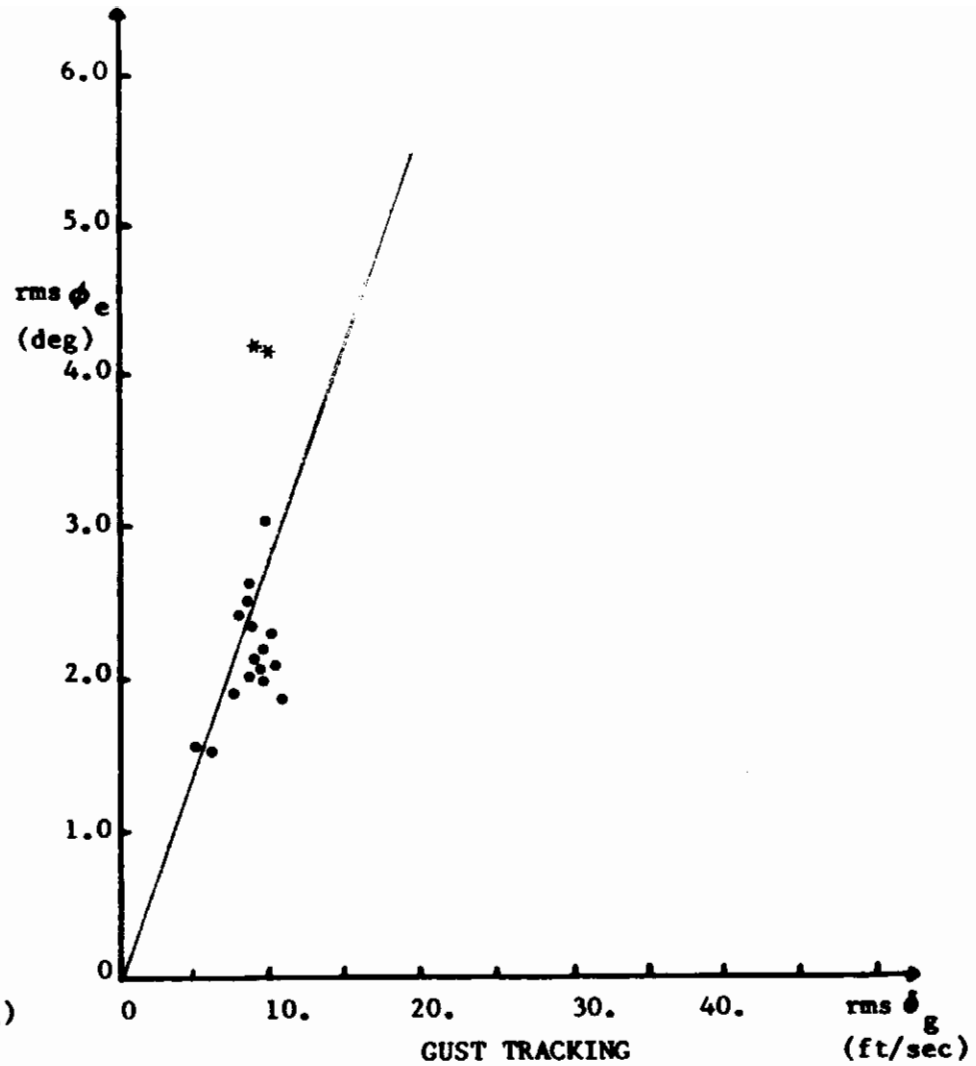

FIGURE 34 F-5 ROLL TASK SIMULATION

• measured * fixed base

—— predicted

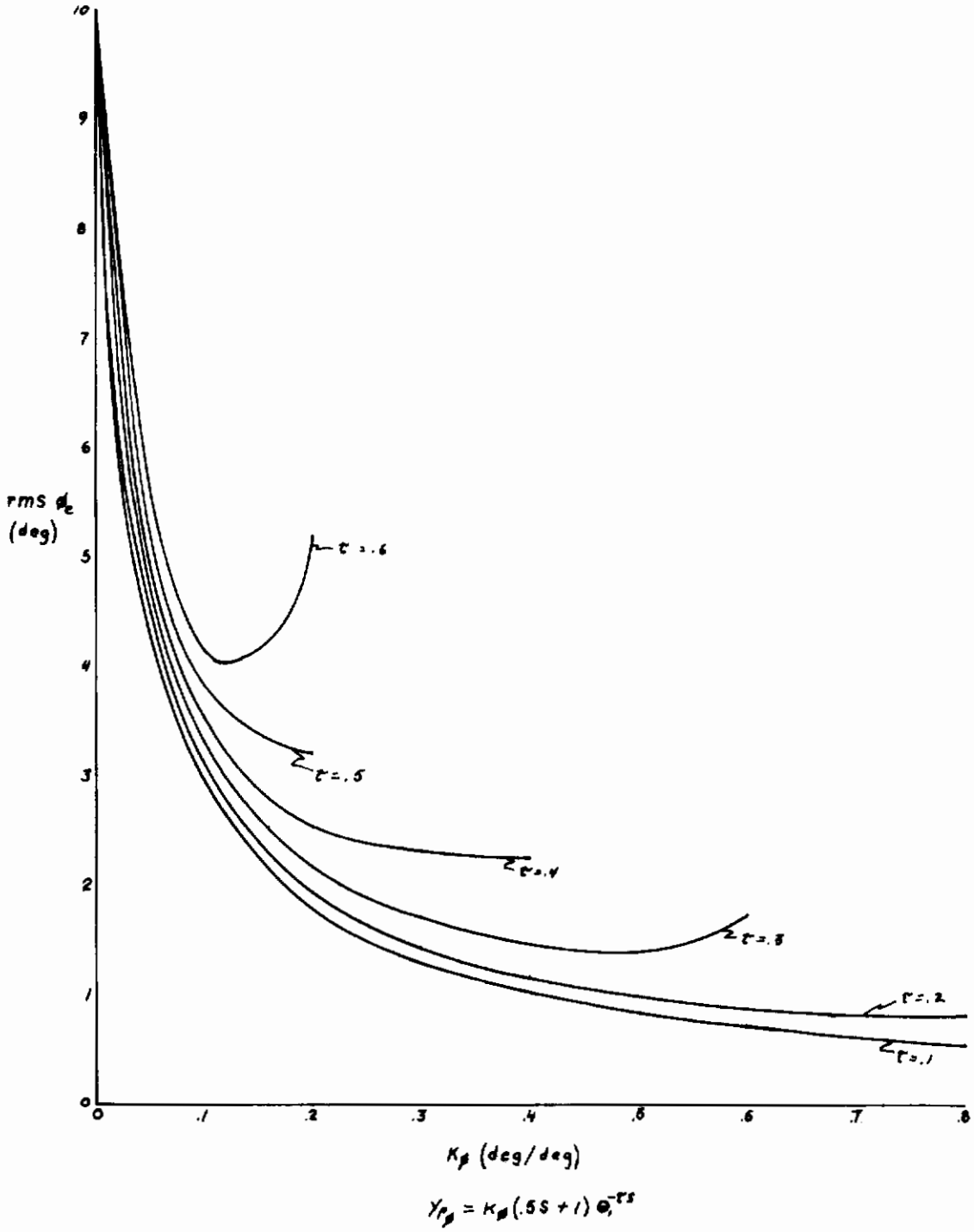

FIGURE 35 F-5 DELAY VARIATION

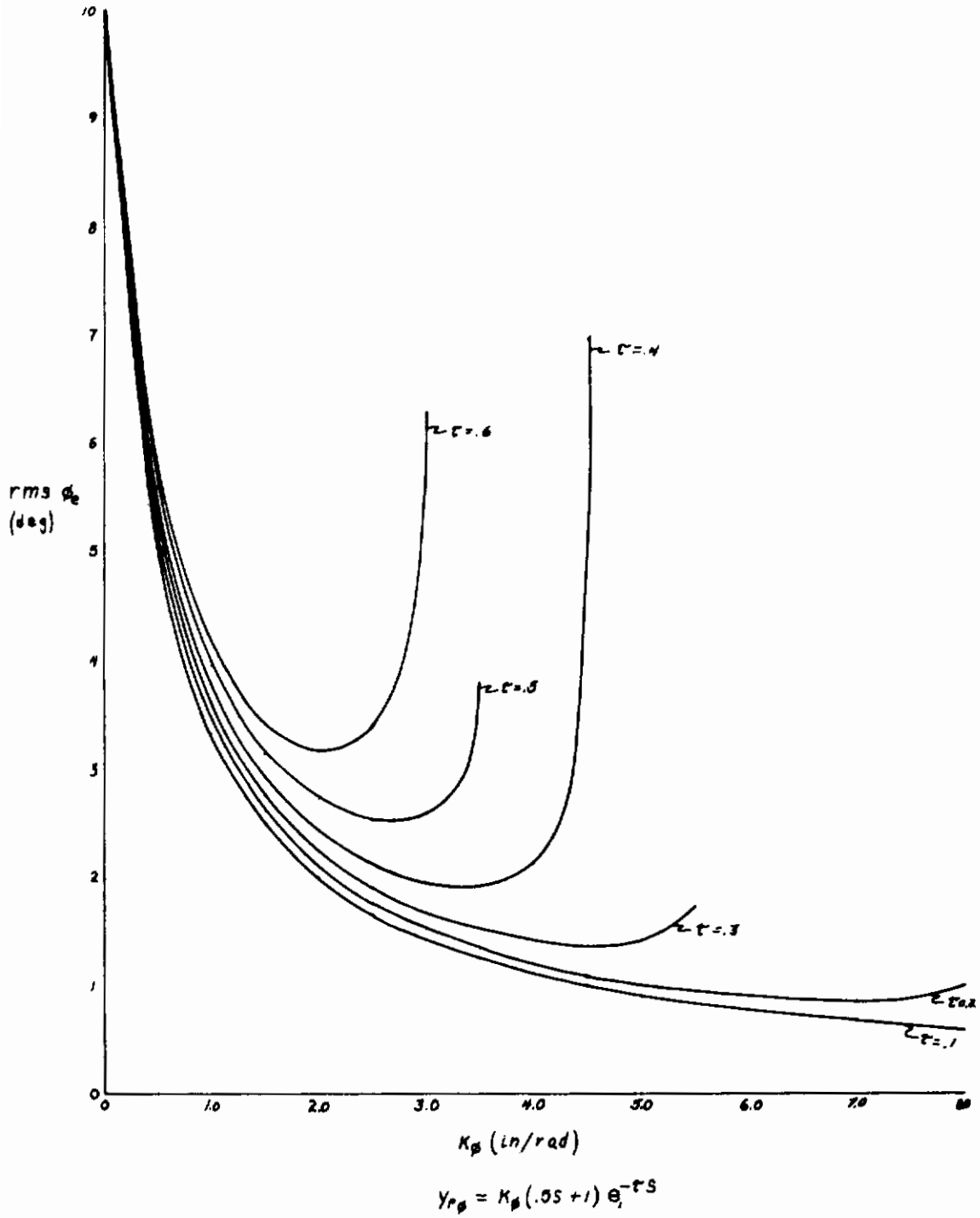

FIGURE 36 T-33 AB-2.6 DELAY VARIATION

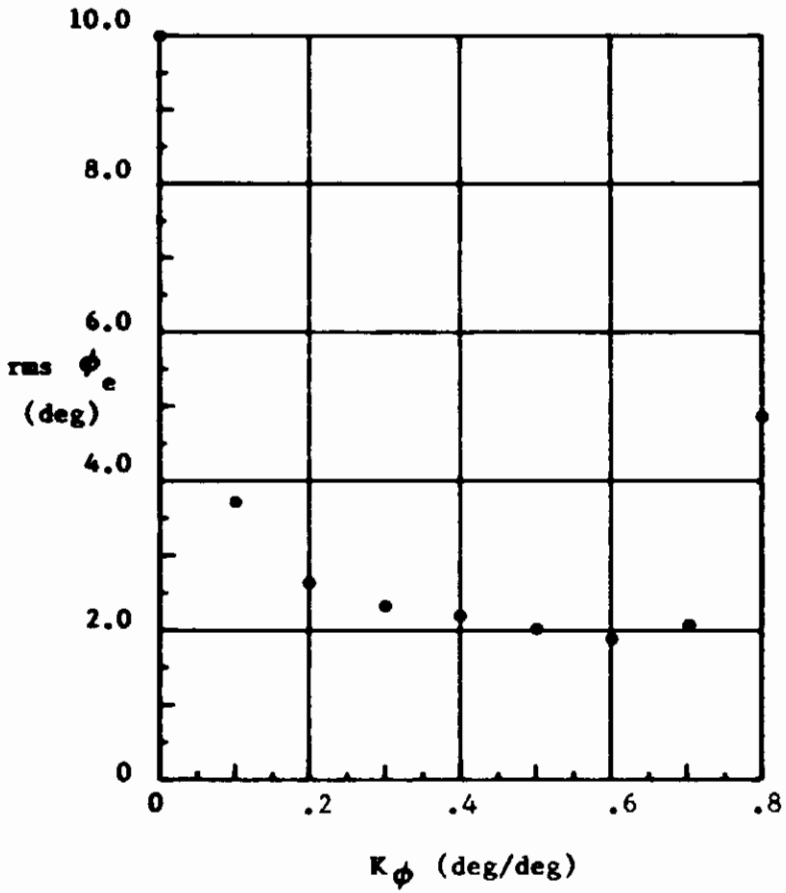

COMMAND TRACKING
RMS COMMAND INPUT = 10°

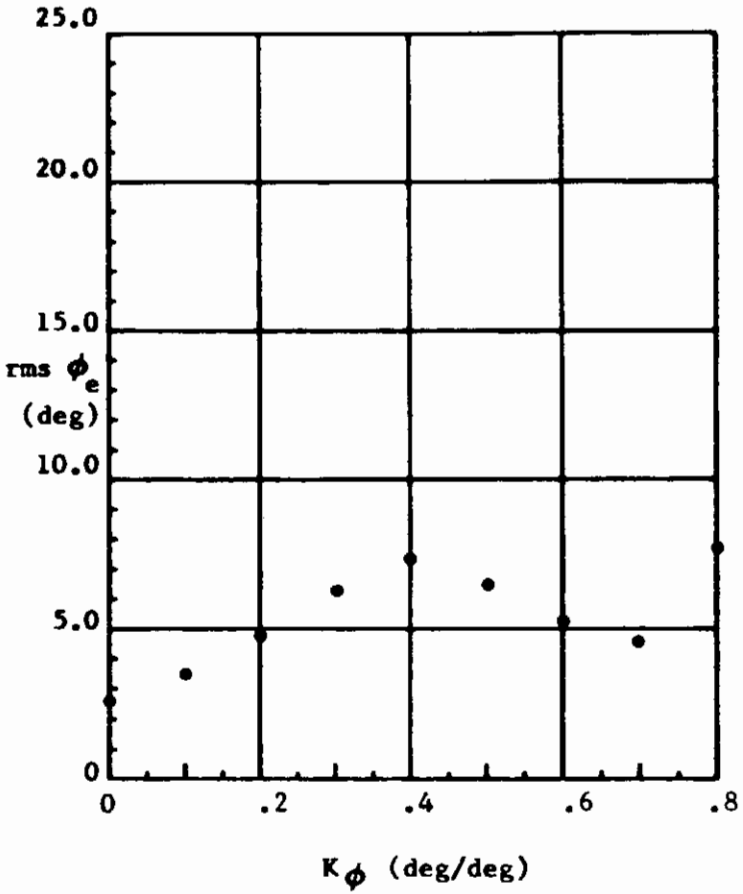

GUST TRACKING
RMS GUST INPUT LEVEL = 10 fps

Pilot Models

$$Y_{p_\beta} = 0$$

$$Y_{p_\phi} = K_\phi (.3S + 1) e^{-.3S}$$

$$Y_{p_\psi} = 0$$

FIGURE 37 **CONFIGURATION** *F-5*

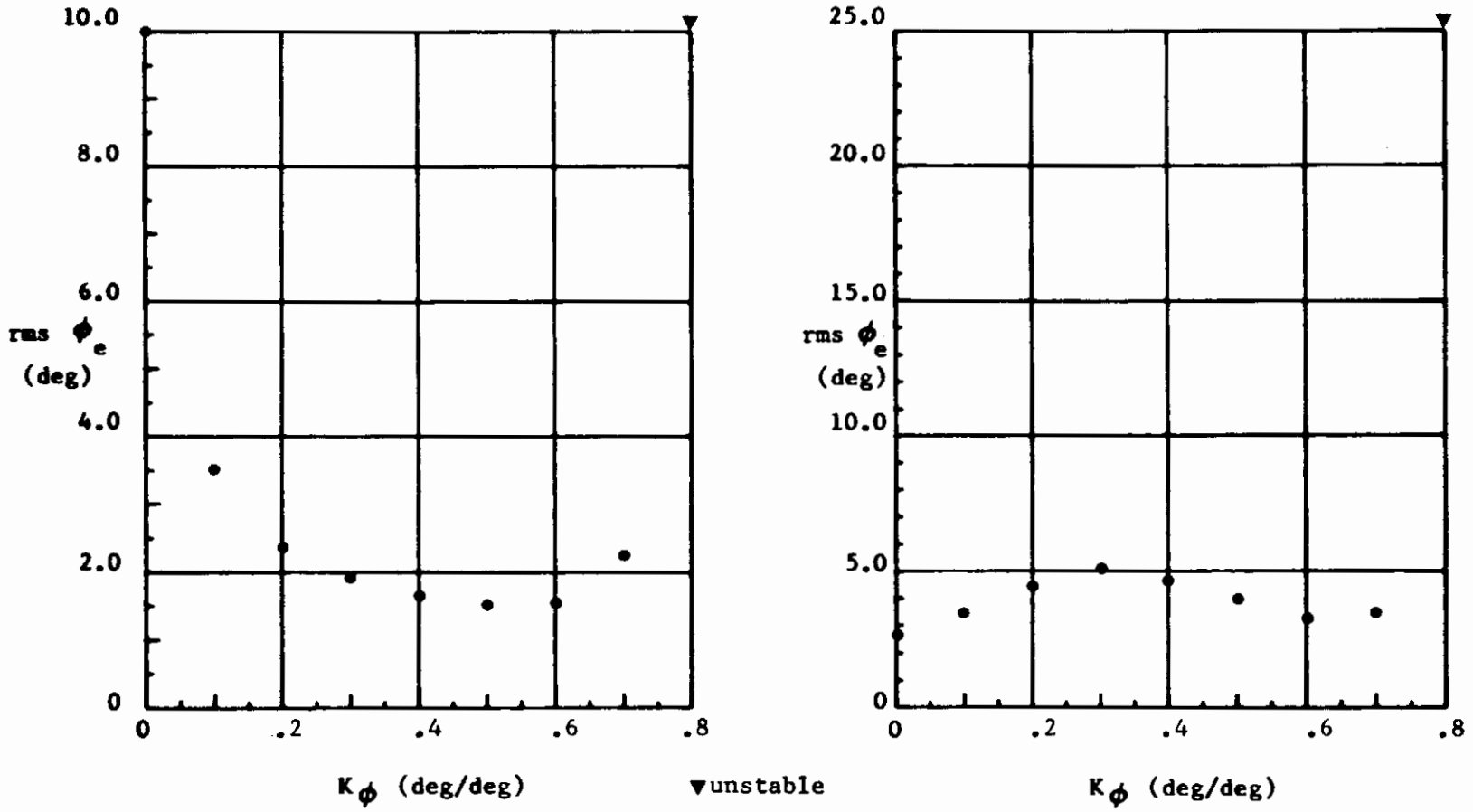

COMMAND TRACKING
RMS COMMAND INPUT = 10°

GUST TRACKING
RMS GUST INPUT LEVEL = 10 fps

Pilot Models

$$Y_{p_\beta} = 0$$

$$Y_{p_\phi} = K_\phi (.4s + 1) e^{-.3s}$$

$$Y_{p_\psi} = 0$$

FIGURE 38 **CONFIGURATION** *F-5*

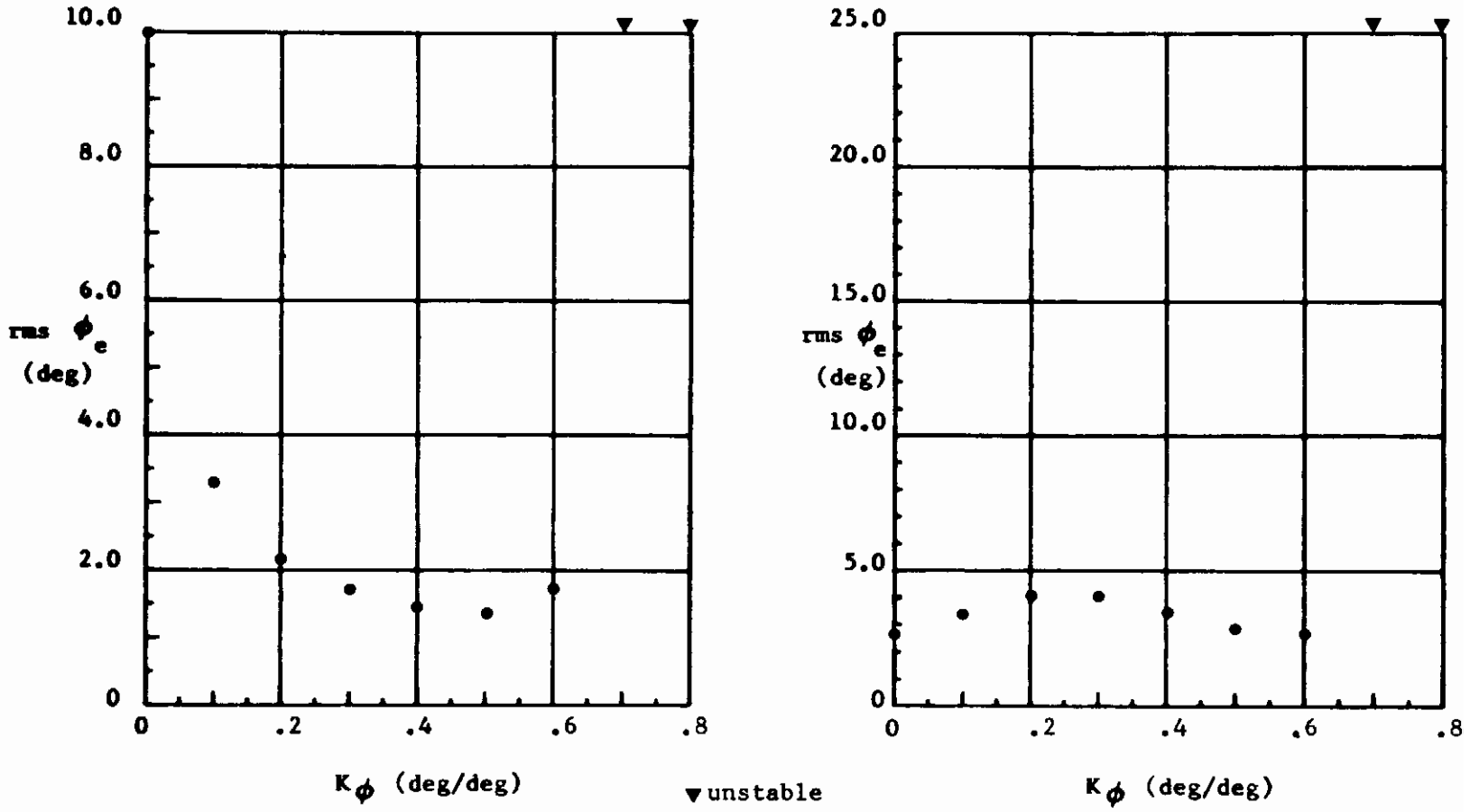

COMMAND TRACKING
RMS COMMAND INPUT = 10°

GUST TRACKING
RMS GUST INPUT LEVEL = 10 fps

Pilot Models

$$Y_{p_\beta} = 0$$

$$Y_{p_\phi} = K_\phi(.5s+1)e^{-.3s}$$

$$Y_{p_\psi} = 0$$

FIGURE 39 **CONFIGURATION** *F-5*

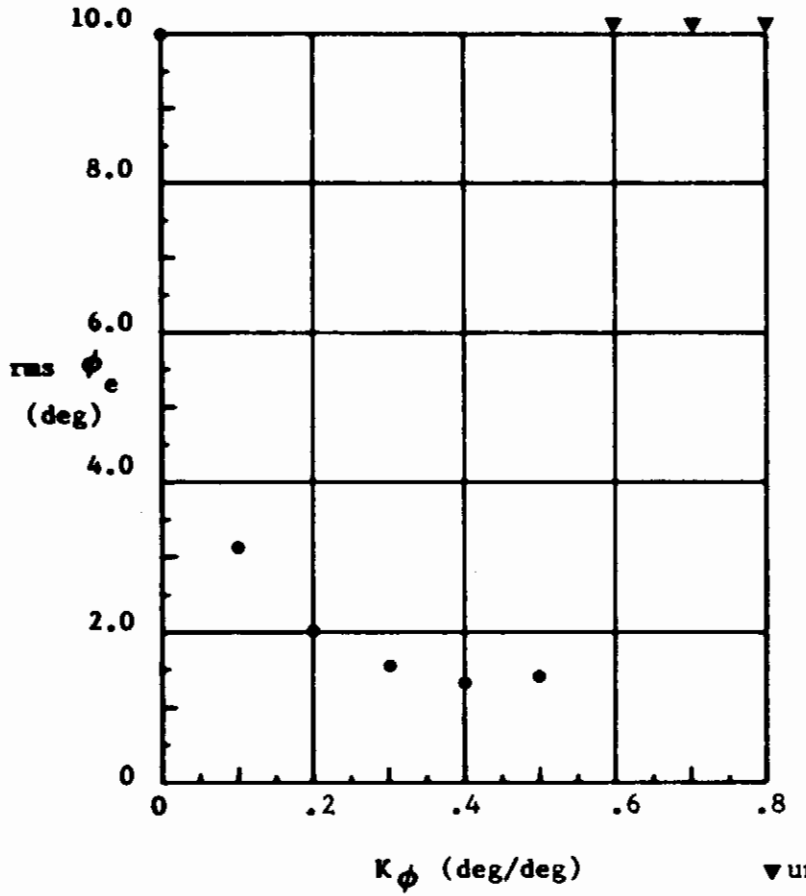

COMMAND TRACKING
RMS COMMAND INPUT = 10°

▼unstable

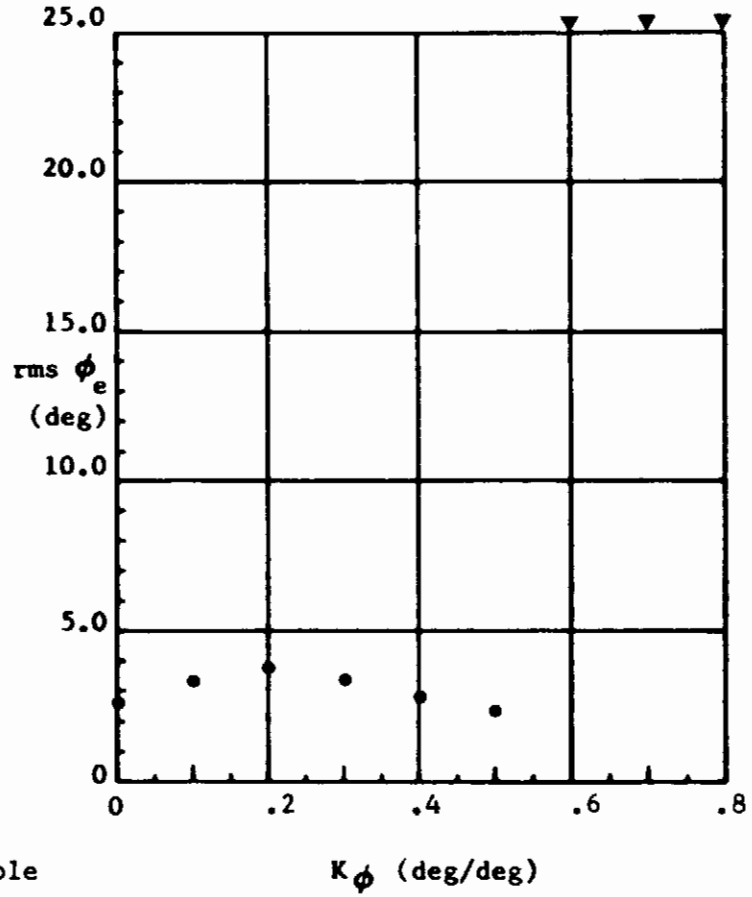

GUST TRACKING
RMS GUST INPUT LEVEL = 10 fps

Pilot Models

$$Y_{p_\beta} = 0$$

$$Y_{p_\phi} = K_\phi (.6S + 1) e^{-.3S}$$

$$Y_{p_\psi} = 0$$

FIGURE 40 **CONFIGURATION** *F-5*

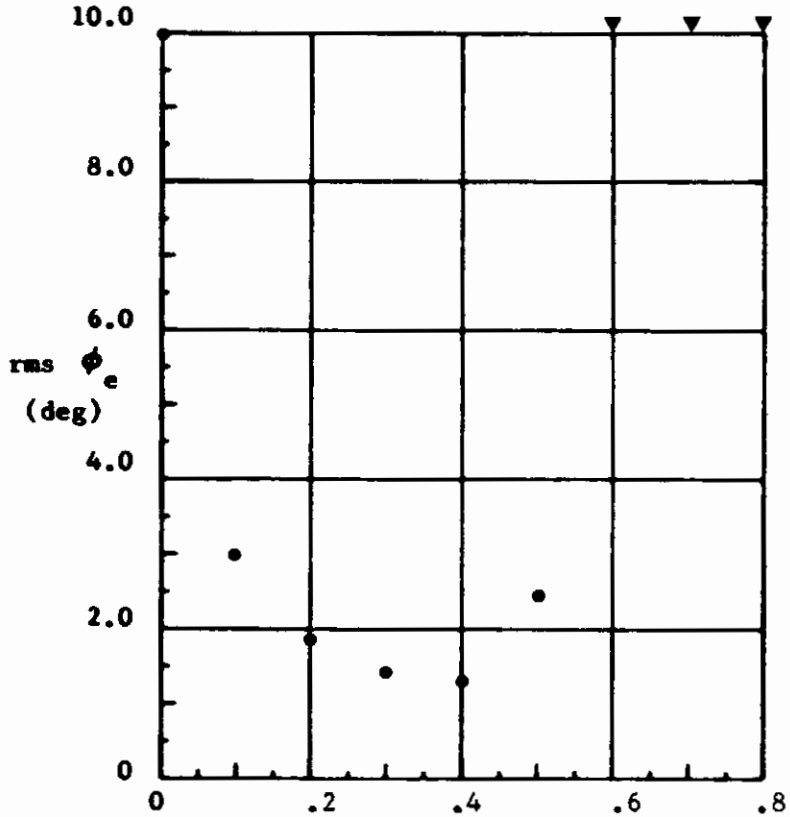

COMMAND TRACKING
RMS COMMAND INPUT = 10°

▼unstable

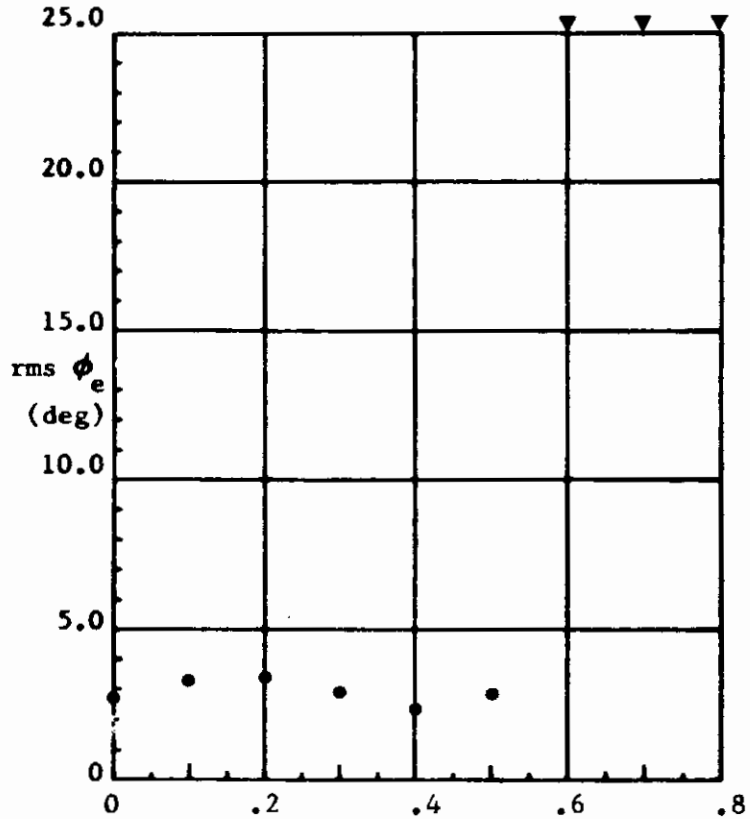

GUST TRACKING
RMS GUST INPUT LEVEL = 10 fps

Pilot Models

$$Y_{p_\beta} = 0$$

$$Y_{p_\phi} = K_\phi (.7s + 1)\, e^{-.3s}$$

$$Y_{p_\psi} = 0$$

FIGURE 41 **CONFIGURATION** *F-5*

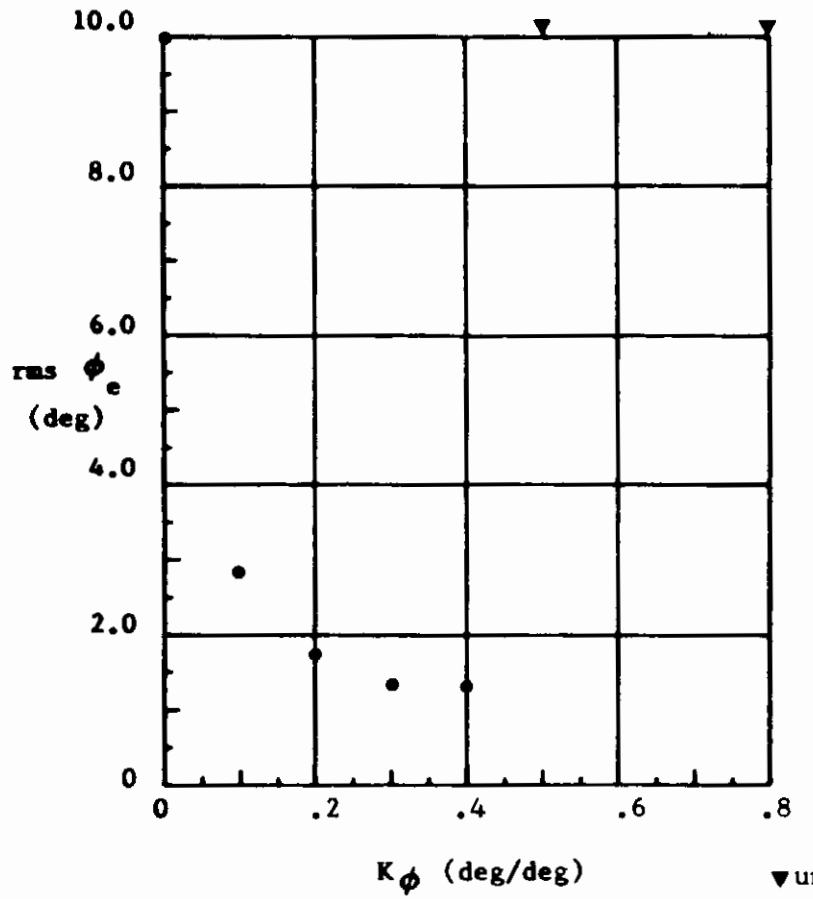

COMMAND TRACKING
RMS COMMAND INPUT = 10°

▼unstable

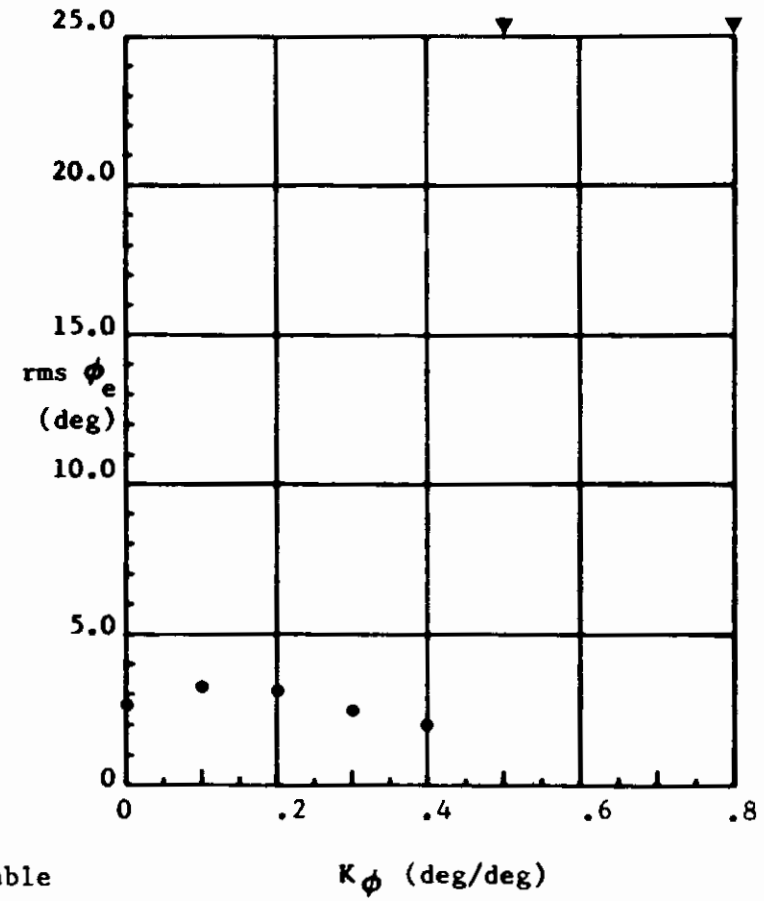

GUST TRACKING
RMS GUST INPUT LEVEL = 10 fps

Pilot Models

$$Y_{p_\beta} = 0$$

$$Y_{p_\phi} = K_\phi (.8s + 1) e^{-.35s}$$

$$Y_{p_\psi} = 0$$

FIGURE 42 **CONFIGURATION** *F-5*

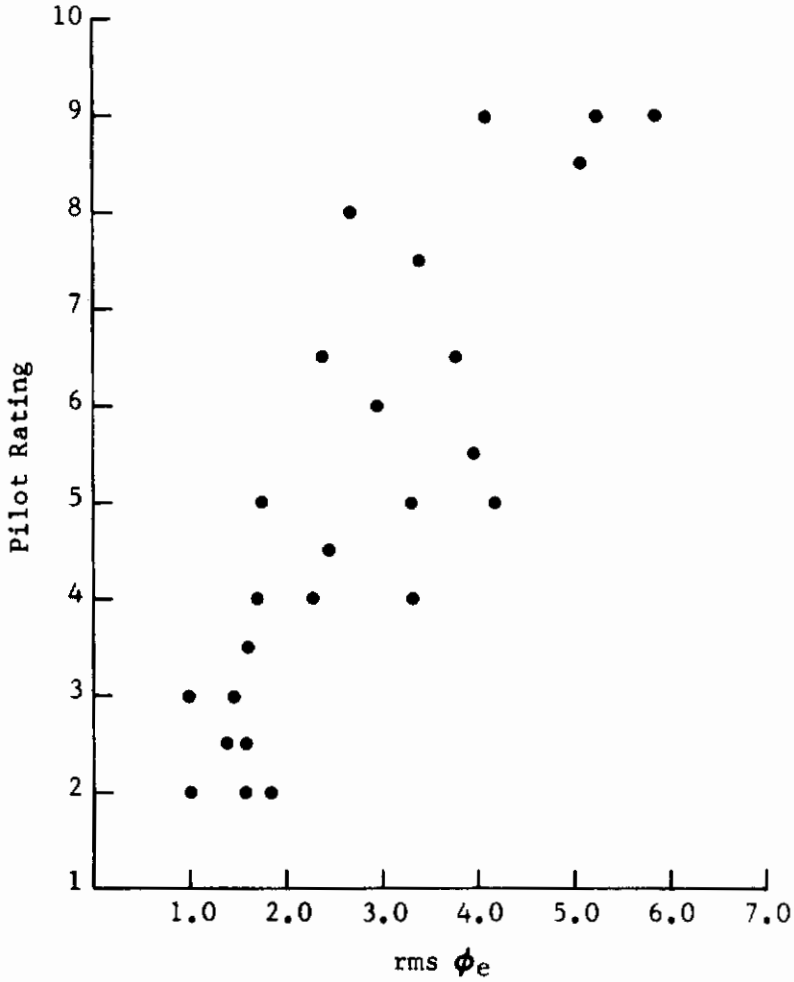

FIGURE 43 PILOT RATING vs BANK ANGLE ERROR FOR GUST RESPONSE

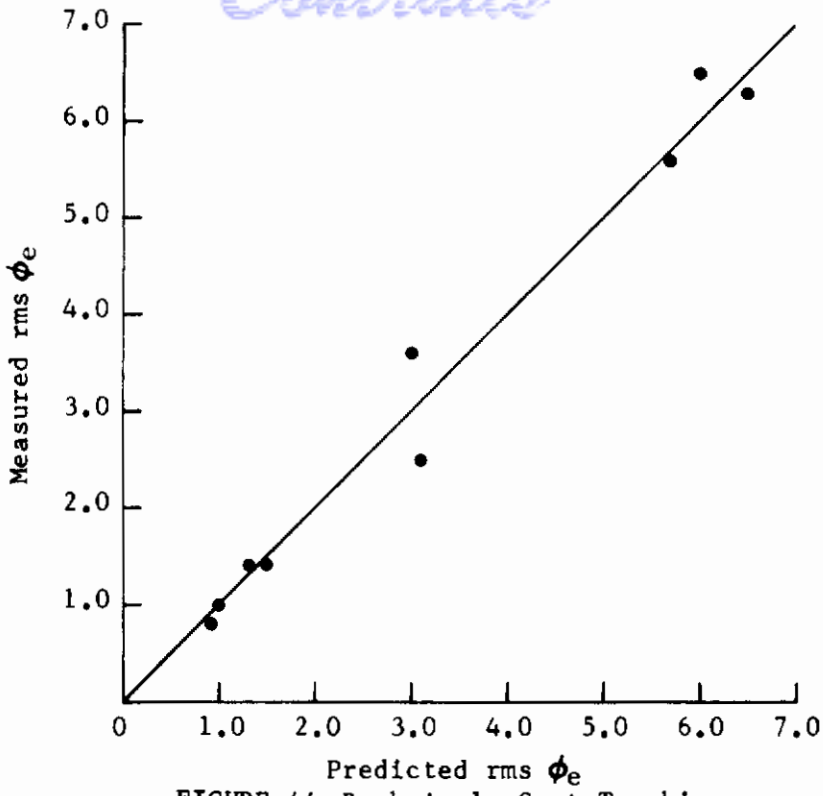

FIGURE 44 Bank Angle Gust Tracking

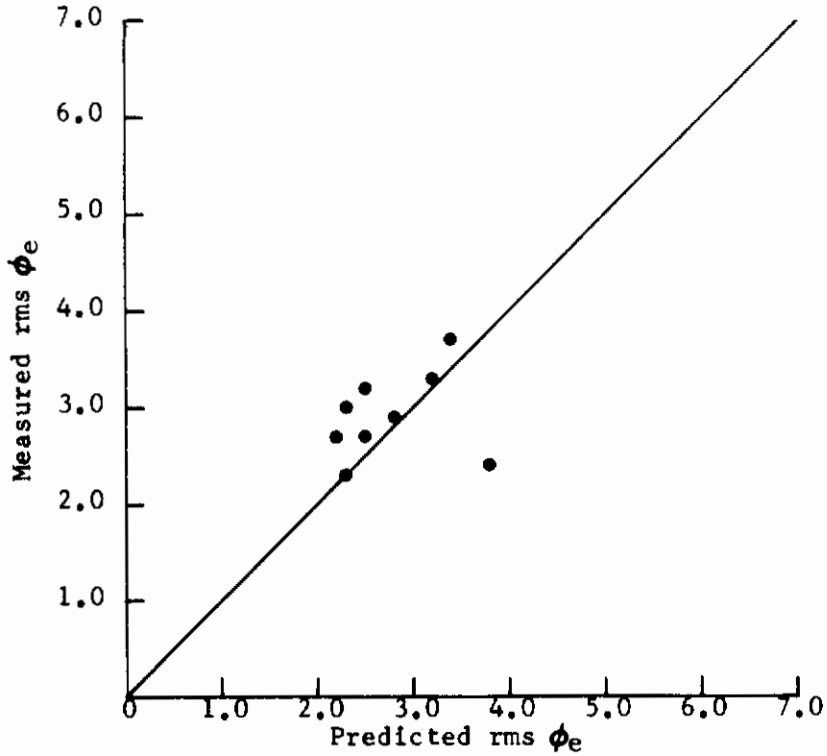

FIGURE 45 Bank Angle Command Tracking

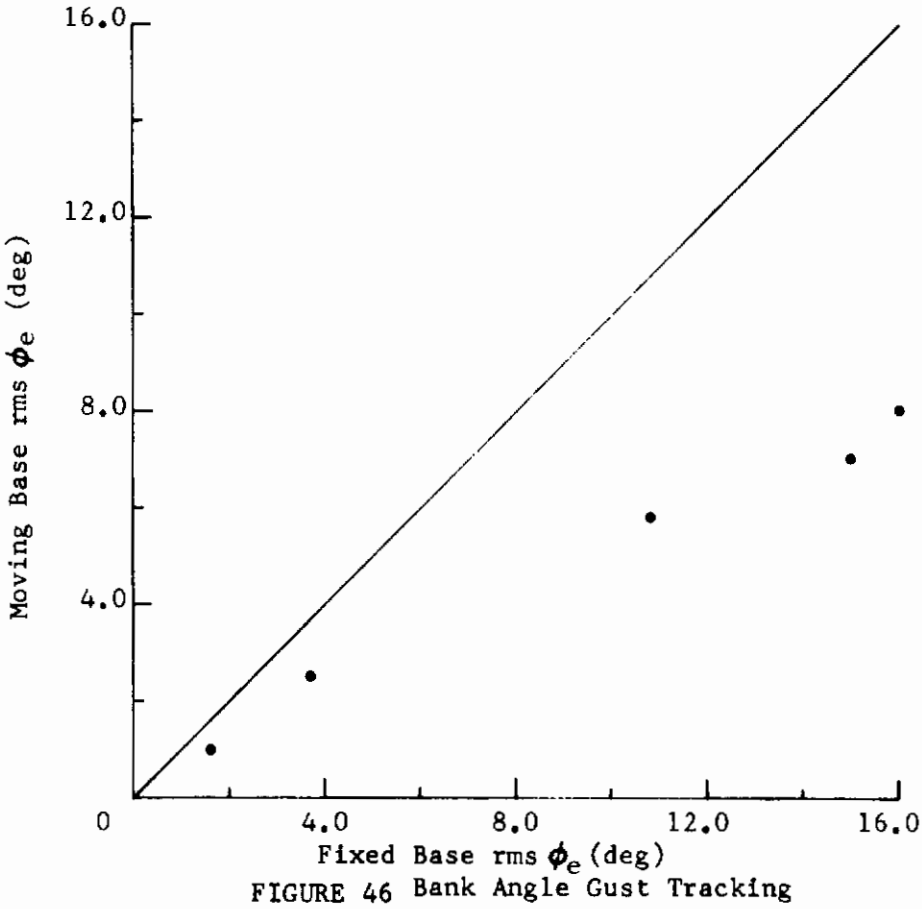

FIGURE 46 Bank Angle Gust Tracking

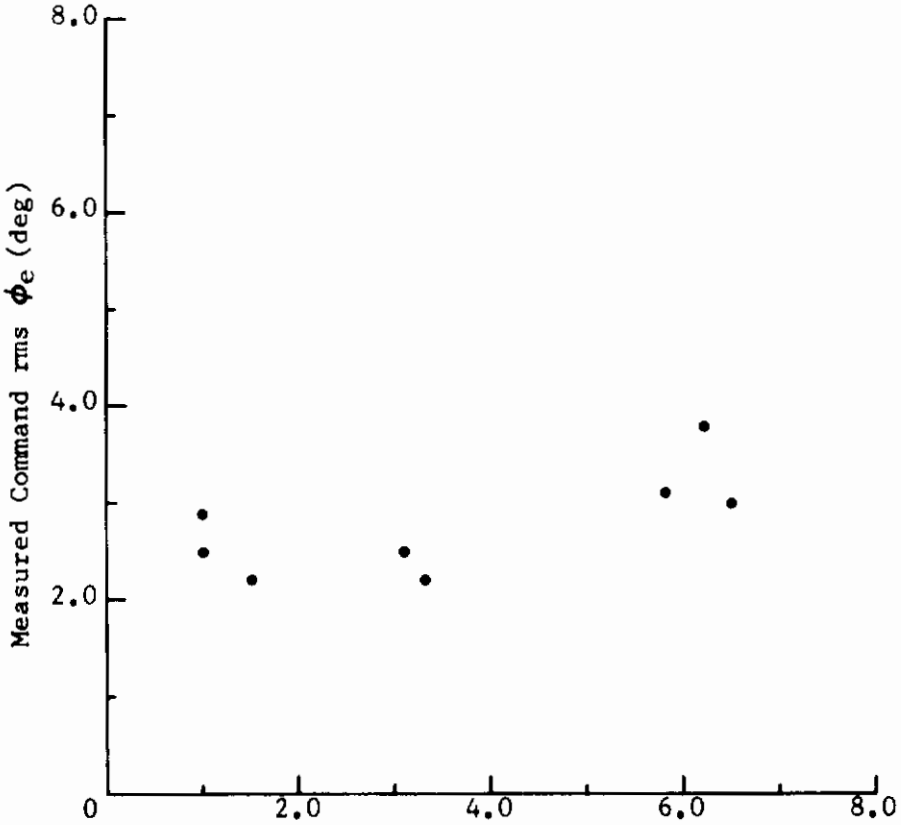

FIGURE 47 Command Tracking vs Gust Tracking

horizontal in the T_L direction along the T_L curve near .5 seconds. Thus, the optimum K_ϕ and T_L used for the F-5 prediction is near optimum for the system. In this way the gain and lead variation prediction graphs are cross sections of the rms ϕ_e surface at the prediction point of T_L and τ, and can be used to determine the changes in T_L and K_ϕ which will move the prediction point closer to the optimum. A modification of this has been used by Anderson and Dillow to optimize with respect to the Anderson pilot rating index.

Since incorporation of gust or command tracking prediction methods into an Anderson formula depends on a strong linear correlation between pilot rating and rms performance, a number of simulation flights were made to obtain pilot ratings. Configurations and turbulence levels were chosen randomly, and the pilot, W.W.K., rated the airplane on a Cooper scale. Twenty-five ratings were obtained and are shown in Figure 43. All configurations are represented in this data, and are usually repeated with different turbulence levels. A table of the performance and configuration for each pilot rating is found in Appendix III.

Two graphs showing predicted versus measured performance for all configurations in command and gust tracking are presented in Figures 44 and 45. They summarize the above cases, and each measured data point is the average of data corresponding to gust levels less than 15 ft/sec. These show the accuracy of the method over the range of predicted responses referenced to 10 ft/sec and 10° rms command tracking signal for all nine airplanes simulated.

In order to demonstrate the importance of both inertial acceleration pilot cues and moving base simulation for flying qualities in turbulence research, a number of flights were made fixed base. Some of this data has already been shown by asterisks in the simulation data graphs, but much of it was off scale. Figure 46 shows fixed base vs moving base averages for five configurations, AB2.6, AB3.3, BC2.2, BC2.3, and F-5. The agreement between fixed and moving base data is not good at low rms ϕ_e levels and becomes less so as this quantity increases.

Figure 47 shows a plot of measured command tracking rms ϕ_e vs gust tracking rms ϕ_e. Each data point represents one configuration and the data was normalized to a 10 ft/sec gust and a 10° tracking signal before averaging. The data points are distributed horizontally which shows that there is no significant correlation between performance of the airplanes in command tracking and in gust tracking. This establishes that flying qualities in turbulence and flying qualities in still air are uncorrelated aspects of airplane performance requiring separate criteria and analysis techniques.

The command tracking performance scores are in good agreement with numerical results reported for the crossover pilot model discussed in Section II. For example, Heifferon and Hannen (Reference 15) compute rms performance for a system having the form

$$Y_p Y_c = \frac{k}{s} e^{-\tau s}$$

tracking a randomly generated signal. They include data corresponding to a time delay of $\tau = .44$ sec and a tracking signal obtained by filtering white noise through the filter H (s) used in the bank angle study. If σ_T is the rms tracking signal level, then the crossover model predicts $\sigma_e/\sigma_T = .2$. The above analyses and simulation have resulted in rms ϕ_e values mainly between 2° and 3° for the rms command tracking signal of 10°. Thus, rms ϕ_e/rms ϕ_c ranges mainly between .2 and .3 so that the optimization procedure used here agrees nicely with the Heifferon and Hannen data on crossover pilot models when this model is applicable.

D. Heading Task Prediction

An analysis of the heading task was completed for the configurations chosen for simulation. The system models for command tracking and gust tracking are shown in Figure 4. Although a parallel bank angle and heading closure model has been used, series closures can equally well be computed by the multiloop analysis program. Some data is available for these series closures (Reference 16), but not a sufficient amount to show a clear superiority over the parallel closure model adopted here for simplicity.

Since the response is slower for heading than bank angle tasks, the breakpoint of the tracking command signal was lowered. The filter used to generate the command signal is represented by

$$H(s) = \frac{K}{(s + .2)^2} \qquad (26)$$

and the difference between the commanded heading and the actual heading was presented on the bank steering bar of the ADI.

Since two axes and two pilot models are involved in the heading task, the time delay τ was increased to $\tau = .45$ seconds (Reference 17) for the turbulence task. This was used in both ϕ and ψ pilot models. The multiloop program was modified to automatically perform a perturbation of the gains K_ϕ and K_ψ. The lowest rms ψ_e was then

regarded as the prediction for the quantities rms ψ_e, rms ϕ and rms β. These were all recorded during the simulation and the results are shown in Figure 48 through 66 where the line shows the predicted values. The command tracking time delay was also $\tau = .45$ seconds.

The accuracy of the multiloop pilot model predictions is good for the majority of configurations and the agreement of the rms values of all lateral control axes between the predictions and the simulation demonstrates the appropriateness of the multiloop pilot model, but the closeness of this agreement seems to depend on the yaw rate due to aileron inputs since pilot W.W.K. reported AB 3.1, AB 3.3 and BC 2.2 to have excessive aileron yaw.

Graphs showing predicted versus measured qualities for the turbulence heading task are shown in Figures 67, 68, and 69. These indicate that the multiloop prediction method agrees well with the simulation results, but, that the rms ψ_e performance levels in turbulence do not differ widely among the configurations. Thus, it is necessary to examine other parameters such as rms ϕ and rms β . Since rms yaw rate appears to be a factor, it should be included in future studies of heading tasks in turbulence. This quality can be computed using a slight modification of the multiloop analysis program and has been found to be important by other investigators, see Reference 13.

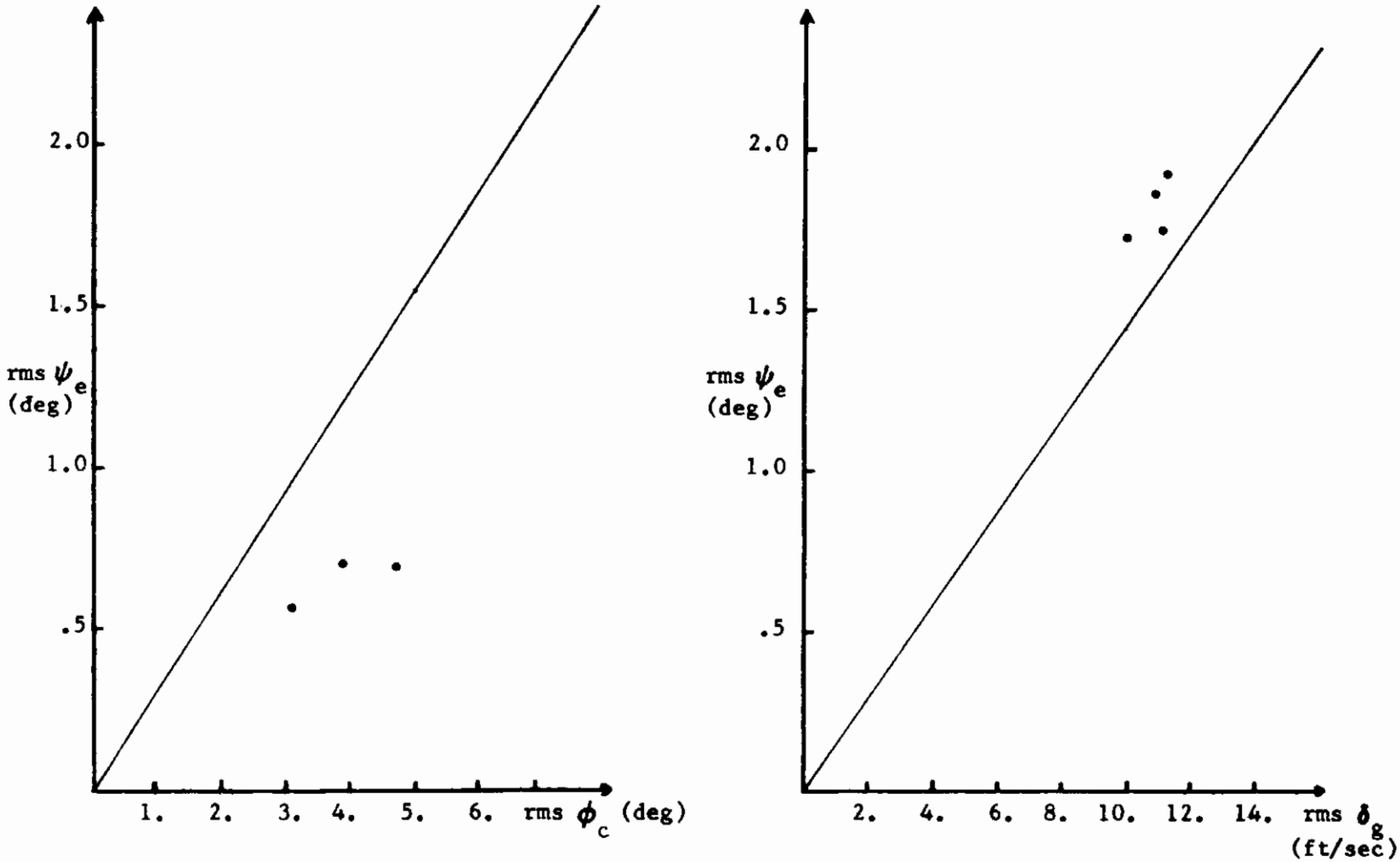

FIGURE 48 T-33 AB 2.6 HEADING TASK SIMULATION

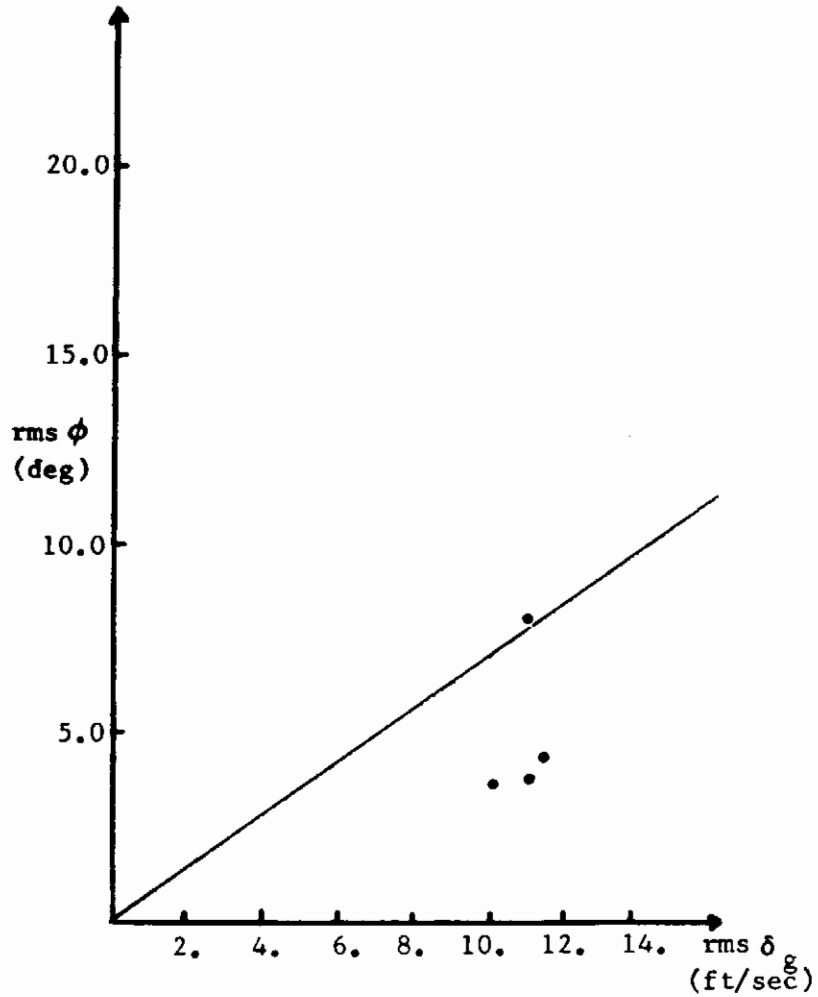

GUST TRACKING

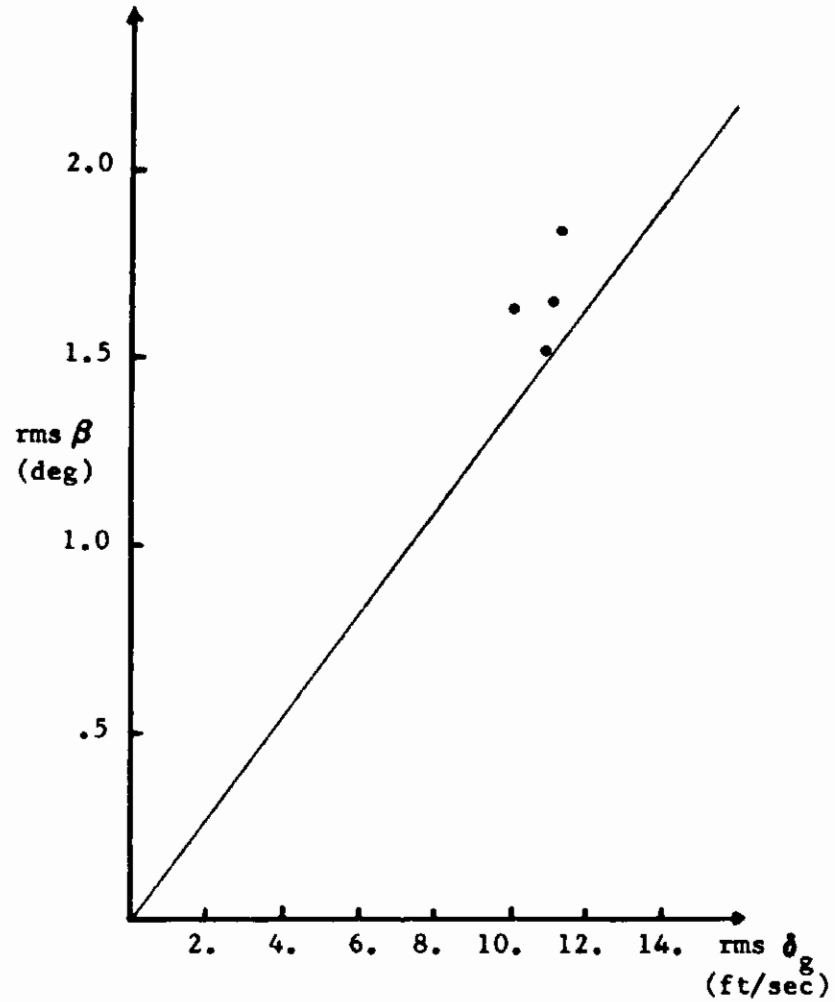

GUST TRACKING

FIGURE 49 T-33 AB 2.6 HEADING TASK SIMULATION

• measured

—— predicted

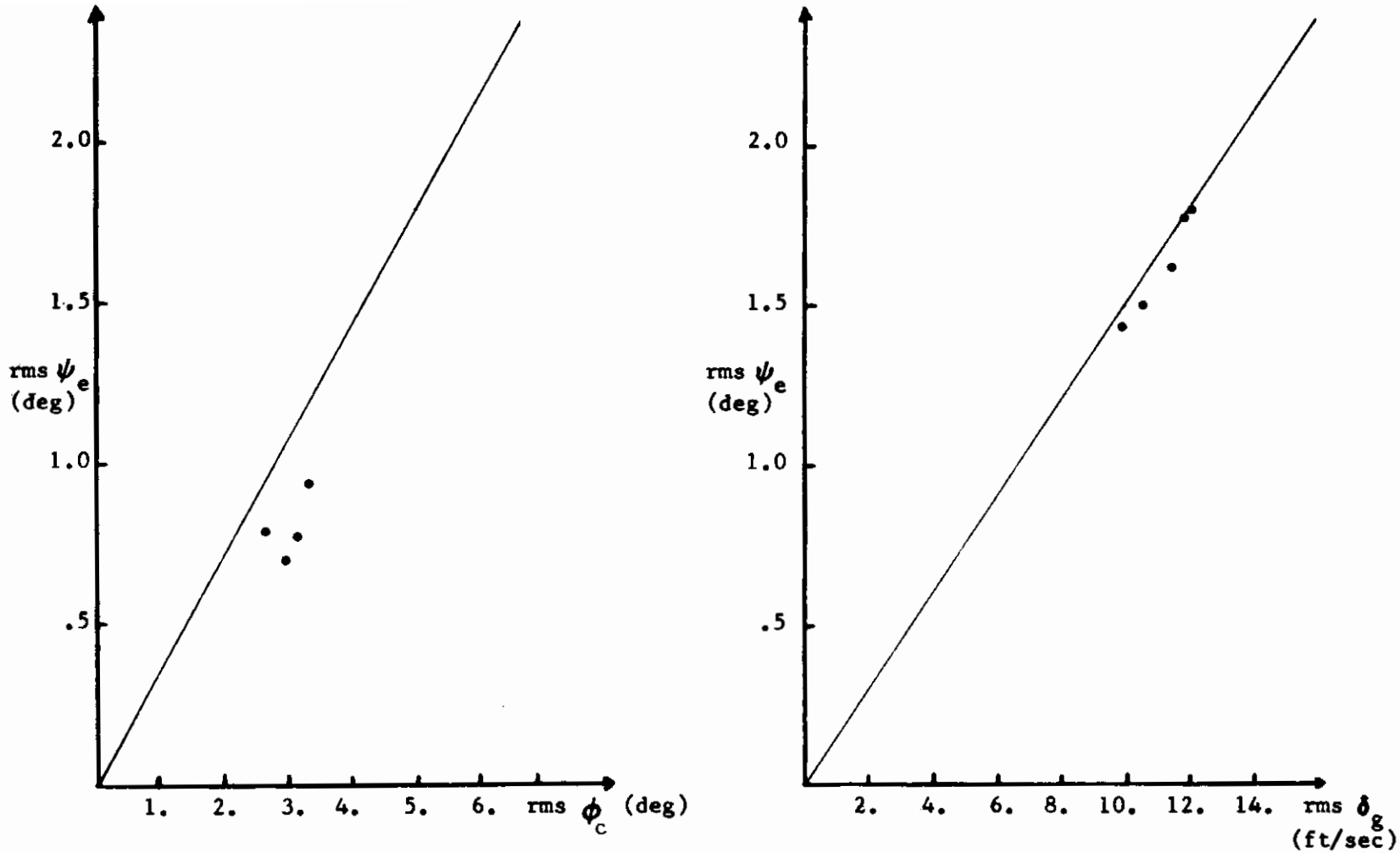

COMMAND TRACKING

GUST TRACKING

FIGURE 50 T-33 AB 2.7 HEADING TASK SIMULATION

• measured

—— predicted

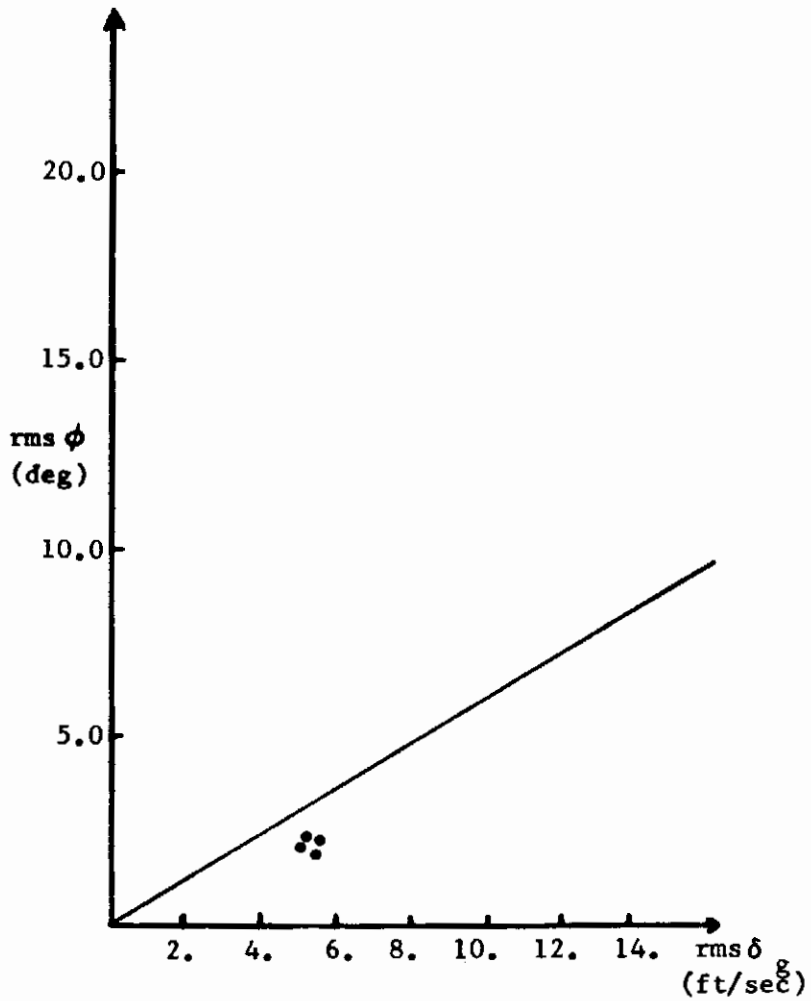

GUST TRACKING

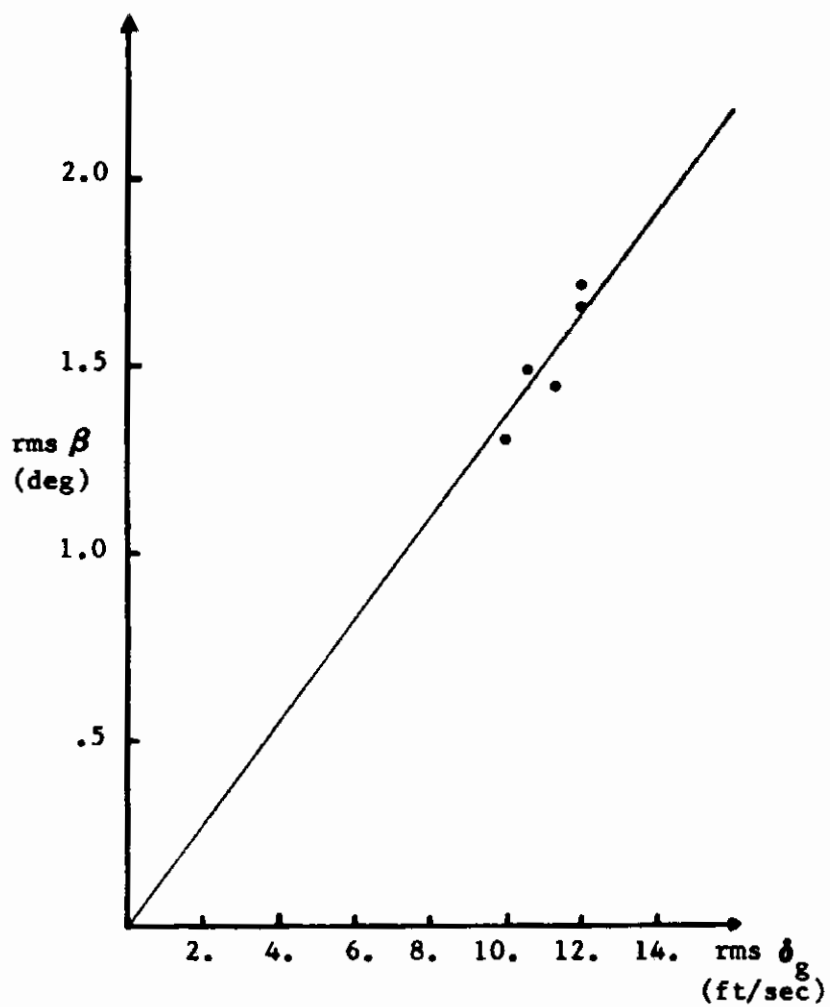

GUST TRACKING

FIGURE 51 T-33 AB 2.7 HEADING TASK SIMULATION

• measured

—— predicted

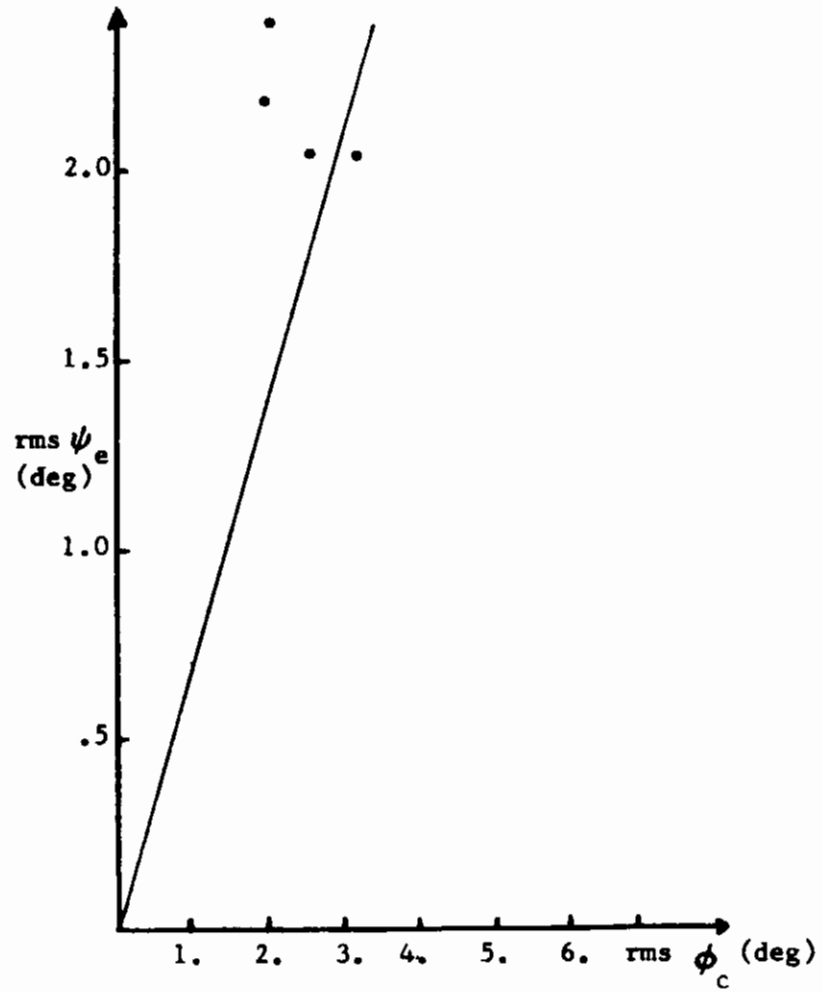

COMMAND TRACKING

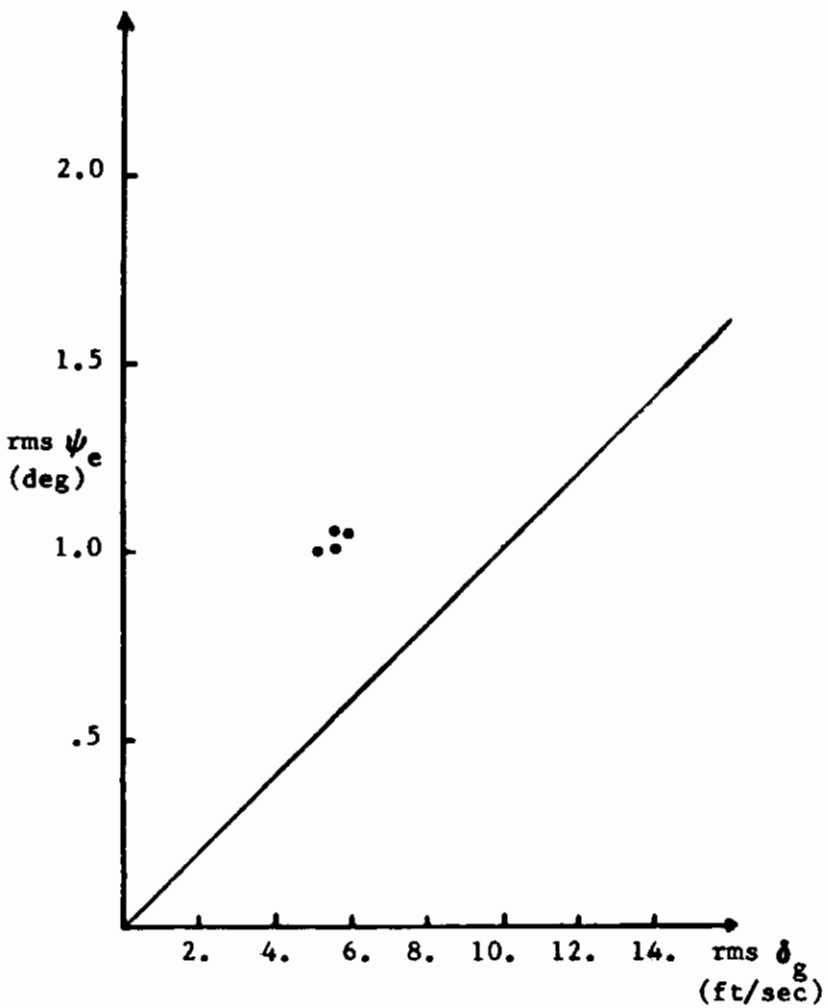

GUST TRACKING

FIGURE 52 T-33 AB 3.1 HEADING TASK SIMULATION

• measured

—— predicted

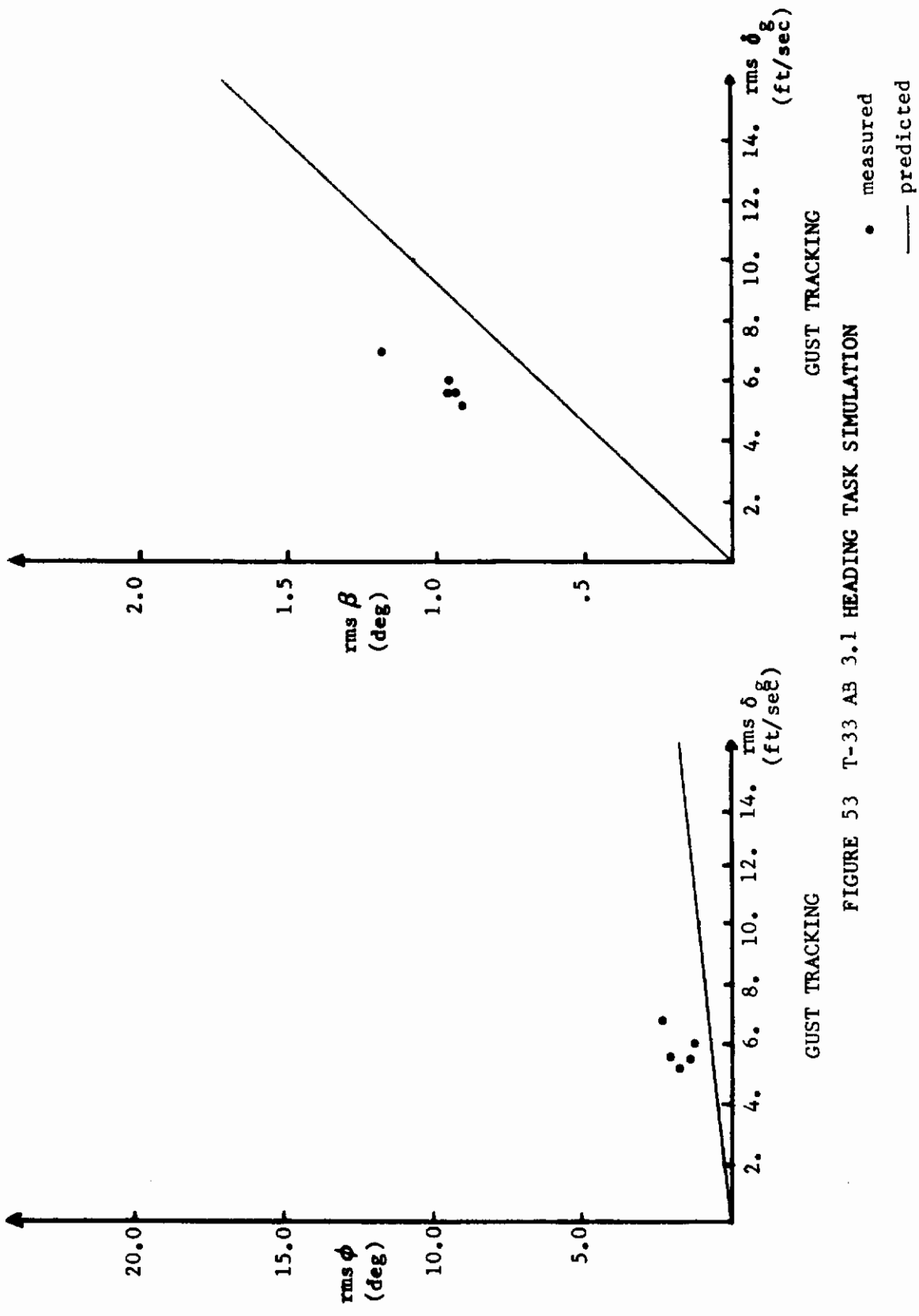

FIGURE 53 T-33 AB 3.1 HEADING TASK SIMULATION

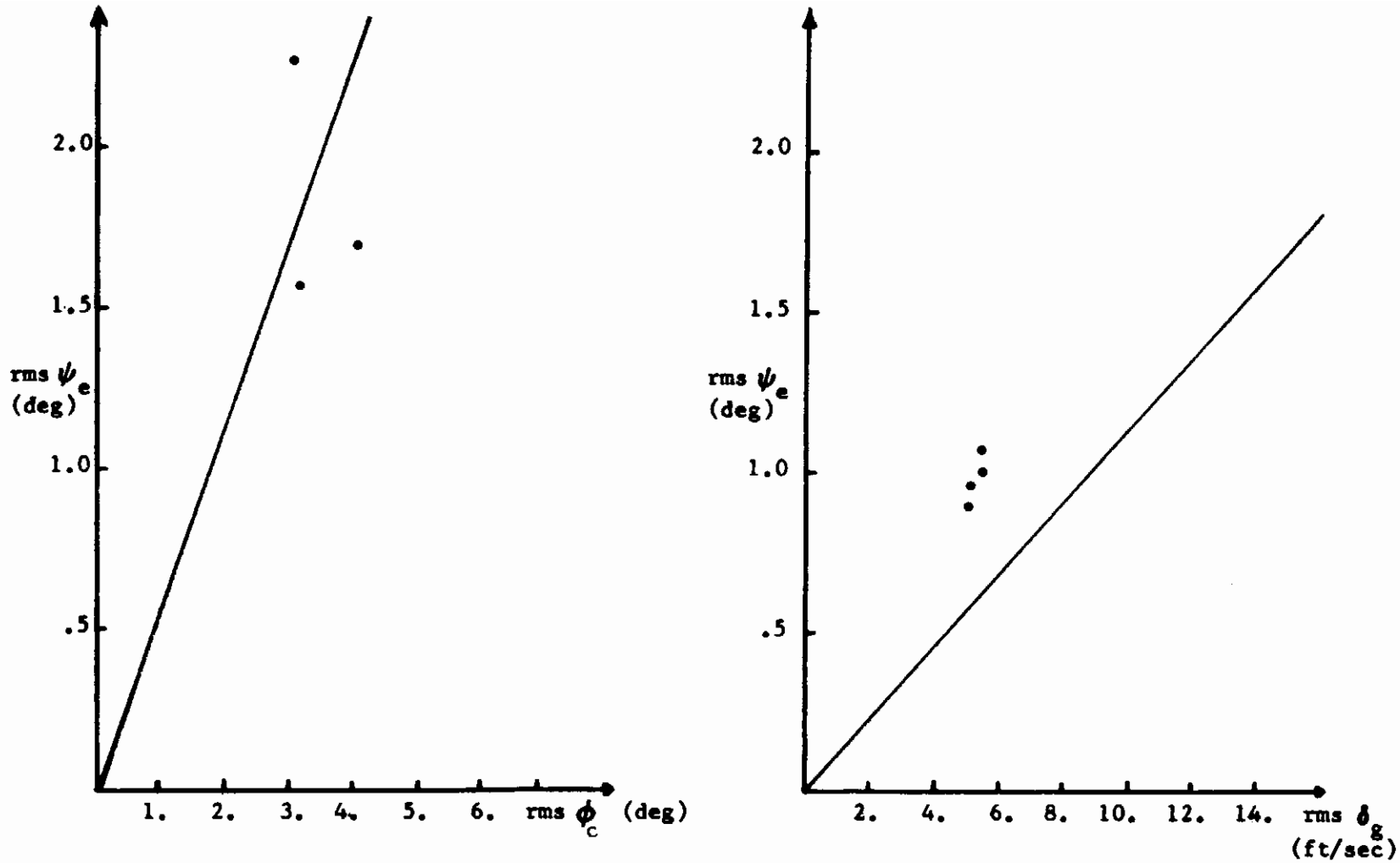

COMMAND TRACKING

GUST TRACKING

FIGURE 54 T-33 AB 3.3 HEADING TASK SIMULATION

• measured

—— predicted

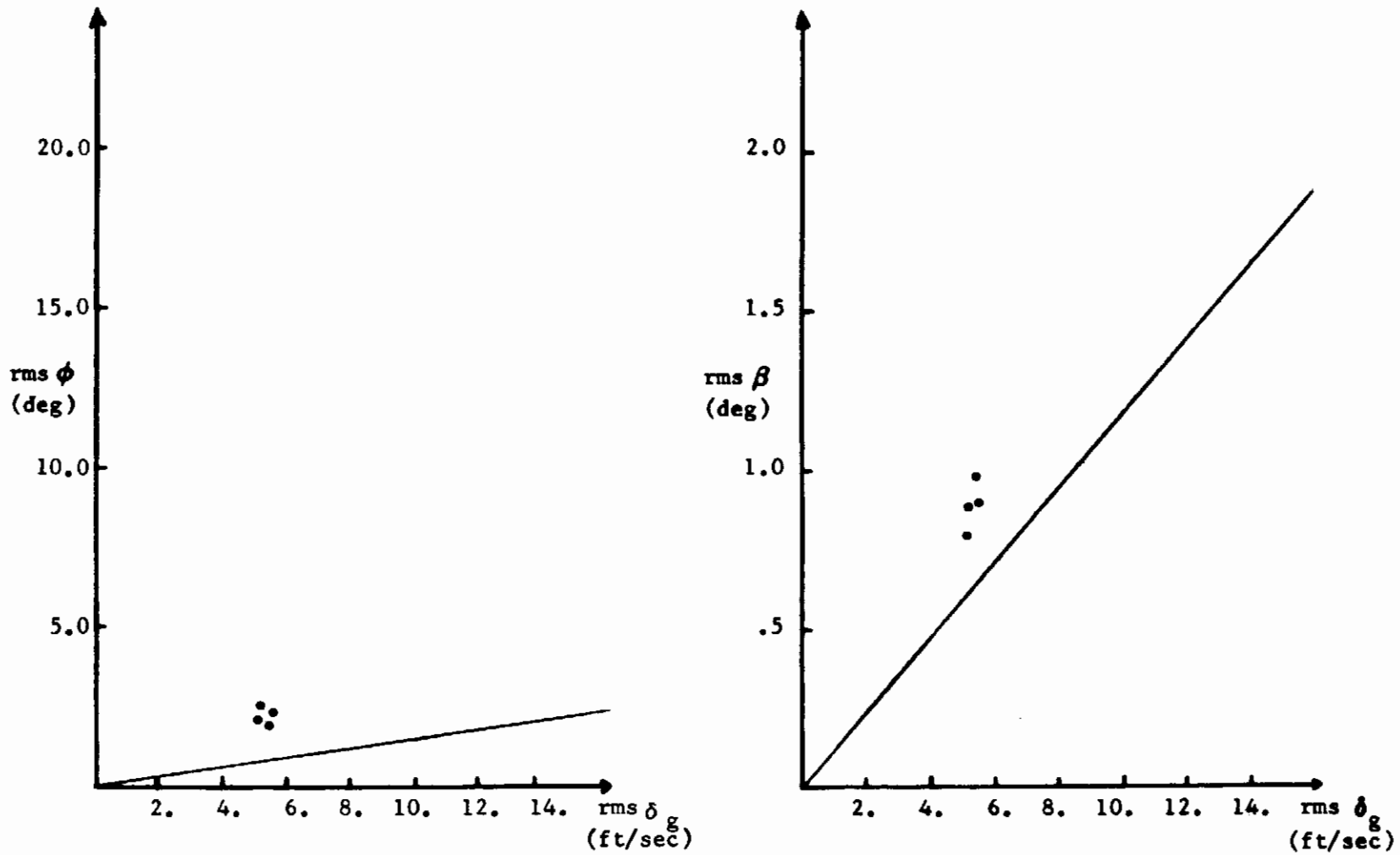

FIGURE 55 T-33 AB 3.3 HEADING TASK SIMULATION

• measured

——predicted

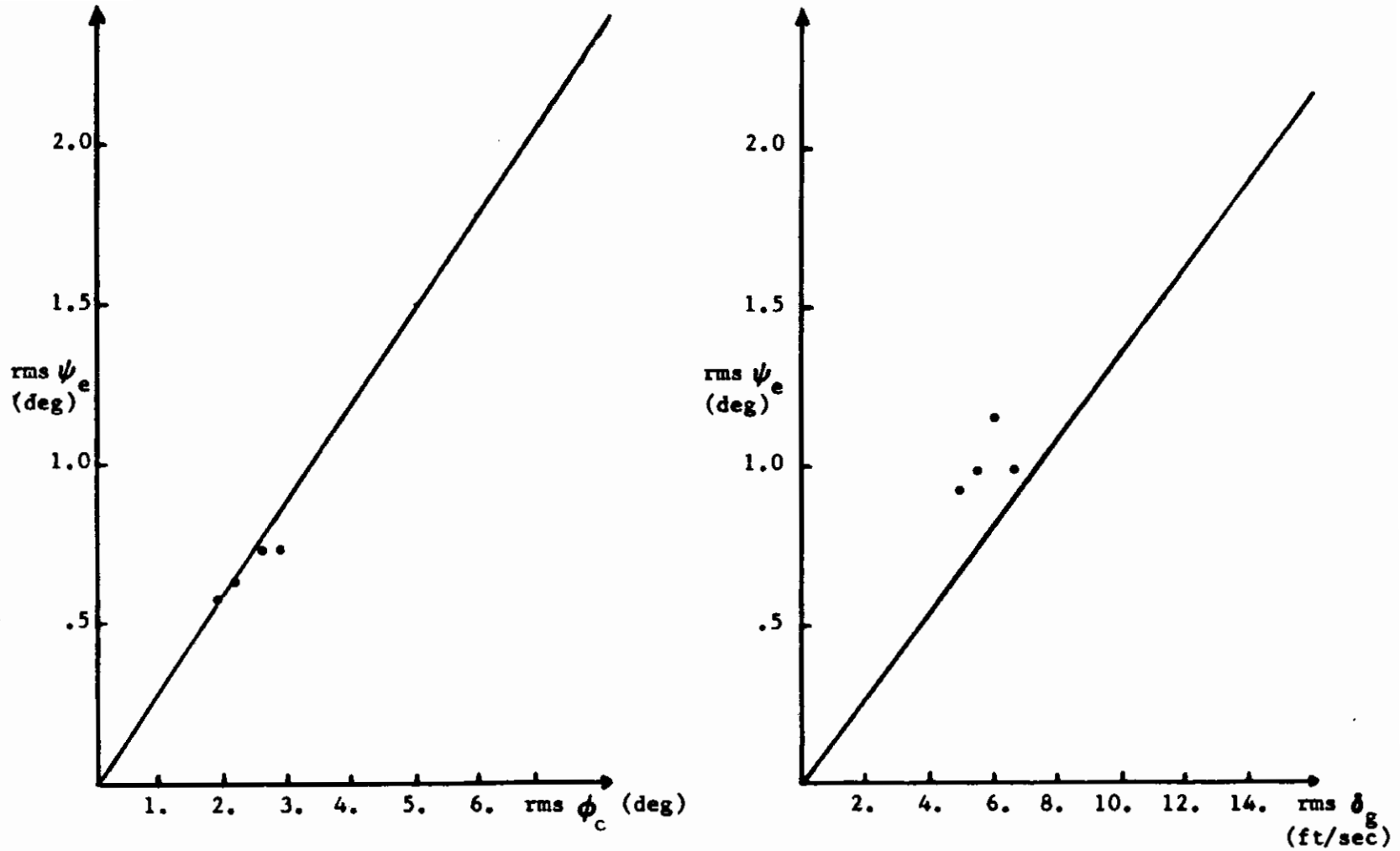

FIGURE 56 T-33 BB 2.3 HEADING TASK SIMULATION

• measured

—— predicted

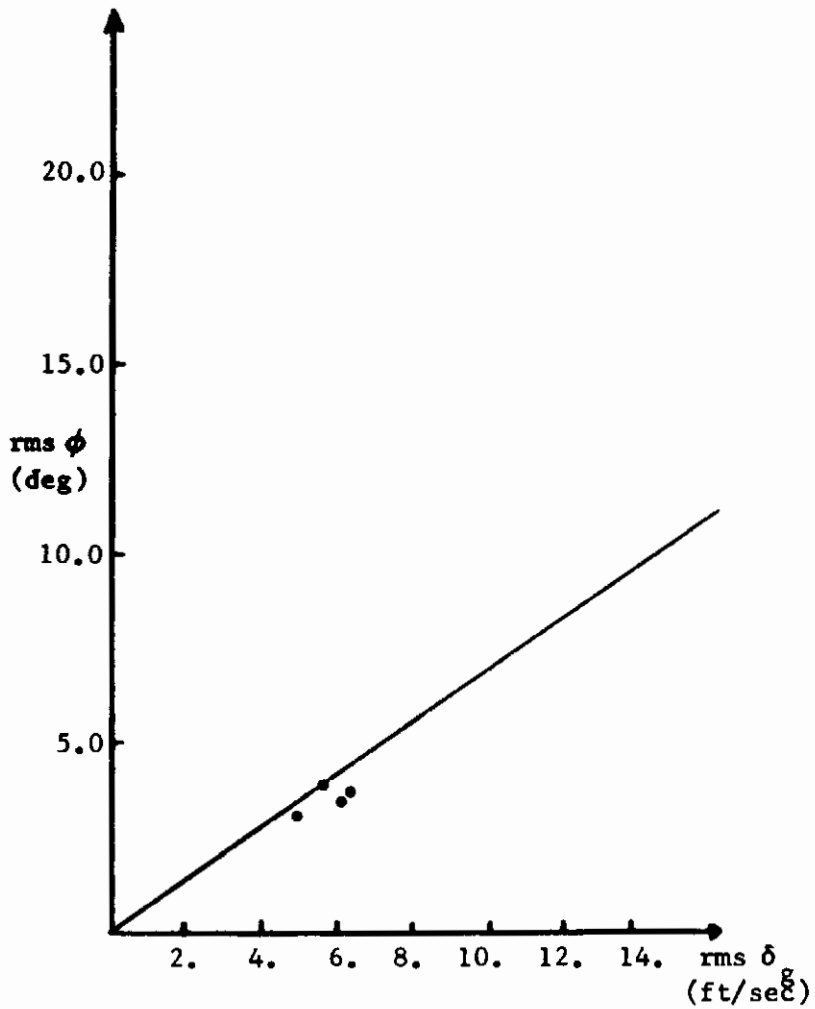

GUST TRACKING

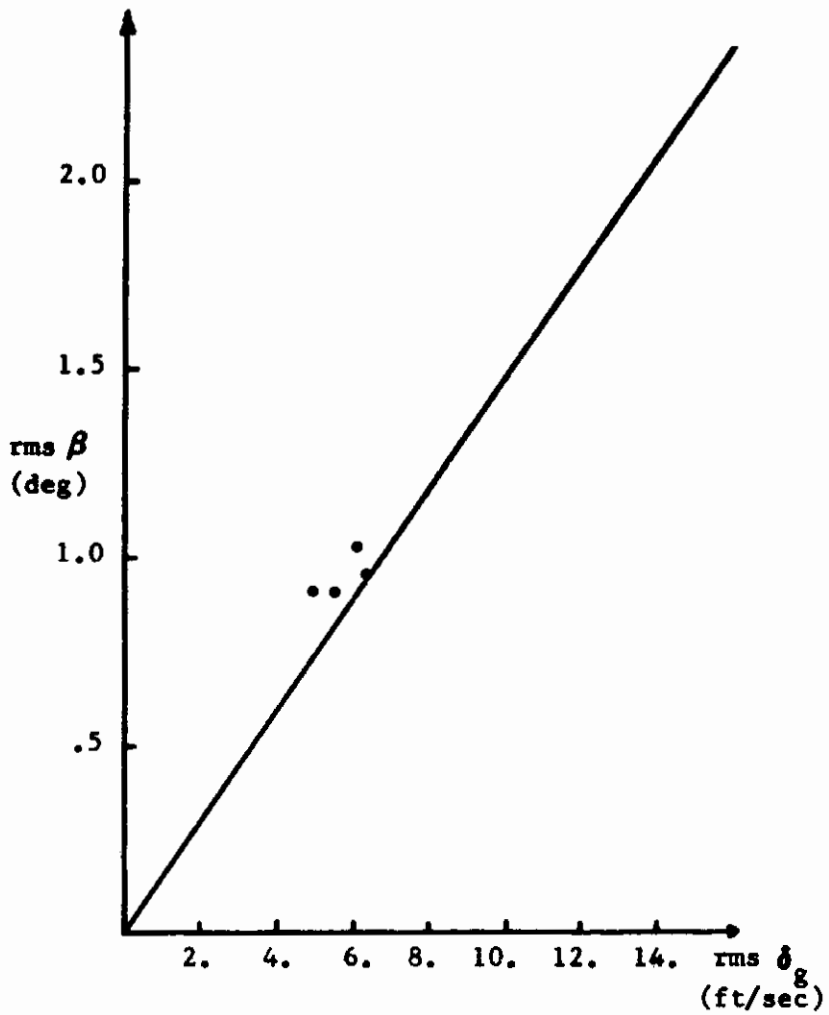

GUST TRACKING

FIGURE 57 T-33 BB 2.3 HEADING TASK SIMULATION

• measured

—— predicted

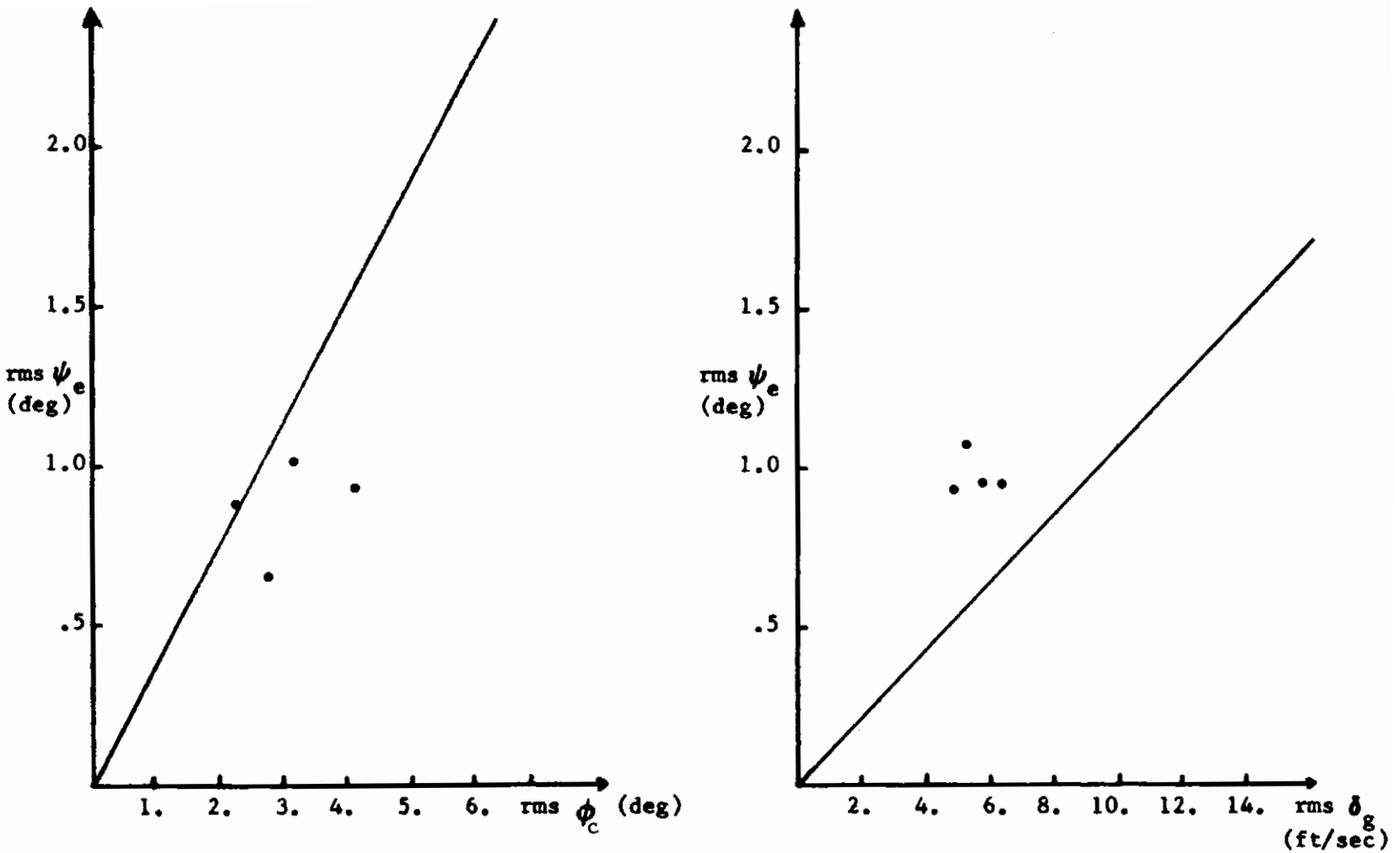

FIGURE 58 T-33 BC 2.2 HEADING TASK SIMULATION

• measured

—— predicted

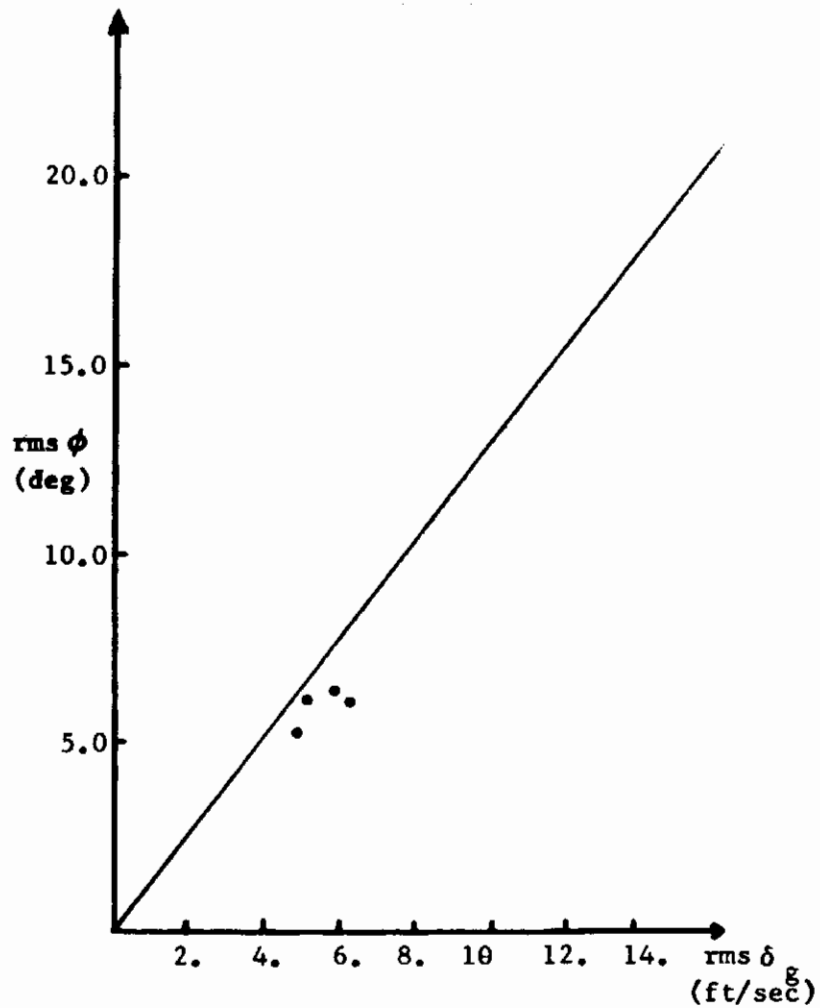

GUST TRACKING

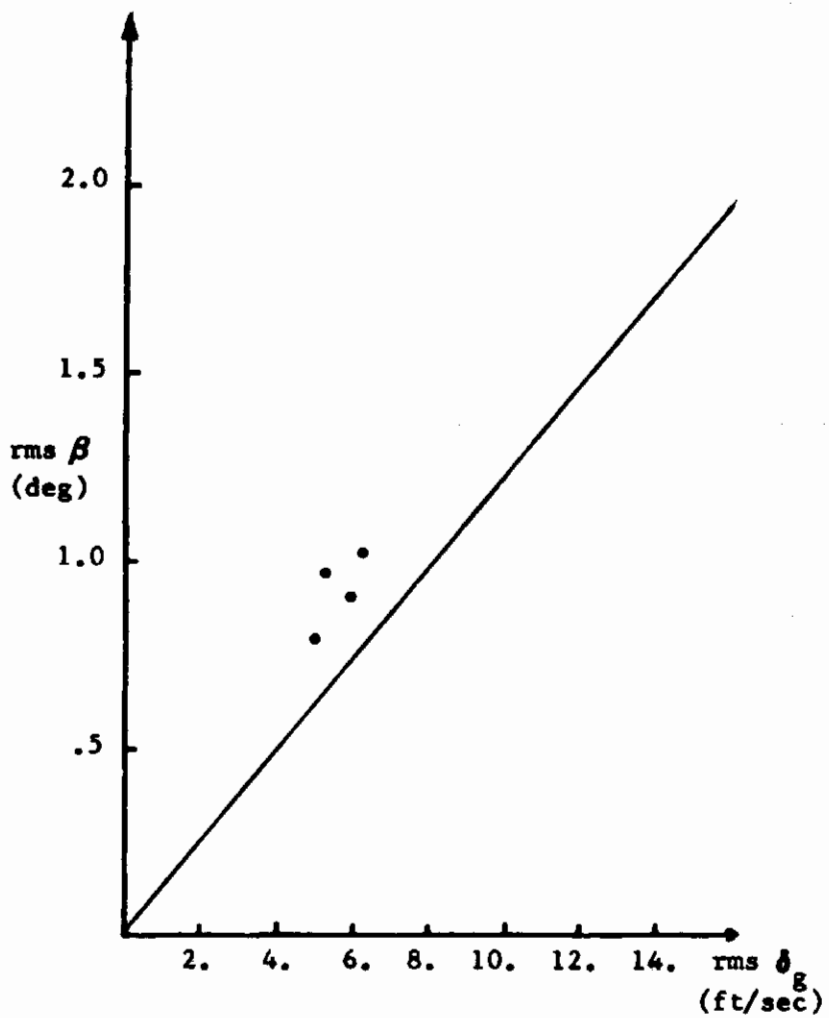

GUST TRACKING

FIGURE 59 T-33 BC 2.2 HEADING TASK SIMULATION

• measured

—— predicted

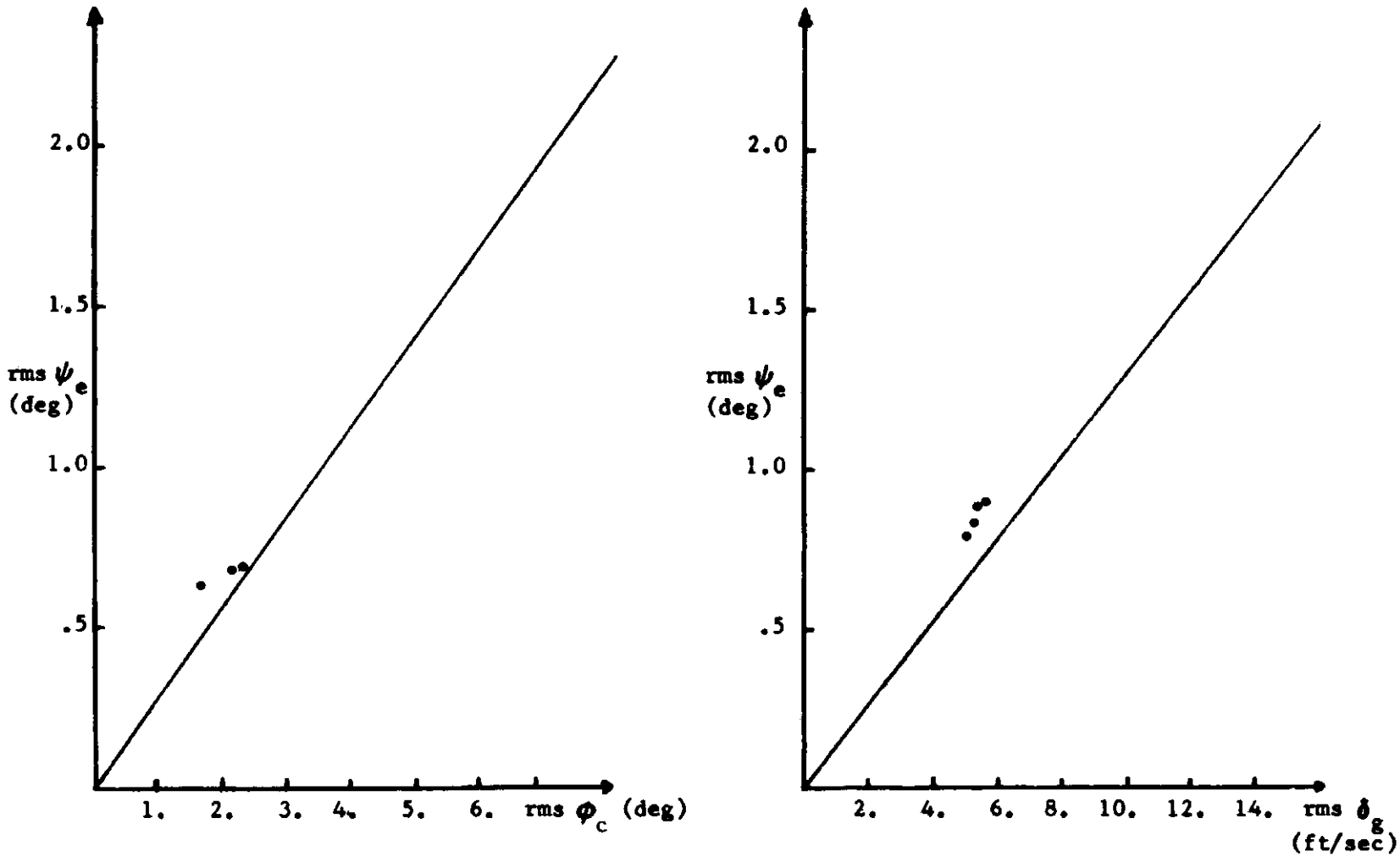

COMMAND TRACKING

GUST TRACKING

FIGURE 60 T-33 BC 2.3 HEADING TASK SIMULATION

• measured

—— predicted

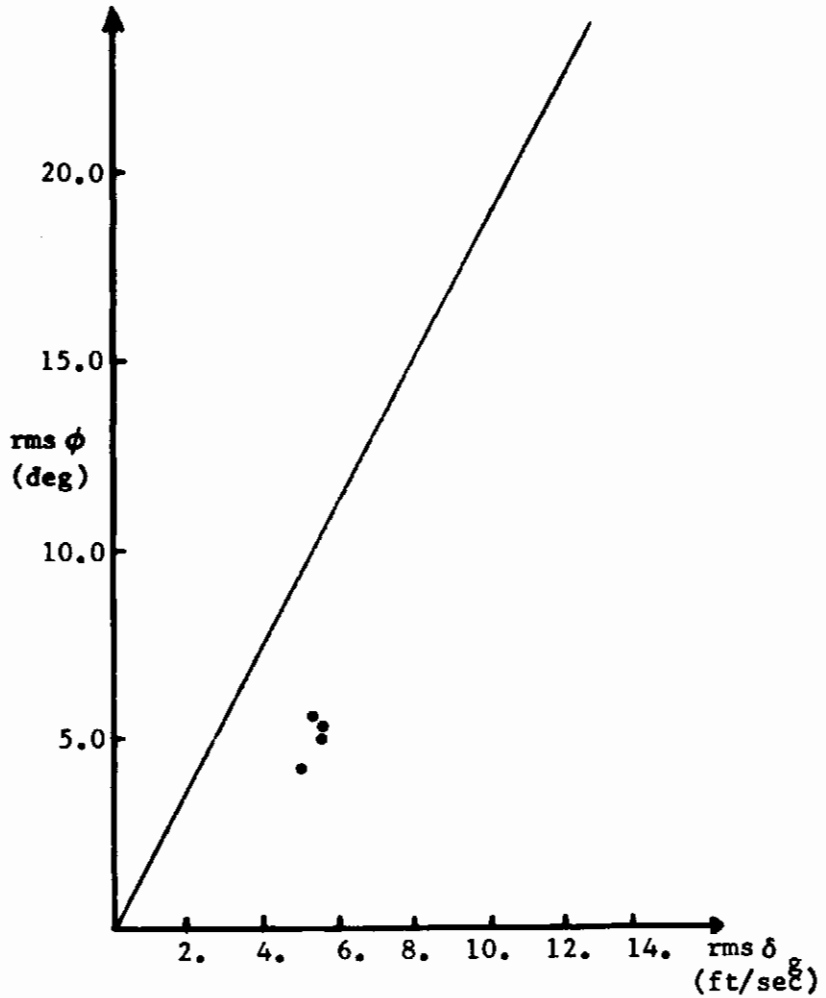

GUST TRACKING

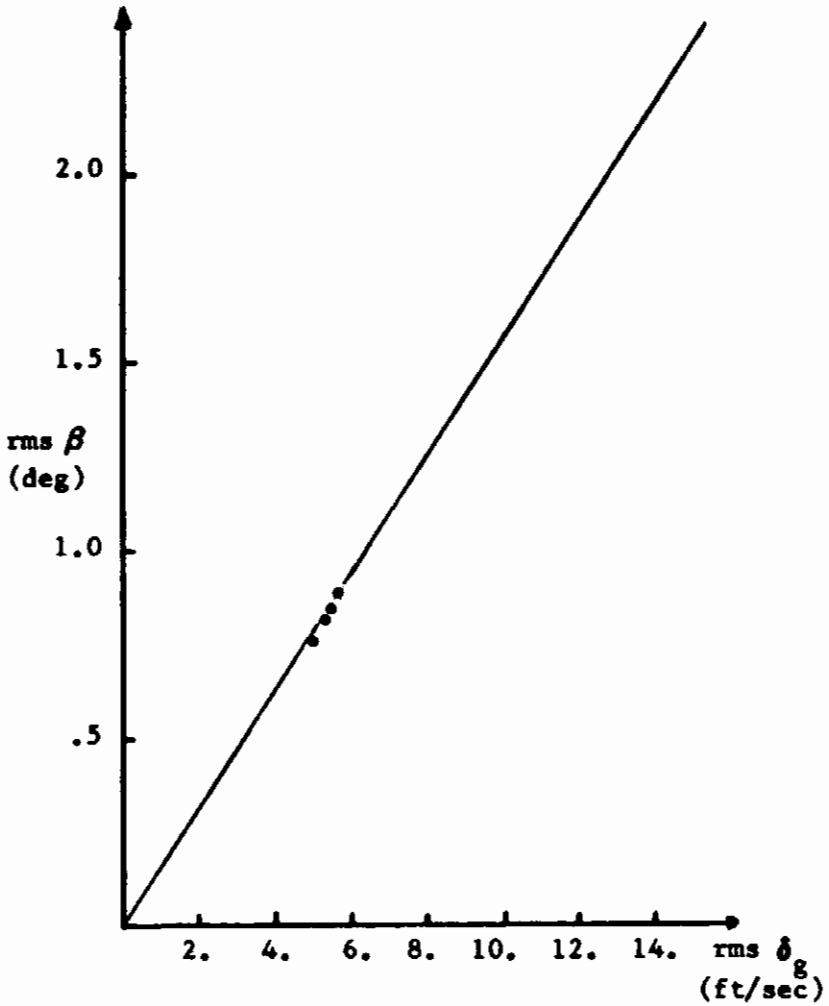

GUST TRACKING

FIGURE 61 T-33 BC 2.3 HEADING TASK SIMULATION

• measured

—— predicted

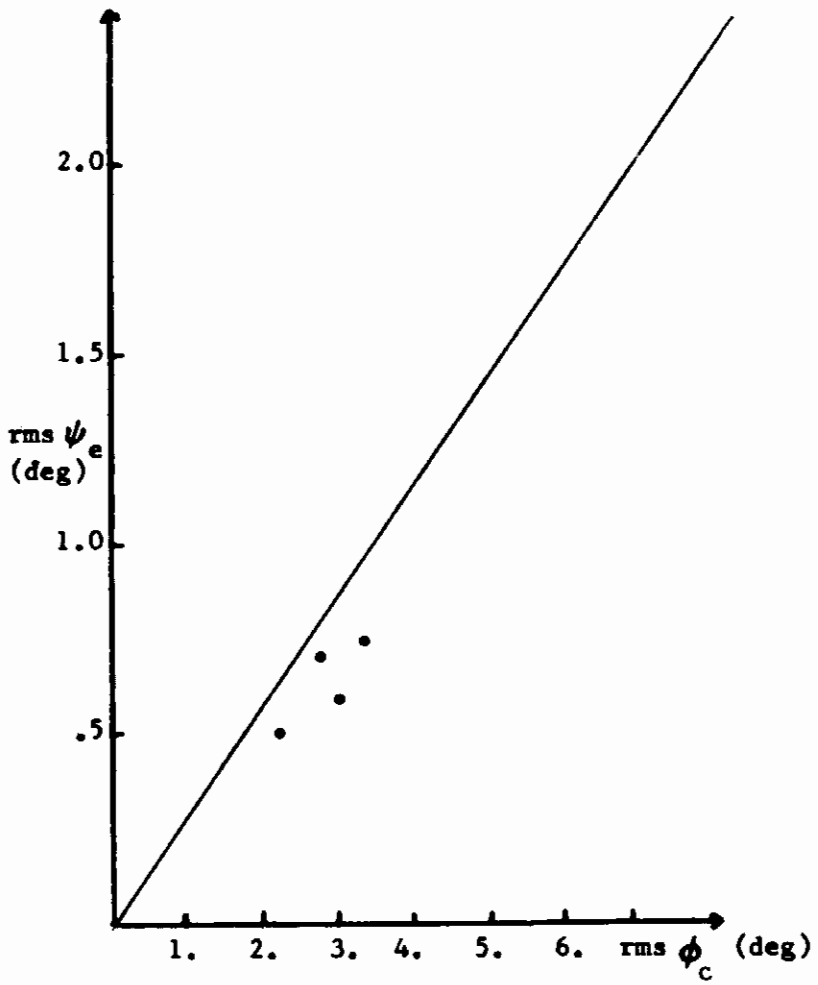

COMMAND TRACKING

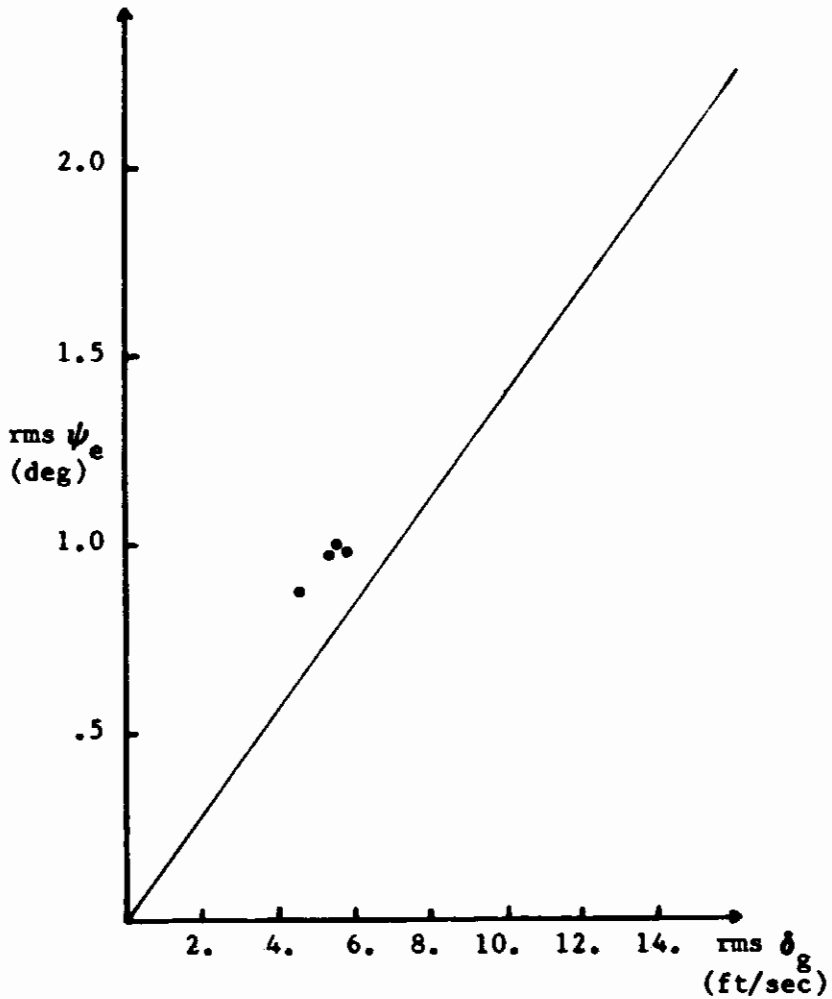

GUST TRACKING

FIGURE 62 T-33 BC 2.4 HEADING TASK SIMULATION

• measured

—— predicted

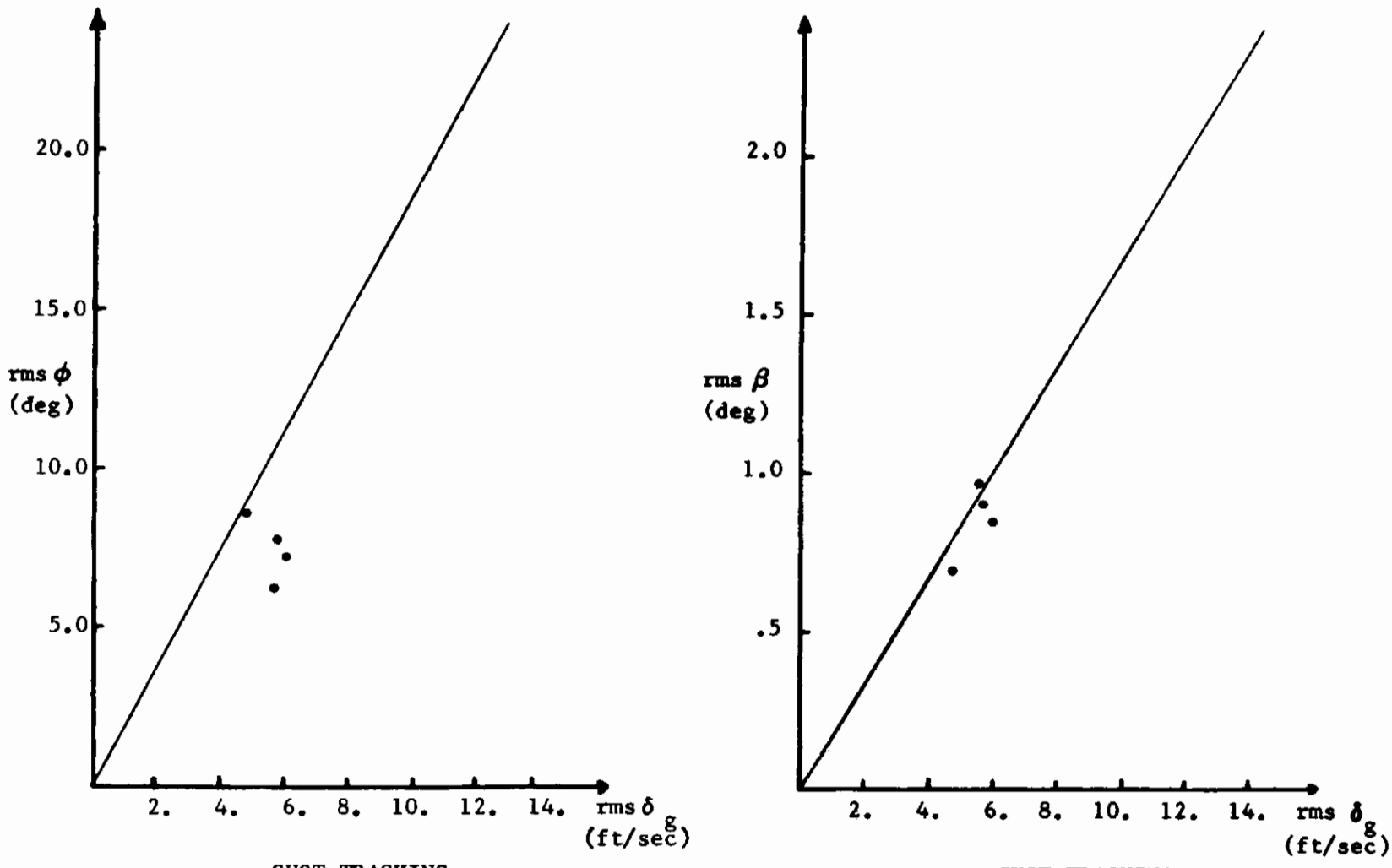

FIGURE 63 T-33 BC 2.4 HEADING TASK SIMULATION

• measured

—— predicted

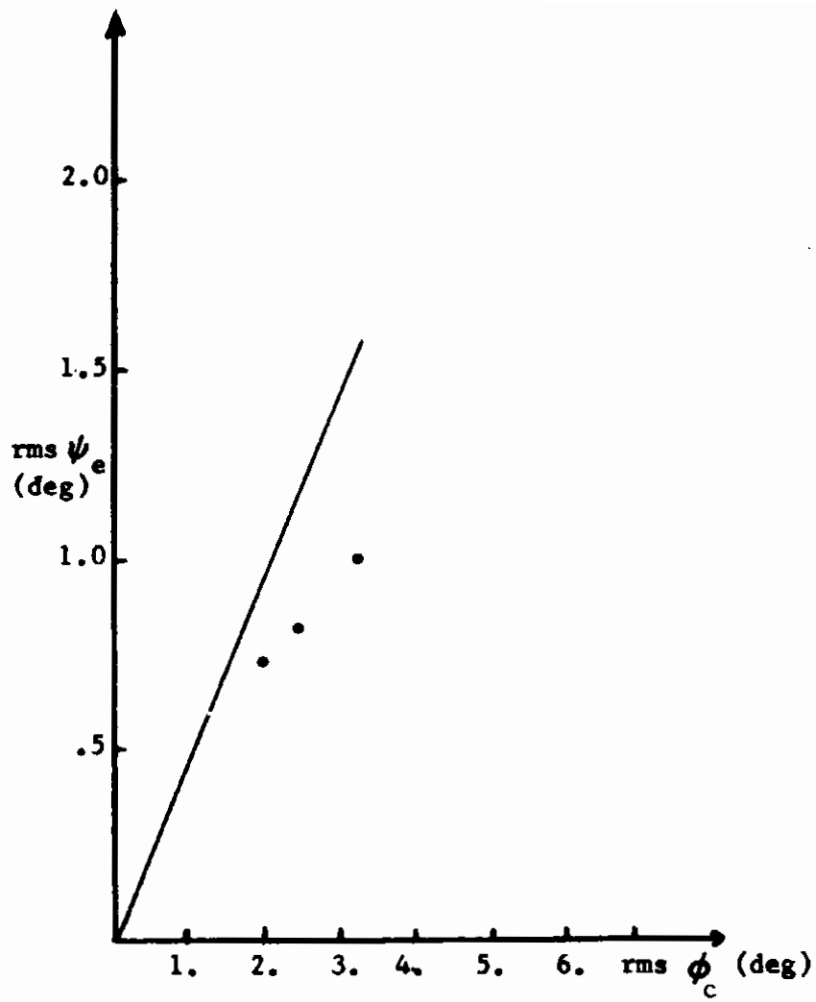

COMMAND TRACKING

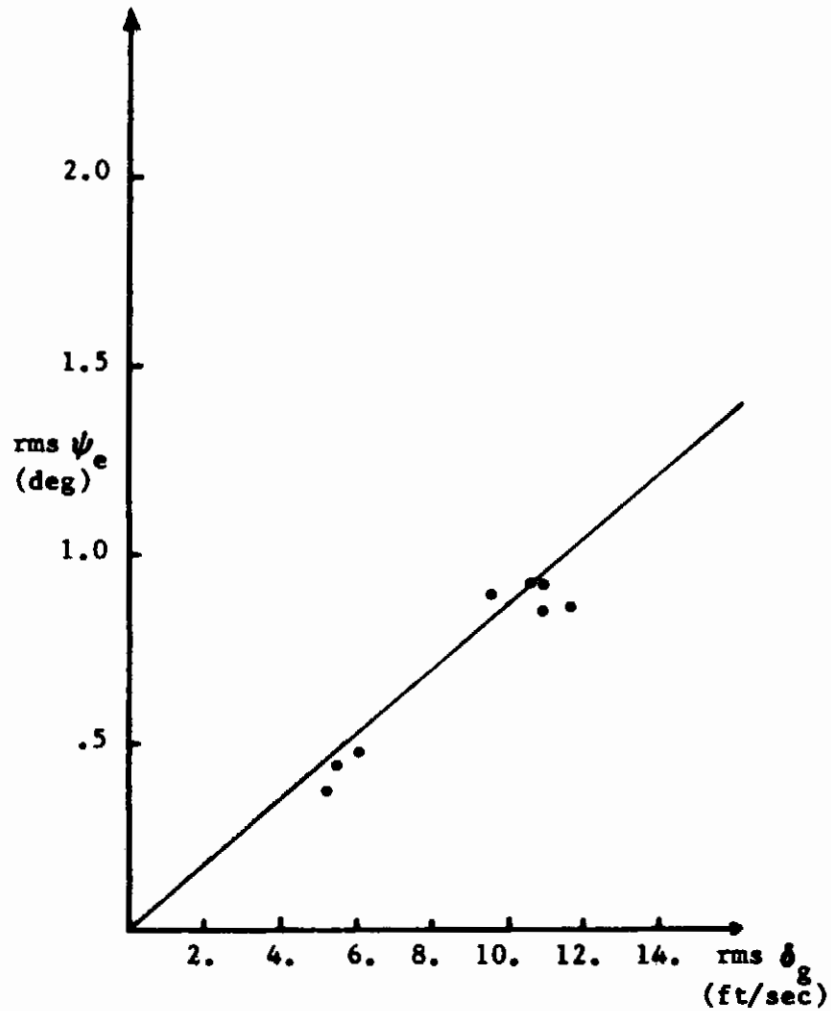

GUST TRACKING

FIGURE 64 F-5 SAS HEADING TASK SIMULATION

• measured

—— predicted

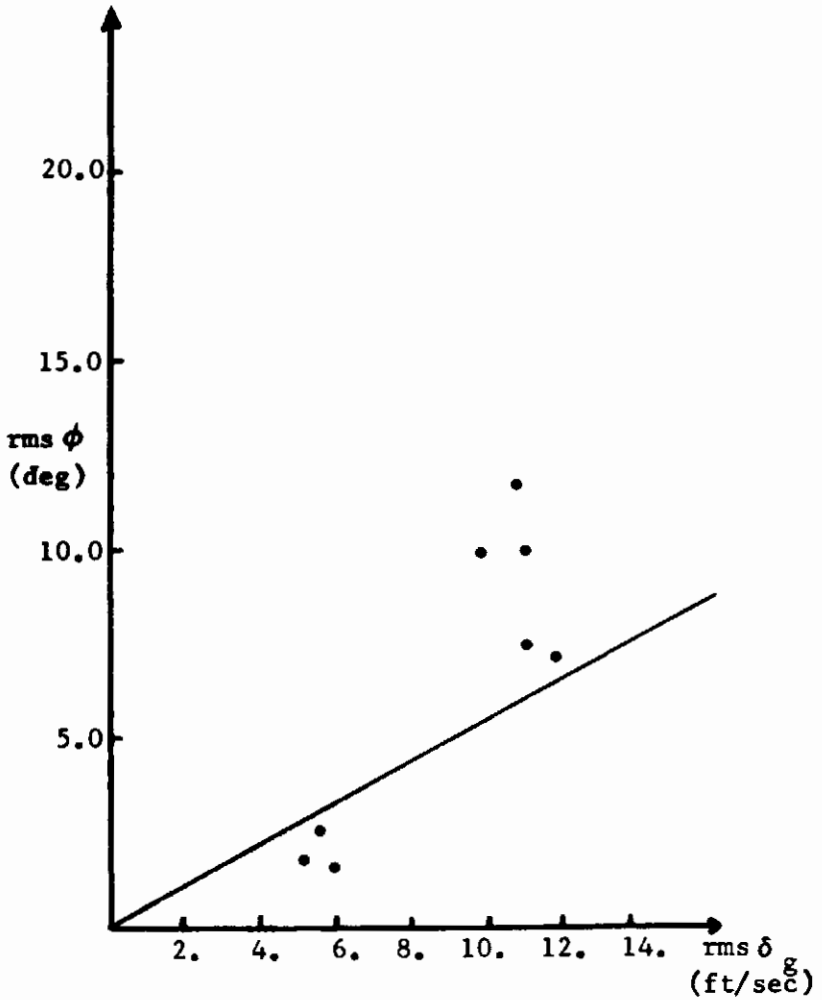

GUST TRACKING

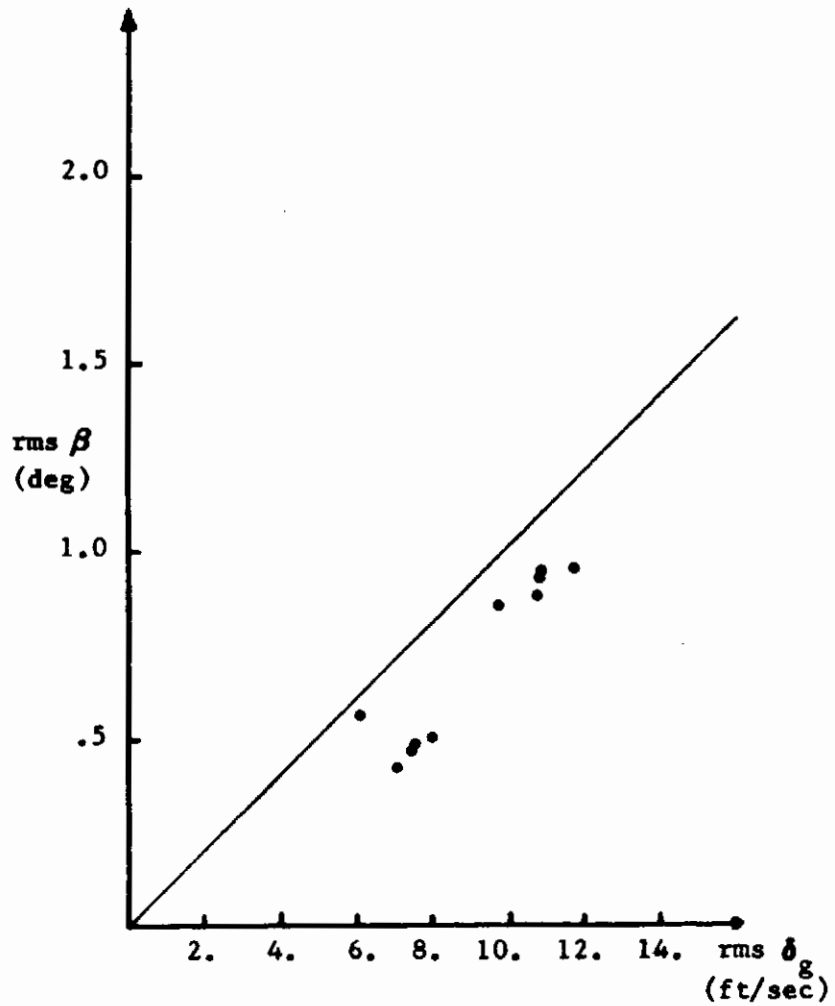

GUST TRACKING

FIGURE 65 F-5 SAS HEADING TASK SIMULATION

• measured

—— predicted

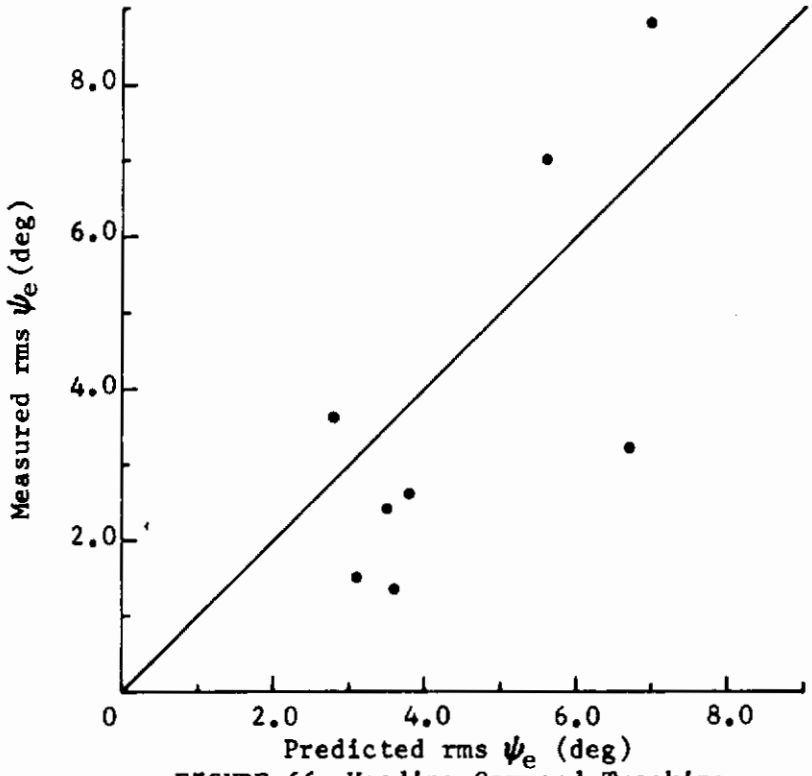

FIGURE 66 Heading Command Tracking

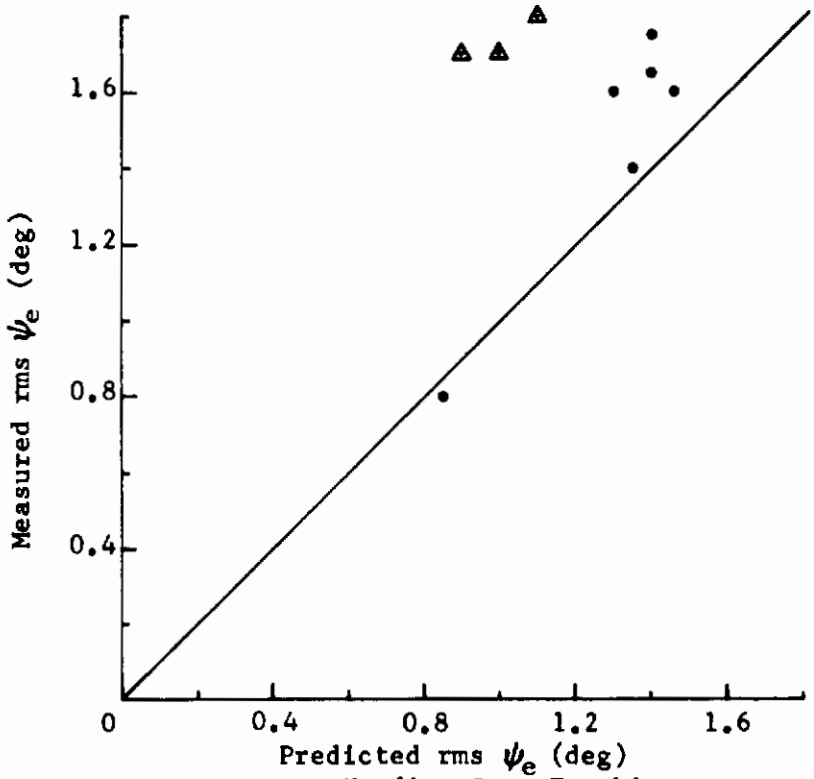

FIGURE 67 Heading Gust Tracking

▲ large aileron yaw

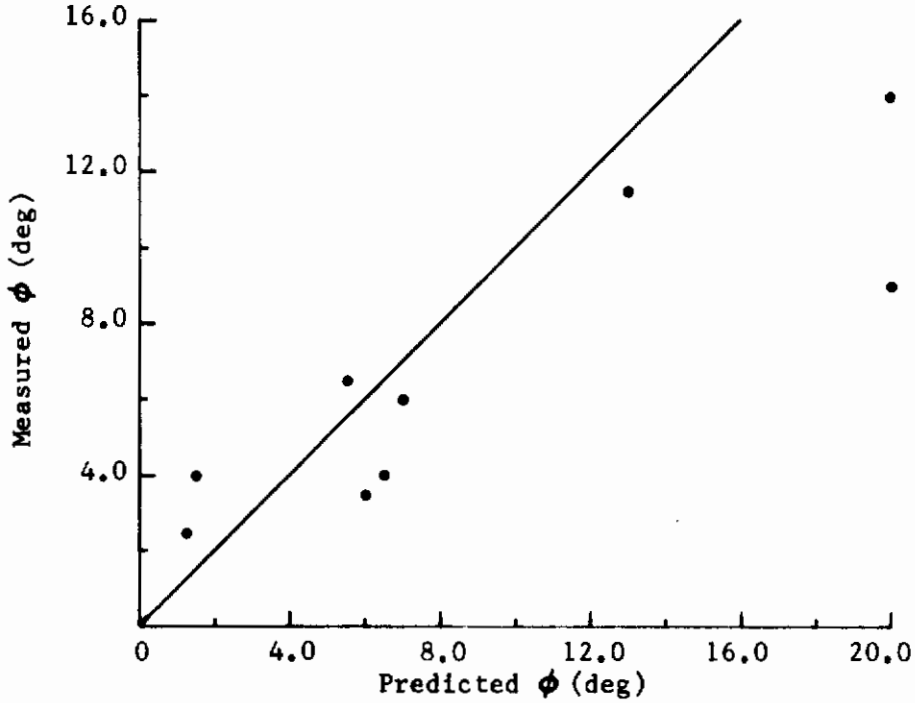

FIGURE 68 Heading Gust Tracking

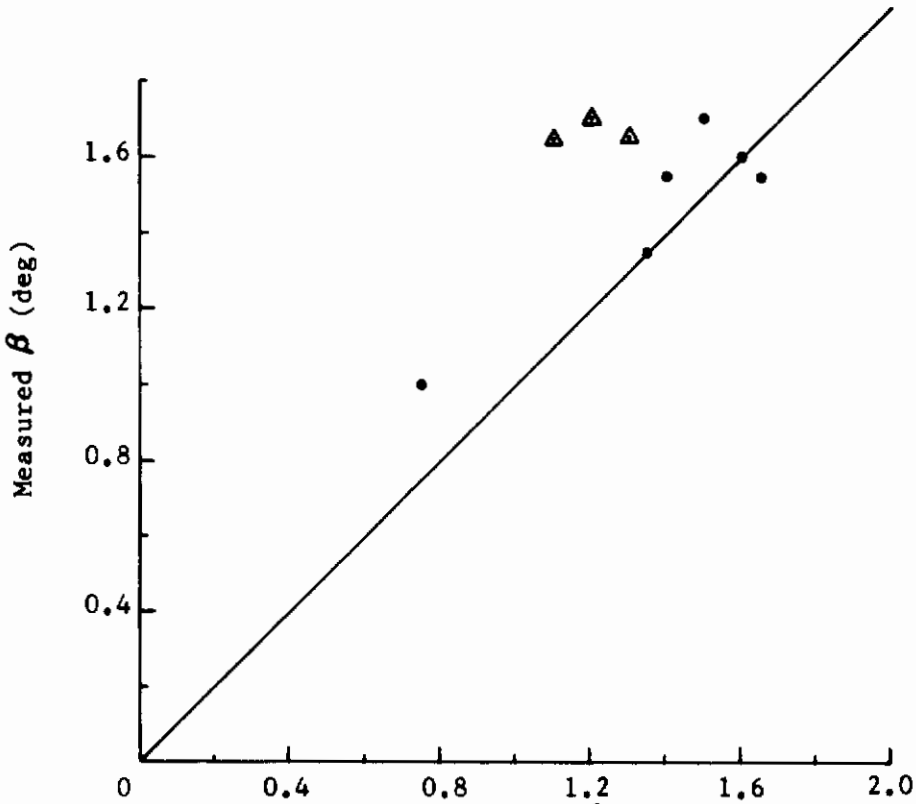

FIGURE 69 Heading Gust Tracking

▲ large aileron yaw

IV. FURTHER CONSIDERATIONS OF SYSTEM ANALYSIS

There are several additional topics relating to pilot-vehicle system modeling that will be briefly discussed in this section. These considerations are in part conjectural but are supported by a limited amount of experimental evidence.

A. Superposition in the Pilot

The analysis and simulation discussed in Section III have dealt with the command tracking and turbulence tracking as separately considered tasks. Since many applications of these methods are concerned with tradeoff design studies of task performance in a turbulent environment, it is necessary to compute the pilot-vehicle system performance for command tracking tasks in a turbulence. The system description is linear so that predictions for this combined task can be obtained by using the principle of linear superposition.

Let q_T and q_g be the error time response of a pilot-vehicle system for command tracking and turbulence tracking respectively and let σ_T and σ_g be the associated rms performance measures. Thus σ_T = rms q_T and σ_g = rms q_g. Then the superimposed tasks have the time response $q_T + q_g$ and the performance σ_{Tg} for the combined task is given by

$$\sigma_{Tg}^2 = \lim_{T\to\infty} \frac{1}{T} \int_0^T (q_T(t) + q_g(t))^2 \, dt \tag{27}$$

$$= \sigma_T^2 + \sigma_g^2 + \lim_{T\to\infty} \frac{2}{T} \int_0^T q_T(t)\, q_g(t)\, dt. \tag{28}$$

Thus if the command signal and the gust are statistically independent, the combined performance is given by

$$\sigma_{Tg} = \sqrt{\sigma_T^2 + \sigma_g^2} \tag{29}$$

In this way the predicted performance of the system for the combined command tracking task in turbulence can be obtained from the separate command and turbulence tracking predictions.

In order to determine if the human pilot follows a linear superposition principle, a number of simulation flights were made in which the pilot was asked to track the bank angle command signal in turbulence. The rms levels of the command signal and gust filters were recorded as well on the rms performance. The expected performances ϕ_{e_T} for command tracking and ϕ_{e_g} for gust tracking can then be obtained from the bank angle prediction graphs. These were averaged in the above rms manner and a comparison of these numbers with the actual measured performance shown in Figure 70 where the line drawn is the line of exact agreement. For comparison, Figure 71 shows the same comparison for predicted values obtained by arithmetic averaging

$$\sigma_{Tg} = \frac{1}{2} (\sigma_T + \sigma_g) \tag{30}$$

The amount of data is not sufficient to perform a linear regression analysis and substantiate the superposition principle for the human pilot. However, the data strongly suggests that this hypothesis is valid and in this way gives a method for predicting the system performance of command tracking in turbulence.

B. Anderson Formulas for Command Tracking in Turbulence

The relationship between bank angle rms error and pilot ratings, Figure 43, indicates that an Anderson formula may be appropriate for predicting pilot ratings for tasks in turbulence. Assuming linear superposition in the pilot, the following formula is the likely candidate for a single axis task

$$PR = K_1 \frac{\sqrt{\sigma_T^2 + \sigma_g^2}}{\sigma_m} + K_2 T_L + K_3 \tag{31}$$

and corresponding formulas may be generated for multiple axis tasks. Anderson has examined the pilot rating data obtained from the bank angle simulation and has found agreement between reported pilot ratings and the above formula, but the data is too scant to regard this as more than a consistency check.

C. Reduced Time Delay as a Model for Acceleration Cues

The failure of fixed base simulation to give performance levels similar to moving base data for bank angle gust tracking, Figure 46, demonstrates the importance of inertial acceleration cues to the pilot. Furthermore, the agreement between

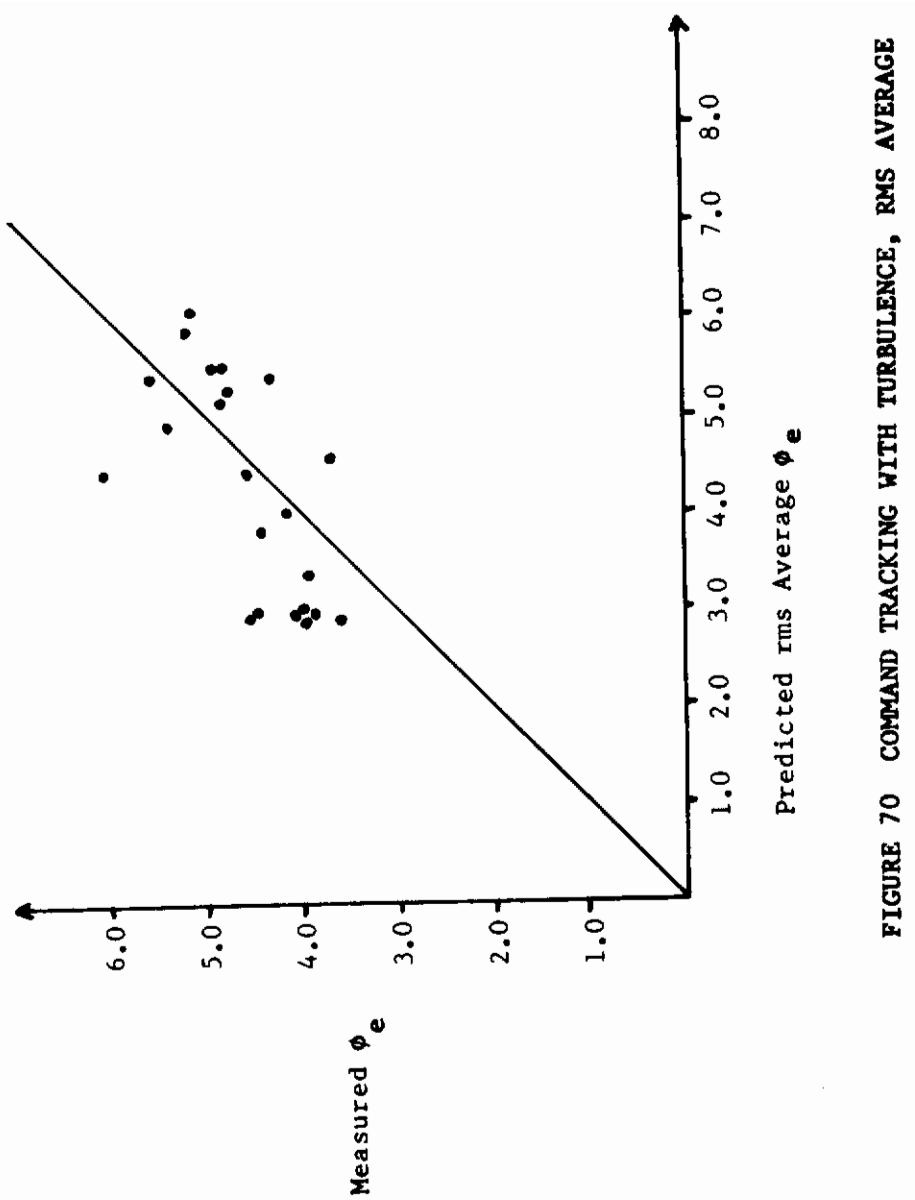

FIGURE 70 COMMAND TRACKING WITH TURBULENCE, RMS AVERAGE

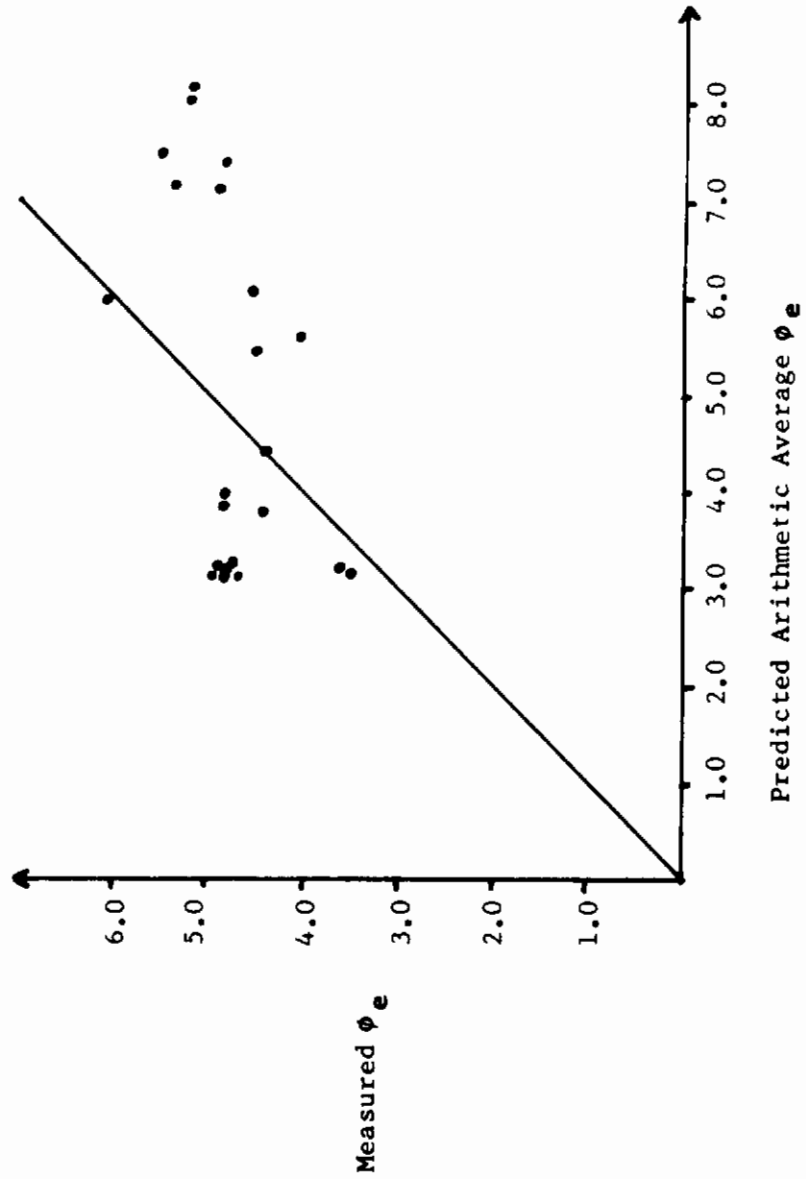

FIGURE 71 COMMAND TRACKING WITH TURBULENCE, ARITHMETIC AVERAGE

measured gust tracking rms ϕ_e and predicted rms ϕ_e shows that the reduced time delay $\tau = .3$ sec serves as a model for these acceleration cues. The following discussion develops a theory of acceleration pilot models and demonstrates the near equivalence of acceleration and reduced time delay pilot models.

Let Y_ϕ be the bank angle pilot model as used above for predicting bank angle gust tracking performance

$$Y_\phi = K_\phi (.5s + 1) e_1^{-.3s} \tag{32}$$

This is the reduced time delay model, the τ being reduced from $\tau = .44$ sec, the value which models command tracking since command tracking does not depend strongly on acceleration cues. On the other hand, the acceleration pilot model is postulated as

$$\overline{Y}_\phi = \overline{K}_\phi (\overline{T}_L s + 1) (.5s + 1) e_1^{-.44s} \tag{33}$$

where $\overline{K}_\phi$ is the gain and $\overline{T}_L$ is the acceleration pilot lead.

In order to assess the effort of the reduced time delay, it is convenient to write

$$e^{-.44s} = e^{-.3s} e^{-.14s} \tag{34}$$

so that

$$e_1^{-.44s} = \left(\frac{s - 6.67}{s + 6.67}\right) \left(\frac{s - 13.3}{s + 13.3}\right) \tag{35}$$

then the acceleration model takes the form

$$\overline{Y}_\phi = \overline{K}_\phi (\overline{T}_L s + 1) (.5s + 1) \left(\frac{s - 6.67}{s + 6.67}\right)\left(\frac{s - 13.3}{s + 13.3}\right) \tag{36}$$

The success of the reduced time delay model suggests that the pilot adopts a $\overline{T}_L$ such that $(\overline{T}_L s + 1)$ effectively cancels the Padé denominator of the reduced part of the time delay $(s + 13.3)$. A comparison of bank angle gust tracking predictions using the reduced τ model and the acceleration model optimized with respect to $\overline{K}_\phi$ is

shown in Figure 72. The close agreement of these two models shows that the reduced τ model is consistent with the acceleration model and furnishes a measure of the amount of acceleration cues used by the pilot.

Configuration	Acceleration Model	Reduced τ Model
AB 2.6	1.25	1.05
AB 2.7	1.27	1.09
AB 3.1	.768	.73
AB 3.3	.719	.68
BB 2.3	4.01	3.1
BC 2.2	5.47	5.7
BC 2.3	5.86	6.44
BC 2.4	6.06	6.64

FIGURE 72 COMPARISON OF ACCELERATION AND REDUCED TIME DELAY PILOT MODELS

V APPLICATION TO AIRPLANE SPECIFICATION AND DESIGN

A. Specification Criteria

This research into flying qualities prediction has developed methods for analytically evaluating certain characteristics of pilot flight including system error prediction for command tracking and attitude hold tasks in turbulence. Since these two basic types of piloted control are independently determined by the airframe dynamics, a closed loop pilot-vehicle specification criterion would be required for each.

There are two ways in which performance predictions can conceivably be used to formulate criteria suitable for possible inclusion in the Military Specification on Flying Qualities of Piloted Aircraft. The first, developing an Anderson rating prediction formula, appears to be promising on the basis of the rms ϕ_e vs pilot rating data of Figure 43. This is similar to the data used by Anderson to develop the VTOL formula of the "Paper Pilot" prediction method and suggests a minimum error and line of regression having a slope somewhat higher than the one used by Anderson. The number of pilot ratings obtained during the simulations were not sufficient to validate a rating formula; this approach will require an extensive simulation of many operational airplanes in varied flight conditions and control modes.

On the other hand, numerical criteria can be directly obtained from the performance prediction data. One promising way of doing this is to assume a standard maximum of Level I pilot workload and refer all calculations to the implied pilot lead. The value used in this investigation is $T_L = .5$ seconds and is a likely choice. Furthermore, the lead variation graphs indicate that for time delays matching the simulator data, this lead is sufficient for Level I Class IV airplanes. Bank angle criteria would then take on a simple form requiring only that the system errors in command tracking and in gust tracking be lower than certain prescribed levels. Furthermore, requirements on the sensitivity of the system to pilot gain can be prescribed. This aspect of handling qualities in turbulence appears to be important to the pilot and can be assessed by the prediction methods.

Both the analytical and simulator data indicate that specification criteria for heading command and turbulence tasks should be based on more than tracking error. Yaw rate and the amount of aileron induced yaw appear to be important and can be easily incorporated into the method. However, analysis is much more difficult with heading than with bank angle and much more analysis and simulation is required before either of these two programs for developing specification criteria can be carried out.

The agreement between the predictions and the simulator data indicate that the multiloop pilot model is accurate for airplanes with low aileron induced yaw so that modifications of the model should be straightforward.

B. Applications to Airplane Design

Even though there is not enough data available to supply numerical specification criteria of the kind discussed above, the performance prediction methods developed during this research program are useful for many design applications. The agreement between the analytic predictions and the simulations not only show that system tracking errors can be predicted at the earliest stages of preliminary design, but that comparisons between designs, or design and operational airplane will be accurate. Furthermore, the identification of the separate parameters of command tracking and attitude hold tracking in turbulence allows tradeoff studies to be made very early in the design effort. These tradeoff and comparison studies include investigations of changes in the aerodynamic and control derivatives, advanced control systems, and any type of control or stability augmentation systems.

C. Design Study Example

The techniques developed during this research were applied in the final design effort of the Northrop A-X aircraft. Favorable response of the aircraft to turbulence was considered essential in order to carry out the desired missions. Since the ability to maintain precise bank angle control is paramount in lateral handling qualities, a study was initiated to evaluate the effect of various design permutations on performance of the aircraft in maintaining zero bank angle in lateral turbulence. Variation of C_{l_β}, C_{n_β}, and a yaw damper were considered.

Analysis was carried out through modification of the computer program described in Appendix IV. A bank angle pilot model of the form $K(T_L s + 1)_e^{-.3s}$ was assumed adequate for the task. Do-loops were then added to the program so that a range of pilot gains would be evaluated for each of several values of pilot lead. The best bank angle performance at each value of lead was then plotted versus the lead. The predicted performance for the configuration under consideration was then estimated to be at the point on the curve where the slope, Δ rms $\phi_e / \Delta T_L$, was -2.5, following the Anderson minimum rating prediction method. For an account of the significance of this, see References 6 and 10.

Partial results of the study are summarized in the table below.

Calculations for rms δg_β = 10 ft/sec	rms Bank Angle Error
Proposed A-X Configuration	0.25°
Effect of Yaw Damper Off	0.35°
Effect of Variations in C_{l_β}	
50% Increase	0.35°
100% Increase	0.50°
Effect of Variations in C_{n_β}	
50% Increase	0.25°
100% Increase	0.25°

A simulation of the A-X was carried out on the Northrop Large Amplitude Flight Simulator and the measured values of rms bank angle error was in close agreement with the figures in the above table.

The experience of this design problem shows that the total system pilot-vehicle prediction techniques were a rapid and accurate way of investigating the variations of the aerodynamics. In addition, the tradeoff studies concerning the yaw damper in still and in turbulent air led to substantial improvement in the proposed A-X configuration.

VI CONCLUSIONS

A method for predicting the performance of the total pilot-vehicle system has been developed for the lateral dynamics of conventional airplanes. This method, which is based on pilot model theory and multiloop analysis, predicts tracking errors for command tracking tasks and also for attitude hold tracking tasks in turbulence. The predictions are in terms of root mean square averages of the system time history and are obtained by means of a fully automated multiloop analysis performance prediction program available from the United States Air Force. Thus, system performance can be evaluated analytically in terms of familiar time domain statistics without the conceptual or computational difficulties of the popular but limited frequency domain methods.

The validity and accuracy of this method has been ascertained by means of moving base simulation on the Northrop Large Amplitude Flight Simulator operating in five degree of freedom motion. A wide range of airplanes were simulated including the F-5 and eight Air Force variable stability T-33 configurations flown by Cornell. These airplanes exhibited very striking differences in performance and the data obtained agrees well with the predicted performance. Full details of the method and the simulation results have been presented in this report and the following items indicate the extent of the applicability and success of the techniques developed during this effort.

A. Bank Angle Study

There were two principal pilot tasks to be evaluated. The first, command tracking of a random signal resulted in good agreement between the predictions and the simulator data for all configurations. The second, holding wings level in the presence of atmospheric turbulence, not only led to even better agreement between the theory and the experiment, but also to the identification of system sensitivity to pilot attention that can be analytically evaluated. Thus, the method demonstrates the ability to identify and assess many crucial features of the total pilot-vehicle system during bank angle tracking modes.

B. Heading Study

Analysis of heading depends on the ability to arrive at multiloop pilot models which will predict the root mean square values of bank angle, sideslip angle, and heading angle error. The method proved to be accurate in this sense for all but three

of the configurations. The three exceptions demonstrated large aileron induced yaw and large yaw rates during the simulation, which indicates the importance of yaw rate in heading task evaluation.

C. Specification Criteria

The accuracy of the method for predicting pilot-vehicle system performance and the simulator data relating this performance with pilot ratings indicates that a pilot rating formula of the kind developed by R.O. Anderson for VTOL airplanes may also be suitable for conventional aircraft. Specification alternatives have also been suggested which include parameters not occurring in an Anderson type formula. Such criteria in terms of the root mean square values of the dynamic variables and the slopes of the prediction graphs may be particularly useful for more complex multi-loop control evaluation. By means of these prediction methods the basic stability characteristics of the airplane can be used to obtain a knowledge of how it will respond when piloted. By specifying this piloted performance, much information about the flying qualities of an airplane can be obtained in addition to the open-loop parameters. Thus the closed-loop pilot-vehicle analysis methods developed here obtain further information from the basic airframe characteristics, especially in turbulence where specific criteria can now be developed.

D. Application to Airplane Design

The usefulness of these techniques in design has already been demonstrated to Northrop in the configuration of the Northrop A-X airplane. Even though specification criteria are not yet available, the method was used to study the effects of varied aero-dynamic derivatives and yaw dampers. Several configurations were compared against one another and against the known flying qualities characteristics of the F-5. This application was essential to the proposed design of the Northrop A-X and showed both the power and versatility of the prediction method.

E. Final Remarks

The usefulness of the above approach to flying qualities, especially in turbulence, has been amply demonstrated. The method has been developed to the point where it is a powerful tool for analysis and design, and the ultimate goal of achieving closed loop pilot-vehicle specification criteria now depends on further high quality simulation or flight testing. The success of the "Paper Pilot" of Anderson and Dillow as well

as the above results indicates that further research along these lines is more than warranted. It is hoped that this report will not only serve as an introduction to this new and active area of research but will also serve to stimulate further work in this direction.

REFERENCES

1. Meeker, J.I., "Evaluation of Lateral-Directoral Handling Qualities of Piloted Re-Entry Vehicle Using Fixed-Base and In-Flight Evaluation", Cornell Aeronautical Laboratory, Inc., NASA CR-778, May 1967.

2. McRuer, D.T., et al, "Human Pilot Dynamics in Compensatory Systems", Systems Technology, Inc., AFFDL-TR-65-15, July 1965.

3. McRuer, D.T., "Analysis of Multiloop Vehicular Control Systems", Systems Technology Inc., ASD-TDR-62-1014, March 1964.

4. Durand, T.S., "Carrier Landing Analysis", STI-TR-137-2, February 1967.

5. Kensinger, J.T., "A Method to Determine the Allowable Error of a Sensor Used to Display Angle of Attack", AFIT, GE/EE/68-9, March 1968 .

6. Anderson, R.O., "A New Approach to the Specification and Evaluation of Flying Qualities", AFFDL-TR-69-120, June 1970.

7. Dillow, James D., "The Paper Pilot — A Digital Computer Program to Predict Pilot Rating for the Hover Task", FDCC TM-69-3, December 1969, (To be published as AFFDL-TR-70-40.)

8. Baron, J. et al, "Application of Optimal Control Theory to the Prediction of Human Performance in a Complex Task", AFFDL-TR-69-81, March 1970.

9. Laning, J.H., and Battin, R.H., "Random Processes in Automatic Control", McGraw Hill, New York 1956.

10. McDonnell, John D., "Pilot Rating Techniques for the Estimation and Evaluation of Handling Qualities", Systems Technology, Inc., AFFDL-TR-68-76, December 1968.

11. Skelton, Grant B., "Investigation of the Effects of Gusts on V/STOL Craft in Transition and Hover", Honeywell Inc., AFFDL-TR-68-85, October 1968.

12. Chalk, C.R., et al, "Background Information and User Guide for MIL-F-8785B (ASG), "Military Specification — Flying Qualities of Piloted Airplanes", AFFDL-TR-69-72, August 1969.

13. Franklin, James A., "Influence of Turbulence on Lateral-Directional Flying Qualities", AIAA Paper No. 70-998, August 1970.

14. Meeker, J.I., and Hall, G.W., "In-Flight Evaluation of Lateral-Directional Handling Qualities for the Fighter Mission", AFFDL-TR-67-98.

15. Heifferon, J.C., and Hannen, R.A., "The Effects of Changes in Input Power Spectra on Human Operator Compensatory Tracking", Proceedings of the Sixth Annual Conference on Manual Control, AFIT, April 1970.

16. McRuer, D.T., et al, "New Approaches to Human-Pilot Vehicle Dynamic Analysis", Systems Technology, Inc., AFFDL-TR-67-150, February 1968.

17. Stapleford, R.L., et al, "Experiments and a Model for Pilot Dynamics with Wind and Motion Inputs", Systems Technology, Inc., NASA CR-1325, May 1969.

18. Tsu, C.N., "A Note About the Effects of Product of Inertia in Lateral Stability", J. Inst. Aeron. Sci., Vol 21, No. 7, July 1954.

APPENDIX I MULTILOOP ANALYSIS

APPENDIX I

MULTILOOP ANALYSIS

In the conventional analysis of linear feedback control systems one of the first objectives is to derive the closed loop transfer functions of interest, for once these are obtained the determination of system behavior is a fairly routine matter. However, the derivation of these closed loop transfer functions can present special problems. If the control system can be represented by a block diagram which explicitly shows every loop and loop closure, the transfer functions can be obtained without difficulty. Unfortunately, such representations cannot always be made. For example, there may be loop closures through a common block in the diagram whose behavior, although linear, is governed by a complex system of linear differential equations. This means that loops closed through such an element do not operate separately but are coupled in their behavior in a complex way by the differential equations. Nevertheless, such coupled loops can be shown to constitute a linear control system. Consequently, a system of this kind possesses transfer functions which are identical in their meaning and analysis with the transfer functions of conventional servo analysis.

Although the notation and terminology are obviously adapted for multiloop control of the airframe, the method will apply directly to any dynamic system that meets the following requirements.

1. The system can have at most three degrees of freedom, hence is governed by no more than three independent dynamic variables q_1, q_2, q_3.
2. The differential equations of the controlled system relating the variables q_1, q_2, q_3 must be linear. These equations are called the vehicle dynamics of the system. They are always presented in the s-plane of the Laplace transform.
3. There should be no more than two inputs to the vehicle (forcing functions) δ_1, δ_2 called deflections which govern the vehicle dynamics.

So far, no restrictions on the control system have been imposed. There is only one restriction.

4. The individual components of the control system, including the pilot, must have linear transfer functions, or be approximated by linear transfer functions, and should be combined in a linear manner within the system.

5. The system may be controlled by, or may have outputs q_4, q_5, . . ., called auxiliary dynamic variables, in addition to q_1, q_2, q_3, but these q_4, q_5 . . . must be linear combinations of q_1, q_2, q_3.

The lateral dynamics of the airframe can be represented in the following way. Let the independent dynamic variables be taken as r, ϕ, β, which must be q_1, q_2, q_3 in some convenient order. Later it will become clear how this order is selected. Since the vehicle dynamics are assumed linear, the equations will be of the form

$$\begin{aligned} a_{11}q_1 + a_{12}q_2 + a_{13}q_3 &= F_{11}\delta_1 + F_{12}\delta_2 \\ a_{21}q_1 + a_{22}q_2 + a_{23}q_3 &= F_{21}\delta_1 + F_{22}\delta_2 \\ a_{31}q_1 + a_{32}q_2 + a_{33}q_3 &= F_{31}\delta_1 + F_{32}\delta_2 \end{aligned} \tag{37}$$

$$\begin{aligned} q_4 &= a_{41}q_1 + a_{42}q_2 + a_{43}q_3 \\ q_5 &= a_{51}q_1 + a_{52}q_2 + a_{53}q_3 \end{aligned} \tag{38}$$

The total pilot vehicle system can be represented in matrix form as in Figure 73, where the indicated matrices are defined by

$$\Delta = \det \left[a \right] \tag{39}$$

$$\left[a \right] = \begin{bmatrix} a_{11} & a_{12} & a_{13} & 0 & 0 \\ a_{21} & a_{22} & a_{23} & 0 & 0 \\ a_{31} & a_{32} & a_{33} & 0 & 0 \\ -a_{41} & -a_{42} & -a_{43} & 1 & 0 \\ -a_{51} & -a_{52} & -a_{53} & 0 & 1 \end{bmatrix} \tag{40}$$

$$\left[q \right] = \begin{bmatrix} q_1 \\ q_2 \\ q_3 \\ q_4 \\ q_5 \end{bmatrix} \qquad \left[q_c \right] = \begin{bmatrix} q_{1c} \\ q_{2c} \\ q_{3c} \\ q_{4c} \\ q_{5c} \end{bmatrix} \tag{41}$$

$$\left[E \right] = \begin{bmatrix} E_{11} & E_{12} \\ E_{21} & E_{22} \\ E_{31} & E_{32} \\ 0 & 0 \\ 0 & 0 \end{bmatrix} \qquad \left[F \right] = \begin{bmatrix} F_{11} & F_{12} \\ F_{21} & F_{22} \\ F_{31} & F_{32} \\ 0 & 0 \\ 0 & 0 \end{bmatrix} \tag{42}$$

$$\left[\delta \right] = \begin{bmatrix} \delta_1 \\ \delta_2 \end{bmatrix} \qquad \left[\eta \right] = \begin{bmatrix} \eta_1 \\ \eta_2 \end{bmatrix} \tag{43}$$

$$\left[G \right] = \begin{bmatrix} G_{11} & G_{12} & G_{13} & G_{14} & G_{15} \\ G_{21} & G_{22} & G_{23} & G_{24} & G_{25} \end{bmatrix} \tag{44}$$

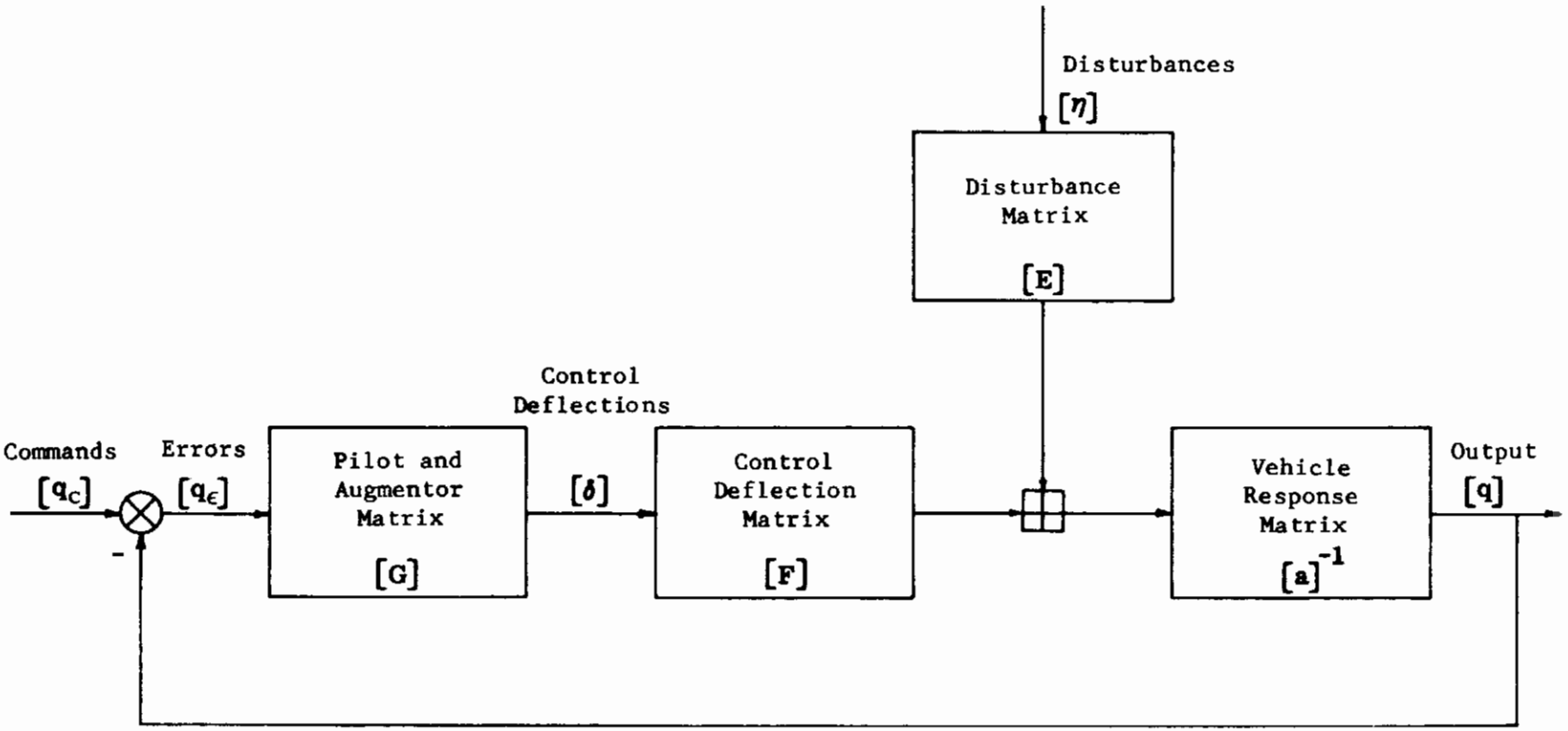

FIGURE 73 MULTILOOP BLOCK DIAGRAM

The system is then represented by the matrix equation

$$\Big[[a] + [F]\,[G]\Big]\,[q] = [F]\,[G]\,[q_c] + [E]\,[\eta] \tag{45}$$

or

$$[q] = \Big[[a] + [F]\,[G]\Big]^{-1}\Big\{[F]\,[G]\,[q_c] + [E]\,[\eta]\Big\} \tag{46}$$

Thus the roots of

$$\Delta_{sys} = \det\Big[[a] + [F]\,[G]\Big] = 0 \tag{47}$$

are the eigenvalues of the total system. This can be expanded in terms of cofactors and written in the following way

$$\Delta_{sys} = \Delta + \sum_{i=1}^{5}\sum_{j=1}^{2} G_{ji} N_{q_i \delta_j} + \sum_{\substack{i=1 \\ i \neq k}}^{5}\sum_{k=1}^{5} G_{1\,i} G_{2k} N^{q_i\, q_k}_{\delta_1\, \delta_2} \tag{48}$$

The two and four index "N" symbols are notations developed in Reference 3 and are defined as follows:

In order to evaluate these terms it is necessary to use the quantities a_{ij}, F_{ij}.

The key to these evaluations is the determinant which defines Δ.

$$\Delta = \det \begin{bmatrix} a_{11} & a_{12} & a_{13} & 0 & 0 \\ a_{21} & a_{22} & a_{23} & 0 & 0 \\ a_{31} & a_{32} & a_{33} & 0 & 0 \\ -a_{41} & -a_{42} & -a_{43} & 1 & 0 \\ -a_{51} & -a_{52} & -a_{53} & 0 & 1 \end{bmatrix} \tag{49}$$

It should be emphasized that the a_{ij} of the first three rows are completely determined by the stability derivatives of the vehicle while the a_{ij} of the last two rows are determined by the linear relation which defines q_4 and q_5.

The quantities $N_{q_i \delta_j}$, $N^{q_i q_j}_{\delta_1 \delta_2}$ can now be expressed as determinants which have five rows and five columns. These determinants are obtained from $|a|$ in the following manner.

$N_{q_i \delta_j}$ is the determinant obtained from $|a|$ by replacing the i^{th} column by the j^{th} column of F corresponding to δ_j.

(replaces q_i column)

$$\left.\begin{matrix} F_{1j} \\ F_{2j} \\ F_{3j} \\ 0 \\ 0 \end{matrix}\right\}$$

$N^{q_i q_j}_{\delta_1 \delta_2}$ is the determinant obtained from $|a|$ by the two replacements

$$\left.\begin{matrix} F_{11} \\ F_{21} \\ F_{31} \\ 0 \\ 0 \end{matrix}\right\} \text{ replaces } i^{th} \text{ column}$$

$$\left.\begin{matrix} F_{12} \\ F_{22} \\ F_{32} \\ 0 \\ 0 \end{matrix}\right\} \text{ replaces } j^{th} \text{ column}$$

Note that $N^{q_i q_j}_{\delta_k \delta_k} = 0$ and $N^{q_i q_i}_{\delta_j \delta_k}$ is not allowed.

Thus, for example,

$$N_{q_3 \delta_1} = \begin{vmatrix} a_{11} & a_{12} & F_{11} & 0 & 0 \\ a_{21} & a_{22} & F_{21} & 0 & 0 \\ a_{31} & a_{32} & F_{31} & 0 & 0 \\ -a_{41} & -a_{42} & 0 & 1 & 0 \\ -a_{51} & -a_{52} & 0 & 0 & 1 \end{vmatrix} \tag{50}$$

$$= \begin{vmatrix} a_{11} & a_{12} & F_{11} \\ a_{21} & a_{22} & F_{21} \\ a_{31} & a_{32} & a_{31} \end{vmatrix}$$

$$N_{\delta_1 \delta_2}^{q_2 q_4} = \begin{vmatrix} a_{11} & F_{11} & a_{13} & F_{12} & 0 \\ a_{21} & F_{21} & a_{23} & F_{22} & 0 \\ a_{31} & F_{31} & a_{33} & F_{32} & 0 \\ -a_{41} & 0 & -a_{43} & 0 & 0 \\ -a_{51} & 0 & -a_{53} & 0 & 1 \end{vmatrix} \tag{51}$$

$$= \begin{vmatrix} a_{11} & F_{11} & a_{13} & F_{12} \\ a_{21} & F_{21} & a_{23} & F_{22} \\ a_{31} & F_{31} & a_{33} & F_{32} \\ -a_{41} & 0 & -a_{43} & 0 \end{vmatrix}$$

These definitions can be used to write the closed loop total system transfer functions. This gives solutions to equation 47 for all input to output choices. Solutions are given here for three systems of increasing complexity: Form I, Form II, and Form III as indicated in Figures 74, 75, and 76. The transfer functions are then given in Equations 52, 53, and 54.

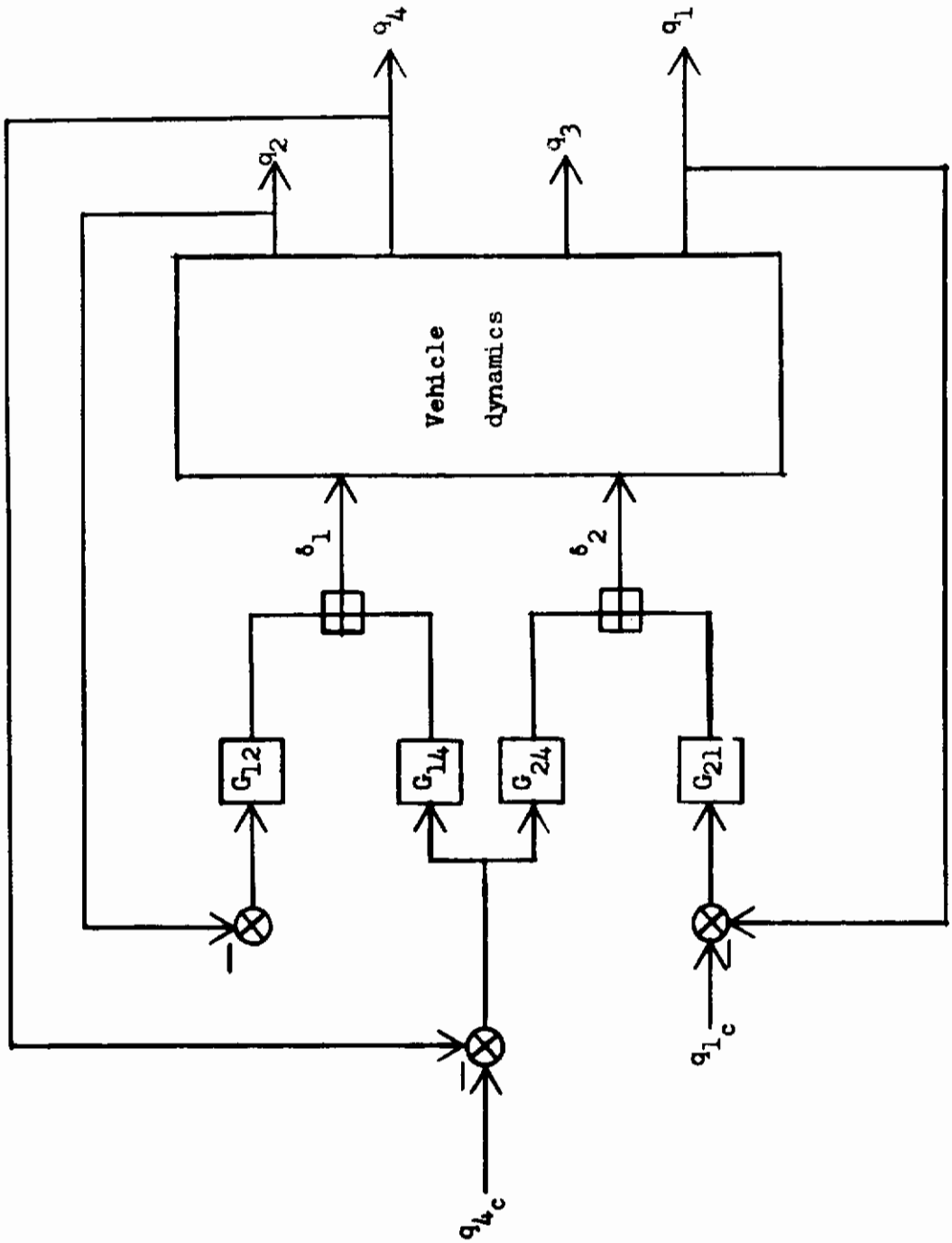

FIGURE 74. FORM I MULTILOOP DIAGRAM

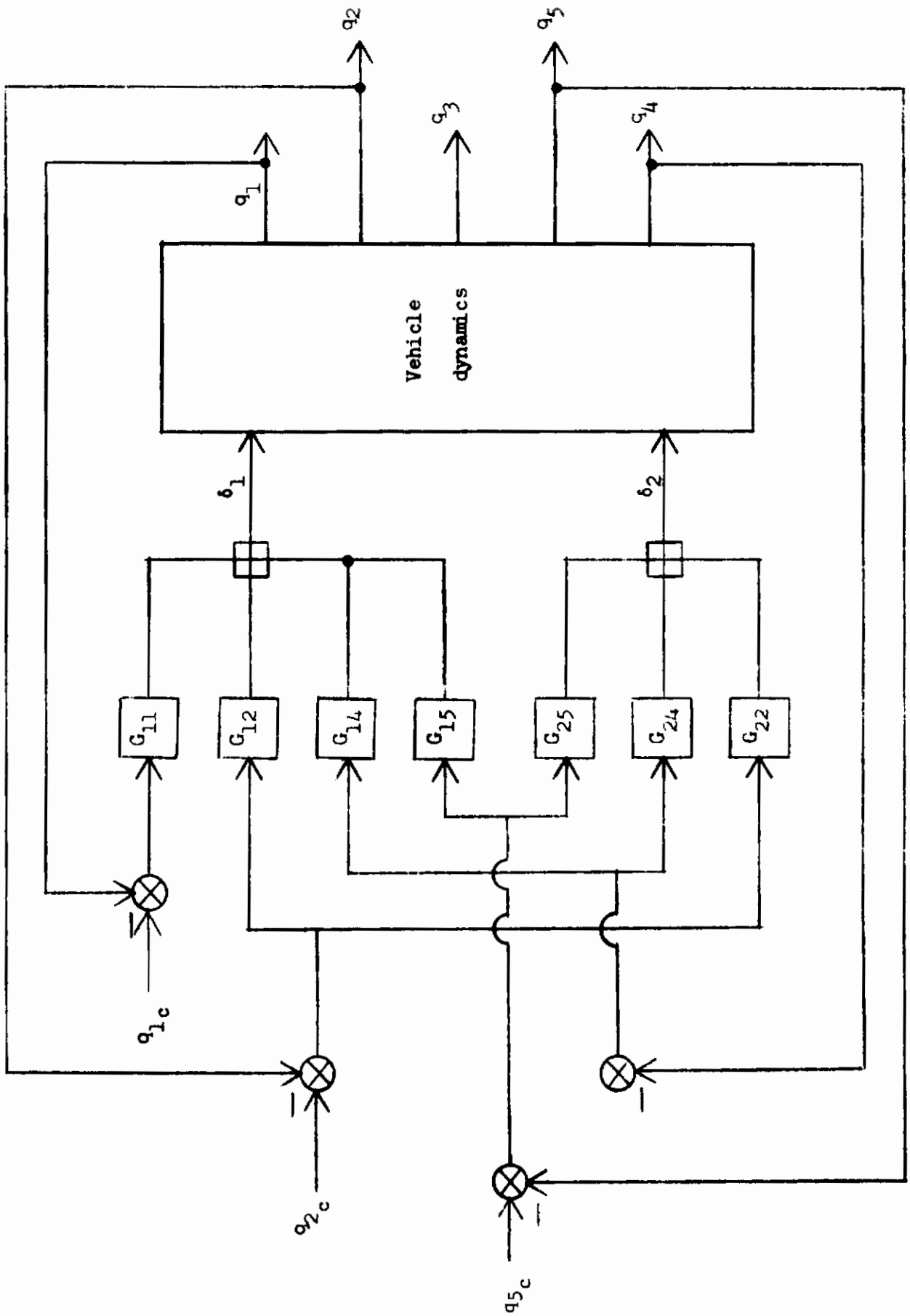

FIGURE 75. FORM II MULTILOOP DIAGRAM

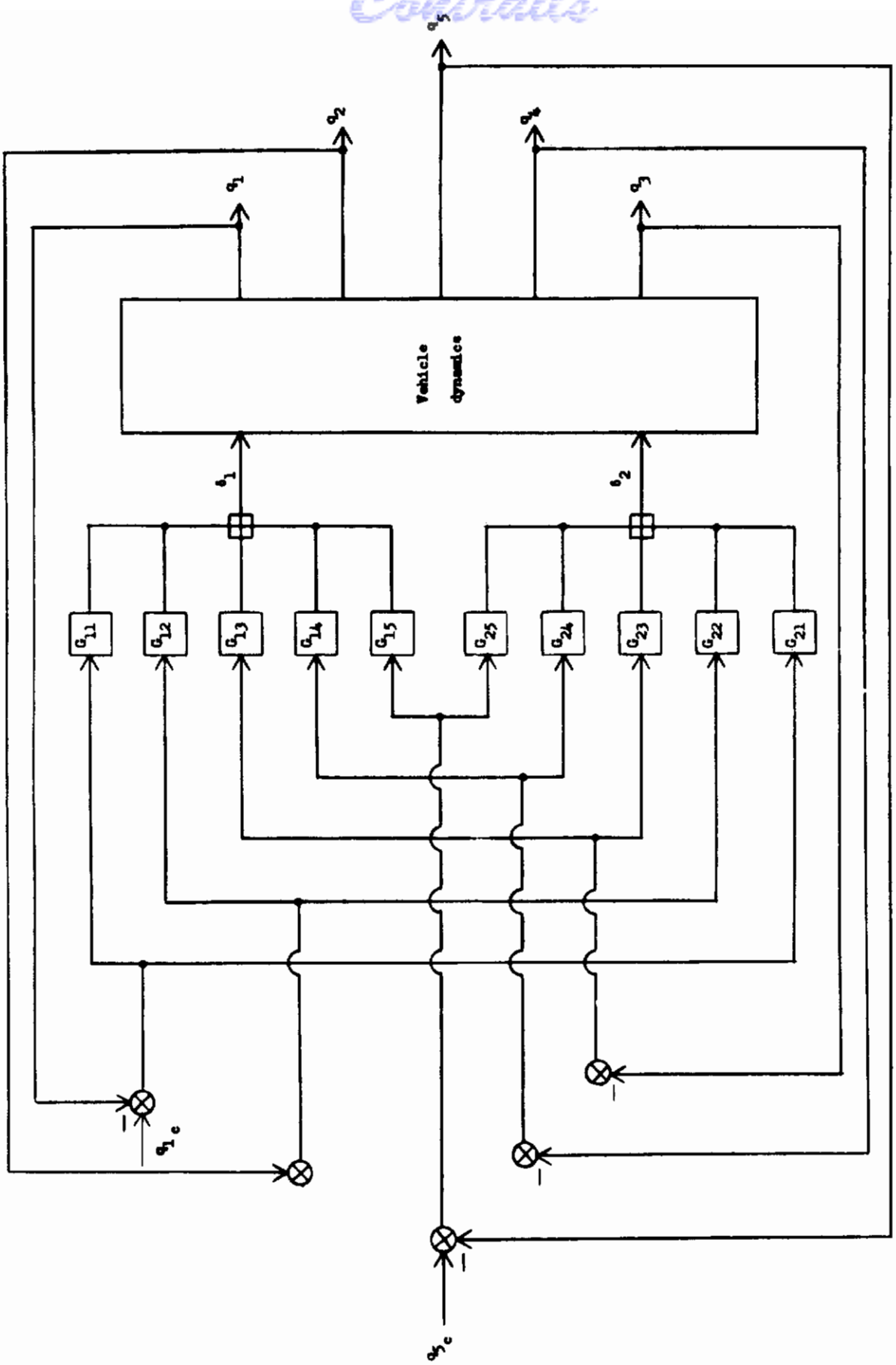

FIGURE 76. FORM III MULTILOOP DIAGRAM

$$\frac{q_i}{q_{1_c}} = \frac{G_{21}\left(N_{q_i\delta_2} + G_{12}N_{\delta_1\delta_2}^{q_2q_i} + G_{14}N_{\delta_1\delta_2}^{q_4q_i}\right)}{\Delta + G_{12}N_{q_2\delta_1} + G_{14}N_{q_4\delta_1} + G_{24}\left(N_{q_4\delta_2} + G_{12}N_{\delta_1\delta_2}^{q_2q_4}\right) + G_{21}\left(N_{q_1\delta_2} + G_{12}N_{\delta_1\delta_2}^{q_2q_1} + G_{14}N_{\delta_1\delta_2}^{q_4q_1}\right)}$$

$i = 1, 2, 3, 4$

$$\frac{q_i}{q_{4_c}} = \frac{G_{14}\left(N_{q_i\delta_1} + G_{21}N_{\delta_1\delta_2}^{q_iq_1}\right) + G_{24}\left(N_{q_i\delta_2} + G_{12}N_{\delta_1\delta_2}^{q_2q_i}\right)}{\Delta + G_{12}N_{q_2\delta_1} + G_{14}N_{q_4\delta_1} + G_{24}\left(N_{q_4\delta_2} + G_{12}N_{\delta_1\delta_2}^{q_2q_4}\right) + G_{21}\left(N_{q_1\delta_2} + G_{12}N_{\delta_1\delta_2}^{q_2q_1} + G_{14}N_{\delta_1\delta_2}^{q_4q_1}\right)}$$

$i = 1, 2, 3, 4$

EQUATION 52. FORM I TRANSFER FUNCTIONS

Let

$$\Delta_{sys} = \Delta_{II} = \Delta + G_{11}N_{q_1\delta_1} + G_{12}N_{q_2\delta_1} + G_{14}N_{q_4\delta_1}$$
$$+ G_{15}N_{q_5\delta_1} + G_{22}N_{q_2\delta_2} + G_{24}N_{q_4\delta_2}$$
$$+ G_{25}N_{q_5\delta_2}$$
$$+ G_{11}G_{22}N^{q_1q_2}_{\delta_1\delta_2} + G_{11}G_{24}N^{q_1q_4}_{\delta_1\delta_2} + G_{11}G_{25}N^{q_1q_5}_{\delta_1\delta_2}$$
$$+ G'_{14}G_{22}N^{q_4q_2}_{\delta_1\delta_2} + G_{14}G_{25}N^{q_4q_5}_{\delta_1\delta_2} + G_{12}G_{25}N^{q_2q_5}_{\delta_1\delta_2}$$
$$+ G_{15}G_{22}N^{q_5q_2}_{\delta_1\delta_2} + G_{15}G_{24}N^{q_5q_4}_{\delta_1\delta_2} + G_{12}G_{24}N^{q_2q_4}_{\delta_1\delta_2}$$

Then

$$\frac{q_i}{q_{1_c}} = \frac{G_{11}\left\{N_{q_i\delta_1} + G_{22}N^{q_iq_2}_{\delta_1\delta_2} + G_{24}N^{q_iq_4}_{\delta_1\delta_2} + G_{25}N^{q_iq_5}_{\delta_1\delta_2}\right\}}{\Delta_{II}}$$

$$i = 1, 2, 3, 4, 5$$

$$\frac{q_i}{q_{5_c}} = \frac{1}{\Delta_{II}}\left\{G_{15}\left(N_{q_i\delta_1} + G_{22}N^{q_iq_2}_{\delta_1\delta_2} + G_{24}N^{q_iq_4}_{\delta_1\delta_2}\right)\right.$$
$$\left. + G_{25}\left(N_{q_i\delta_2} + G_{11}N^{q_1q_i}_{\delta_1\delta_2} + G_{12}N^{q_2q_i}_{\delta_1\delta_2} + G_{14}N^{q_4q_i}_{\delta_1\delta_2}\right)\right\}$$

$$i = 1, 2, 3, 4, 5$$

EQUATION 53. FORM II TRANSFER FUNCTIONS

$$\frac{q_i}{q_{2_c}} = \frac{1}{\Delta_{II}} \left\{ G_{12} \left(N_{q_i \delta_1} + G_{24} N^{q_i q_4}_{\delta_1 \delta_2} + G_{25} N^{q_i q_5}_{\delta_1 \delta_2} \right) \right.$$

$$\left. + G_{22} \left(N_{q_i \delta_2} + G_{11} N^{q_1 q_i}_{\delta_1 \delta_2} + G_{14} N^{q_4 q_i}_{\delta_1 \delta_2} + G_{15} N^{q_5 q_i}_{\delta_1 \delta_2} \right) \right\}$$

$$i = 1, 2, 3, 4, 5$$

EQUATION 53. FORM II TRANSFER FUNCTIONS (Concluded)

$$\text{Let } \Delta_{sys} = \Delta_{III} = \Delta + \sum_{i=1}^{5} \sum_{j=1}^{2} G_{ji} N_{q_i \delta_j} + \sum_{i=1}^{5} \sum_{k=1}^{5} G_{1_i} G_{2_k} N^{q_i q_k}_{\delta_1 \delta_2}$$

$$\frac{q_i}{q_{1_c}} = \frac{1}{\Delta_{III}} \left\{ G_{11} \text{ (sum of terms containing } G_{11} \text{ with } q_i \text{ replacing } q_1) \right.$$

$$\left. + G_{21} \text{ (sum of terms containing } G_{21} \text{ with } q_i \text{ replacing } q_1) \right\}$$

where the terms summed are selected from Δ_{III}. $i = 1, 2, 3, 4, 5$

$$\frac{q_i}{q_{5_c}} = \frac{1}{\Delta_{III}} \left\{ G_{15} \text{ (sum of terms containing } G_{15} \text{ with } q_i \text{ replacing } q_5) \right.$$

$$\left. + G_{25} \text{ (sum of terms containing } G_{25} \text{ with } q_i \text{ replacing } q_5) \right\}$$

EQUATION 54. FORM III TRANSFER FUNCTIONS

APPENDIX II GUIDE TO THE MULTILOOP ANALYSIS PROGRAM

APPENDIX II GUIDE TO THE MULTILOOP ANALYSIS PROGRAM

INTRODUCTION

The rating of an aircraft using an analytical formula which is a function of closed-loop pilot-vehicle performance and pilot workload requires a method of calculating the required formula variables. The multiloop analysis technique was selected to perform this task because it produces transfer functions composed of parts which are intuitively related to physical system parameters. However, the technique requires the laborious calculation of many polynomials as explained in Appendix I. The primary purpose of the multiloop analysis digital program is to relieve the investigator of the chore of performing the multiloop analysis calculations.

In order to be used as a versatile research tool, the program has remained very general in nature. The flow chart of Figure 77 gives a general description of the logic involved in the program setup. Note that inputs may be either dimensional or dimensionless aircraft parameters. The multiloop polynomials required are calculated and the transfer functions are then formulated. The program may additionally be used to calculate the rms performance of a command tracking task or a turbulence disturbance. In all cases, the program has been kept as modular as possible so that parts may be interchanged or removed to meet specific requirements.

Program Elements

The Program is designed to accept dimensionless derivatives in the stability axis system or dimensional derivatives in the stability axis system but using the conversion to the prime notation convention (Reference 18). If dimensionless parameters are entered, the program will convert them to the dimensional, prime system notation convention. For completeness, the operations used in this conversion are given in Table I.

The equations of motion describing the vehicle are expressed in the stability axis system because of simplicity. The equations used are listed below in Table II.

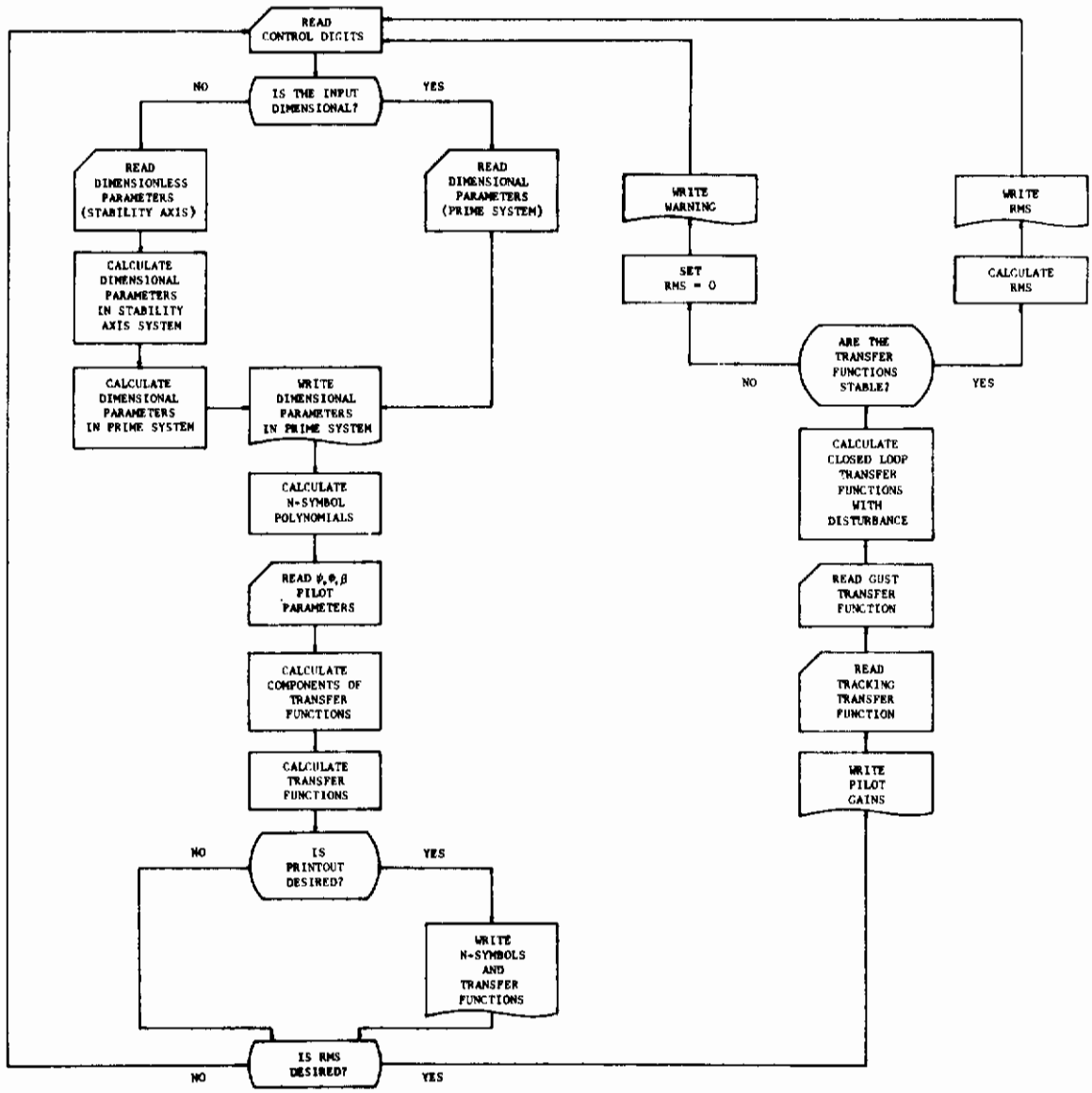

FIGURE 77. MULTILOOP ANALYSIS PROGRAM FLOW CHART

TABLE I. TRANSFORMATION TO DIMENSIONAL DERIVATIVES

$$Y_v = \frac{\rho U_o S}{2m} C_{y_\beta}$$

$$L_v = \frac{\rho U_o S b}{2 I_{xx}} C_{l_\beta}$$

$$L_\beta = U_o L_v$$

$$N_v = \frac{\rho U_o S b}{2 I_{zz}} C_{n_\beta}$$

$$N_\beta = U_o N_v$$

$$L_p = \frac{\rho U_o S b^2}{4 I_{xx}} C_{l_p}$$

$$N_p = \frac{\rho U_o S b^2}{4 I_{zz}} C_{n_p}$$

$$L_r = \frac{\rho U_o S b^2}{4 I_{xx}} C_{l_r}$$

$$N_r = \frac{\rho U_o S b^2}{4 I_{zz}} C_{n_r}$$

$$Y^*_{\delta r} = \frac{1}{U_o} Y_{\delta_r} = \frac{\rho U_o S}{2m} C_{y_{\delta r}}$$

$$L_{\delta r} = \frac{\rho U_o^2 S b}{2 I_{xx}} C_{l_{\delta r}}$$

$$N_{\delta r} = \frac{\rho U_o^2 S b}{2 I_{zz}} C_{n_{\delta r}}$$

$$Y^*_{\delta a} = \frac{1}{U_o} Y_{\delta_a} = \frac{\rho U_o S}{2m} C_{y_{\delta a}}$$

$$L_{\delta a} = \frac{\rho U_o^2 S b}{2 I_{zz}} C_{l_{\delta a}}$$

$$N_{\delta a} = \frac{\rho U_o^2 S b}{2 I_{zz}} C_{n_{\delta a}}$$

TRANSFORMATION TO PRIME NOTATION CONVENTION

$$L'_i = \frac{L_i + (I_{xz}/I_{xx}) N_i}{1 - (I_{xz}^2/I_{xx}I_{zz})}$$

$$N'_i = \frac{N_i + (I_{xz}/I_{zz}) L_i}{1 + (I_{xz}^2/I_{xx}I_{zz})}$$

TABLE II. EQUATIONS OF MOTION

$$(-g/U_o \cos\theta_o)\phi + (1-g/U_o \frac{1}{s} \sin\theta_o)\, r + (s - Y_v)\beta = Y^*_{\delta a}\,\delta a + Y^*_{\delta r}\,\delta r + Yv\,\delta g_\beta$$

$$s(s-L'_p)\phi + (-L'_r)\, r + (-L'_\beta)\beta = L'_{\delta a}\,\delta a + L'_{\delta r}\,\delta r + L'_\beta\,\delta g_\beta$$

$$(-sN'_p)\phi + (s-N'_r)\, r + (-N'_\beta)\beta = N'_{\delta a}\,\delta a + N'_{\delta r}\,\delta r + N'_\beta\,\delta g_\beta$$

$$\left(\frac{1}{s}\sec\theta_o\right) r = \psi$$

Note that the pitch angle, θ_o, has not been assumed to be zero. Hence, the equation may be used to describe vehicle dynamics during a dive. If θ_o is large, the resulting effective rotation of the gravity vector significantly modifies the dynamic modes. Also note that the coefficients Y_r and Y_p have been deleted from the equations. The effect of these two parameters is usually not significant. However, this assumption should be checked in each case and particularly in those cases where the aircraft under investigation is unconventional. The reader should also note that in addition to the normal lateral forcing function inputs of aileron, δa, and rudder, δr, a δg_β has been included. This input represents the disturbance caused by the change in β resulting from lateral, v, turbulence. Hence, the input β- gust, δg_β, was included. The coefficients (Y_v, L'_β, N'_β) which distribute this input over the equations of motion are simply the static force and moment coefficient of the normal sideslip angle, β. This relationship will adequately describe the effects of the v gust inputs.

The block diagram shown in Figure 1 depicts the pilot-vehicle system which can be investigated using the program. Provisions have been made for the pilot to control heading, bank angle, and sideslip with an additional control loop for a yaw-rate damper. The required transfer functions are given in Table III in the proper multiloop analysis notation. The N- symbol polynomials (i.e., $N_{\psi_{\delta_a}}$, . . .) are computed by evaluating the proper determinants. The expressions for these N- symbols are given in Table IV. Comments within the digital program give the areas where each N- symbol is calculated. Program notation follows the multiloop analysis notation very closely; i.e., $N_{\psi_{\delta_a}}$ becomes N/SI/DA in the program.

TABLE III. REQUIRED TRANSFER FUNCTIONS

$$\Delta'' = \Delta + Y_\phi N_{\phi_{\delta a}} + Y_\psi N_{\psi_{\delta a}} + Y_\beta N_{\beta_{\delta r}} + Y_r N_{r_{\delta r}} + Y_\phi Y_r N_{\delta a \delta r}^{\phi r} + Y_\phi Y_\beta N_{\delta a \delta r}^{\phi \beta} + Y_\psi Y_\beta N_{\delta a \delta r}^{\psi \beta}$$

$$\frac{\beta}{\delta g_\beta} = \frac{N_{\beta_{\delta g_\beta}} + Y_\phi N_{\delta g_\beta \delta a}^{\beta \phi} + Y_\psi N_{\delta g_\beta \delta a}^{\beta \psi} + Y_r N_{\delta g_\beta \delta r}^{\beta r}}{\Delta''}$$

$$\left| \begin{array}{l} r \to \delta r \\ \beta \to \delta r \\ \phi \to \delta a \\ \psi \to \delta a \end{array} \right.$$

$$\frac{\phi}{\delta g_\beta} = \frac{N_{\phi_{\delta g_\beta}} + Y_\psi N_{\delta g_\beta \delta a}^{\phi \psi} + Y_\beta N_{\delta g_\beta \delta r}^{\phi \beta} + Y_r N_{\delta g_\beta \delta r}^{\phi r}}{\Delta''}$$

$$\left| \begin{array}{l} r \to \delta r \\ \beta \to \delta r \\ \phi \to \delta a \\ \psi \to \delta a \end{array} \right.$$

$$\frac{\psi}{\delta g_\beta} = \frac{N_{\psi_{\delta g_\beta}} + Y_\phi N_{\delta g_\beta \delta a}^{\psi \phi} + Y_\beta N_{\delta g_\beta \delta r}^{\psi \beta}}{\Delta''}$$

$$\left| \begin{array}{l} r \to \delta r \\ \beta \to \delta r \\ \phi \to \delta a \\ \psi \to \delta a \end{array} \right.$$

TABLE III. REQUIRED TRANSFER FUNCTIONS (Concluded)

$$\frac{\psi}{\psi_e} = \frac{Y_\psi\left(N_{\psi\,\delta a} + Y_\beta\, N^{\psi\ \beta}_{\delta a\ \delta r}\right)}{\Delta + Y_\phi\, N_{\phi\,\delta a} + Y_r\, N_{r\,\delta r} + Y_\beta\, N_{\beta\,\delta r} + Y_\phi Y_r\, N^{\phi\ r}_{\delta a\ \delta r} + Y_\phi\, Y_\beta\, N^{\phi\ \beta}_{\delta a\ \delta r}}$$

$$\left|\begin{array}{l} r \rightarrow \delta r \\ \beta \rightarrow \delta r \\ \phi \rightarrow \delta a \\ \psi \rightarrow \delta a \end{array}\right.$$

$$\frac{\phi}{\phi_e} = \frac{Y_\phi\left(N_{\phi\,\delta a} + Y_r\, N^{\phi\ r}_{\delta a\ \delta r} + Y_\beta\, N^{\phi\ \beta}_{\delta a\ \delta r}\right)}{\Delta + Y_\psi N_{\psi\,\delta a} + Y_r\, N_{r\,\delta r} + Y_\beta\, N_{\beta\,\delta r} + Y_\psi\, Y_\beta\, N^{\psi\ \beta}_{\delta a\ \delta r}}$$

$$\left|\begin{array}{l} r \rightarrow \delta r \\ \beta \rightarrow \delta r \\ \phi \rightarrow \delta a \\ \psi \rightarrow \delta a \end{array}\right.$$

$$\frac{\beta}{\beta_e} = \frac{Y_\beta\left(N_{\beta\,\delta r} + Y_\phi\, N^{\beta\ \phi}_{\delta r\ \delta a} + Y_\psi\, N^{\beta\ \psi}_{\delta r\ \delta a}\right)}{\Delta + Y_\phi N_{\phi\,\delta a} + Y_\psi\, N_{\psi\,\delta a} + Y_r\, N_{r\,\delta r} + Y_\phi Y_r N^{\phi\ r}_{\delta a\ \delta r}}$$

$$\left|\begin{array}{l} r \rightarrow \delta r \\ \beta \rightarrow \delta r \\ \phi \rightarrow \delta a \\ \psi \rightarrow \delta a \end{array}\right.$$

TABLE IV. N-SYMBOL POLYNOMIALS

$$\Delta = s^4 + (-N_{r'} - Y_v - L_{p'})\, s^3 + (N_{\beta'} + N_{r'}\, Y_v + L_{p'}\, N_{r'} + L_p\, Y_v - N_p L_{r'})\, s^2 + (-(g/U_o)\cos\theta_o\, L_{\beta'} - N_{\beta'}\, L_{p'} - N_{r'}\, Y_v\, L_{p'} + N_{p'}\, L_{\beta'} + L_{r'}\, Y_v\, N_{p'} - N_{\beta'}\, (g/U_o)\sin\theta_o)\, s + (-(g/U_o)\cos\theta_o\, L_{r'}\, N_{\beta'} + (g/U_o)\cos\theta_o\, N_{r'}\, L_{\beta'} + (g/U_o)\sin\theta_o\, (L_{p'}\, N_{\beta'} - N_{p'}\, L'_{\beta})$$

$$N^{r\ \beta}_{\delta a\, \delta r} = \left(N'_{\delta a}\, Y^*_{\delta r} - Y^*_{\delta a}\, N'_{\delta r}\right) s^2 + \left(L'_p\, Y^*_{\delta a}\, N'_{\delta r} - L'_p\, N'_{\delta a}\, Y^*_{\delta r} + N_{p'}\, Y^*_{\delta r}\, L'_{\delta a} - N_{p'}\, Y^*_{\delta a}\, L'_{\delta r}\right) s + \left((g/U_o)\cos\theta_o\, N'_{\delta a}\, L'_{\delta r} - (g/U_o)\cos\theta_o\, L'_{\delta a}\, N'_{\delta r}\right)$$

$$N^{r\ \phi}_{\delta r\, \delta a} = (L'_{\delta a}\, N'_{\delta r} - N'_{\delta a}\, L'_{\delta r})\, s + \left(-Y_v L'_{\delta a}\, N'_{\delta r} + Y_v\, N'_{\delta a}\, L'_{\delta r} + L'_{\beta}\, Y^*_{\delta a}\, N'_{\delta r} - L'_{\beta}\, N'_{\delta a}\, Y^*_{\delta r} - N'_{\beta}\, Y^*_{\delta a}\, L'_{\delta r} + N'_{\beta}\, L'_{\delta a}\, Y^*_{\delta r}\right)$$

$$N_{r_{\delta r}} = (N_{\delta r})\, s^3 + (Y^*_{\delta r}\, N_{\beta'} - N'_{\delta r}\, Y_v - N'_{\delta r}\, L'_p + N'_p\, L'_{\delta r})\, s^2 + (-Y^*_{\delta r}\, L'_p\, N'_{\beta} + L'_p\, N'_{\delta r}\, Y_v + N'_p\, Y^*_{\delta r}\, L'_{\beta} - N'_p\, L'_{\delta r} Y_v)\, s + \left((g/U_o)\cos\theta_o\, L'_{\delta r}\, N'_{\beta} - (g/U_o)\cos\theta_o\, N'_{\delta r}\, L'_{\beta}\right)$$

TABLE IV. N-SYMBOL POLYNOMIALS (Continued)

$$s\,N_{\phi_{\delta a}} = (L'_{\delta a})\,s^3$$

$$+ (Y^*_{\delta a}\,L'_\beta - L'_{\delta a}\,Y_v - L'_{\delta a}\,N'_r + N'_{\delta a}\,L'_r)\,s^2$$

$$+ (Y^*_{\delta a}\,L'_r\,N'_\beta - Y^*_{\delta a}\,N'_r\,L'_\beta + L'_{\delta a}\,N'_\beta + N'_r\,Y_v\,L'_{\delta a} - N'_{\delta a}\,L'_\beta - N'_{\delta a}\,L'_r\,Y_v)\,s$$

$$+ (g/U_o)\,(\sin\theta_o)\,(N'_{\delta a}\,L'_\beta - L'_{\delta a}\,N'_\beta)$$

$$s\,N_{\psi_{\delta_a}} = \Big[(-N'_{\delta a})\,s^3$$

$$+ (Y_v\,N'_{\delta a} - N'_\beta\,Y^*_{\delta a} + L'_p\,N'_{\delta a} - N'_p L'_{\delta a})\,s^2$$

$$+ (-L'_p\,Y_v\,N'_{\delta a} + L'_p\,N'_\beta\,Y^*_{\delta a} + N'_p\,Y_v\,L'_{\delta a} - N'_p\,L'_\beta\,Y^*_{\delta a})\,s$$

$$+ (g/U_o\cos\theta_o\,L'_\beta\,N'_{\delta a} - g/U_o\cos\theta_o\,L'_{\delta a}\,N'_\beta)\Big] \Big/ -\cos\theta_o$$

$$N_{\beta_{\delta_r}} = (Y'_{\delta r})\,s^3$$

$$+ (-N'_{\delta r} - Y^*_{\delta r}\,L'_p - N'_r\,Y'_{\delta r})\,s^2$$

$$+ \Big((g/U_o)\cos\theta_o\,L'_{\delta r} + L'_p\,N'_{\delta r} - L'_{\delta r}\,N'_p + Y'_{\delta r}\,L'_p\,N'_r - Y'_{\delta r}\,L'_r\,N'_p$$

$$+ (g/U_o)\sin\theta_o\,N'_{\delta r}\Big)s$$

$$+ \Big((g/U_o)\cos\theta_o\,L'_r\,N'_{\delta r} - (g/U_o)\cos\theta_o\,L'_{\delta r}\,N'_r - (g/U_o)\sin\theta_o\,L'_p\,N'_{\delta r}$$

$$+ (g/U_o)\sin\theta_o\,L'_{\delta r}\,N'_p\Big)$$

$$s\,N^{\phi\ \beta}_{\delta a\ \delta r} = (Y^*_{\delta r}\,L'_{\delta a} - Y^*_{\delta a}\,L'_{\delta r})\,s^2$$

$$+ (Y^*_{\delta a}\,L'_{\delta r}\,N'_r - Y^*_{\delta a}\,L'_r\,N'_{\delta r} - L'_{\delta a}\,N'_{\delta r} + L'_{\delta r}\,N'_{\delta a} - Y^*_{\delta r}\,L'_{\delta a}\,N'_r + Y^*_{\delta r}\,L'_r\,N'_{\delta a})s$$

$$+ (L'_{\delta a}\,N'_{\delta r}\,(g/U_o)\sin\theta_o - L'_{\delta r}\,N'_{\delta a}\,(g/U_o)\sin\theta_o)$$

TABLE IV. N-SYMBOL POLYNOMIALS (Continued)

$$N_{\beta_{\delta g_\beta}} = (-Y_v)\, s^3$$
$$+ (L'_p\, Y_v + N'_\beta + Y_v\, N'_r)\, s^2$$
$$+ (-g/U_o \cos\theta_o\, L'_\beta - L'_p\, N'_\beta - g/U_o \sin\theta_o\, N'_\beta$$
$$+ N'_p\, L'_\beta + N'_p\, L'_r\, Y_v - L'_p\, Y_v\, N'_r)\, s$$
$$+ (-g/U_o \cos\theta_o\, L'_r\, N'_\beta + (g/U_o \cos\theta_o\, L'_\beta\, N'_r$$
$$+ (g/U_o \sin\theta_o\, N'_\beta\, L'_p - g/U_o \sin\theta_o\, L'_\beta\, N'_p)$$

$$sN^{\beta\ \phi}_{\delta g_\beta\ \delta a} = (Y^*_{\delta a}\, L'_\beta - L'_{\delta a}\, Y_v)\, s^2$$
$$+ (L'_{\delta a}\, N'_\beta - N'_{\delta a}\, L'_\beta + L'_r\, Y^*_{\delta a}\, N'_\beta - L'_r\, N'_{\delta a}\, Y_v$$
$$- N'_r\, Y^*_{\delta a}\, L'_\beta + N'_r\, L'_{\delta a}\, Y_v)\, s$$
$$+ (-(g/U_o) \sin\theta_o\, L'_{\delta a}\, N'_\beta + (g/U_o) \sin\theta_o\, N'_{\delta a}\, L'_\beta)$$

$$N^{\beta\ r}_{\delta g_\beta \delta a} = (Y^*_{\delta a}\, N'_\beta - N'_{\delta a}\, Y_v)\, s^2$$
$$+ (-L'_p\, Y^*_{\delta a}\, N'_\beta + N'_{\delta a}\, L'_p\, Y_v + N'_p\, Y^*_{\delta a}\, L'_\beta - N'_p\, L'_{\delta a}\, Y_v)s$$
$$+ ((g/U_o) \cos\theta_o\, L'_{\delta a}\, N'_\beta - (g/U_o) \cos\theta_o\, N'_{\delta a}\, L'_\beta)$$

$$N_{\phi_{\delta g_\beta}} = (-L'_\beta)s^2$$
$$+ (L'_\beta\, N'_r - N'_\beta\, L'_r)s$$

TABLE IV. N-SYMBOL POLYNOMIALS (Continued)

$$sN^{\phi\ \beta}_{\delta g_\beta \delta r} = (L'_{\delta r}\, Y_v - L'_\beta\, Y^*_{\delta r})\, s^2$$
$$+ (L'_\beta\ N'_{\delta r} - N'_\beta\ L'_{\delta r} + L'_r\, Y_v\, N'_{\delta r}$$
$$- L'_r\, N'_\beta\ Y^*_{\delta r} - N'_r\, Y_v\, L'_{\delta r} + N'_r\, L'_\beta\ Y^*_{\delta r})s$$
$$+ (-g/U_o) \sin\theta_o\, L'_\beta\, N'_{\delta r} + (g/U_o) \sin\theta_o\, N'_\beta\ L'_{\delta r})$$

$$N^{\phi\ r}_{\delta g_\beta \delta r} = \left(- L'_\beta\, N'_{\delta r} + N'_\beta\, L'_{\delta r}\right)s$$

$$N_{r_{\delta g\beta}} = (- N'_\beta)\ s^3$$
$$+ (L'_p\, N'_\beta - N'_p\, L'_\beta)\, s^2$$

$$N^{r\ \phi}_{\delta g_\beta \delta a} = \left(N'_{\delta a}\, L'_\beta - L'_{\delta a}\, N'_\beta\right)s$$

$$N^{r\ \beta}_{\delta g_\beta \delta r} = \left(Y_v\, N'_{\delta r} - N'_\beta\, Y^*_{\delta r}\right)s^2$$
$$+ \left(- L'_p\, Y_v\, N'_{\delta r} + L'_p\, N'_\beta\, Y^*_{\delta r} \quad + N'_p\, Y_v\, L'_{\delta r} - N'_p\, L'_\beta\, Y^*_{\delta r}\right)s$$
$$+ \left((g/U_o) \cos\theta_o\, L'_\beta\, N'_{\delta r} - (g/U_o) \cos\theta_o\, N'_\beta\, L'_{\delta r}\right)$$

$$N^{\psi\ \beta}_{\delta a \delta r} = \frac{\sec\theta_o}{s}\, N^{r\ \beta}_{\delta a \delta r}$$

$$N^{\phi\ \psi}_{\delta g_\beta \delta a} = \frac{\sec\theta_o}{s}\, N^{\phi\ r}_{\delta g_\beta \delta a}$$

TABLE IV. N-SYMBOL POLYNOMIALS (Concluded)

$$N_{\psi \delta g_\beta} = \frac{\sec \theta_o}{s} N_{r_{\delta g_\beta}}$$

$$N^{\psi\ \beta}_{\delta g_\beta \delta r} = \frac{\sec \theta_o}{s} N^{r\ \beta}_{\delta g_\beta \delta r}$$

$$N^{\psi\ \phi}_{\delta g_\beta \delta a} = \frac{\sec \theta_o}{s} N^{r\ \phi}_{\delta g_\beta \delta a}$$

$$N^{\phi\ r}_{\delta g_\beta \delta a} = \left(- L'_\beta N'_{\delta a} + N'_\beta L'_{\delta a}\right) s$$

$$N^{\beta\ r}_{\delta g_\beta \delta r} = \left(Y_{\delta r} N'_\beta - N'_{\delta r} Y_v\right) s^2$$

$$\left(- L'_p Y_{\delta r} N'_\beta + N'_{\delta r} L'_p Y_v + N'_p Y'_{\delta r} L'_\beta - N'_p L'_{\delta r} Y_v\right)$$

$$+ (g/U_o) \cos \theta_o \left(L'_{\delta r} N'_\beta - N'_{\delta r} L'_\beta\right)$$

$$N^{\beta\ \ \psi}_{\delta g_\beta \delta a} = \frac{\sec \theta_o}{s} N^{\beta\ \ r}_{\delta g_\beta \delta a}$$

Pilot transfer functions may be entered into the program as the ratio of two polynomials. For example, the heading pilot, Y_ψ is expressed as:

$$Y_\psi = (\text{Gain}) \frac{(\text{Pilot Compensation Numerator})}{(\text{Pilot Compensation Denominator})} \cdot \frac{(\text{Time Delay Approximation Numerator})}{(\text{Time Delay Approximation Denominator})}$$

The complete list of pilot transfer functions is given in Table V in the notation that will be used in referring to them.

TABLE V. PILOT MODEL NOTATION

$$Y_\psi = K_\psi \frac{P_{\psi 1}}{P_{\psi 2}} \cdot \frac{D_{\psi 1}}{D_{\psi 2}}$$

$$Y_\phi = K_\phi \frac{P_{\phi 1}}{P_{\phi 2}} \cdot \frac{D_{\phi 1}}{D_{\phi 2}}$$

$$Y_\beta = K_\beta \frac{P_{\beta 1}}{P_{\beta 2}} \cdot \frac{D_{\beta 1}}{D_{\beta 2}}$$

$$Y_r = K_r \frac{P_{r1}}{P_{r2}}$$

The labeling of variables within the digital program has been contrived to be in phonetic agreement with the notation of Table IV. The numerator coefficients of the pilot compensation part of Y are labeled PSI1(n). The remaining polynomials are labeled similarly.

Because the pilot transfer functions are ratios of polynomials, the fractions must be cleared in the expressions for the transfer functions. This is accomplished in a straight-forward manner by multiplying the numerator and denominator of each transfer function by a factor F defined by:

$$F = s\, P_{\psi_2}\, P_{\phi_2}\, P_{\beta_2}\, D_{\psi_2}\, D_{\phi_2}\, D_{\beta_2}\, P_{r2}$$

The results of this operation are given in Table VI. Again, labeling of variables in the program correspond closely to those of Table VI; i.e., the coefficients of $\Delta\psi$ become DSI (n). Note that this method of clearing fractions implies that if a pilot model is not to be considered, all polynomials should be set to 1.0 and the gain to 0.0.

The calculation of system response to a command tracking signal is described below for the bank angle command task. A block diagram of the system is given in Figure 78. Note that the ϕ/ϕ_ϵ transfer function contains all possible loop closures, not just the bank angle loop, but that the command to all loops except bank angle is zero. The transfer function required for performance evaluation is $\phi_{\epsilon/W.N.}$ Manipulation of the system in Figure 78 gives the result:

$$\frac{\phi_\epsilon}{W.N.} = \frac{\phi_{c/W.N.}}{1 + \phi/\phi_\epsilon} \tag{55}$$

Similar expressions may be derived for heading and sideslip by replacing ϕ in the above relationship with the parameter of interest.

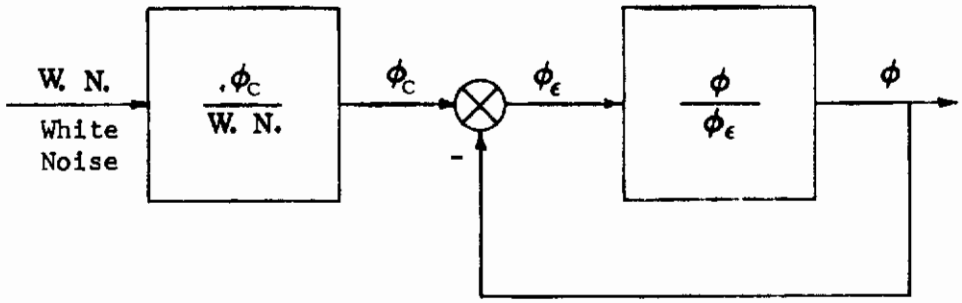

FIGURE 78. BANK ANGLE COMMAND BLOCK DIAGRAM

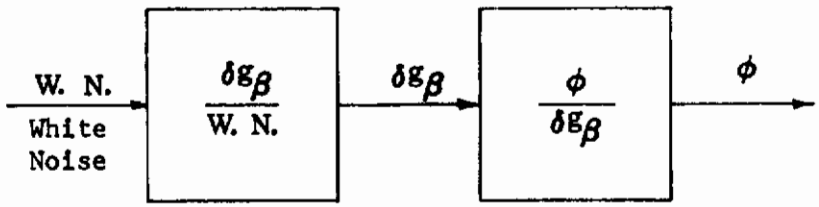

FIGURE 79. BANK ANGLE TURBULENCE BLOCK DIAGRAM

TABLE VI. TRANSFER FUNCTIONS

$$\frac{\beta}{\beta_g} = \frac{FN''_{\beta_{\delta g_\beta}}}{F\Delta''}$$

$$\frac{\psi}{\beta_g} = \frac{FN''_{\psi_{\delta g_\beta}}}{F\Delta''}$$

$$\frac{\phi}{\beta_g} = \frac{FN''_{\phi_{\delta g_\beta}}}{F\Delta''}$$

$$F\Delta'' = \Delta_1 + K_\phi\Delta_\phi + K_\psi\Delta_\psi + K_\beta\Delta_\beta + K_r\Delta_r + K_\phi K_\beta\Delta\phi\beta + K_\psi K_\beta\Delta\psi\beta + K_r K_\phi\ \Delta r\phi$$

where

$$\Delta 1 = SP_{\psi 2}\, P_{r2}\, P_{\phi 2}\, P_{\beta 2}\, D_{\psi 2}\, D_{\phi 2}\, D_{\beta 2}\, (\Delta)$$

$$\Delta\phi = P_{r2}\, P_{\psi 2}\, P_{\phi 1}\, P_{\beta 2}\, D_{\psi 2}\, D_{\phi 1}\, D_{\beta 2}\, (SN_{\phi\delta a})$$

$$\Delta\psi = P_{r2}\, P_{\psi 1}\, P_{\phi 2}\, P_{\beta 2}\, D_{\psi 1}\, D_{\phi 2}\, D_{\beta 2}\, (SN_{\psi\delta a})$$

$$\Delta\beta = SP_{\psi 2}\, P_{r2}\, P_{\phi 2}\, P_{\beta 1}\, D_{\psi 2}\, D_{\phi 2}\, D_{\beta 1}\, (N\beta_{\delta r})$$

$$\Delta r = S\ P_{r1}\, P_{\psi 2}\, P_{\phi 2}\, P_{\beta 2}\, D_{\psi 2}\, D_{\phi 2}\, D_{\beta 2}\, (N_{r\delta r})$$

$$\Delta\phi\beta = P_{r2}\, P_{\psi 2}\, P_{\phi 1}\, P_{\beta 1}\, D_{\psi 2}\, D_{\phi 1}\, D_{\beta 1}\, (SN^{\phi\ \beta}_{\delta a\delta r})$$

$$\Delta\psi\beta = P_{r2}\, P_{\psi 1}\, P_{\phi 2}\, P_{\beta 1}\, D_{\psi 1}\, D_{\phi 2}\, D_{\beta 1}\, (SN^{\psi\ \beta}_{\delta a\delta r})$$

$$\Delta r\phi = S\, P_{r1}\, P_{\psi 2}\, P_{\phi 1}\, P_{\beta 2}\, D_{\phi 1}\, D_{\psi 2}\, D_{\beta 2}\, (N^{r\ \phi}_{\delta r\delta a})$$

TABLE VI. TRANSFER FUNCTIONS (Continued)

$$FN''_{\beta\,\delta g_\beta} = s\,P_{r_2}\,P_{\psi_2}\,P_{\phi_2}\,P_{\beta_2}\,D_{\psi_2}\,D_{\phi_2}\,D_{\beta_2}\left(N_{\beta\,\delta g_\beta}\right) + K_\phi\,P_{\psi_2}\,P_{r_2}\,P_{\phi_1}\,P_{\beta_2}\,D_{\psi_2}\,D_{\phi_1}\,D_{\beta_2}\left(s\,N^{\beta\ \phi}_{\delta g_\beta\ \delta a}\right) + K_\psi\,P_{r_2}\,P_{\psi_1}\,P_{\phi_2}\,P_{\beta_2}\,D_{\psi_1}\,D_{\phi_2}\,D_{\beta_2}\left(s\,N^{\beta\ \psi}_{\delta g_\beta\ \delta a}\right) + K_r\,s\,P_{r_1}\,P_{\psi_2}\,P_{\phi_2}\,P_{\beta_2}\,D_{\psi_2}\,D_{\phi_2}\,D_{\beta_2}\left(N^{\beta\ r}_{\delta g_\beta\ \delta r}\right)$$

$$FN''_{\phi\,\delta g_\beta} = s\,P_{\psi_2}\,P_{r_2}\,P_{\phi_2}\,P_{\beta_2}\,D_{\psi_2}\,D_{\phi_2}\,D_{\beta_2}\left(N_{\phi\,\delta g_\beta}\right) + K_\beta\,P_{r_2}\,P_{\psi_2}\,P_{\phi_2}\,P_{\beta_1}\,D_{\psi_2}\,D_{\phi_2}\,D_{\beta_1}\left(s\,N^{\phi\ \beta}_{\delta g_\beta\ \delta r}\right) + K_\psi\,P_{r_2}\,P_{\psi_1}\,P_{\phi_2}\,P_{\beta_2}\,D_{\psi_1}\,D_{\phi_2}\,D_{\beta_2}\left(s\,N^{\phi\ \psi}_{\delta g_\beta\ \delta a}\right) + s\,K_r\,P_{r_1}\,P_{\psi_2}\,P_{\phi_2}\,P_{\beta_2}\,D_{\psi_2}\,D_{\phi_2}\,D_{\beta_2}\left(N^{\phi\ r}_{\delta g_\beta\ \delta r}\right)$$

$$FN''_{\psi\,\delta g_\beta} = P_{\psi_2}\,P_{r_2}\,P_{\phi_2}\,P_{\beta_2}\,D_{\psi_2}\,D_{\phi_2}\,D_{\beta_2}\left(s\,N_{\psi\,\delta g_\beta}\right) + K_\phi\,P_{r_2}\,P_{\psi_2}\,P_{\phi_1}\,P_{\beta_2}\,D_{\psi_2}\,D_{\phi_1}\,D_{\beta_2}\left(s\,N^{\psi\ \phi}_{\delta g_\beta\ \delta a}\right) + K_\beta\,P_{r_2}\,P_{\psi_2}\,P_{\phi_2}\,P_{\beta_1}\,D_{\psi_2}\,D_{\phi_2}\,D_{\beta_1}\left(s\,N^{\psi\ \beta}_{\delta g_\beta\ \delta r}\right)$$

Command Transfer Functions:

$$\frac{\psi}{\psi_\epsilon} = \frac{K_\psi\,(\Delta\psi + K_\beta\Delta\psi\beta)}{\Delta_1 + K_\phi\Delta_\phi + K_\beta\Delta_\beta + K_\phi K_\beta\,\Delta_{\phi_\beta} + K_r\,\Delta_r + K_r\,K_\phi\Delta_{r\phi}}$$

$$\frac{\phi}{\phi_\epsilon} = \frac{K_\phi\,(\Delta\phi + K_\beta\Delta\phi\beta + K_r\,\Delta_{r\phi})}{\Delta_1 + K_\psi\,\Delta_\psi + K_\beta\,\Delta_\beta + K_\psi\,K_\beta\,\Delta_{\psi_\beta} + K_r\Delta_r}$$

$$\frac{\beta}{\beta_\epsilon} = \frac{K_\beta(\Delta_\beta + K_\phi\,\Delta_{\phi\beta} + K_\psi\,\Delta_{\psi\beta})}{\Delta_1 + K_\phi\Delta_\phi + K_\psi\Delta_\psi + K_r\,\Delta_r + K_r\,K_\phi\Delta_{r\phi}}$$

Remember that the command signal goes only to the loop of interest and the command to the remaining loops is zero.

The response to gust disturbances is formulated as shown in the block diagram of Figure 76. The command to all control loops during the gust disturbance is zero. Therefore, the output of the system is the error. In the example given $\phi = \phi_\epsilon$. Hence, the required transfer function is:

$$\frac{\phi}{W.N.} = \frac{\beta_g}{W.N.} \frac{\phi}{\beta_g} \tag{56}$$

Transfer functions for heading and sideslip may be obtained by substituting for ϕ as before.

The rms system performance is calculated by evaluating the integral form:

$$I_n = \frac{1}{2\pi_j} \int_{-j\infty}^{j\infty} \left| \frac{c\ (s)}{a\ (s)} \right|^2 ds \tag{57}$$

This evaluation is performed digitally through the use of an Air Force subroutine explained in FDCC TM 65-17. Verification for transfer functions of order 10 have indicated accuracy to five significant figures.

Output Format

A sample of the program output format is given in Figure 80. The labeling of the output is largely self-explanatory once the operation of the program is understood.

Input Format

The input format is given in Figure 81.

Cautions in Program Use

1. The axis of the yaw rate gyro of a yaw rate damper may not coincide with the stability axis system. Hence, inappropriate use of the yaw rate damper loop in design can lead to erroneous results.
2. If a pilot model is not to be used, all its numerator and denominator polynomials should be set to 1.0 and its gain to 0.0.
3. In interpreting rms results, remember that the three command tracking results represent the command signal applied at three different points, while the gust results represent reaction to the single lateral disturbance.
4. The rms calculations may become inaccurate for system orders >10. The program uses a scaling factor in an attempt to keep numbers involved below 10^{38}. However, if an overflow message results or erratic rms values are generated, the scaling should be checked.

DIMENSIONAL DERIVATIVES...PRIME AXIS SYSTEM

YV= -0.50022262E 00 YDR= 0.86149395E-01 YDA=-0.11984501E-01 NB= 0.89688988E 01 NP= 0.11286491E 00

NR= -0.54589915E 00 NDR=-0.72979650E 01 NDA= 0.35173190E 00 LB= -0.29062820E 02 LP= -0.18557234E 01

LR= 0.40454578E 00 LDA= 0.20227386E 02 LDR= 0.62888346E 01

DELTA				
0.10000000E 01	0.29018450E 01	0.11137622E 02	0.15150860F 02	0.54879194E 00
N/R/DA/B/DR				
-0.57160936E-01	0.99107325E-01	0.67194271E 01		
N/R/DR				
-0.72979650E 01	-0.15711156E 02	-0.52681952E 01	-0.69824448E 01	
N/R/DR/PHI/DA				
-0.14983073E 03	-0.60304962E 02			
SN/PHI/DA				
0.20227386E 02	0.21650894E 02	0.19738101E 03	0.0	
SN/SI/DA				
0.35173190E 00	0.30041351E 01	0.13083353E 01	0.85944252E 01	
N/B/DR				
0.86149395E-01	0.75048628E 01	0.13198586E 02	0.21558259E-01	
SN/PHI/DA/B/DR				
0.18179445E 01	0.15080000E 03	0.0		
N/B/DGB				
0.50022262E 00	0.10170243E 02	0.15150875E 02	0.54879194E 00	
SN/B/DGB/PHI/DA				
0.10466498E 02	0.19738101E 03	0.0		
N/B/DGB/R/DA				
0.68456471E-01	0.13083363E 01	0.85944252E 01		
N/PHI/DGB				
0.29062820E 02	0.12237040E 02	0.0		
SN/PHI/DGB/B/DR				
-0.64207268E 00	0.15650926E 03	0.0		
N/PHI/DGB/R/DA				
0.19163969E 03	0.0			
N/R/DGB				
-0.89688988E 01	-0.13363611E 02	0.0	0.0	
N/R/DGB/PHI/DA				
-0.19163969E 03	0.0			
N/R/DGB/B/DR				
0.28779411E 01	0.52681971E 01	0.69824448E 01		
SN/SI/DA/B/DR				
-0.57160936E-01	0.99107325E-01	0.67194271E 01		
SN/PHI/DGB/SI/DA				
0.19163969E 03	0.0			

FIGURE 80 MULTILOOP ANALYSIS PROGRAM OUTPUT

```
SN/B/DGB/SI/DA
      0.68456471E-01      0.13083363E 01      0.85944252E 01
SN/SI/DGB
     -0.89688988E 01     -0.13363611E 02      0.0                 0.0
SN/SI/DGB/PHI/DA
     -0.19163969E 03      0.0
SN/SI/DGB/B/DR
      0.28779411E 01      0.52681971E 01      0.69824448E 01
N/PHI/DGB/R/DR
     -0.15569553E 03      0.0
N/B/DGB/R/DR
     -0.28779411E 01     -0.52681952E 01     -0.69824448E 01

              THE SI PER SI ERROR TRANSFER FUNCTION IS BELOW
NUMERATOR
      0.12310612E 00      0.34560575E 01      0.33529053E 02      0.76873688E 02     -0.94295508E 03
     -0.85397617E 04     -0.32584902E 05     -0.73473750E 05     -0.11677744E 06     -0.13692981E 06
     -0.83205188E 05
DENOMINATOR
      0.10000000E 01      0.37638596E 02      0.61827563E 03      0.58839063E 04      0.36466926E 05
      0.15728781E 06      0.49084038E 06      0.11201160E 07      0.18283030E 07      0.20276060E 07
      0.14098390E 07      0.49838250E 06      0.0
              THE PHI PER PHI ERROR TRANSFER FUNCTION IS BELOW
NUMERATOR
      0.70795841E 01      0.15104362E 03      0.10301030E 04      0.83967041E 02     -0.37368824E 05
     -0.25230219E 06     -0.93022681E 06     -0.21987640E 07     -0.30924570E 07     -0.19100690E 07
      0.0
DENOMINATOR
      0.10000000E 01      0.37638596E 02      0.62003320E 03      0.59213242E 04      0.36721102E 05
      0.15730113E 06      0.48159250E 06      0.10578960E 07      0.15990050E 07      0.14852620E 07
      0.64840525E 06      0.34558098E 05      0.83205117E 04
              THE B PER B ERROR TRANSFER FUNCTION IS BELOW
NUMERATOR
      0.30152284E-01      0.32154884E 01      0.58927155E 02      0.34252710E 03     -0.61402637E 03
     -0.16603543E 05     -0.84988188E 05     -0.21693388E 06     -0.30854275E 06     -0.24393513E 06
     -0.91798938E 05     -0.15951406E 04
DENOMINATOR
      0.10000000E 01      0.37641617E 02      0.61858496E 03      0.58894531E 04      0.36497824E 05
      0.15721875E 06      0.46927431E 06      0.11124720E 07      0.18098680E 07      0.20040990E 07
      0.13971240E 07      0.50289556E 06      0.81610000E 04
              THE N/B/DGB NUMERATOR IS BELOW
      0.50022262E 00      0.27470581E 02      0.61277222E 03      0.74420313E 04      0.54881328E 05
      0.25743606E 06      0.77940719E 06      0.15143460E 07      0.18500570E 07      0.13606290E 07
      0.50289556E 06      0.81610000E 04
              THE N/PHI/DGB NUMERATOR IS BELOW
      0.29062820E 02      0.10162549E 04      0.15015898E 05      0.12172094E 06      0.58713006E 06
      0.17043320E 07      0.28528910E 07      0.24672060E 07      0.96004994E 06      0.33059163E 06
      0.0
```

FIGURE 80 (continued)

```
                    THE N/SI/DGB NUMERATOR IS BELOW
 -0.89688988E 01     -0.31849609E 03     -0.47952266E 04     -0.39952922E 05     -0.20191906E 06

 -0.63967619E 06     -0.12745790E 07     -0.15770160E 07     -0.11741380E 07     -0.43999075E 06
  0.66303125E 04
                    THE OPEN LOOP DENOMINATOR FOR THE B GUST IS BELOW
  0.10000000E 01      0.37638596E 02      0.61826318E 03      0.58835586E 04      0.36463570E 05
  0.15728006E 06      0.49093463E 06      0.11209690E 07      0.18315600E 07      0.20349520E 07
  0.14215160E 07      0.51207538E 06      0.83205117E 04

SI=    -0.1000      KPHI=    -0.2500      KB=    -0.1000

     THE RMS ERROR OF SI/SI ERROR IS 0.97792E 01

     THE RMS ERROR OF PHI/PHI ERROR IS 0.65218E 01

     THE RMS ERROR OF B/B ERROR IS 0.98353E 01

     THE RMS ERROR OF N/B/DGB IS 0.11418E 01

     THE RMS ERROR OF N/PHI/DGB IS 0.32177E 01

     THE RMS ERROR OF N/SI/DGB IS 0.10312E 01
```

FIGURE 80 (Concluded)

KEY PUNCH FORM - GENERAL PURPOSE

Form 20-708 (R-1 69)

JOB TITLE					ENGINEER	PAGE 1 of 3
DPWA SERIAL NO.	PRE.	NDP JOB NO.	DASH	FOR ORGN NO.	ANALYST	DATE

INPUT FOR MULTILOOP ANALYSIS PERFORMANCE PROGRAM

The necessary input format for the program is described below, along with required explanations. Note that the symbol * before a line indicates the data card as opposed to explanations.

* | N | N | N |

+1 indicates dimensional input; -1 indicates dimensionless input.

+1 by-pass tracking & gust filter inputs & rms calculations; -1 indicates tracking & gust filter data and gives rms.

+1 by-pass N-symbol and transfer function print outs; -1 gives all print-outs.

Dimensional Input ($'$ axis system)

A*

Y_v	Y'_{sr}	Y'_{sa}	N'_β	N'_p	N'_r	
N'_{sr}	N'_{sa}	L'_β	L'_p	L'_r	L'_{sa}	
L'_{sr}	u_o	Θ_o	0			

Dimensionless Input (stability axis system)

B*

C_{y_β}	$C_{y_{sr}}$	$C_{y_{sa}}$	C_{n_β}	C_{n_p}	C_{n_r}	
$C_{n_{sr}}$	$C_{n_{sa}}$	C_{ℓ_β}	C_{ℓ_p}	C_{ℓ_r}	$C_{\ell_{sa}}$	
$C_{\ell_{sr}}$	ρ	S	u_o	b	Mass	
I_{xx}	I_{zz}	I_{xz}	Θ_o (deg)	g		

N.B. either A or B above must be included in each data set.

* | m | n_1 | n_2 | n_3 |

Integer indicating the number of coefficients in the Pade denominator.

Integer indicating the number of coefficients in the Pade numerator.

Integer indicating the number of coefficients in the Pilot denominator.

Integer indicating the number of coefficients in the Pilot numerator.

* | Ψ_n | Ψ_{n-1} | Ψ_{n-2} | Ψ_{n-3} | Ψ_{n-4} | |

Ψ_n = s^{nd} coefficient of the Pilot numerator.

FIGURE 81 MULTILOOP PROGRAM INPUT

KEY PUNCH FORM - GENERAL PURPOSE

Form 20-708 (R-1 69)

JOB TITLE | ENGINEER | PAGE 2 OF 3

DPWA SERIAL NO. | PRE | NCP JOB NO | DASH | FOR ORGN NO. | ANALYST | DATE

$Y_{n-1} = s^{n-2}$ coefficient of the pilot numerator,

etc.

N.B. No more than 5 coefficients may be entered

* coefficients of the pilot denominator are entered in the same manner as those of the Y_{pilot} numerator.

* coefficients of the Pade numerator are entered in the same manner as those of the Y_{pilot} numerator.

* coefficients of the Pade denominator are entered in the same manner as those of the Y_{pilot} numerator.

* K_y

K_y is the gain of the Y_{pilot} model.

*

*

* The Φ_{pilot} model and Pade approximation are entered here in the same manner as the Y_{pilot} model and Pade

* approximation preceeding.

*

*

*

* The β_{pilot} model and Pade approximation are entered here in the same manner as the Y_{pilot} model and Pade

* approximation preceeding.

*

*

* K | N

N — Integer indicating the number of coefficients in the yaw rate damper denominator ≤ 5.

K — Integer indicating the number of coefficients in the yaw rate damper numerator ≤ 5.

* Y_{r_n} | $Y_{r_{n-1}}$ | $Y_{r_{n-2}}$ | $Y_{r_{n-3}}$ | $Y_{r_{n-4}}$

FIGURE 81 (CONTINUED)

KEY PUNCH FORM - GENERAL PURPOSE

Form 2[illegible] (R.[illegible] 69)

JOB TITLE					ENGINEER	PAGE 3 of 3
OPWA SERIAL NO.	PRE	NEXT JOB NO.	DASH	FOR ORGN. NO.	ANALYST	DATE

$y_{r_n} = s^{n-1}$ coefficient of the yaw rate damper numerator.

$y_{r_{n-1}} = s^{n-2}$ coefficient of the yaw rate damper numerator.

etc.

* Coefficients of the yaw rate damper denominator are entered in the same manner as the numerator.

* K_r

K_r is the gain of the yaw rate damper.

The above data must appear in each data set. If rms calculations are desired, the following data must be entered.

* I I

Integer indicating the number of coefficients in the tracking filter denominator.

Integer indicating the number of coefficients in the tracking filter numerator.

* τ_n | τ_{n-1} | ... | ... | ... | τ_0

τ_n = the coefficient of s^n in the tracking filter numerator.

τ_{n-1} = the coefficient of s^{n-1} in the tracking filter numerator.

etc. for as many cards as necessary to enter the numerator coefficients.

NB The product of the numerator of the system transfer function and the tracking filter numerator is limited to order 28 (29 coefficients).

* The tracking filter denominator is entered here in the same manner as the numerator above.

NB The product of the denominator of the system transfer function and the tracking filter denominator is limited to order 29 (30 coefficients).

*

* The gust filter is entered here in the same manner as the tracking filter preceeding.

*

As many complete data sets may be "stacked" as desired.

FIGURE 81 (CONCLUDED)

APPENDIX III SIMULATION

LIST OF SYMBOLS FOR APPENDIX III

A_{y_p}	- Side acceleration at the pilot's station, ft/sec^2	
A_{z_p}	- Normal acceleration at the pilot's station, ft/sec^2	
A_{gust}, B_{gust}, C_{gust}	- Gust filter constants, 1/sec or 1/sec^2	
A_{tc}	- Tracking filter time constant, 1/sec	
b	- Airplane wing span, ft	
C_D	= $D/\frac{1}{2}\rho V_o^2 S$,	Airplane drag coefficient
C_{D_o}	- Drag coefficient at zero angle of attack	
C_{D_α}	= $\partial C_D/\partial\alpha$,	Nondimensional drag coefficient derivative with respect to angle of attack, 1/rad
$C_{D_\alpha 2}$	= $\partial C_D/\partial\alpha^2$,	Nondimensional drag coefficient derivative with respect to angle of attack squared, 1/rad^2
C_l	= $L/\frac{1}{2}\rho V_o^2 Sb$,	Airplane rolling moment coefficient
C_{l_r}	= $\partial C_l/\partial(rb/2V_o)$,	Nondimensional rolling moment coefficient derivative with respect to yawing rate, 1/rad
C_{l_β}	= $\partial C_l/\partial\beta$,	Nondimensional rolling moment coefficient derivative with respect to sideslip, 1/rad
C_L	= $L/\frac{1}{2}\rho_o V_o^2 S$,	Airplane lift coefficient
C_{L_o}	- Lift coefficient at zero angle of attack	
C_{L_α}	= $\partial C_L/\partial\alpha$,	Nondimensional lift coefficient derivative with respect to angle of attack, 1/rad
$C_{L_{\delta e}}$	= $\partial C_L/\partial\delta e$,	Nondimensional lift coefficient derivative with respect to elevator control, 1/rad
C_n	= $N/\frac{1}{2}\rho_o V_o^2 Sb$,	Airplane yawing moment coefficient
C_{n_p}	= $\partial C_n/\partial(pb/2V_o)$,	Nondimensional yawing moment coefficient derivative with respect to rolling rate, 1/rad

$C_{n_{\delta as}}$ = $\partial C_n / \partial \delta_{as}$, Yawing moment coefficient derivative with respect to aileron control 1/in

D - Drag, lb

g - Acceleration due to gravity, ft/sec^2

h - Altitude, ft

I_x - Moment of inertia about x-axis, ft-lb-sec^2

I_y - Moment of inertia about y-axis, ft-lb-sec^2

I_z - Moment of inertia about z-axis, ft-lb-sec^2

I_{xz} - Product of inertia, ft-lb-sec^2

$K = \left| 1 - (I_{xz}^2 / I_x I_z) \right|^{-1}$

K_{aug} - Yaw augmenter gain, in/ft/sec

K_{gust} - Gust filter gain, rad/volt-sec

$K_{p_1} = \dfrac{Kq_o S b}{I_x} \left(\dfrac{\partial C_{l_\beta}}{\partial \alpha} \right)$, 1/sec^2

$K_{p_2} = \dfrac{Kq_o S b^2}{2 V_o I_x} \left(\dfrac{\partial C_{l_r}}{\partial \alpha} \right)$, 1/sec

$K_{p_3} = \dfrac{Kq_o S b^2 I_{xz}}{2 V_o I_x I_z} \left(\dfrac{\partial C_{n_p}}{\partial \alpha} \right)$, 1/sec

$K_{p_4} = -\dfrac{Kq_o S b I_{xz}}{I_x I_z} \left(\dfrac{\partial C_{n_{\delta as}}}{\partial \alpha} \right)$, 1/in-sec^2

$K_{p\theta}$ - Simulator-beam vertical drive signal compensation gain term, rad/volt

$K_{p\psi}$ - Simulator-beam lateral drive signal compensation gain term, rad/volt

$K_{r_1} = \dfrac{Kq_o S b^2}{2 V_o Iz} \left(\dfrac{\partial C_{n_p}}{\partial \alpha} \right)$, 1/sec

$K_{r_2} = \dfrac{Kq_o S b}{I_z} \left(\dfrac{\partial C_{n_{\delta as}}}{\partial \alpha} \right)$, 1/in-sec

K_{r_3} = $\frac{Kq_o S b I_{xz}}{I_x I_z}\left(\frac{\partial C_{\ell_\beta}}{\partial \alpha}\right)$, $1/sec^2$

K_{r_4} = $\frac{Kq_o S b^2 I_{xz}}{2 V_o I_x I_z}\left(\frac{\partial C_{\ell_r}}{\partial \alpha}\right)$, $1/sec$

K_{tc} - Tracking filter gain, rad/volt-sec^2

K_θ - Simulator-cockpit pitch drive signal gain

$K_{\ddot{\theta}}$ - Simulator-beam vertical drive signal washout gain

K_{θ_M} - Simulator-cockpit pitch drive signal compensation gain term, rad/volt

K_ϕ - Simulator-cockpit roll drive signal washout gain

K_{θ_M} - Simulator-cockpit yaw drive signal compensation gain term, rad/volt

K_ψ - Simulator-cockpit yaw drive signal washout gain

$K_{\ddot{\psi}}$ - Simulator-beam lateral drive signal washout gain

K_{ψ_M} - Simulator-cockpit yaw drive signal compensation gain term, rad/volt

l_B - Distance between simulator cockpit gimbal center and simulator beam gimbal center, ft

l_x - Distance from airplane center of gravity to the pilot's station along the x-axis, ft

L - Rolling moment, ft-lb; Lift, lb

L_p = $(1/I_x)(\partial L/\partial p)$, $1/sec$

L_r = $(1/I_x)(\partial L/\partial r)$, $1/sec$

L_β = $(1/I_x)(\partial L/\partial \beta)$, $1/sec^2$

$L_{\delta as}$ = $(1/I_x)(\partial L/\partial \delta as)$, $1/sec^2$ - in

$L_{\delta rp}$ = $(1/I_x)(\partial L/\partial \delta r p)$, $1/sec^2$ - in

L_i' = $\left|L_i + (I_{xz}/I_x) N_i\right| \cdot K$; $i = \beta, \beta_{as}, \delta_{rp}, p, r$

m - W/g, lb-sec^2/ft

M - Pitching moment, ft-lb

M_q = $(1/I_z)(\delta M/\delta q)$, $1/sec$

M_α = $(1/I_z)\ (\partial M/\partial \alpha)$, $1/sec^2$

$M_{\dot{\alpha}}$ = $(1/I_z)\ (\partial M/\partial \dot{\alpha})$, $1/sec$

M_{δ_e} = $(1/I_z)\ (\partial M/\partial \delta_e)$, $1/sec^2$

N - Yawing moment, ft-lb

N_g - Noise generator signal, Gaussian, 50 Hz bandwidth, infinite random sequence length

N_p = $(1/I_z)\ (\partial N/\partial p)$, $1/sec$

N_r = $(1/I_z)\ (\partial N/\partial r)$, $1/sec$

N_β = $(1/I_z)\ (\partial N/\partial \beta)$, $1/sec^2$

$N_{\partial as}$ = $(1/I_z)\ (\partial N/\partial \delta_{as})$, $1/sec^2$-in

$N_{\partial r_p}$ = $(1/I_z)\ (\partial N/\partial \delta_{rp})$, $1/sec^2$-n

$N_{y_{cg}}$ - Side acceleration at airplane center of gravity, g units

$N_{z_{cg}}$ - Normal acceleration at airplane center of gravity, g units

N_i' = $\left[N_i + (I_{xz}/I_x)L_i\right] \cdot K$; $i = \beta,\ \delta_{as},\ \delta_{rp},\ p,\ r$

p - Roll rate, rad/sec

q_o = $1/2\,\rho V_o^2$, dynamic pressure, lbs/ft^2

r - Yaw rate, rad/sec

s - Laplace operator, 1/sec

T_{sx} - Thrust, lb

T_{θ_1} - Simulator-beam vertical drive signal rate washout constant, sec

T_{θ_2} - Simulator-beam vertical drive signal position washout constant, sec^2

T_{ψ_1} - Simulator-beam lateral drive signal rate washout constant, sec

T_{ψ_2} - Simulator-beam lateral drive signal position washout constant, sec^2

V_o	- Initial true velocity, ft/sec
ΔV	- Perturbation true velocity, ft/sec
W	- Airplane weight, lb
x, y, z	- Stability axes (i.e., a right hand orthogonal body-axis system with origin at the center of gravity, the z-axis in the plane of symmetry and the x-axis aligned with the relative wind of zero sideslip trimmed flight)
Y	- side force, lb
Y_β	= $(1/m V_o)$ $(\partial Y/\partial \beta)$, 1/sec
$Y_{\delta_{rp}}$	= $(1/m V_o)$ $(\partial Y/\partial \delta_{rp})$, 1/sec-in
α	- Angle of attack, rad
β	- Angle of sideslip, rad
δ_{as}	- Aileron stick deflection, in
δ_e	- Elevator deflection, rad
δ_{rp}	- Rudder pedal deflection, in
θ	- Pitch angle, rad
θ_{BD}	- Washed-out simulator-beam vertical drive signal with compensation
θ_{BW}	- Washed-out simulator-beam vertical drive signal without compensation
θ_M	- Simulator-cockpit pitch drive signal without compensation
ρ	- Atmospheric density, lbs-sec^2/ft^4
τ_1, τ_2	- Simulator-beam lateral drive signal compensation time constants, sec
τ_3, τ_4	- Simulator-beam vertical drive signal compensation time constants, sec
τ_{aug}	- Yaw augmenter time constant, sec
τ_{θ_M}	- Simulator-cockpit pitch drive signal compensation time constant, sec
τ_{ϕ_M}	- Simulator-cockpit roll drive signal compensation time constant, sec
τ_{ϕ_W}	- Simulator-cockpit roll drive signal washout time constant, sec
τ_{ψ_M}	- Simulator-cockpit yaw drive signal compensation time constant, sec
τ_{ψ_W}	- Simulator-cockpit yaw drive signal washout time constant, sec

ϕ	- Roll angle, rad
ϕ_M	- Washed-out simulator-cockpit roll drive signal without compensation
ψ	- Yaw angle, rad
ψ_{BD}	- Washed-out simulator-beam lateral drive signal with compensation
ψ_{BW}	- Washed-out simulator-beam lateral drive signal without compensation
ψ_M	- Washed-out simulator-cockpit yaw drive signal without compensation

APPENDIX III: SIMULATION

INTRODUCTION

The following discussion presents the experiments performed on the Northrop Large Amplitude 3-Axis Flight Simulator. The experiments were designed to gather information pertaining to lateral handling qualities during precision tracking tasks. The simulator dynamics and the tasks were carefully controlled to provide the best possible data. Descriptions of the simulator, the tasks, and the pilots follow:

SIMULATION

An external view of the Northrop 3-Axis Large Amplitude Flight Simulator is shown in Figure 82. The motion system of the moving base simulator employs a gimballed cockpit suspended at the end of a beam as shown. The three rotational degrees of freedom are obtained through the gimbals. The beam is pivoted on a clevis and driven by front and rear hydraulic actuators to provide vertical translation. Lateral translation is derived through a pivoting mechanism between the clevis and the post, driven by hydraulic actuators.

A satisfactory level of fidelity in the output characteristics of the simulator response must be achieved within the limitations imposed by the following constraints:

1. Available hydraulic power imposes magnitude limits on acceleration and velocity motion response.
2. Total travel of the simulator sets limits on displacement.
3. The motion control servo sets upper and lower limits on the dynamic response of the simulator.
4. Coulomb and breakaway friction exist in the output of the servodrive. The motion performance capability of the simulator is summarized in Table VII. Figure 83 shows a typical response of the simulator translation motion system to sinusoidal inputs, and indicates how velocity saturation sets amplitude limits on motion response over midrange frequencies. Acceleration saturation determines amplitude limits at high frequencies, and position saturation sets displacement limits at low frequency.

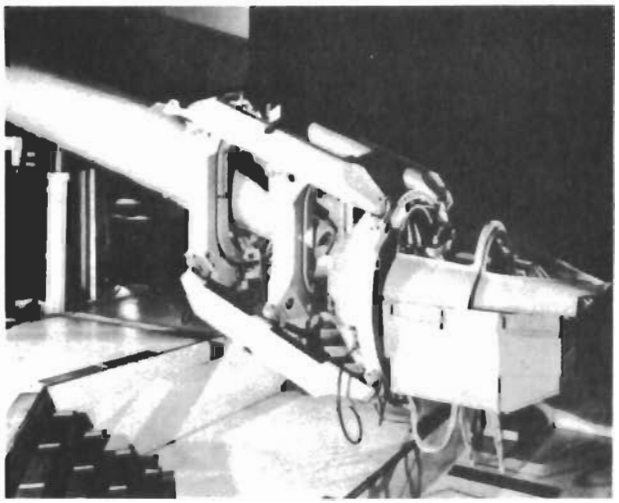

LARGE-AMPLITUDE 3-AXIS FLIGHT SIMULATOR

FIGURE 82

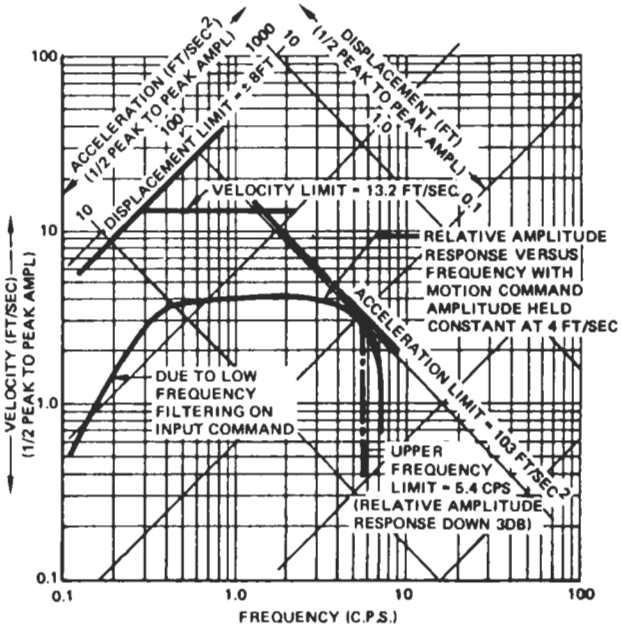

RESPONSE OF VERTICAL TRANSLATED MOTION SYSTEM AT PILOT'S STATION TO STEADY SINUSOIDAL MOTION

FIGURE 83

TABLE VII. PERFORMANCE SUMMARY LARGE-AMPLITUDE 3-AXIS FLIGHT SIMULATOR

				TWO-PLACE COCKPIT –		ONE-PLACE COCKPIT –	
				BEAM STATIONARY	BEAM MAX ACCEL	BEAM STATIONARY	BEAM MAX ACCEL
		DISPLACE-MENT	VELOCITY	ACCEL-ERATION	ACCEL-ERATION	ACCEL-ERATION	ACCEL-ERATION
BEAM	VERTICAL	±10 FEET	±16.2 FT/SEC	–	±4.8 g	–	±5.8 g
	LATERAL	±4 FEET	±21.6 FT/SEC	–	±1.8 g	–	±2.2 g
COCKPIT	PITCH	±30°	±1.1 RAD/SEC	±24.4 RAD/SEC²	±14.4 RAD/SEC²	SAME AS TWO-PLACE COCKPIT	
	YAW	±30°	±1.5 RAD/SEC	±20.3 RAD/SEC²	±15.0 RAD/SEC²		
	ROLL	±45°	±2.7 RAD/SEC	±35.3 RAD/SEC²	±29.1 RAD/SEC²		

An external visual display is also available for use with the simulator. However, all experiments were performed under instrument flight rules and no external visual display was used.

A pictorial description of the drive philosophy is given in Figure 84. Note that the essential requirements are that beam movements provide linear acceleration cues and that cab movements provide rotational and attitude cues. In practice, the drive system filters must be "tuned" to provide the maximum possible fidelity within the limits of the equipment. Since the tasks involved in this simulation required no large amplitude maneuvers, very good motion cues could be obtained without fear of reaching simulator limits. The frequency response obtained by "tuning" the simulation is given in Figure 85. Details of the drive equation and vehicle dynamics are given in Tables II through XIV. Note that the full five degrees of freedom of the simulator were used in conjunction with the six-degree-of-freedom representation of the vehicle on the analog computers.

Four distinct tasks were evaluated during the simulation. The tasks are described below.

1. Follow a commanded random bank angle.

   A signal generated by filtering white noise with $\frac{s}{(s + 0.5)^2}$ was used to indicate the command bank angle. The difference between this signal and the actual bank angle was applied to the vertical needle of the ADI. The pilot's instructions were to keep the needle centered by varying bank angle with the ailerons while not allowing altitude to vary "too much." The rudder was not to be used.

2. Maintain zero bank angle in the presence of turbulence.

   A Dryden form lateral, or v, directional velocity gust of varying intensities was introduced through the equations of motion. The actual bank angle, which in this case was the error, was presented on the vertical needle of the ADI. The pilot's instructions were to keep the needle centered by controlling bank angle with the ailerons while not allowing altitudes to vary "too much." The rudder was not to be used.

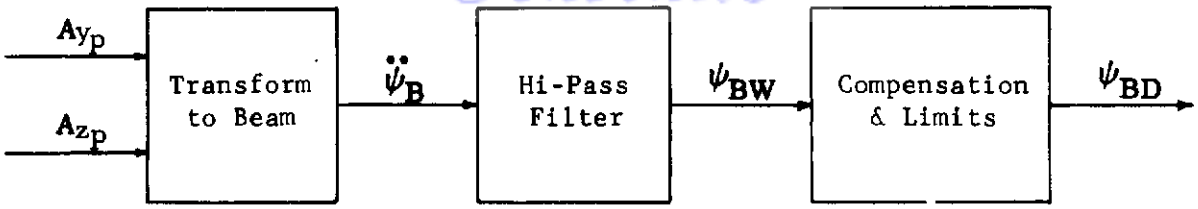

Beam Yaw

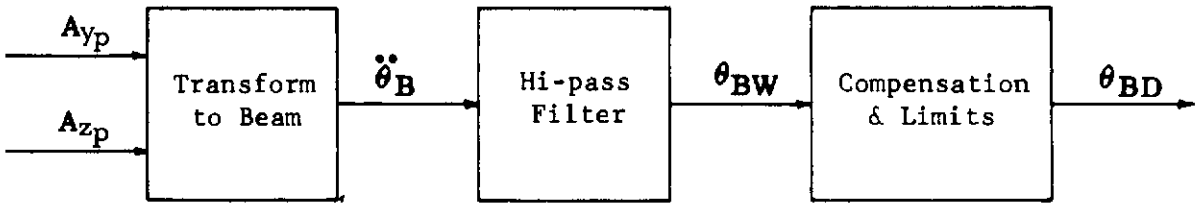

Beam Pitch

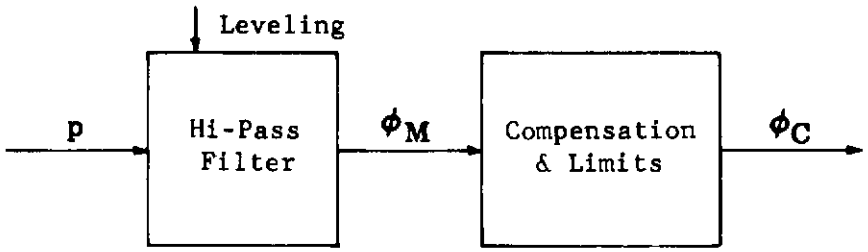

Cab Roll

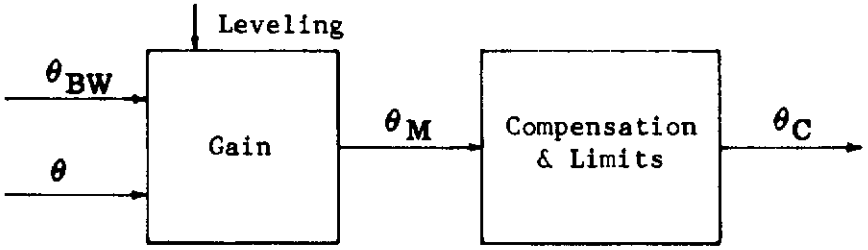

Cab Pitch

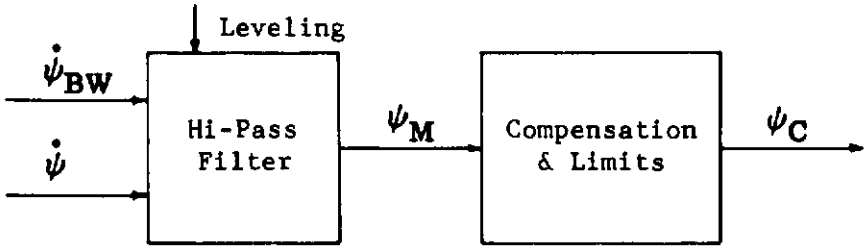

Cab Yaw

FIGURE 84 SIMULATOR DRIVE PHILOSOPHY

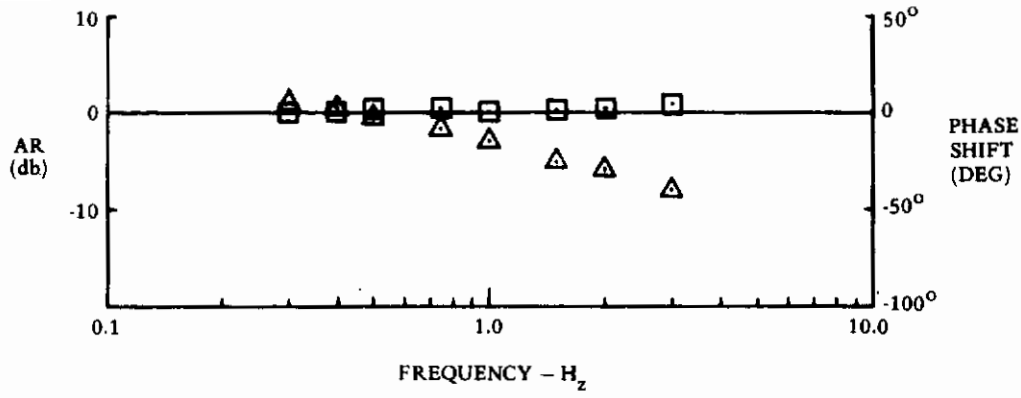

CAB PITCH

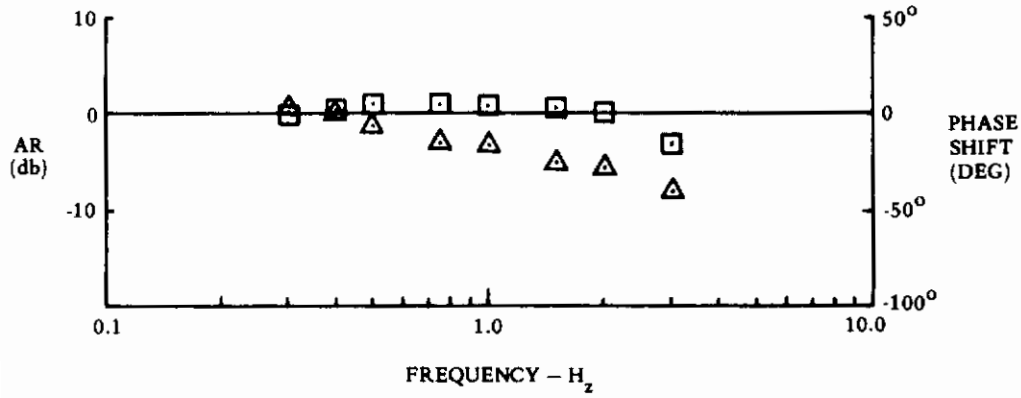

CAB YAW

△ PHASE

⊡ AMPLITUDE

FIGURE 85. SIMULATOR FREQUENCY RESPONSE

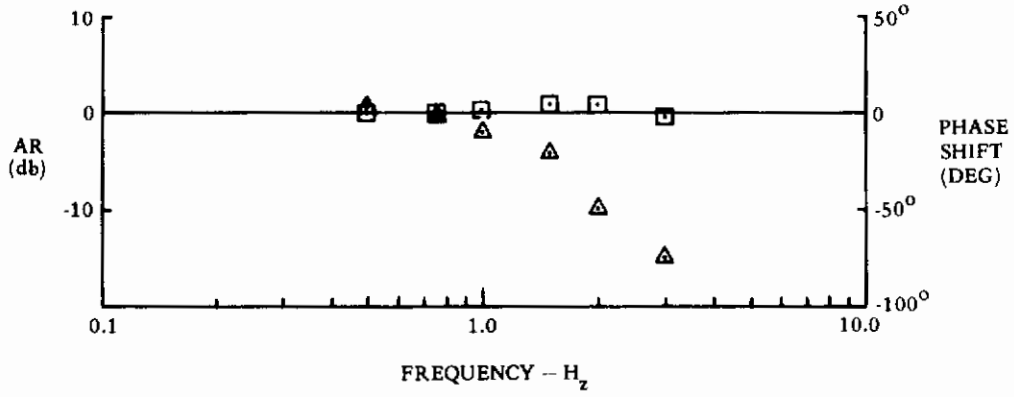

BEAM YAW

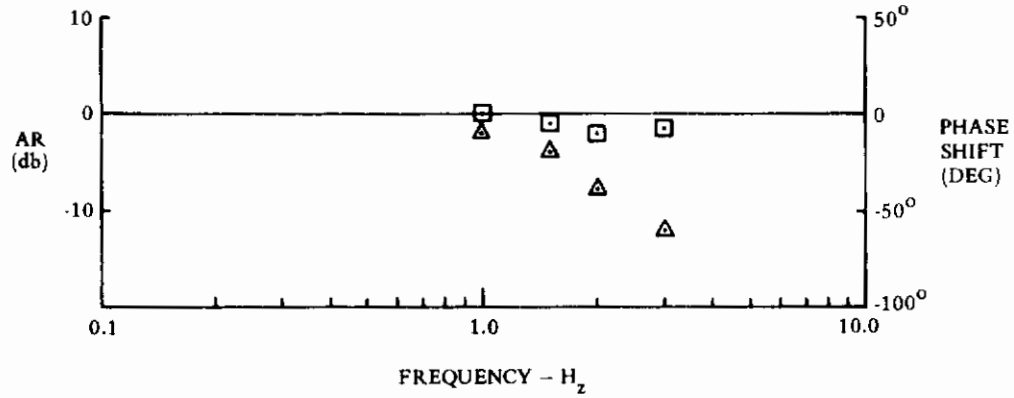

BEAM PITCH

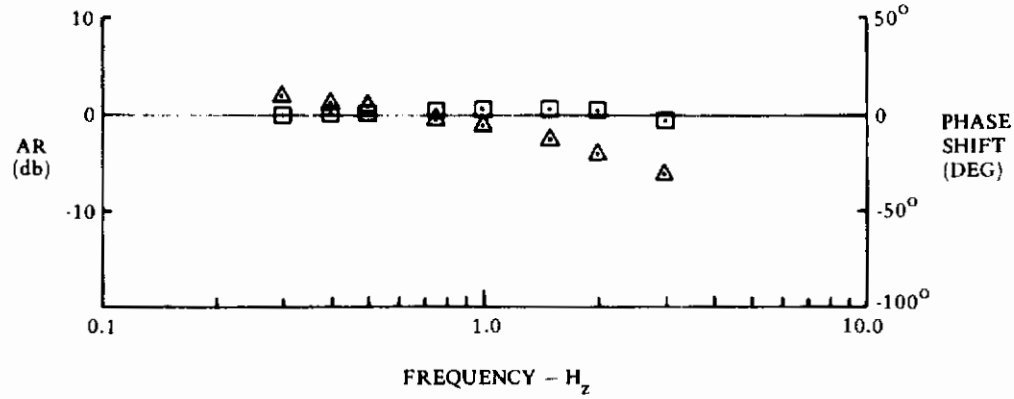

CAB ROLL

FIGURE 85. (concluded)

3. Follow a commanded random heading.

   A signal generated by filtering white noise with $\frac{k}{(s + 0.2)^2}$ was used to indicate the commanded heading. The difference between this heading and the actual aircraft heading was presented on the vertical needle of the ADI. The pilot's instructions were to keep the needle centered by using the ailerons while not allowing altitude to drift "too much". The rudder was not to be used.

4. Maintain a heading of 0 degrees in the presence of turbulence.

   A Dryden form v gust of varying intensities was introduced through the equations of motion. The actual heading signal was applied to the vertical needle of the ADI. The pilot's instructions were to keep the needle centered by using the ailerons while not allowing altitude to drift "too much". The rudder was not to be used.

   Three pilots were used during the simulation. Their respective qualifications are listed below.

Pilot: W.W.K., Prime pilot for the tests.

This pilot is currently employed in the Northrop Aircraft Division Research and Development Department. At Northrop he has participated as an engineer-pilot in several conventional aircraft and VTOL simulation studies, including an auto-rotation and stability augmentation failure study of the CH-46 helicopter, and A-X dive bombing evaluations. He has flown the Northrop T-38A and F-5B, and the experimental S-1. Prior to joining Northrop, he served in the U.S. Navy as an operational pilot with the fleet and as a test pilot at the Naval Air Test Center, Patuxent River, Maryland. He is a graduate of the U.S. Naval Test Pilot School. He holds conventional airplane and helicopter commercial flying licenses and has approximately 4000 hours of flying time.

Pilot: R.L.M. has flown the Large Amplitude 3-X Flight Simulator for A-X air-to-ground delivery simulation, comparison of this ground based simulator to in-flight simulator, and several other Northrop projects. His experience includes approximately 550 hours in WW II trainers and bombers and 100 recent hours in civilian light aircraft.

Pilot: T.E.M. has flown the Large Amplitude 3-X Flight Simulator for a study involving comparison of the ground based simulator and an in-flight simulator. He currently has accumulated approximately 250 hours of flight time in various single engined, light, civilian aircraft.

TABLE VIII. LATERAL-DIRECTIONAL AIRFRAME EQUATIONS

$$\dot{\beta} = \frac{Y_s}{m V_o} + \frac{g \sin\phi}{V_o} + \alpha\, p - r$$

$$\beta_{iner} = \int \dot{\beta}\, dt$$

$$\beta_{aero} = \beta_{iner} + \beta_{gust}$$

$$\frac{Y_s}{m V_o} = Y_\beta \beta_{aero} + Y_{\delta_{rp}} \delta_{rp}$$

$$\dot{p} = L'_\beta \beta_{aero} + L'_p\, p + L'_r\, r + L'_{\delta_{as}} \delta_{as} + L'_{\delta_{rp}} \delta_{rp}$$

$$+ K_{p_1} \alpha\beta_{aero} + K_{p_2} \alpha r + K_{p_3} \alpha p + K_{p_4} \alpha\delta_{as}$$

$$\dot{r} = N'_\beta \beta_{aero} + N'_p\, p + N'_r\, r + N'_{\delta_{as}} \delta_{as} + N'_{\delta_{rp}} \delta_{rp}$$

$$+ K_{r_1} \alpha p + K_{r_2} \alpha\delta_{as} + K_{r_3} \alpha\beta_{aero} + K_{r_4} \alpha r$$

$$a_{y_p} = V\beta_{aero} + l_x \dot{r} - g \sin\phi + V_o (\dot{\beta} + r)$$

$$N_{y_{cg}} = \frac{a_{y_o}}{g} - \frac{l_x \dot{r}}{g}$$

$$\frac{S_{rp_{aug}}}{r} = \frac{-K_{aug}\, s}{T_{aug}\, s + 1}$$

TABLE IX. LONGITUDINAL AIRFRAME EQUATIONS

$$\dot{V} = \frac{X_s}{m} + \frac{T_{sx}}{m} - g\theta + g\alpha\cos\phi$$

$$\Delta V = \int \dot{V}\, dt$$

$$V = V_o + \Delta V$$

$$\frac{X_s}{m} = q_o S\left(C_{D_o} + C_{D_\alpha}\alpha + C_{D_{\alpha 2}}\alpha^2\right) + \frac{2q_o S\Delta V}{V_o}\left(C_{D_o} + C_{D_\alpha}\alpha + C_{D_{\alpha 2}}\alpha^2\right)$$

$$\frac{T_{sx}}{m} = \text{Constant}$$

$$\dot{\alpha} = \frac{Z_s}{V_o m} + \frac{g\cos}{V_o} + q$$

$$\frac{Z_s}{m} = q_o S\left(C_{L_o} + C_{L_\alpha}\alpha + C_{L_{\delta_e}}\delta_e\right) + \frac{2q_o S\Delta V}{V_o}\left(C_{L_o} + C_{L_\alpha}\alpha\right)$$

$$\dot{q} = M_\alpha\alpha + M_{\delta_e}\delta_e + M_{\dot{\alpha}}\dot{\alpha} + M_q q$$

$$a_{z_p} = \dot{V}\alpha - \ell_x\dot{q} - g\cos\phi - V_o(q - \dot{\alpha})$$

$$N_{z_{cg}} = -\frac{a_{z_p}}{g} - \frac{\ell_x\dot{q}}{g}$$

$$\dot{h} = V\theta - \alpha\cos\phi - \beta\sin\phi$$

TABLE X. EULER ANGLE EQUATIONS

$$\dot{\psi} = r \cos\phi + q \sin\phi$$

$$\dot{\phi} = p + \theta \dot{\psi}$$

$$\dot{\theta} = q \cos\phi - r \sin\phi$$

TABLE XI. SIMULATOR BEAM EQUATIONS

$$\ddot{Y}_M = a_{Y_p} \cos\phi - a_{Z_p} \sin\phi$$

$$\ddot{\psi}_B = \dot{Y}_M / \ell_B$$

$$\psi_{BW} = \frac{K_{\ddot{\psi}} \ddot{\psi}_B}{s^2 + \frac{s}{T_{\psi_1}} + \frac{1}{T_{\psi_2}}}$$

$$\psi_{BD} = \frac{(\tau_1 s + 1)(\tau_2 s + 1)\ \psi_{BW}}{K_{p_\psi}}$$

$$\ddot{Z}_M = a_{Z_p} \cos\phi + a_{Y_p} \sin\phi + q$$

$$\ddot{\theta}_B = \ddot{Z}_B / \ell_B$$

$$\theta_{BW} = \frac{K_{\ddot{\theta}} \ddot{\theta}_B}{s^2 + \frac{s}{T_{\theta_1}} + \frac{1}{T_{\theta_2}}}$$

$$\theta_{BD} = \frac{(\tau_3 s + 1)(\tau_4 s + 1)\ \theta_{BW}}{K_{p_\theta}}$$

TABLE XII. SIMULATOR COCKPIT EQUATIONS

$$\phi_M = \frac{K_\phi (p - \dot{\theta} \tan \psi) + \dot{\psi}_{BW} \sin \left(\theta_M + \theta_{BW}\right)}{s + \frac{1}{\tau_{\phi_W}}}$$

$$\phi_C = \frac{\left(\tau_{\phi_M} s + 1\right) \phi_M}{K_{\phi_M}}$$

$$\dot{\theta}_M + \dot{\theta}_{BW} = \frac{K_\theta \dot{\theta}}{\cos \psi} - \psi_{BW} \sin \left(\theta_M + \theta_{BW}\right) \sin \psi_M$$

$$\theta_C = \frac{\left(\tau_{\theta_M} s + 1\right) \theta_M}{K_{\theta_M}}$$

$$\psi_M = \frac{K_\psi \dot{\psi} - \dot{\psi}_{BW} \cos \left(\theta_M + \theta_{BW}\right) \cos \psi_M}{s + \frac{1}{\tau_{\psi_W}}}$$

$$\psi_C = \frac{\left(\tau_{\psi_M} s + 1\right) \psi_M}{K_{\psi_M}}$$

TABLE XIII. GUST SIMULATION

$$\beta_{gust} = \left(N_g\right)\left(K_{gust}\right) \frac{s + A_{gust}}{s^2 + B_{gust}\, s + C_{gust}}$$

TABLE XIV. TRACKING SIGNAL

$$\phi_{tc} \text{ or } \psi_{tc} = \left(N_g\right) \frac{K_{tc}}{\left(s + A_{tc}\right)^2}$$

TABLE XV. ROOT MEAN SQUARE COMPUTATIONS

$$x_{ms} = \frac{1}{100} \int_0^{100} \left[x(t)\right]^2 dt \quad \text{(Analog Computer)}$$

$$x_{rms} = \left(x_{ms}\right)^{\frac{1}{2}} \quad \text{(Hand Calculation)}$$

Bank angle task, $x(t)$: $V_o\beta_{gust}$, ϕ_{tc}, ϕ_ϵ

Heading task, $x(t)$: $V_o\beta_{gust}$, ψ_{tc}, ψ_ϵ, β, ϕ

TABLE XVI. SIMULATOR COCKPIT INSTRUMENTS

Attitude Director Indicator (ADI)	
Pitch Indicator:	θ
Roll Indicator:	ϕ
Bank Steering Bar (Tracking Command Display):	$\phi_\epsilon = \phi - \phi_{tc}$
or:	$\psi_\epsilon = \psi - \psi_{tc}$
Turn Needle (mechanized as a ball):	$\frac{N_{y_{cg}}}{(0.1\,s + 1)^2}$
Horizontal Situation Indicator (HSI):	ψ
Airspeed Indicator:	$V_o + \Delta V$
Altimeter:	$\int \dot{h}\, dt + h_o$
Vertical Velocity Indicator:	$\dot{h}$
G-meter:	$N_{z_{cg}}$

TABLE XVII. T-33 DATA

ALL CONFIGURATIONS

m = 385 slugs

g = 32.2 ft/sec^2

V_o = 590 fps

ℓ_x = 6 ft

K_{p_1} = -87.25/sec^2

K_{p_2} = 3.57/sec

K_{p_3} = -0.04685/sec

K_{p_4} = 0.0036/in-sec^2

K_{r_1} = -1.634/sec

K_{r_2} = 0.1259/in-sec^2

K_{r_3} = -1.175/sec^2

K_{r_4} = 0.0482/sec

C_{D_o} = 0.0217

C_{D_α} = 0.172/rad

$C_{D_\alpha}^2$ = 0.057/rad^2

T_{s_X} = Adjusted to trim initial V to zero

C_{L_o} = 0.264

C_{L_α} = 6.47/rad

$C_{L_{\delta_e}}$ = 0.368/rad

$L'_{\delta_{rp}}$ = -0.188/sec^2-in

$N'_{\delta_{rp}}$ = 0.460/sec^2-in

$Y_{\delta_{rp}}$ = -0.00503/sec-in

S = 234.8 ft^2

b = 37.54 ft

$\bar{c}$ = 6.72 ft

q_o = 200 lbs/ft^2

I_x = 17,100 slug-ft^2

I_y = 21,000 slug-ft^2

I_z = 36,400 slug-ft^2

I_{xz} = 490 slug-ft^2

K_{aug} = 0

A_{gust} = 0.342/sec

B_{gust} = 1.185/sec

C_{gust} = 0.348/sec^2

K_{gust} = Adjusted to give desired gust rms

K_{tc} = Adjusted to give desired tracking command signal rms

Bank-Angle Task: A_{tc} = 0.5/sec

Heading Task: A_{tc} = 0.2/sec

TABLE XVIII. T-33 SIMULATED CONFIGURATIONS

CONFIG-URATION	DERIVATIVE								
	L'_{β}	L'_{p}	L'_{r}	$L'_{\delta_{as}}$	N'_{β}	N'_{p}	N'_{r}	$N'_{\delta_{as}}$	$1/v$
	$1/SEC^2$	$1/SEC^2$	$1/SEC^2$	$1/SEC^2$-in	$1/SEC^2$	$1/SEC^2$	$1/SEC^2$	$1/SEC^2$-in	$1/SEC^2$
AB 2.6	-13.34	-2.493	0.7300	2.460	6.012	-0.0125	-0.3510	0.0517	-0.1616
AB 2.7	-13.34	-2.493	0.7300	1.990	6.012	-0.0125	-0.3510	0.0935	-0.1616
AB 3.1	-10.58	-2.195	1.195	1.030	5.289	-0.3904	-0.7061	-0.1330	-0.1559
AB 3.3	-10.58	-2.195	1.195	1.500	5.289	-0.3904	-0.7061	0	-0.1559
BB 2.3	-44.14	-2.738	2.058	3.320	5.544	0.0148	-0.2782	0	-0.1589
BC 2.2	-41.48	-0.7456	4.110	1.588	5.039	0.0437	-0.3769	-0.0540	-0.1487
BC 2.3	-41.48	-0.7456	4.110	1.885	5.039	0.0437	-0.3769	-0.0130	-0.1487
BC 2.4	-41.48	-0.7456	4.110	1.467	5.039	0.0437	-0.3769	0	-0.1487

TABLE XIX. F-5 DATA

m	=	385 slugs
g	=	32.2 ft/sec^2
V_o	=	718 fps
ℓ_x	=	11 ft
q_o	=	528.2 lbs/ft^2
Y_β	=	0.5002/sec
$Y_{\delta_{rp}}$	=	0.00861/sec-in
L'_β	=	29.06/sec^2
L'_p	=	-1.856/sec
L'_r	=	0.4045/sec
$L'_{\delta_{as}}$	=	2.023/sec^2 -in
$L'_{\delta_{rp}}$	=	-0.0628/sec^2 -in
N'_β	=	8.969/sec^2
N'_p	=	0.00705/sec
$N'_{\delta_{rp}}$	=	0.7298/sec^2 -in
$N_{\delta_{as}}$	=	0.0352/sec^2 -in
N'_r	=	-0.5459/sec
T_{aug}	=	0.5 sec
K_{aug}	=	4 in/rad/sec
A_{gust}	=	0.413
B_{gust}	=	1.531
C_{gust}	=	0.516
S	=	170 ft^2

All other data the same as the T-33 configurations

TABLE XX. SIMULATOR DATA

l_B	=	23.34 ft
$\tau_1 \tau_2$	=	0.1545 sec^2
$\tau_1 + \tau_2$	=	0.667 sec
$1/K_{p_\psi}$	=	387 volts/rad
T_{ψ_1}	=	0.500 sec
T_{ψ_2}	=	0.200 sec^2
$K_{\ddot{\psi}}$	=	0.200
$\tau_3 \tau_4$	=	0.016 sec^2
$\tau_3 + \tau_4$	=	1.016 sec
$1/K_{p_\theta}$	=	121.7
T_{θ_1}	=	0.100 sec
T_{θ_2}	=	0.03185 sec^2
$K_{\ddot{\theta}}$	=	0.500
K_ϕ	=	0.400
τ_{ϕ_W}	=	1.00 sec
τ_{ϕ_M}	=	0.473 sec
$1/K_{\phi_M}$	=	60.5 volts/rad
K_θ	=	0.400
τ_{θ_M}	=	1.220 sec
$1/K_{\theta_M}$	=	115.5 volts/rad
K_ψ	=	0.400
τ_{ψ_W}	=	2.000 sec
τ_{ψ_M}	=	0.355 sec
$1/K_{\psi_M}$	=	123.0 volts/rad

TABLE XXI. BANK ANGLE PILOT RATING DATA

Configuration	rms δg_{β}	rms ϕ_e	Cooper Rating PR
AB 2.6	13.03	1.59	2.0
AB 2.6	23.55	3.33	4.0
AB 2.6	34.27	4.16	5.0
AB 2.6	9.46	1.59	2.5
AB 2.6	16.50	1.73	5.0
AB 2.7	12.46	1.43	3.0
AB 2.7	21.05	2.37	6.5
AB 2.7	33.41	2.66	8.0
AB 3.1	11.58	.97	3.0
AB 3.1	27.09	1.88	5.0
AB 3.3	12.26	1.01	2.0
AB 3.3	23.33	1.69	4.0
BB 2.3	5.79	2.28	4.0
BB 2.3	11.24	3.92	6.5
BB 2.3	15.54	5.04	8.5
BB 2.3	7.37	2.42	4.5
BB 2.3	4.69	1.60	3.5
BB 2.3	14.08	3.75	6.5
BC 2.2	10.31	5.83	9.0
BC 2.2	6.89	3.39	7.5
BC 2.3	10.50	4.09	9.5
BC 2.3	10.51	4.09	9.0
BC 2.3	5.72	3.29	5.0
BC 2.4	12.39	5.21	9.0
BC 2.4	5.12	2.92	6.0

Unclassified
Security Classification

DOCUMENT CONTROL DATA - R & D

(Security classification of title, body of abstract and indexing annotation must be entered when the overall report is classified)

1. ORIGINATING ACTIVITY (Corporate author) Northrop Corporation Aircraft Division Hawthorne, California	2a. REPORT SECURITY CLASSIFICATION Unclassified 2b. GROUP

3. REPORT TITLE

Airplane Flying Characteristics in Turbulence

4. DESCRIPTIVE NOTES (Type of report and inclusive dates)

Final Report — 11 November 1969 to 11 September 1970

5. AUTHOR(S) (First name, middle initial, last name)

Edward D. Onstott
Ernest P. Salmon

6. REPORT DATE November 1970	7a. TOTAL NO. OF PAGES 188	7b. NO. OF REFS 18
8a. CONTRACT OR GRANT NO. F33615-70-C-1156 b. PROJECT NO. 8219 c. Task 821904 d.	9a. ORIGINATOR'S REPORT NUMBER(S) NOR 70-139 9b. OTHER REPORT NO(S) (Any other numbers that may be assigned this report) AFFDL-TR-70-143	

10. DISTRIBUTION STATEMENT

This document has been approved for public release and sale; its distribution is unlimited.

11. SUPPLEMENTARY NOTES	12. SPONSORING MILITARY ACTIVITY Air Force Flight Dynamics Laboratory Air Force Systems Command

13. ABSTRACT

A method for predicting the performance of the total pilot-vehicle system has been developed for the lateral dynamics of Class IV airplanes. This method, which is based on pilot model theory and multiloop analysis, predicts tracking errors for command tracking tasks and also for attitude hold tracking tasks in turbulence. The predictions are in terms of root mean square time domain statistics and are obtained by means of a fully automated multiloop analysis performance prediction program available from the United States Air Force. Thus, system performance can be evaluated analytically in terms of familiar time domain root mean square statistics. The validity and accuracy of this method have been ascertained by means of moving base simulation on the Northrop Large-Amplitude Flight Simulator operating in five-degree-of-freedom motion.

DD FORM 1 NOV 65 1473

Unclassified
Security Classification

14. KEY WORDS	LINK A		LINK B		LINK C	
	ROLE	WT	ROLE	WT	ROLE	WT
Pilot Model Theory						
Multiloop Analysis						
Turbulence						
Pilot-Vehicle Performance						
Turbulence Simulation						
Performance Prediction methods						
Flying Qualities						